Evaluation of the Effects of *L*-2-oxothiazolidine-4-carboxylate or Quercetin on Developing Scar Tissue in Rats using Synchrotron Infrared Microspectroscopy

by

Richard Wiens

A Thesis submitted to the Faculty of Graduate Studies of

The University of Manitoba

in partial fulfilment of the requirements of the degree of

Doctor of Philosophy

Department of Chemistry

University of Manitoba

Winnipeg, Manitoba, Canada

THE UNIVERSITY OF MANITOBA

FACULTY OF GRADUATE STUDIES

*****

COPYRIGHT PERMISSION

Evaluation of the Effects of *L*-2-oxothiazolidine-4-carboxylate or Quercetin on Developing Scar Tissue in Rats using Synchrotron Infrared Microspectroscopy

By

Richard Wiens

A Thesis/Practicum submitted to the Faculty of Graduate Studies of The University of Manitoba in partial fulfillment of the requirement of the degree

Of

Doctor of Philosophy

Abstract

Synchrotron infrared microspectroscopy was used as part of a multi-disciplinary research project to evaluate the effects of two therapeutic agents, L-2-oxothiazolidine-4-carboxylate (OTC) and quercetin, on the wound healing of laminectomized rats. Synchrotron light sources were used to achieve the necessary spatial resolution (~10 microns) to image the heterogeneous wound area. Our hypothesis is that post-surgical inflammation and oxidative stress following laminectomy can be reduced by systemic administration of L-2-oxo-thiazolidine-4-carboxylate (OTC) or quercetin, and that reducing the levels of inflammation and oxidative stress will result in better wound healing.

As part of a Natural Sciences and Engineering Research Council Collaborative Health Research Project (NSERC-CHRP) to test the effects of OTC and quercetin on wound healing, male wistar rats underwent lumbar laminectomies. The rats were placed in one of three treatment groups (saline control, OTC, or quercetin), and sacrificed at three different time points (3, 21, and 63 days post surgery) in the wound healing process. Infrared data was collected on the scar tissue, and analyzed for levels of collagen, phosphates, sugars, and lipids. The 3 day animals showed little collagen, but large amounts of phosphates. The 21 day animals had larger amounts of collagen than the 3 day animals, and a decrease in phosphates. The 63 day animals had a contracted wound area. There was less scar tissue in the 63 day animals, but the collagen had a more intense infrared signature. While we were able to image the wound

area using infrared microspectroscopy, there was no statistical evidence for improvement in the wound healing process based on treatment type. In addition to the studies on OTC and quercetin, it was noticed that the inherently polarized light from a synchrotron source resulted in changes in the IR spectra. These changes were the result of the polarized synchrotron light interacting with the oriented collagen fibres in the wound healing area. Tissue sections from the Achilles tendon of a rat were used to model the effects of polarized light on the IR spectrum of oriented samples.

List of Published Papers

1. Wiens, R., Rak, M., Cox, N., Abraham, S., Juurlink, B. H. J., Kulyk, W. M., and Gough, K. M. G. Synchrotron FTIR microspectroscopic analysis of the effects of anti-inflammatory therapeutics on wound healing in laminectomized rats. Analytical and Bioanalytical Chemistry, 387, 1679-1689, 2007.

2. Gough, K. M., Zielinkski, D., Wiens, R., Rak, M., and Dixon, I. M. C. Fourier transform infrared evaluation of microscopic scarring in the cardiomyopathic heart – Effects of chronic AT1 suppression. Analytical Biochemistry, 316, 232-242, 2003.

List of Abbreviations

AD	Alzheimer's Disease
AGE	Advanced glycation end products
CNS	Central nervous system
ATP	Adenosine triphosphate
COX2	Cyclo-oxygenase 2
DMX	Dimethotrexate
L-Cys	Cysteine
EGF	Epidermal growth factor
FBS	Failed back syndrome or Failed back surgery syndrome (FBSS)
FGF-2	Fibroblast growth factor 2
FPA	Focal Plane Array
FTIR	Fourier Transform Infrared
GAG	Glycosaminoglycans
L-Glu	Glutamic acid
Gly	Glycine
GSH	Glutathione
IGF-1	Insulin growth factor 1
IL-1	Interleukin 1
IL-4	Interleukin 4
IL-6	Interleukin 6
LDL	Low density lipoprotein
MMP	Matrix metalloproteinase
MS	Multiple sclerosis
NFκB	Nuclear factor kappa B
NSAID	Non-steroidal anti-inflammatory drugs
NSERC-CHRP	Natural Sciences and Engineering Research Council – Collaborative Health Research Project
NSLS	National Synchrotron Light Source
PDGF	Platelet derived growth factor
RA	Rheumatoid arthritis
Pi	Inorganic phosphate
SCS	Spinal cord stimulation
SOD	Superoxide dismutase
SPARC	Secreated protein acidic rich in cysteine
SRC	Synchrotron Radiation Center
TGF-β	Transforming Growth Factor β
TIMP	Tissue inhibitor of metalloproteinases
TNF-β	Tumor necrosis factor β

Acknowledgements

I would like to thank the following people without whose help and support this thesis would not be possible:

My supervisor: Dr. Kathleen Gough.

Past and current group members of the Gough research group. Especially: Margaret Rak (Ph. D, 2007), Meghan Gallant (Ms. Chemistry, 2007), Vincent Okoli, Fred Zeiler, and Mitch Bushuk.

My Advisory Committee: Dr. Ian Dixon, Dr. Torsten Hegmann, and Dr. Phil Hultin.

Everyone in the Department of Chemistry

The synchrotron beamline staff at SRC (Dr. Bob Julian) and NSLS (Drs. Lisa Miller, Randy Smith, and Neb Marinkovic).

Our collaborators at the University of Saskatchewan: Nicky Cox (Masters, 2008), Suraj Abraham, Dr. B. Juurlink, and Dr. B. Kulyk.

Financial Support:
NSERC-CHRP

My family

Table of Contents

List of Figures

List of Tables

Chapter 1: Introduction

1.1. Project Overview

1.1.1. Overview

The research presented in this thesis is part of a Collaborative Health Research Project. The principle investigator was Professor Kathleen Gough from the Department of Chemistry at the University of Manitoba. Research was also conducted in the laboratories of Professor Bernhard J. Juurlink and Professor William Kulyk from the Department of Anatomy and Cellular Biology at the University of Saskatchewan.

1.1.2. Background

Failed back surgery syndrome (FBSS) is a post operative disorder characterized by chronic pain that may arise from a variety of underlying causes including:

1) Traumatization of a nerve root,

2) spondylitis,

3) Epidural fibrosis, and

4) Local arachnoiditis.

Peridural scarring, or the excessive formation of scar tissue following spinal surgery, is one of the important contributing factors that result in persistent pain and disability in many individuals who have undergone elective back surgery.

The chronic pain characteristic of FBSS is principally treated with either a combination of pharmacological analgesic therapy and rehabilitation, or spinal cord stimulation (SCS). Both of these therapies have proven to be less effective than originally thought, and both have inherent disadvantages. Long term analgesic drug therapies carry a risk of addiction for the patient, while SCS requires another invasive procedure to implant the electrodes. In addition, both conventional drug therapy and SCS merely alleviate the pain; neither treatment deals with the underlying causes.

1.1.3. Hypothesis

Our hypothesis is that post-surgical inflammation and oxidative stress following laminectomy can be reduced by systemic administration of *L*-2-oxo-thiazolidine-4-carboxylate (OTC) or quercetin, and that reducing the levels of inflammation and oxidative stress will result in better wound healing (Section 1.2).

1.1.4. Research Methods and Goals

The overall project employs a three pronged approach to monitoring the effects of the treatments in the wound healing process. Since the lumbar spine is the most common location for elective spinal surgery, a rat model of lumbar spinal surgery was chosen for our investigations.

Synchrotron Fourier transform infrared (FT-IR) microspectroscopy has been used to show localized distribution of compounds of biological interest including collagen, lipids, and sugars. This research was conducted in the laboratory of Professor Kathleen Gough by Ph. D student Richard Wiens and Margaret Rak, Ph. D.

Conventional immunohistochemistry procedures have been conducted to look at general morphological features of the tissue (H&E staining) as well as to show localized distribution of macrophages, mast cells, and lymphocytes. This research, as well as the surgeries and tissue sectioning was performed by a Master's student, Nicky Cox, in the laboratory of Professor Bernhard Juurlink at the University of Saskatchewan.

Real time PCR has been used to create molecular probes specific to certain compounds of biological interest, including different types of collagens, and these probes can be applied to tissue sections to indicate the distribution of biological compounds throughout a tissue section. This research was performed by Ph. D. student Suraj Abraham, in the laboratory of Professor William Kulyk at the University of Saskatchewan.

By comparing the information obtained from the three different techniques we hope to gain some insight into the process of wound healing itself, as well as conducting a preliminary analysis of the efficacy of the two treatments in reducing the harmful effects of inflammation and oxidative stress post surgery.

1.1.5. My Objectives

This thesis documents the collection and analysis of infrared data from tissues taken from the animals, as well as some infrared data on Achilles tendon to model the effects of the polarized synchrotron light on the infrared data.

Animals were placed in one of three treatment groups, either saline control, OTC treated, or quercetin treated. In addition, each of the three treatment groups was split into three sub groups based on time after surgery at which the animals were sacrificed. Animals were sacrificed at 3 days, 21 days, and 63 days post surgery, for a total of 9 sub groups of animals. Six animals from each of the sub groups were analyzed to account for inter-animal variation. This led to a total of 54 animals in the study.

FTIR data was collected primarily at the Synchrotron Radiation Center in Madison, WI, with some data being collected at National Synchrotron Light Source at Brookhaven National Laboratory and at the Canadian Light Source in Saskatoon, SK.

In addition to the FTIR data, immunohistochemical staining for Smad proteins was attempted. Smad proteins are a part of the TGF-β signaling pathway. The TGF-β family of proteins has a diverse array of functions depending on a variety of situational factors. TGF-β serves a variety of functions in the wound healing process, and changes in Smad protein levels may indicate changes in the wound healing pathology of different treatment types.

1.2. Collagen

1.2.1. General Overview of Collagen

Collagen is the most abundant protein in humans, comprising approximately 25% by mass of the total protein in our bodies, and exists in all but the most basic of living organisms (Miller, E. J. 1982). Twenty-eight different types of collagen have been identified in the literature, but 90% of the collagen found in the human body is of type I, II, III, or IV. Type I collagen is found in bone and tendon and type II collagen is the main component of cartilage. Type III collagen is found in the reticular fibres that support the soft tissues of the liver, bone marrow, and the lymphatic system. Type IV collagen forms the basal lamina, which supports the epithelium. The two types of collagen that are of the most interest in this research are the type I and III fibril-forming collagens.

Collagen fibres have two main characteristics that are crucial in enabling them to serve their roles in tissue and tendons. First, a collagen fibril has a very high tensile strength, allowing it to provide structure and support to the surrounding tissue. Second, collagen fibrils have a high level of elasticity, allowing them to bend and flex in tendons. The high tensile strength and elasticity of collagen fibres are a result of their unusual amino acid composition, and the secondary and tertiary structures that this sequence allows the fibril to adopt. Collagen molecules are composed of repeating triplets of Gly-XXX-YYY, where XXX is often proline, and YYY is often hydroxyproline. The inclusion of glycine at every third position in the sequence is critical as the glycine side chain, a simple

hydrogen atom, is the only side chain small enough to fit into the interior of the collagen triple helix. A molecule of collagen is composed of approximately 1000 amino acids arranged into a left handed helix (Kadler, K. 1994). Three collagen chains will twist together to form a right handed super coil that is stabilized by hydrogen bonding and cross-linking. Figure 1 shows the different regions of a collagen molecule. The N-propeptide (A) and C-propeptide (E) regions are cleaved extracellularly, leaving the triple helical domain (C) with N-telopeptide (B) and C-telopeptide (D) regions.

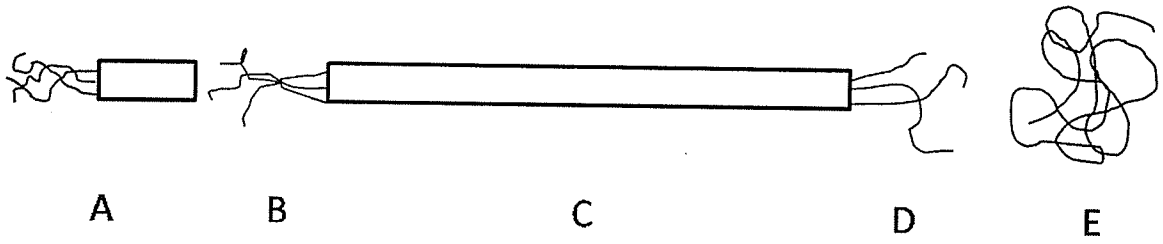

Figure 1: Schematic representation of a collagen molecule.
A) N-propeptide, B) N-telopeptide, C) Triple Helical Domain,
D) C-telopeptide, E) C-propeptide.
Block regions denote triple helical structure.

The main form of type I collagen in humans is found in the extra-cellular matrix of tendon, bone, and ligaments (Kadler, K. 1994). It is a heterotrimer comprised of two identical α1(I) chains and one α2(I) chain. There are also small amounts of a homotrimer of three α1(I) chains found in embryonic tissues and in people with osteogenesis imperfecta (Kadler, K. 1994).

Type III collagen exists as a homotrimer of three α1(III) molecules and can be found in hollow organs, dermis, placenta and uterus (Kadler, K. 1994). Type

III collagen is also commonly associated with type I collagen in developing tissues.

1.2.2. Collagen Synthesis

Collagen synthesis is a complex process involving numerous co-translational and post-translational modifications, both inside and outside the cell. Intracellular steps include the hydroxylation of lysine and proline residues, glycosylation of hydroxylysine residues, and formation of the triple helical procollagen molecule. Extracellular steps include cleavage of the C and N terminal propeptides to form the collagen molecule, followed by fibril formation and cross-linking.

Collagen is synthesized on ribosomes in the rough endoplasmic reticulum of fibroblasts. Hydroxylation and glycosylation occur while the individual chains are being translated and after synthesis is complete (Kadler, K. 1994).

Hydroxylation of lysine (Figure 2) requires that the lysine be in the Gly-XXX-Lys formation (Kadler, K. 1994). Hydroxylation is carried out by lysyl hydroxylase and requires Fe^{2+} ions, 2-oxoglutarate, ascorbate, and molecular oxygen (Davidson, J. M. 1981). One atom of molecular oxygen is incorporated into the 2-oxoglutarate while the other serves to hydroxylate the lysine residue. The 2-oxoglutarate is then decarboxylated to yield succinate and carbon dioxide. Hydroxylysine residues serve as sites for glycosylation of the collagen molecule as well sites for oxidation and the subsequent formation of crosslinks in larger collagen fibres.

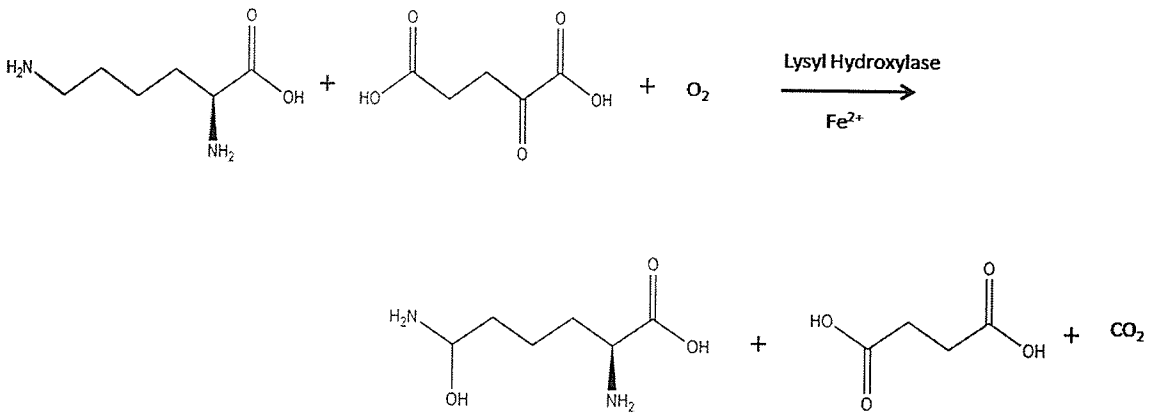

Figure 2: Hydroxylation of a lysine residue by lysyl hydroxylase.

Hydroxylation of prolyl residues is carried out in a similar manner.

Hydroxylation of proline residues occurs at both the three and four position of the side chain (Davidson, J. M. 1981). Hydroxylation at the 4 position only occurs if the proline residue occupies the Gly-XXX-Pro position, similar to the case of lysine. The hydroxylation of proline is enzyme catalyzed by prolyl 4-hydroxylaze and requires the presence of Fe^{2+} ions, 2-oxoglutarate, ascorbate, and molecular oxygen. The hydroxylation of proline by prolyl 4-hydroxylaze induces a change in the collagen backbone that promotes the folding of the molecule into its triple helical structure.

Hydroxylation of proline residues can also occur at the three position, although it is relatively infrequent. For this hydroxylation to occur, proline must occupy at both the XXX and YYY positions of the Gly-XXX-YYY triplet, and the proline residue at the YYY position must be 4-hydroxyproline. Hydroxylation at the three position is catalyzed by a separate enzyme, prolyl 3-hydroxylaze, but little is known about the effects of the presence or absence of 3-hydroxyproline in the collagen backbone.

Collagen molecules contain O-linked galactose monosaccharides and glucosyl galactose disaccharides attached to hydroxylysyl residues. The number of glycosylation sites varies as a result of both normal and abnormal conditions. The degree of glycosylation is dependent on the type of collagen, the tissue where the collagen is present, and can also vary if mutations in the collagen genes are caused by disease. Type I collagen contains few (2) sites of glycosylation compared to type IV collagen (46) per 1000 residues (Miller, E.J. 1982).

Glycosylation of hydroxylysyl residues is catalyzed by two enzymes, hydroxylysyl galactosyltransferase and galactosyl hydroxylysyl glucotransferase, which attach galactose monosaccharides and galactosyl glucose disaccharides respectively (Myllyla, R. 1976, Myllyla, R. 1975). The glycosylation of the hydroxylysyl residues requires that the collagen substrate be in a non-triple-helical structure (Kadler, K. 1994). In addition to the sugars found on the triple helical portion of the procollagen molecule, the C- and N-propeptides can contain N-linked sugars attached to asparagine residues.

The formation of the procollagen molecule from the propeptide chains begins with association of the three individual chains at their C-termini. This association is followed by the formation of a nucleus of triple helical structure and propagation of the nucleus from the C-terminal to the N-terminal in an orderly fashion

Most of the studies investigating the folding of the collagen molecule into its triple helical conformation involve type III collagen. Type III collagen lends itself well to the study of folding, and particularly refolding, because it contains three interchain disulfide bonds near the C-terminus, which allows for the maintenance of particular registration of the individual proα chains so that proper refolding occurs (Engel, J. 1991).

The folding of the collagen III molecule occurs in two phases. The first phase is short, involving the folding of the molecule from the disulfide bonds in the C-terminus, up to the first *cis*-bond along the path of the chains. The inclusion

of numerous proline and hydroxyproline residues encourages the unfolded chains to form peptide bonds in the *cis*-configuration. However, in order for the collagen molecule to fold into the proper triple helical structure all peptide bonds must be in the *trans*-configuration (Engel, Jurgen 1991).

Byers et al (Byers, P. H., 1975), via a series of related experiments, showed that the interchain disulfide bonds form in the *C*-propeptide region of procollagen. They began by digesting procollagen from chick embryos with tadpole collagenase, which lyses the procollagen molecule into PC^A (procollagen A, encompassing the N-terminus) and PC^B (procollagen B, encompassing the *C*-terminus) fragments. Gel electrophoresis was conducted on the fragmented procollagen, before and after reduction of disulfide bonds. Two bands that appeared near the α1 marker remained unchanged after reduction, while the band that appeared between the α1 and β markers migrated further after reduction of the disulfide bonds, showing that only one of the two fragments included disulfide bonds. That the migrating band was the fragment containing the *C*-terminus is shown by comparison of the procollagen electrophoresis data to that of collagen.

After the triple helical structure is formed, the collagen molecule is extruded from the rough endoplasmic reticulum into the Golgi apparatus, and from there to the extra cellular space (Kadler, K. 1994, Davidson J. M. 1981). The extracellular steps in the formation of collagen fibrils are: 1) Conversion of the procollagen molecule to collagen by cleavage of the *C*- and *N*-terminal propeptides by *C*- and *N*-peptidases, 2) The end to end aggregation of collagen

molecules into collagen fibrils, and 3) The stabilization of the collagen fibrils by the formation of interchain crosslinks through hydroxylysyl residues.

The removal of the *N*-propeptide is catalyzed by type I/II procollagen *N*-peptidase, or type III procollagen *N*-peptidase, depending on the type of collagen. The enzyme has been purified from calf tendon and chick embryo leg tendons (Hojima, Y. 1989, Kohn, L. D. 1974). It is composed of four different subunits with catalytic activity assigned to the larger 161 and 135 KDa subunits (Kadler, K. 1994). Type I/II *N*-peptidase cleaves a specific [– Pro – Gln –] bond in the proα1(I) chain and a [– Ala – Gln –] bond in the proα2(I) chain. Type III procollagen *N*-peptidase selectively cleaves the *N*-propeptide from type III collagen. Both proteinases require Zn^{2+} and Ca^{2+} ions for full activity.

In vitro studies show that fibril self assembly is initiated upon enzymatic removal of the *C*-propeptide, carried out by a separate enzyme (Kadler, K. 1994). *C*-propeptidases have been purified from chick leg tendon and mouse fibroblasts. The *C*-propeptidase cleaves the Ala-Asp bonds in proα1(I) and proα2(I) chains. The *C*-propeptidase is also a metalloproteinase and requires the presence of Ca^{2+} and Zn^{2+} for maximum activity.

The resulting triple helical structure of type I collagen is composed of three (2 α1(I) and 1 α2(I)) polypeptide chains wound together into a right handed super helix. There are approximately 3.33 residues/turn; the adjacent chains are staggered by one residue to accommodate the glycine residues of different chains into the overall structure (Kadler, K. 1994, Rich, A. 1961). The triple helix

is stabilized by two types of interchain hydrogen bonds (Ramachandran, G. N. 1973, Ramachandran, G. N. 1968):

1. Between the N-H group of the glycyl residue and the C=O group of amino acid residue in the second position of the neighbouring chain.
2. Water molecule bonding with the O-H group of the 4-hydroxyprolyl residue in the third position of the triplet.

There are three different possible orientations for the type I collagen heterotrimer, with the α2(I) chain occupying one of the three different positions. The lead chain is generally referred to as the A chain, and it is in this position that the α2(I) chain is usually found (Bender, E. 1982).

The aggregation of collagen molecules into fibrils is accompanied by the formation of intra- and inter-molecular crosslinks between lysyl and hydroxylysyl residues (Bender, E. 1982). The formation of crosslinks is catalyzed by lysyl oxidase which removes the amino group from lysyl and hydroxylysyl residues in the telopeptide region at either end of the triple helical region. The resultant aldehydes react with ε-amino groups or other aldehydes to form a variety of cross-linked species. The newly formed crosslinks are reducible, but over time they will react to form non-reducible crosslinks. The formation of these crosslinks provides much of the high tensile and mechanical strength necessary for extended tissue integrity.

The two major bifunctional crosslinks that form in skin, cornea and other soft tissues are (Bender, E. 1982):

1. An aldol condensation reaction between two allysine residues on an α1(I) and α2(I) chain, and

2. A Schiff-base cross-link formed between allysyl residue in the telopeptide and a lysine or hydroxylysine residue in the triple helix of a neighbouring fibril.

The reaction of a bifunctional crosslink with a histidine residue can produce a non-reducible tri-functional crosslink called histidinohydroxylysinonorleucine. Tetrafunctional crosslinks are also possible, but it is not known whether these are naturally occurring cross-links or an artifact of the in vitro acid hydrolysis and borohydride reductions used in these studies.

The second pathway, in which the crosslinks are derived from hydroxylysyl residues, occurs most often in weight bearing tissues and mineralized tissues. Two main bifunctional crosslinks are formed. The first, dehydrodihydroxylysinonorleucine is formed from the condensation of a hydroxyallysine and hydroxylysine, and undergoes rearrangement into the second, more common, form; hydroxylysino-5-oxo-norleucine. The two trifunctional crosslinks, hydroxylysylpyridinoline and lysyl-pyridinoline, arise from the reaction of three hydroxylysines or two hydroxylysines and one lysine.

Finally, in addition to the common crosslinks formed through hydroxylysine residues, there are additional crosslinks such as isotrityrosine, histidinoalanine and lysino-alanine.

1.3. Failed Back Syndrome

1.3.1 Failed Back Syndrome

Failed Back Syndrome (FBS) is a diagnosis applied to patients that have undergone elective back surgery in an effort to relieve back pain, but do not gain relief from their symptoms even after completion of the surgical procedure (Anderson, V.C. 2000; Hazard, R. G. 2006; Onesti, S. T. 2004; Robertson, J. T. 1996; Slipman, C. W. 2002; Burton, C. V. 1981; Coskun, E. 2000). The pain experienced by patients suffering from FBS can occur in the lower back, hip, thigh, or lower leg (Robertson, J. T. 1996). FBS can involve either outright failure or recurrence of pain after temporary relief. Cases of outright failure are usually the result of improper diagnosis or surgical procedures (Crock, H. V. 1976). There are numerous potential causes of relapsing pain including: true recurrence of disc herniation, new disc herniation at a different disc, epidural fibrosis and local arachnoiditis, symptomatic arthritis, and spondylitis (Fritsch, E. K. 1996).

The chronic pain characteristic of FBS can be mechanical or neuropathic, can occur axially or radicularly, and may be complicated by coexisting musculoskeletal disorders or orthopaedic issues (Onesti, S. T. 2004). Mechanical pain is increased by load bearing activities such as standing or walking while neuropathic pain is a more constant pain associated with a radicular distribution. Radicular pain is caused by inflammation or irritation of the nerve root, and can be felt along the nerve. A common cause of radicular pain is sciatica. The result of inflammation of the sciatic nerve, pain radiates along the nerve from the lower

spine through the gluteal muscles to the upper thigh, calf, and foot. Unlike radicular pain, which can be felt throughout the lower half of the body even though it originates in the lower back, axial lower back pain is usually confined to the lower back. Axial back pain is not felt throughout the legs. Axial lower back pain can be caused by a degenerate disc, facet joint problems, or damage to ligaments, muscles, and tendons.

Peridural fibrosis commonly follows surgical procedures and contributes to FBS in multiple ways (Robertson, J. T. 1996, Georges, C. 2004). Peridural fibrosis involves the formation of scar tissue around the dura and nerve roots and causes compression of the nerve roots. In addition to the pain caused by compression of the nerve roots, everyday activities can lead to the production of phospholipase A_2. Phospholipase A2 hydrolyzes acyl bonds of phospholipids releasing arachidonic acid and lysophospholipids. Arachadonic acid is modified by cyclooxygenases yielding eicosanoids (including prostaglandins and leukotrienes) that serve as inflammatory mediators (Robertson, J. T. 1996). Both the direct effects of phospholipase A2 and the subsequent modifications of the arachidonic acid can contribute to the pain and inflammation in Failed Back Syndrome.

Treatment for failed back syndrome can involve further surgical procedures, spinal cord stimulation, pharmacological regimens and rehabilitation, and some or all of these methods can be used in conjunction to ameliorate the chronic pain.

Further surgical procedures are aimed at decompression of all neural elements, restoration of physiologic balance, and fixation of unstable elements. It may also involve the removal of prior instrumentation and incorporation of additional disc segments. Additional surgical procedures are often more complex and present a greater risk of side effects including spinal fluid leakage and wound infection, which can occur in 5-7% of patients.

In addition to corrective surgical procedures, patients may undergo implantation of a spinal cord stimulation (SCS) device. SCS is an invasive technique that involves implantation of a catheter and electrodes. The procedure is based on the theory that stimulation of a large, myelinated, somatosensory fibre will inhibit the transmission of pain signals to the brain (Metzlack, R. 1965). Once implanted, the device applies an electric current that overwhelms the dorsal horn neurons, preventing them from transmitting pain signals to the brain. One of the major difficulties of SCS therapy is the requirement of implanting the electrodes in such a way that they provide parathesia to the painful area without stimulating the dorsal roots. The efficacy of SCS therapy is variable. Kumar et al conducted a study of 60 patients who underwent SCS therapy. Only 15% of the patients were able to return to work due to decreased pain and drug intakes (Kumar, K. 2002). Kumar et al also estimated the cost of SCS therapy over five years to be around $29,000.

The two major components of pharmacological treatment are epidural injections of corticosteroids to treat inflammation and opioids such as morphine to relieve pain. While there is a risk of addiction in the long term use of narcotics,

the treatment is safe if properly monitored. The efficacy of the treatment is uncertain however. Carete *et al* completed a study to monitor the effect of corticosteroids and found that at three months the patients had not experienced a positive effect on pain, sensory deficits, or function. Another study (Devulder, J. 1999) examined 60 patients with fibrosis and found that after six months only 27% had experienced more than 50% pain relief. One of the difficulties associated with the injection of corticosteroids is proper placement of the needle. Injection as close as possible to the site of fibrosis is important due to the limited ability of the injected medium to diffuse through the epidural space. Correct location of the injection site is complicated by alterations in the anatomy of the lower back as a result of multiple surgical procedures (Anderson, V. C. 2000; Rowlingson, J. 1999). Fredman et al (Fredman, B. 1999) conducted a study in which they investigated the ability of fluoroscopy to assist in determining the correct position for injection, and found that even experienced doctors only found the correct injection site 47% of the time without fluoroscopy.

Opioids have been used to treat pain for many years (Conigliaro, D. A. 1996; Savage, S. R. 1999). Common opioids include morphine, codeine, oxycodone, and methadone. These compounds produce their analgesic effects by stimulation of mu-receptors in the brain, and have no upper limit to their ability to relieve pain, although patients undergoing long term treatment for chronic pain may develop a tolerance and need to have their dosages increased (Savage, S.R. 1999). Recent studies (Conigliaro, D. A. 1996; Savage, S. R. 1999) have shown that while the long term use of opioids can be safe, with a low incidence of

abuse and addiction, the possibility of developing dependence still exists. Jamison et al (Jamison, R. N. 1998) reported a study comparing the non-steroidal anti inflammatory drug (NSAID) naproxen with short acting oxycodone and a titrated dose of oxycodone and sustained release morphine. Patients underwent treatment for a year during which they were monitored weekly. While the mean pain level was lower for the two opioid groups, there was no overall change in the Health Status Questionnaire or Symptom Checklist 90 evaluations conducted at the beginning and end of the 12 month treatment period. One method for controlling side effects is intraspinal delivery of the opioid, instead of oral administration. Directly delivering morphine to the spine greatly lowers the amount of opioid necessary, and can prove useful in the cases where oral delivery would require dosages with unacceptable risks of side effects (Anderson, V. C. 2000). The direct delivery requires implantation of a morphine pump, which requires another invasive procedure, similar to the implantation of electrodes for SCS. A study by Anderson et al (Anderson, V. C. 1999) indicated that 50% of patients achieved at least a 25% reduction in pain after two years of treatment, but 20% of patients experienced adverse pharmacological events or device related complications. The five year cost of conventional pharmacologic treatment is estimated to be about $38,000 dollars (Kumar, K. 2002), more than that of spinal cord stimulation.

Both conventional pharmacology and SCS attempt to treat the pain without dealing with the underlying causes of the pain. While successive surgeries are concerned with remedying the underlying causes, they are far from successful,

and most patients diagnosed with FBS have already undergone multiple surgical procedures. The chance of structural abnormalities as well as further scar tissue formation is enhanced in patients that have undergone multiple surgeries, and the ability to combat fibrosis is paramount in improving treatment.

1.4. Wound Healing

1.4.1 Wound Healing Process

The critical function of cutaneous wound healing is the rapid closure of the defect to restore barrier function and maintain the physical integrity of the skin rather than the maintenance of complete form and function (O'Leary, R. 2002). This process results in the formation of cutaneous scars that are devoid of hair, sweat, sebaceous glands, and melanocytes. The wound healing process is generally categorized into three stages:

1. The inflammatory phase, lasting for 1-3 days post injury and characterized by a high density of cellular material,
2. The granulation phase, lasting for 2-6 days post injury, during which the matrix of granulation tissue is laid down, and
3. The remodelling phase, which lasts for 3-4 weeks or even longer. During this phase the granulation tissue is replaced by mature scar tissue, consisting mostly of type I collagen.

The inflammatory phase begins right after injury when activated platelets in the wound area aggregate and degranulate, releasing a variety of cytokines including platelet-derived growth factor (PDGF) and transforming growth factor β (TGF-β). Neutrophils and monocytes are attracted to the wound area by cytokines including TGF-β and monocyte chemoattractant 1. Neutrophils and monocytes cleanse the wound and surrounding tissue of foreign particles,

bacteria, and dead cellular material (Monaco, J. L. 2003; O'Leary, R. 2002; Park, J. E. 2004; Singer, A. J. 1999). Neutrophils arrive first but are replaced over the first two days by monocytes. These monocytes undergo differentiation into macrophages, and the macrophages serve a variety of functions. Macrophages and neutrophils employ surface receptors that enable them to recognize foreign material, bind to it, and subsequently engulf the foreign material, removing it from the wound area (Monaco, J. L. 2003). Upon ingestion by the inflammatory cells, bacteria and debris are digested by oxygen radicals and hydrolytic enzymes (Monaco, J. L. 2003). In addition to their role in phagocytosis, macrophages contribute to wound debridement via the production of reactive chemical species including nitric oxide, oxygen, and peroxide radicals (Park, J. E. 2004). While their role in wound debridement is important, the main contribution of macrophages to the wound healing process is the production of a wide variety of cytokines that are involved in subsequent phases of the wound healing process. The cytokines produced by macrophages include TGF-β, interleukin-1 (IL-1), insulin-like growth factor 1 (IGF-1), fibroblast growth factor 2 (FGF-2), and PDGF. These cytokines serve a variety of functions, and the same cytokine can have different effects depending on its concentration. TGF-β is known to be a macrophage chemoattractant in concentrations of 10^{-15} M, but is required in much higher concentrations (10^{-9} M) before it is capable of stimulating collagen synthesis in fibroblasts (Cohen, I. K. 1993). The different cytokines fulfill various roles in angiogenesis, stimulation of migration and proliferation of fibroblasts, wound vascularisation and extracellular-matrix synthesis and remodelling. In the

later stages of the inflammatory phase, eosinophils are recruited by macrophage-produced cytokines. Eosinophils are associated with fibrotic conditions, and produce a variety of matrix synthesis mediators (TGF-β, IL-4, IL-6, and TNF-β) in addition to anti-fibrotic agents (IL-2 and interferon-γ). Eosinophil sonicate has been shown to increase the rate of proliferation and collagen synthesis of fibroblasts, as well as the rate of contraction of the collagen matrix (Levi-Schaffer, 1999). At the end of this phase, a wound only has approximately 3% of the strength of that of unbroken skin.

The granulation phase begins two to six days post injury, and overlaps with the inflammatory phase. At the start of the granulation phase, the wound area is composed of a matrix rich in fibrin and fibronectin. During the granulation phase, this matrix is replaced by granulation tissue. Granulation tissue consists mostly of type I and III collagens, as well as other proteins such as thrombospondin I and secreted protein acidic rich in cysteine (SPARC). Collagen is produced by fibroblasts and is essential to the wound healing process. The production of collagen is mediated by TGF-β, PDGF, and epidermal growth factor (EGF). Aberrations in wound healing are often the result of improper collagen production or deposition. In patients with diabetes impaired activation of inflammatory cells results in limited collagen deposition and poor wound healing. While insufficient collagen deposition is a potential hazard in the wound healing process, it is also possible for the production and deposition of collagen to proceed long after the process should have slowed and stopped, resulting in the formation of hypertrophic scars and keloid formation. Proteoglycans are also an important

part of granulation tissue. They consist of a protein molecule linked to a variable number of glycosaminoglycans (GAGs). Proteoglycans bind proteins and alter their orientation, influencing their activity. Dermatan sulphate is an example of a proteoglycan that orients collagen in such a way as to facilitate the formation of collagen fibrils. One protein missing from the wound healing matrix is elastin. Elastin contributes to the elasticity of dermal tissue, and its absence in scar tissue causes increased stiffness of the scar. Once the granulation tissue has been synthesized the wound begins to contract. The contraction phase begins about a week after injury, and is characterized by the presence of myofibroblasts. Myofibroblasts are characterized by actin rich filaments, similar to that of smooth muscle cells, multi-lobed nuclei, and abundant rough endoplasmic reticulum. The contraction process likely requires stimulation by TGF-β and PDGF, attachment of fibroblasts to the collagen matrix, and crosslinks between individual collagen fibrils. At the end of the granulation phase, the strength of healing wound is about 20% that of unbroken skin.

The final phase of wound healing is the remodelling phase which begins about three weeks after the initial injury. It is during the remodelling phase that a wound regains much of the strength of unbroken tissue, although it will not ever be as strong as it was pre-injury, reaching a maximum strength of about 80% relative to unbroken tissue. In the remodelling phase, collagen synthesis is balanced by collagen breakdown, carried out by matrix metalloproteinases (MMPs). MMPs are a family of enzymes that break down extracellular matrices, and their functions are mediated by tissue inhibitors of metalloproteinases

(TIMPs). During the remodelling process, the scar tissue undergoes significant changes. By the end of the contraction phase, the cellular rich milieu of the early healing process has begun to be replaced by a fine array of collagen fibres. During the remodelling phase, the tissue becomes less cellular due to cytokine mediated apoptosis and these collagen fibres are replaced by thicker fibres, oriented parallel to skin stresses. In addition, the number of intra- and inter-fibrillar crosslinks is increased, greatly increasing the mechanical strength of the repaired wound. The ratio of type I collagen to type III continues to increase, and the amount of water and proteoglycans decrease.

1.5. Oxidative Stress and Inflammation

1.5.1. Diseases with an underlying component of oxidative stress and inflammation

Diseases with an underlying component of oxidative stress and inflammation become more common as a human being ages (Juurlink, B. H. J. 2001). Cells and tissues experience oxidative stress when the compounds that scavenge strong oxidizing species are unable to cope with an increased concentration of strong oxidizing species. Inflammation is a result of the body's response to foreign particles, including bacteria, virions, and foreign DNA, characterized by the production of pro-inflammatory cytokines (Brod, S. A. 2000). Three conditions that include oxidative stress and inflammation components affecting the human population, especially as they age, are autoimmunity, Alzheimer's disease, and atherosclerosis.

The term autoimmune disease encompasses a variety of different disorders, including multiple sclerosis (MS), type I diabetes, and rheumatoid arthritis (RA) (Brod, S. A. 2001).

Multiple Sclerosis is a condition in which the immune system attacks and destroys the oligodendrocytes of the central nervous system (CNS) (Rosati, G. 2001). Oligodendrocytes are responsible for producing and maintaining the myelin sheath, a fatty layer that surrounds the neurons. Demylenation prevents the neurons in the brain from properly transmitting their signals, and the disease

progresses to varying stages of physical and cognitive disability, depending on the individual patient.

Type I diabetes results from the destruction of the insulin producing β islet cells in the pancreas by inflammatory cells (Rother, K. I. 2007). There is no known cure for type I diabetes, and those suffering from the disease must receive regular insulin injections to make up for the lack of endogenously produced insulin.

Rheumatoid arthritis involves the inflammation of tissue, primarily in the joints, although it can also occur in organs such as the lungs and skin (Majithia, V. 2007). The joints of patients with RA become swollen, and stiffness can hinder or prevent function. Extra-articular arthritis also occurs in 15% of patients (Turesson, C. 2003). The most commonly affected joints are those of the hands, feet, and spine, although larger joints such as the shoulder and hip can also be affected. There is no known cure for RA, although many different treatments are available. The two main foci for treatment are the prevention of further loss of function, and relief of pain caused by the inflammation (Hasler, P. 2006; O'Dell, J. 2004). Disease modifying anti rheumatic drugs (DMARDs), including dimethotrexate and sulfalazine, inhibit the expression of t cell activation and expression. Dimethotrexate (DMX) is favoured by pharmacologists because of its relatively high compatibility with other anti-rheumatoid medications. However, DMX is used in higher concentrations as an anti-cancer drug, and at higher concentrations inhibits the production of folic acid, required for the synthesis of new DNA.

DMARDs are usually combined with anti-inflammatories and analgesics such as NSAIDs and acetaminophen or opiates.

Alzheimer's Disease (AD) is the most common cause of dementia in humans (Juurlink, B. H. J. 2001, Brod, S. A. 2000). AD has two forms, most commonly affecting the elderly (> 65 years of age), although an early onset form is also possible. AD is characterized by the presence of plaques in the brain, made up of aggregates of improperly cleaved β-amyloid fragments, and neurofibrillary tangles. There are several indicators of increased oxidative stress in patients exhibiting AD. The presence of advanced glycation end products (AGEs), many of which are 4-hydroxynonenal, indicate significant lipid peroxidation. Similarly, the intake of vitamin E, which has been shown to inhibit lipid peroxidation, has proven to slow the progression of AD. The use of NSAIDs has been shown to retard the progression of AD. It is hypothesized that the mechanism involves the inhibition of the pro-inflammatory enzyme cyclo-oxygenase-2 (COX2) whose upregulation in AD is mediated by the transcription complex factor nuclear factor kappa B (NFκB).

Atherosclerosis is characterized by chronic inflammation of the arterial walls (Glagov, S. 1987; Kunitomo, M. 2007). There are many factors that predispose individuals to atherogenesis, the majority of which involve increasing the oxidative stress on the endothelium (Juurlink, B. H. J. 2001). Atherosclerosis begins with the oxidation of low density lipoproteins (LDLs) by hypochlorous acid Macrophages are recruited to the site to clear out the oxidized LDLs, but are unable to digest them. The macrophages eventually burst, depositing more of the

oxidized LDL on the arterial wall, which in turn causes the body to recruit more macrophages, establishing a negative feedback loop. The build up of arterial plaques results in a narrowing of the arteries, reducing blood flow to the organs. In addition, the soft plaques can rupture, leading to the formation of a thrombosis, a blood clot that can block the flow of blood to the tissue. If the clot is not removed and blood flow is not restored, tissue necrosis can occur in less than five minutes. The most well known type of thrombosis occurs in the heart, leading to myocardial infarction, commonly known as a heart attack.

Oxidative stress and inflammation contribute to numerous diseases affecting humankind. The treatments for most of these afflictions involve treating the symptoms of the disease, and few have a known cure. Of particular concern is that many of these conditions are more likely to affect the elderly. As medical care and living conditions improve, more people can expect to live longer lives and experience an increased risk of acquiring these diseases.

1.5.2. Mechanisms of Oxidative Stress

Oxidative stress is the result of an imbalance between the level of oxidizing species and species that scavenge the strong oxidizers (Juurlink, B. H. J. 2001). The production and scavenging of oxidizing species involve many interconnected pathways. Three percent of oxygen is incompletely reduced during respiration, and gives rise to superoxide ($O_2^{\cdot -}$) anions (Fridovich, I. 1986). In addition to being strong oxidizing species in their own right, superoxide anions can combine to form singlet oxygen, or react with nitric oxide to create peroxynitrous acid (Juurlink, B. H. J). The peroxynitrous acid can disassociate to yield hydroxyl radicals and nitrogen dioxide radicals. Superoxide anions can be scavenged by an enzyme (superoxide dismutase, SOD) to form molecular oxygen, but this creates hydrogen peroxide, a strong oxidant on its own. Hydrogen peroxide can be scavenged by glutathione peroxidise (GPx) which requires glutathione as an electron donor. Hydrogen peroxide can also give rise to hydroxyl radicals if transition metal ions are present to serve as the electron donor. Hydroxyl radicals, whether they are the result of hydrogen peroxide or peroxynitrous radicals, can react with lipids to produce lipid radicals which initiate a chain reaction by forming lipid peroxyl radical. These lipid peroxyl radicals can react with another lipid to form another lipid radical, continuing the chain.

Increasing the amount of glutathione present in the cell would allow for the scavenging of more oxidizing species. Glutathione is a tripeptide consisting of cysteine, glutamate, and glycine. Glutathione is unusual in that the peptide

linkage of the cysteine and glutamate residues occurs between the amide group of the cysteine peptide and the side chain of the glutamate peptide.

In addition to the direct scavenging of oxidizing species, it is also possible to decrease the concentration of transition metal ions that create harmful oxidizing radicals. Compounds that serve to chelate and remove these metal ions from the cellular milieu could provide benefits in the form of reduced oxidative stress.

1.5.3. Glutathione and L-2-oxothiazolidine-4-carboxylate

Glutathione (GSH) is a tripeptide consisting of cysteine, glutamate, and glycine (Anderson, M. E. 1998; Kamencic, H. 2001; Zhang, Z. 2002). Glutathione contains an unusual linkage in that the cysteine and glutamate residues are bonded together through the amino group of the glutamate side chain. This linkage prevents hydrolysis of glutathione from by most peptidases. The formation of glutathione from its component peptides is a two step process:

$$\text{L-Glu + L-Cys + ATP} \rightleftharpoons \text{L-}\gamma\text{-Glu --- L-Cys + ADP + Pi} \qquad (1)$$

$$\text{L-}\gamma\text{-Glu --- L-Cys + Gly + ATP} \rightleftharpoons \text{GSH + ADP + Pi} \qquad (2)$$

The rate limiting step in this two step procedure is the incorporation of cysteine (1). Thus, increasing the amount of intracellular cysteine should enable the cell to produce greater quantities of cysteine more rapidly. The cysteine produced is then used by cells to produce GSH. Attempts to increase GSH levels by direct administration of GSH are unsuccessful. Cells do not take up GSH in significant amounts, and the GSH is degraded extracellularly.

L-2-oxothiazolidine-4-carboxylic acid (OTC) (Figure 3a) is a cysteine precursor. It is an analog of 5-oxoproline, and can be a substrate for 5-oxoprolinase. It is believed that 5-oxoprolinase reacts with the OTC to yield S-carboxycysteine which is hydrolyzed to cysteine and carbon dioxide. OTC treatment has been shown to promote better healing by decreasing oxidative stress and inflammation secondary to spinal cord injuries (Kamencic 2001), and

has been tested in clinical studies for patients with amyotrophic lateral sclerosis (Cudkowicz 1999), and those infected with HIV (Barditch-Crovo 1998).

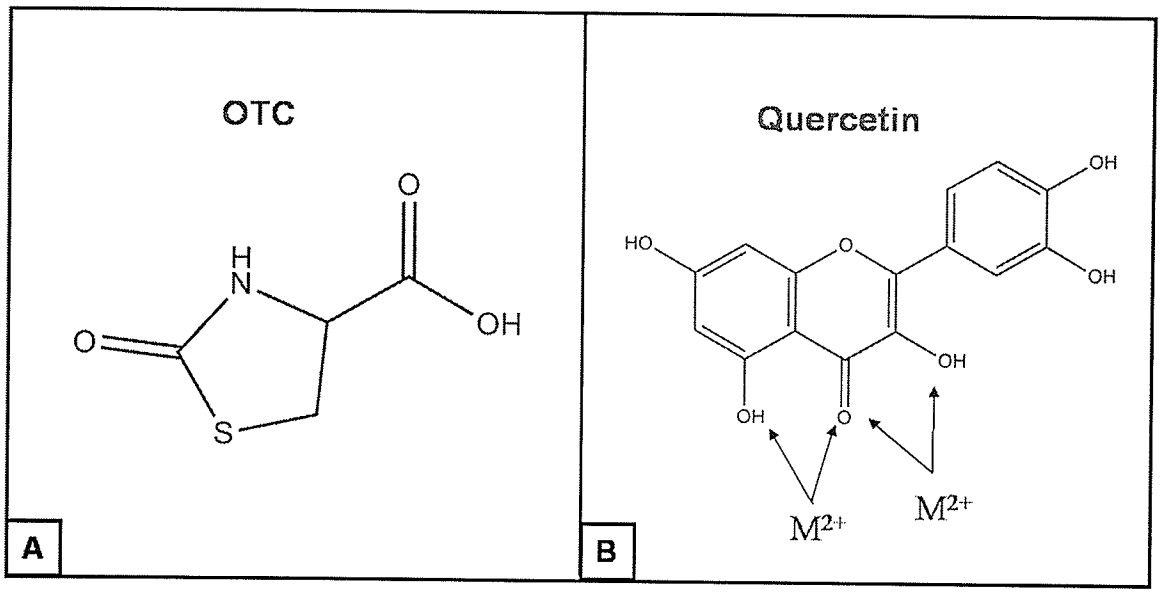

Figure 3: Structures of treatment molecules.
OTC (A) undergoes a ring opening reaction to yield the amino acid cysteine. Arrows in B indicate potential sites for chelation of oxidizing metal ions.

1.5.4. Quercetin

Quercetin (Figure 3b) is a polyphenolic compound belonging to a group of related compounds known as flavonoids (Erlund, I. 2004). To date, some 6000 different flavonoids are known, although the number of bio-active compounds is significantly lower. Flavonoids are potent anti-oxidants, but can contribute beneficial health affects through a number of different mechanisms.

Quercetin is found in a variety of fruits and vegetables including apples and onions, as well as beverages such as wine and tea (Erlund, I. 2004). The highest concentration of quercetin is found in onions, but due to the low amounts of onions consumed, the largest percentage of dietary quercetin comes from apples, tea and wine.

Quercetin has been shown to have antioxidative, anticarcinogenic, anti-inflammatory, anti-aggregatory, and vasodilating effects (Erlund, I. 2004; Myhrstad, M. C. W. 2002; Schultke, E. 2003). These effects can be the result of many different mechanisms including metal chelation (antioxidative), scavenging of radicals (antioxidative), enzyme inhibition (antioxidative, anticarcinogenic) and/or effects on gene expression (anticarcinogenic, anti-inflammatory).

Flavonoids such as quercetin serve to upregulate phase 2 enzymes in the body. Phase 2 enzymes serve to remove harmful reactive oxygen species, often by forming glutathial-xenobiotic adducts (Juurlink, B. H. J. 2001).

1.6. Infrared Spectroscopy

1.6.1 Introduction to Infrared Spectroscopy

Spectroscopy is the production, measurement, and interpretation of electromagnetic spectra caused by the interaction of matter and radiation, as a function of energy. The molecular information present in a spectrum depends on the energy of radiation used to produce the spectrum. Infrared (IR) spectroscopy provides information on the vibrational and rotational motion of molecules. Energies in infrared spectroscopy are conventionally expressed in units of wavenumbers, with units of cm^{-1}. The equation for energy (1) is rewritten in terms of $\bar{v}$ (2), where $\bar{v}$ is the inverse of the wavelength of radiation (Atkins, P. W. 1998).

$$E = \frac{hc}{\lambda} \quad (1)$$

$$E = hc\bar{v} \quad (2)$$

$$\bar{v} = \frac{1}{\lambda}$$

Infrared spectroscopy is generally divided into three different subgroups: far infrared spectroscopy, mid infrared spectroscopy, and near infrared spectroscopy. Far IR (10-400 cm^{-1}) spectroscopy, so called because it is far from the visible portion of the spectrum, is lowest in energy and primarily used to obtain information on the pure rotational modes of gas phase molecules. Mid IR (800-4000 cm^{-1}) spectroscopy provides vibrational and rotational information on a wide variety of important compounds: most organics (including proteins, lipids, and

sugars), small molecules (carbon dioxide, water, etc). In the near infrared portion (4000-14000 cm^{-1}) of the spectrum, the radiation has sufficient energy to excite overtone vibrations. This thesis will focus on the mid-infrared portion of the spectrum, where the majority of the information arises from bond vibrations of the molecules.

Each of the atoms in a molecule has three degrees of freedom. The individual atoms can move along the x, y, and z axes in three dimensional space. Depending on the direction of motion of individual atoms, the molecule can undergo translation, rotation, or vibration. Translation of a molecule requires the molecule to move through space, and results in a change in the centre of mass of the molecule, but no change in inter-atomic distance or orientation of the atoms with respect to each other. The rotation of a molecule about an axis leads to a change in orientation of the molecule, but does not result in a change in the centre of mass or inter-atomic distances.

Vibration of a molecule is characterized by a change in the inter-atomic distances, but there is no change in the molecule's centre of mass or orientation. Since each atom has three degrees of freedom, the total number of degrees of freedom for a molecule is 3*N, where N is the number of atoms in the molecule. The number of vibrations for a given molecule is thus 3*N minus the number of translational and rotational modes. For a simple linear molecule like HCl, rotation (2) and translation (3) account for five of the degrees of freedom. If the hydrogen and chlorine atoms both move in the same direction, along the same axis, there will be no change in the H-Cl bond length, and no change in the orientation of the

molecule. The entire molecule will have translated itself along the axis of movement. Since the atoms can move along each of the three spatial axes, translation accounts for three of the degrees of freedom. If the hydrogen and chlorine atoms move in opposite directions along an axis other than that of the H-Cl bond, the molecule will rotate about that axis. Rotation thus accounts for two more degrees of freedom that the molecule possesses. This leaves only one mode of vibration, caused by the movement of the two atoms in opposite directions along the axis of the bond, resulting in a stretching of the H-Cl bond. The case is similar for a non linear molecule like H_2O, except there is an additional rotational mode. This leaves three degrees of freedom for the molecule, corresponding to the three vibrational modes of water. The three vibrational modes of water (Figure 4) are:

1) A symmetric stretch of the O-H bonds, where the bonds stretch and contract together,
2) An asymmetric stretch where one of the O-H bonds stretches while the other contracts,
3) And a bending, or scissoring vibration, where the two hydrogen atoms move towards each other, without breaking the plane of the molecule.

Figure 5 is a spectrum of air, showing the infrared active vibrations of CO_2 and H_2O.

The number of vibrations for a linear molecule is given by the formula 3*N-5, where N is the number of atoms in the molecule, while a non linear molecule,

has 3*N-6 vibrations, to account for the extra rotational mode. The infrared spectrum can be pretty simple for small molecules, given the relatively small number of vibrations. A molecule like water only has 3*(3) – 6 = 3 vibrations, but for large molecules, especially proteins like collagen, the situation is more complicated. A collagen molecule is composed of three individual chains, held together by crosslinks and hydrogen bonds. Each of the individual chains has about 1000 amino acids. The simplest amino acid, glycine, has 10 atoms in it. This means that a collagen molecule is going to have more than 30,000 modes of vibration, potentially resulting in a very complicated infrared spectrum.

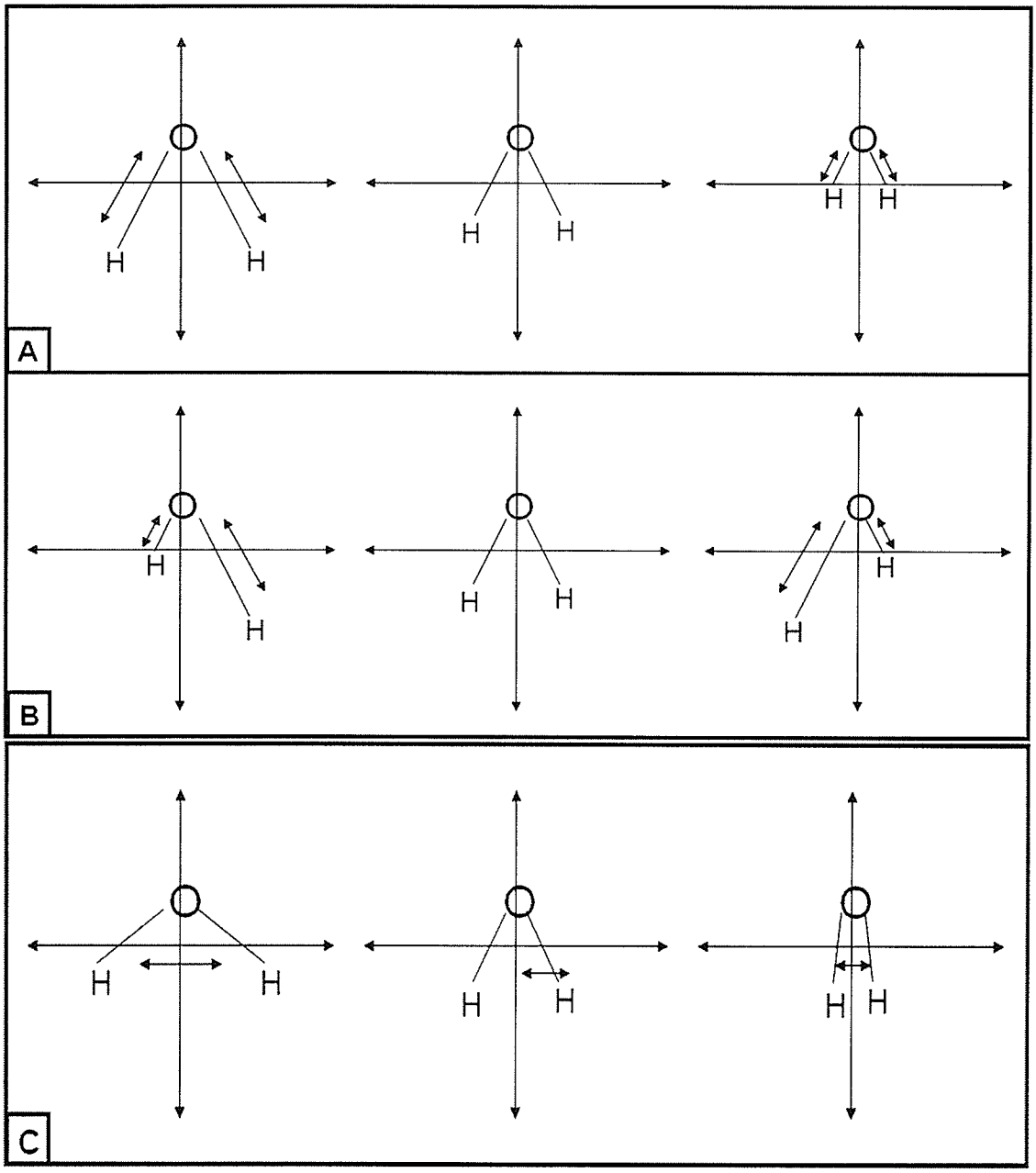

Figure 4: The three vibrational modes of water:

A. Symmetric stretching of the O-H bonds,

B. Asymmetric stretching of O-H bonds,

C. Scissoring motion.

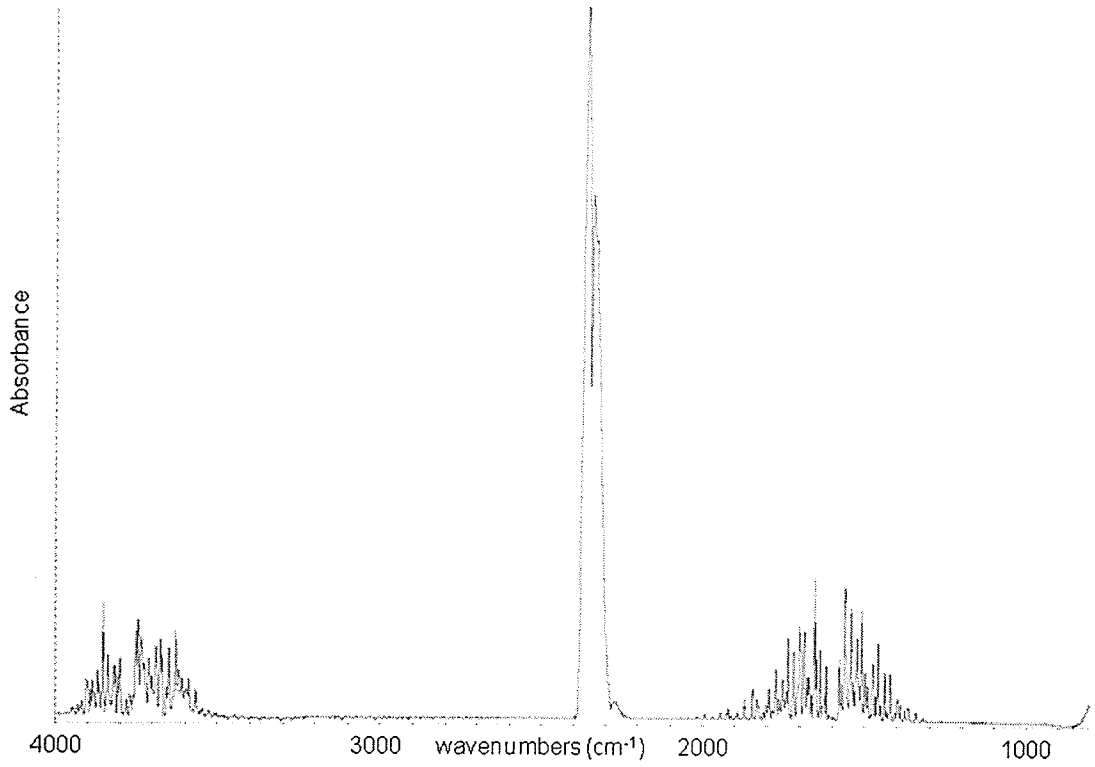

Figure 5: Infrared Spectrum of gas phase CO_2 and water. Intense band at 2200 cm^{-1} is the asymmetric stretch of CO_2. The bending vibration of H_2O is shown around 1600 cm^{-1}, and the high frequency bands at 3300 cm^{-1} are the stretching modes of H_2O.

An infrared spectrum is a two dimensional plot showing the absorbance of light as a function of energy. A sample is irradiated by infrared light, and some of this light is absorbed to excite transitions from the ground vibrational state to an excited vibrational state. A detector records the intensity of light that has passed through the sample, and compares this intensity with a background reading of the light's intensity without having passed through a sample. The absorbance is defined as:

$$A = -\log\left(\frac{I}{I_0}\right)$$

Where I is the intensity of light that has passed through a sample and I_0 is the intensity of the incident light. The absorption of infrared light by a molecule is a quantized process. This means that only photons whose energy precisely matches that of a molecular vibration will be absorbed, and the vibration will be represented by a peak in the infrared spectrum at the frequency of absorption.

However, not all molecular vibrations will produce a band in the infrared spectrum. In order for a vibration to absorb infrared light, there must be a change in the permanent dipole moment from the ground vibrational state to the excited vibrational state. This can be proven by examining the transition moment for infrared absorption:

$$R = \left\langle X_i \middle| (r - r_e) * \left(\frac{d\mu}{dr}\right) \middle| X_i \right\rangle$$

X_i is the wavefunction that represents the ground vibrational state, X_j is the wavefunction that represents the excited vibrational state, and $d\mu/dr$ is the change in the dipole moment. Since $\langle X_i | X_j \rangle = 0$, there must be a change in the dipole moment for a vibration to be IR active. As an example, the symmetric stretching mode of CO_2, where both C=O bonds are expanding or contracting in unison is predicted to show up at a frequency of 1340 cm^{-1}. The ground vibrational state, with the molecule at rest, has no permanent dipole moment, so in order for the vibration to be IR active the excited vibrational state must have a dipole moment. The symmetric stretching motion will alter the individual dipole moments of C=O bonds from the rest state, but they will still be of equal intensity with respect to each other, and opposite in direction, meaning that the stretched molecule will have no permanent dipole moment, equivalent to the molecule at rest. This means that there is no absorption of IR light at the frequency of this vibration, and no corresponding band in the infrared spectrum. The vibration is said to be infrared inactive. The requirement for a change in the dipole moment between initial and final states is known as a *selection rule*, a requirement for a transition to occur with a nonzero probability. In addition to the absence of peaks corresponding to IR inactive vibrations, there may be fewer peaks in a spectrum than predicted due to degenerate vibrations. Degenerate vibrations are vibrations that occur at the same frequency. Raman spectroscopy, which has a different selection rule than infrared spectroscopy, can provide complementary data on molecular vibrations. The aforementioned symmetric stretch of CO_2 is raman active, even though it's not IR active.

1.6.2 Instrumentation – Grating Monochromators and Interferometers

Prior to the development of modern Fourier Transform infrared (FTIR) spectrometers, a conventional spectrometer employed a monochromator with either a prism or diffraction grating to produce an infrared peak.

In such an instrument, light from a source passes through an entrance slit and impinges upon a collimating mirror (Griffiths, P. R. 1975) (Figure 6). The collimated light is projected onto a prism which disperses the light, made up of various energies, into its constituent parts. Photons of different energies will be focused to different positions depending on the wavelength of the photons. The prism can be rotated, changing the wavelength of light that impinges upon the exit slit, allowing for the collection of bands representing absorptions of different energies.

The amount of energy that reaches the detector is a function of the exit slit width (Griffiths, P. R. 1975). The exit slit width also determines the spectral resolution of the device. If the entrance slit allows light of 400-4000 cm^{-1} to pass through, and the exit slit is 8 cm^{-1} wide, then the spectral resolution is 16 cm^{-1} (see Figure 7 for spectra recorded at different resolutions), but only about 0.2% of the light from the source reaches the detector (8/3600). This lack of light means that in order to achieve a reasonable signal to noise ratio, data must be accumulated over a long period of time at each point, and a total of 450 data points over the 3600 cm^{-1} span must be collected.

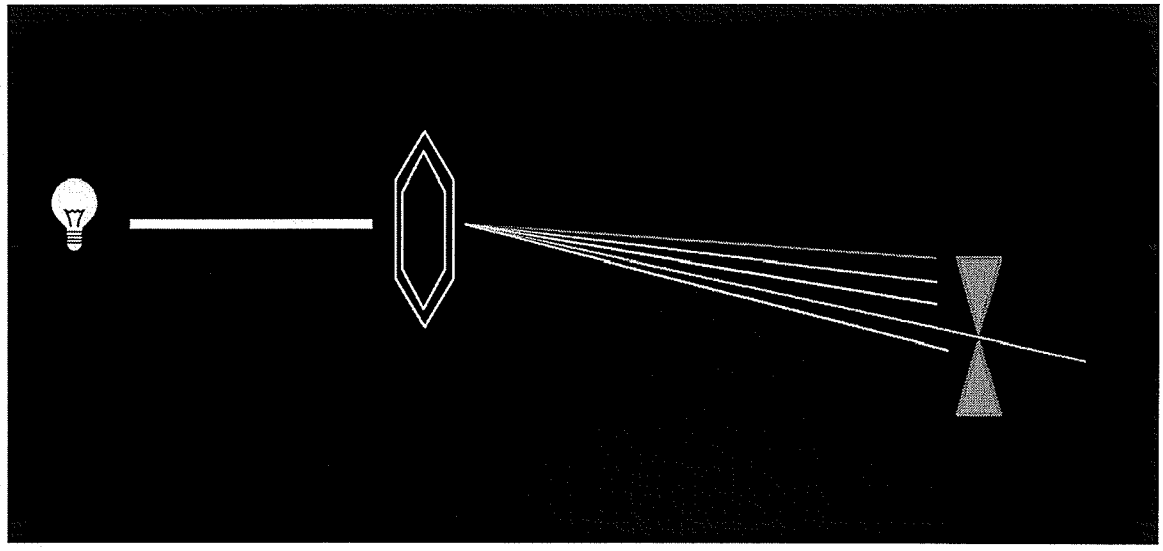

Figure 6: Diffraction monochromator.

The incident light is separated into its component wavelengths by the prism, and only one of these wavelengths can pass through the exit slit at a time. The prism can be rotated so that the particular wavelength of light passing through the exit slit can be changed.

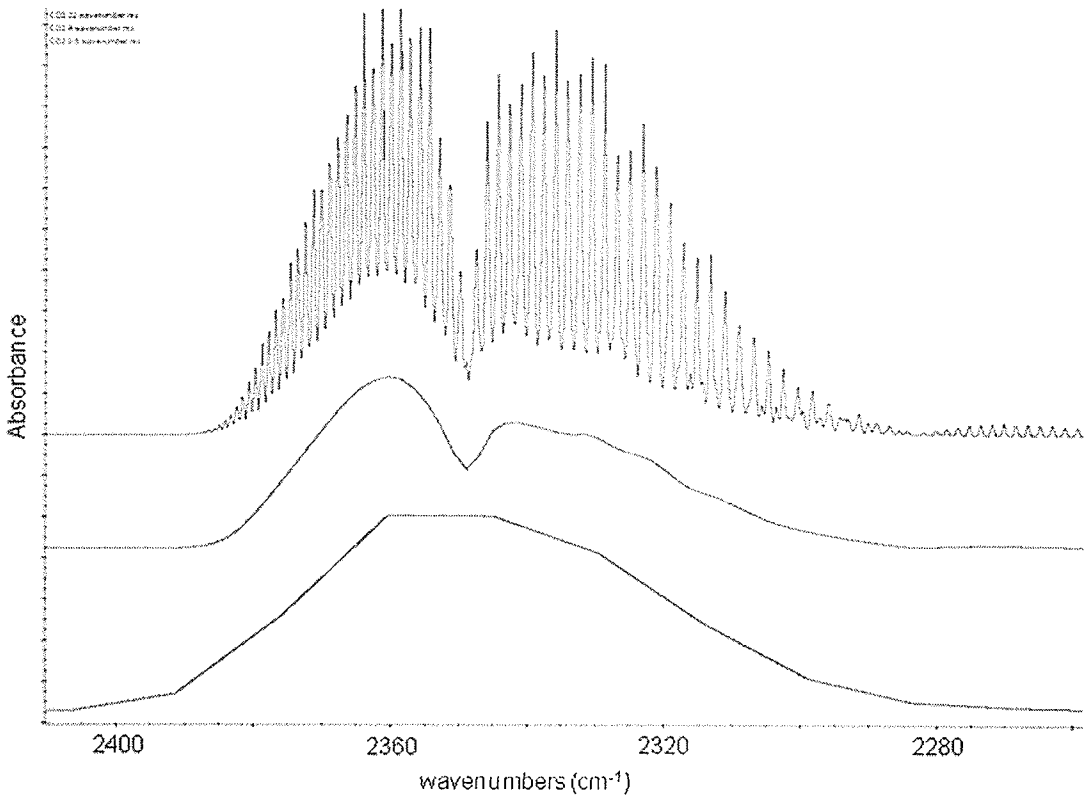

Figure 7: Asymmetric stretching of CO_2, collected at different spectral resolutions.
Red: 0.5 cm^{-1}, purple: 4 cm^{-1}, and Blue: 32 cm^{-1}.

The Michelson interferometer (Figure 8), named for its creator, addresses the problem of long acquisition time necessary to achieve an acceptable signal to noise ratio (Griffiths, P. R. 1975). The Michelson interferometer consists of a beamsplitter that separates the incident light into two different beams, perpendicular to each other. One of the beams impinges upon a fixed mirror, while the other strikes a moving mirror. The two beams are then recombined, and the difference in their intensities can be determined as a function of the different distances that the individual beams have traversed. Lord Rayleigh recognized the relationship between the interferogram and the spectrum of the light that gave rise to the interferogram. By applying a mathematical operation known as a Fourier Transform, named for its discoverer, Joseph Fourier, an interferogram could be converted into a spectrum. The first numerical Fourier transform of an interferogram into a spectrum was done in 1949 by Fellgett. One of the principle advantages to using an interferometer instead of a monochromator is that spectral data can be collected for a broad range of frequencies, all at one time. This advantage is known as Fellgett's advantage, and greatly reduces the time necessary to acquire an infrared spectrum.

Acquisition of infrared spectra via an interferometer instead of a monochromator was limited by the lack of computing power in the 1950's and 60's necessary to perform the calculations for the Fourier transform. While calculating the Fourier Transform of a spectrum of medium resolution, with only 1,000 data points, might take just a few minutes, high resolution experiments with 10,000 data points would require calculation times of several hours, negating the

time gained by Felgett's advantage. In the mid 1960's two developments increased the feasibility of Fourier transform spectroscopy. The first was the application of the Fast Fourier Transform algorithm by Cooley and Tukey (Cooley, J. W. 1965). This method allowed for the transformation of spectra with high resolution in only a few minutes, while low to mid resolution spectra could be computed in a few seconds. The second development was less specific, and has affected many different fields. The development of more sophisticated solid-state devices and integrated computers increased computational power available to scientists across many disciplines, enabling them to conduct experiments and analyze data much more efficiently. Today FTIR spectrometers with dedicated computers are commercially available from several companies and our used for a variety of purposes.

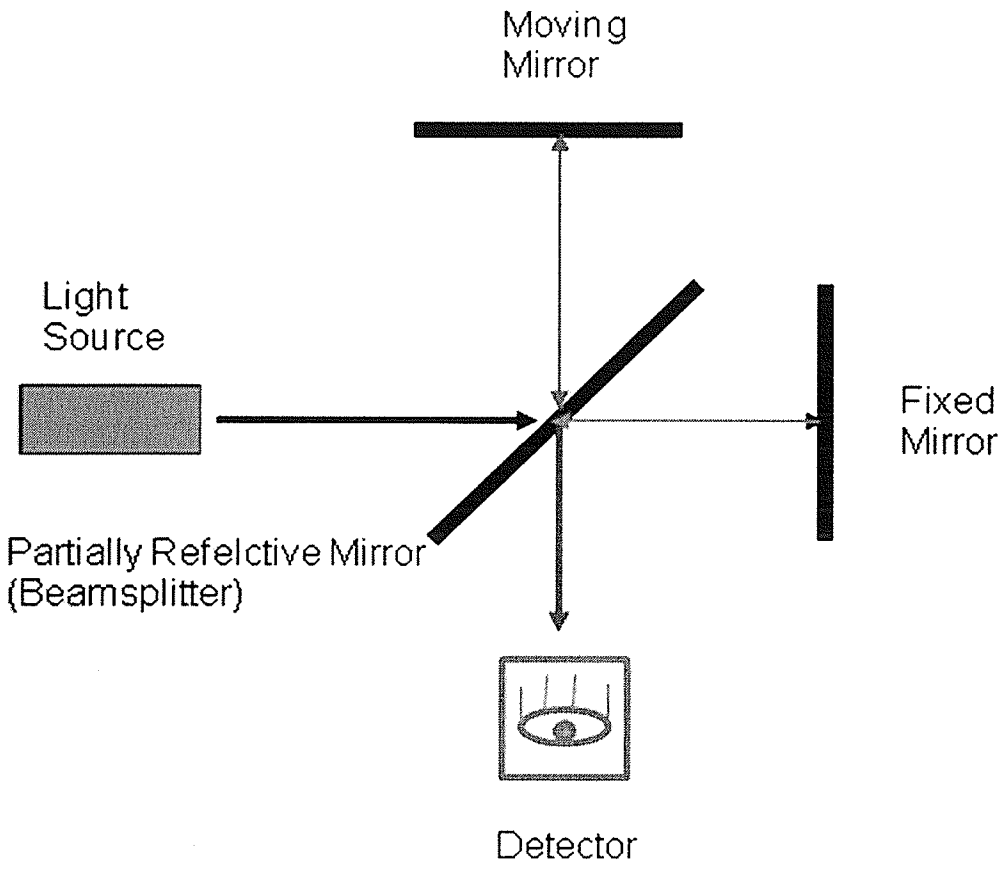

Figure 8: Schematic representation of the Michelson interferometer. Light from a source is reflected to a moving mirror or transmitted to a fixed mirror. The light reflects off the two mirrors and recombines before arriving at the detector. Interference after reflection from the two mirrors can be either constructive or destructive depending on the difference between the path lengths set by the moving mirror.

1.6.3 Infrared Sources – Globar vs Synchrotron

Conventional benchtop FTIR spectrometers employ a ceramic Globar that, when heated, functions as a blackbody emitter (Smith, T. I. 2002). A Globar source has several advantages. The Globar is cheap and relatively easy to manufacture, and under most ordinary conditions of bulk sample analysis provides more than enough power to obtain spectra with adequate signal to noise ratios in an appropriate amount of time. However, when examining spectra via microspectroscopic techniques, the spatial resolution desired increases such that the aperture must be narrowed to the point where the amount of light that impacts the sample is insufficient to acquire spectra with acceptable signal to noise ratios without impractically long accumulation times.

The brightness of the light source is given by the power per unit area. The total power emitted by the Globar source is very high, but the brightness is quite low. As a result, a large area is necessary for enough light to reach the detector (Figure 9a). To achieve the desired spatial resolution for microspectroscopic analysis, a different source must be found.

In the 1950's and 60's, scientists began to use synchrotron radiation for spectroscopic experiments (Burattini, E. E. 1991). In a synchrotron, electrons are accelerated to relativistic speeds (99.9999% the speed of light), and placed into a storage ring where they orbit. The storage ring is not a perfect circle. The ring is composed of long straight stretches interrupted by curved bending magnets and undulators. When the electrons approach the curved sections of the ring they

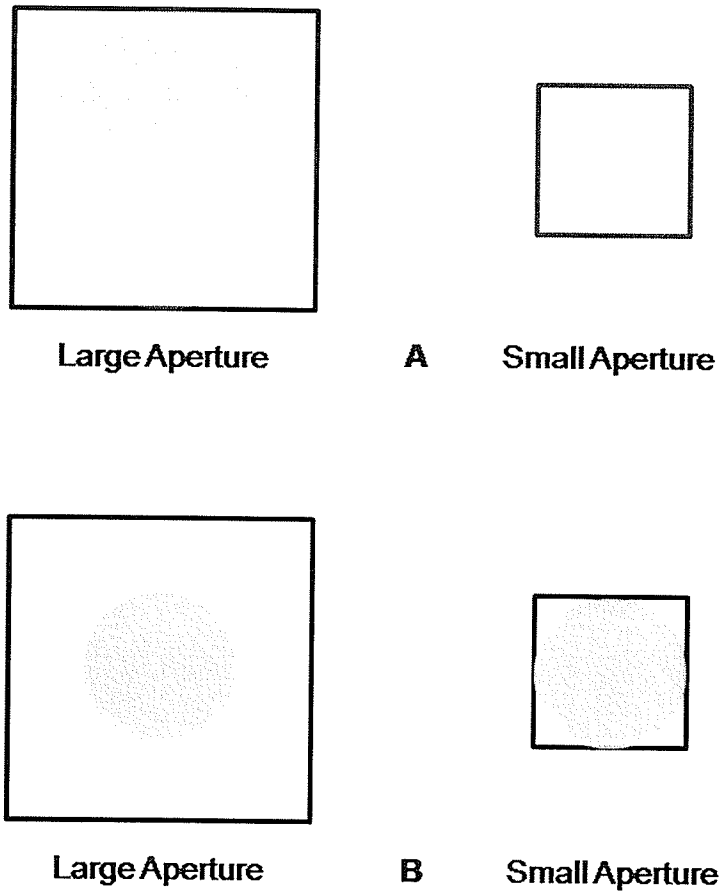

Figure 9: Power and Brightness.
Representation of total intensity of light passing through an aperture for globar (a) and synchrotron sources (b).

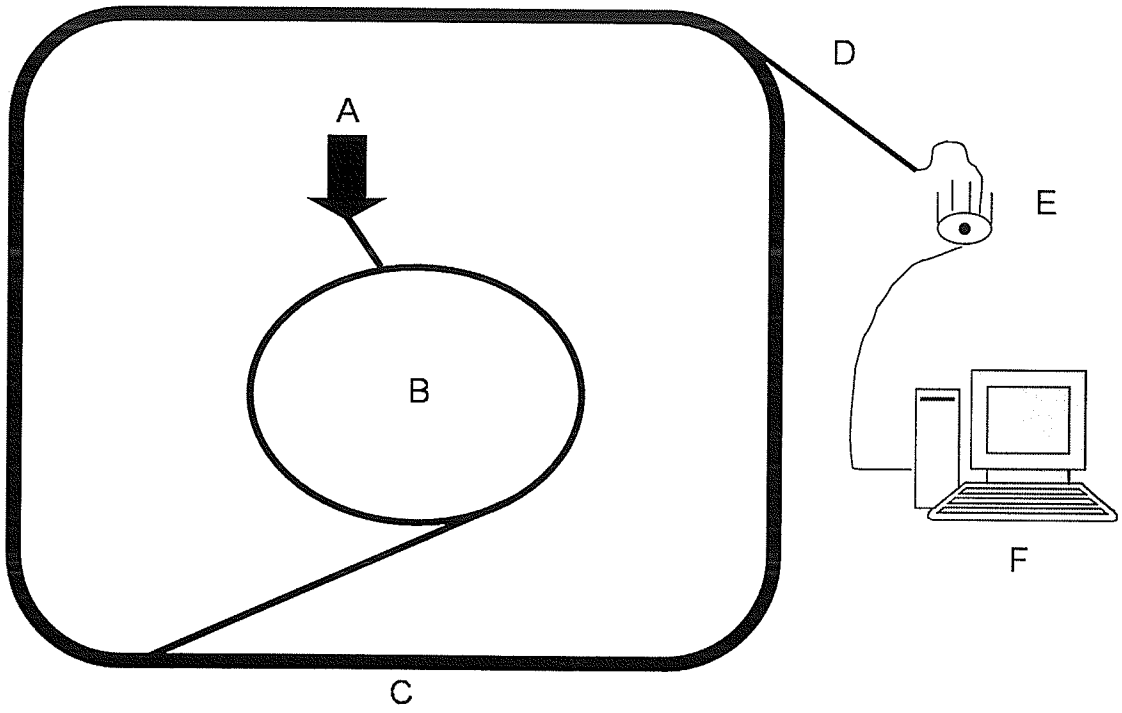

Figure 10: Diagram of a synchrotron including electron source (A), booster ring (B), storage ring (C), beamline (D), IR microscope with detector (E) and workstation (F).

undergo a change in momentum, and this causes them to give off energy in the form of photons. These photons can be used as a broadband source for a wide variety of experiments from the x-ray and UV energy range to longer wavelengths suitable for infrared analyses. In addition to spanning a broad range of frequencies in the electromagnetic spectrum, synchrotron radiation is very bright. Brightness is a measurement of power per unit area, and the brightness of the synchrotron is three orders of magnitude higher than a conventional globar. Both the synchrotron beam and the globar function as point sources. As point sources the light they emit expands, but angle of the light from the synchrotron is much smaller than the angle of the light emitted by the globar. Since the width of the light beam is narrower for the synchrotron, it is more easily focused, contributing to the higher brightness of the synchrotron. This concentration of light in a small area (Figure 9B) provides for a source that is approximately 1000 times brighter than a conventional globar source, allowing for spectra to be collected at diffraction limited spatial resolutions in less than a minute. This increase in power yields tremendous increases in signal to noise ratios, especially at higher spatial resolutions, over spectra acquired with a globar. Synchrotron sources have been shown to increase S/N ratios by a factor of 20 (Carr, G. L. 1995). Since S/N ratio increases as the square root of the number of scans, increasing the S/N ratio by a factor of 20 means that data collection time can be decreased by a factor of 400 with no loss in spectral quality. Simply put, a spectrum that would take an hour to collect with a Globar source can be collected at a synchrotron in under 10 seconds.

1.6.4 The Mid Infrared Spectrum

The mid infrared spectrum is a very information rich portion of the spectrum. Mid infrared light is high enough in energy to excite rotational and vibrational modes of molecules, but not high enough to cause changes in electronic structure. Spectra can be collected from compounds in solid, liquid or gas phases. Solid phase spectra can be collected in four different forms.

First, an analyte can be ground together with dry KBr and pressed into a pellet. KBr is transparent to IR light, and the resulting spectrum will just contain spectral features arising from the compound of interest. Samples can also be prepared as a Nujol mull, where the compound of interest is mixed with a mixture of hydrocarbons. This method is used primarily in organic chemistry, but suffers from the fact that information arising from regions of the spectrum involving carbon and hydrogen modes will be lost as the Nujol will absorb in these areas. Third, samples can be prepared as a thin film. The sample is dissolved in a suitable solvent and applied to a window that is transparent to IR light. The solvent is left to evaporate and a thin film is left behind. This method is useful for large molecules, proteins, and sugars. Finally, tissue sections can be prepared for infrared spectroscopic analysis by freezing them in liquid nitrogen immediately after harvesting, then sectioning with a cryotome. Thin sections (5-10 microns) are placed on suitable IR substrates and can then be examined via infrared microscopy. As most samples involved in this work are tissue sections, this form of sample preparation will be focused on in discussing the infrared spectra of the constituent components of these samples.

1.6.5 Infrared Spectra of Collagens

The infrared spectrum of collagen was first recorded in the 1940's. Figure 11 shows a spectrum of type I collagen with the regions of interest to our study: Sugars and phosphates (A), collagen fingerprint (B), Amide I (C) and C-H stretch region (D). The two most intense peaks are the Amide I and Amide II bands, at 1670 cm^{-1} and 1550 cm^{-1}, respectively. The Amide I band arises from the stretching of the carbonyl bonds of the peptide backbone, and its position can give information on the secondary structure of the protein of interest (Lazarev, Y. A. 1985). The triple helical nature of collagen results in an asymmetrical band whose maximum is at approximately 1670 cm^{-1}, with a lower frequency shoulder around 1655 cm^{-1}. The Amide II band is a combination of C-N stretching of the carbon backbone, along with an N-H bending motion. While all protein spectra will contain Amide I and II absorptions, collagen has a unique set of bands centred on the Amide III vibration at 1240 cm^{-1}. This quartet of bands at 1204, 1240, 1284, and 1338 cm^{-1} is characteristic of collagen, although the specific bond vibrations that contribute to this profile are not well characterized.

In addition to the bands arising from vibrations of the Amide groups, collagen also contains spectral features arising from C-O-C ring vibrations and C-H stretching vibrations. The profile for pure collagen between 1000 and 1100 cm^{-1} shows two more intense bands at approximately 1080 cm^{-1} and 1030 cm^{-1}, sitting on top of broad band. The 1080 and 1240 cm^{-1} bands in collagen overlap with the symmetric and asymmetric stretching vibrations of phosphate groups, present in lipid bilayers for example, and one most be careful in choosing which

bands to use for identifying the amount of collagen present in a sample. The profile for the C-H stretching region (2850-3000 cm^{-1}) is also unusual (Figure 12). Normally this region is characterized by two sets of bands, the symmetric stretches of CH_2 and CH_3 groups, and the asymmetric stretches of CH_2 and CH_3 groups. In collagen, the usual pair of doublets is replaced with a series of three peaks, with the symmetric CH_2 band virtually disappearing.

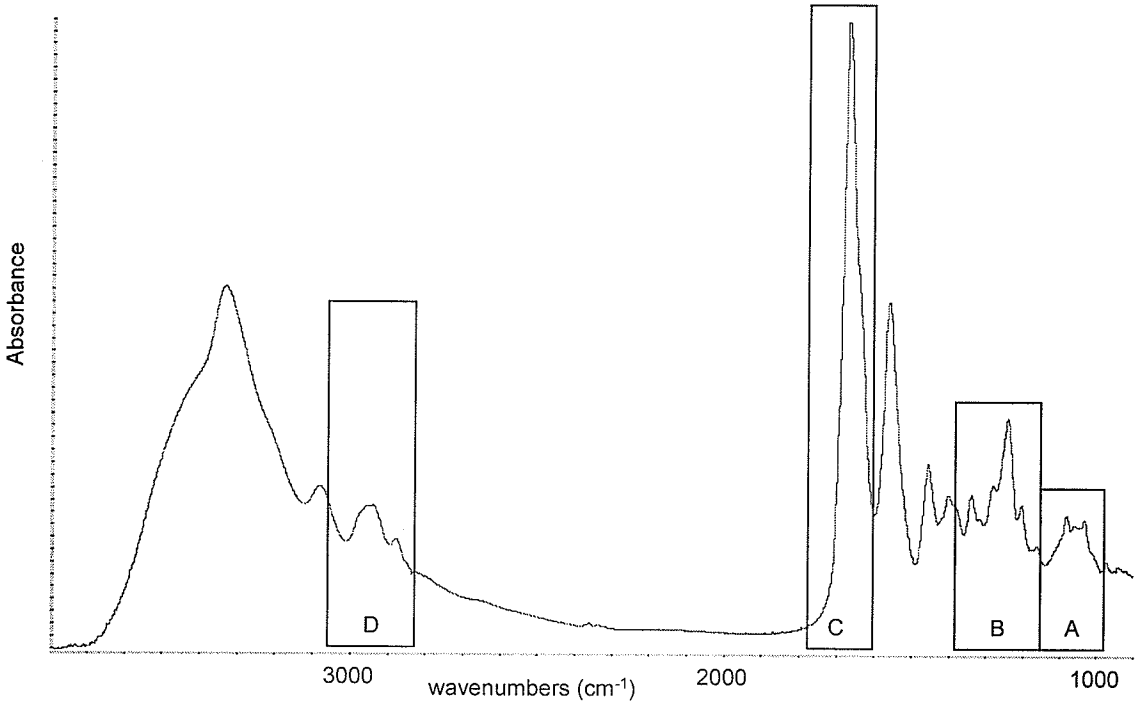

Figure 11: Infrared spectrum of a thin film of pure Type I collagen from a rat tail. Spectral regions of interest include sugars and phosphates (A), collagen fingerprint (B), amide I (C), and C-H stretch (D).

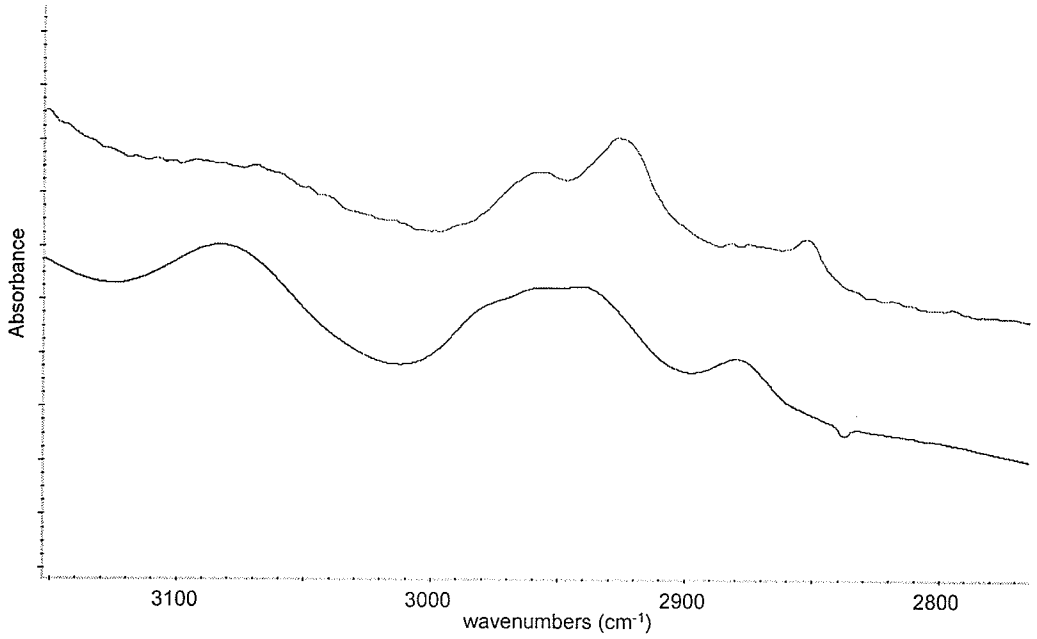

Figure 12: CH stretch region of the infrared spectrum of collagen (blue) and a lipid (red). Lipid contains two sets of two bands (asymmetric and symmetric stretching of CH2 and CH3 groups); while the collagen profile consists of a broad band around 2950 cm-1 and a single band at 2880 cm-1.

The infrared spectrum of collagen does not vary much with the type of collagen sample prepared if the sample is prepared as a thin film from a solution (Fig 13), but if the collagen is present in tissue, the spectrum can have large changes in intensity depending on the ordered nature of the collagen fibrils, if the incident infrared light is polarized (Section 3.5). The Amide bands (I, II, and III) are most affected by changes in the polarization of the incident light. Changes in polarization can result in changes to both the relative intensities of individual bands, as well as general band shape.

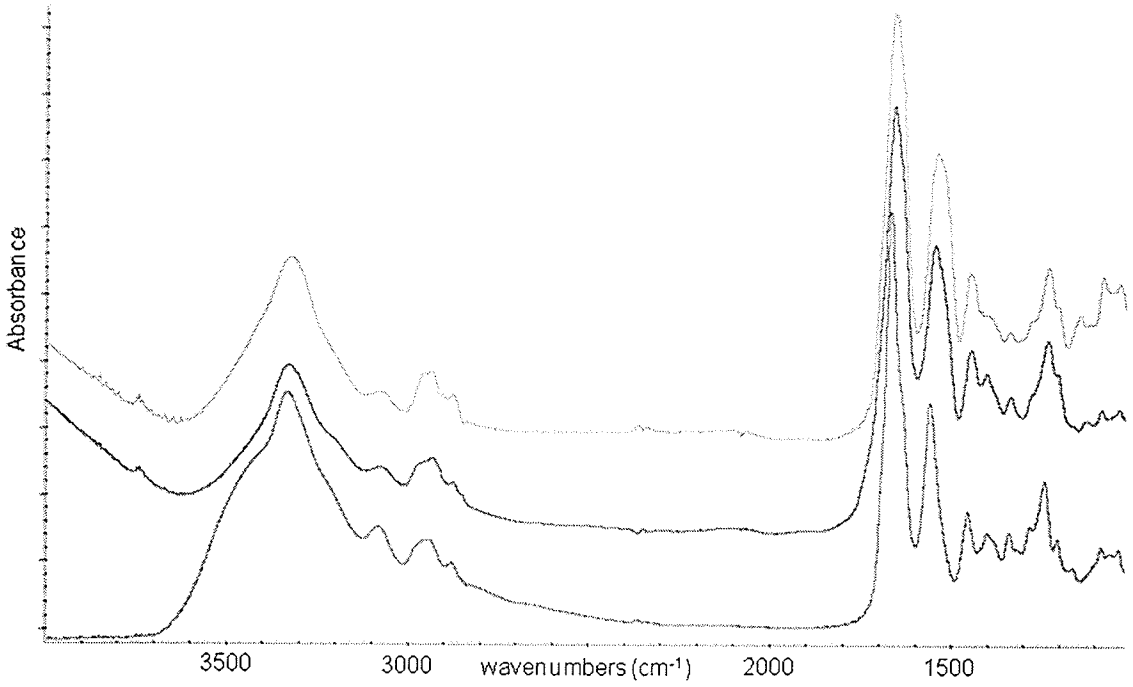

Figure 13 – Infrared Spectra of Type I collagen (red), type III collagen (purple) and type VI collagen (green).

1.6.6 Infrared Spectra of Carbohydrates

Carbohydrates are organic compounds, either aldehydes or ketones. In addition to the aldehyde or ketone functional group, carbohydrates include many hydroxyl groups, usually one on each carbon not involved in the aldehyde or ketone group. The generic chemical formula for a carbohydrate is $(CH_2O)_n$, where $n > 3$. Although this formula is generally consistent, some compounds that fit this formula are not categorized as carbohydrates, and some compounds that do not meet this formula are categorized as carbohydrates.

The infrared absorptions of carbohydrates (Figure 14) can be classified into three groups. The first group consists of O-H and C-H stretching vibrations that occur around 3300 and 2900 cm^{-1} respectively. The exact position of the bands will depend on the carbohydrate(s) involved, as well as the chemical state. The O-H stretching vibration is a very broad band, and overlaps with the N-H and O-H stretching modes of proteins and other biomolecules. This makes the O-H vibration a poor choice for determining the amount of carbohydrates present in tissue samples. Spectra of carbohydrates also result in fairly intense bands in the C-H stretching region of the spectrum. Given that virtually every biological compound will contain C-H stretching vibrations, using these bands for analysis of carbohydrate levels in tissues is also unadvised. In addition to the higher frequency stretching vibrations, carbohydrates possess many vibrations at frequencies under 1500 cm^{-1}. Included in these low frequency bands are bending vibrations of CH_2 groups (1200-1500 cm^{-1}), as well as stretching and bending of the carbohydrate ring (900-1200 cm^{-1}). These carbohydrate ring vibrations are

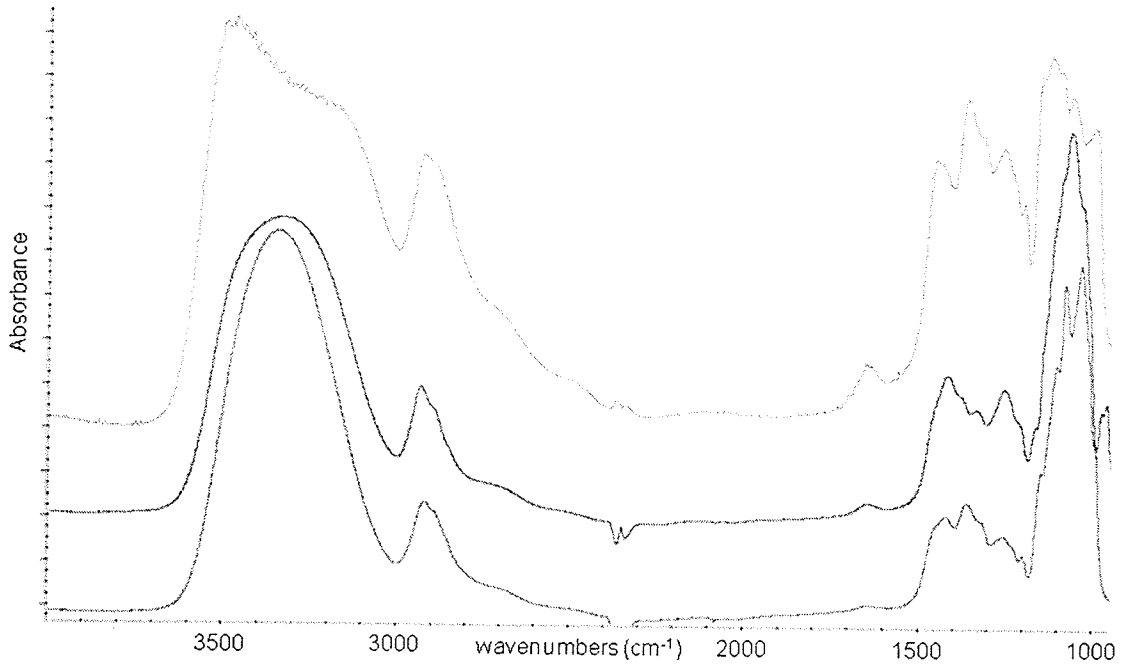

Figure 14 – Infrared spectra of different sugars.
Dextrose (red), mannose (purple), and glucose (green).

useful for monitoring changing levels of carbohydrates across a tissue sample, but care must be taken to differentiate these vibrations from the symmetric stretching of phosphate groups, which can occur in the same region. The third groups of vibrations consists of low frequency bending modes of the rings, which generally fall outside the region of the spectrum used in mid infrared spectroscopy (< 800 cm^{-1}).

1.6.7 Infrared Spectra of Lipids

Lipids are naturally occurring, fat soluble molecules. Lipids include fatty acyls, sterol lipids (cholesterol), as well as glycerolipids and glycerophospholipids. Fatty acyls include fatty acids, fatty amides, and fatty esters, and can be acted upon by enzymes to yield prostaglandins, leukotrienes, and thromboxanes, which are involved in inflammation. The fatty acyls are generated by chain elongation of a malonyl or methylmalonyl – Coenzyme A (CoA) group. This process results in a long hydrophobic tail that can be saturated or unsaturated, attached to a polar headgroup. Sterol lipids consist of a fused four ring system, similar to steroids, and contribute to cell membrane structure. Glycerolipids consist of mono-, di-, and tri-substituted glycerols. Glycerolipids include triglycerides, one of the main storage mechanisms for fat in mammals. Glycerophospholipids are similar to glycerolipids, except that they contain a phosphate group. Glycerophospholipids play an important role as a bilayer that forms the cellular membranes in animals, as well as being important components of cell signalling pathways.

The structure of lipids results in two groups of bands in the infrared spectrum (Figure 15), those arising from the long hydrophobic group, and those resulting from vibrations of the polar head group. The hydrophobic chains, consisting mainly of CH_2 groups, will result in very intense bands at the CH_2 and CH_3 stretching frequencies around 2850 cm^{-1}. In addition to their high intensities, ratioing the intensity of the CH_2 band to the CH_3 band can help to differentiate the CH_2 band of lipids from the CH_2 bands of other constituent components. The polar headgroups will result in bands around 1720 cm^{-1} (C=O stretch) as well as

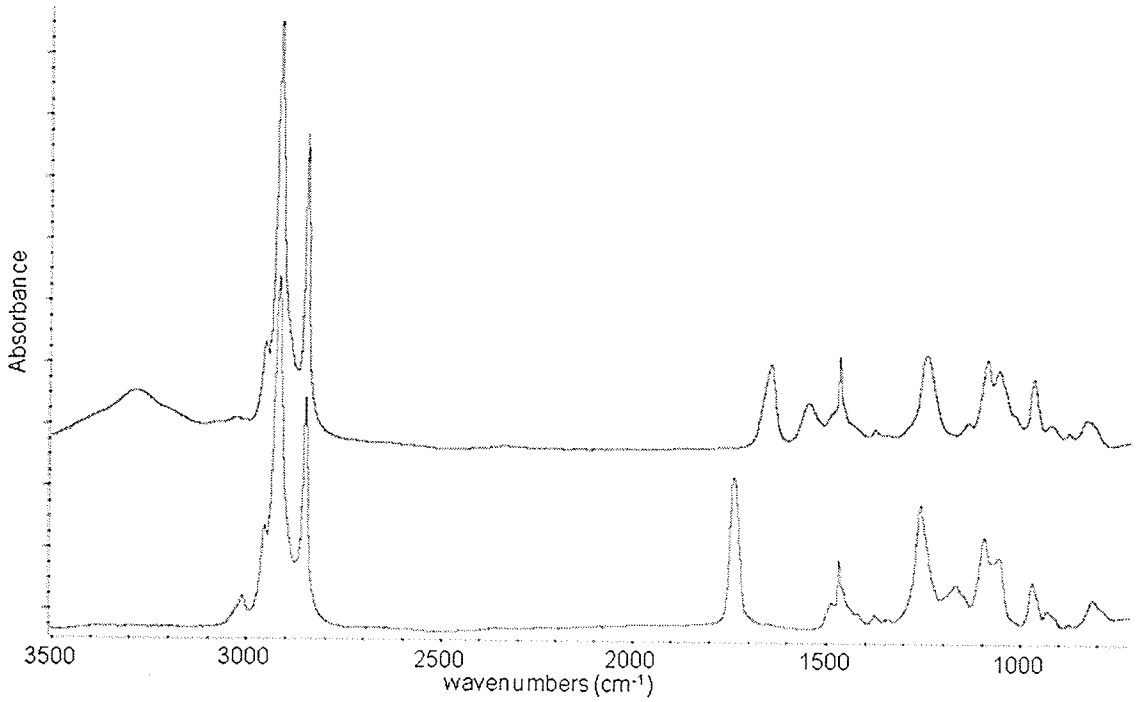

Figure 15 – Infrared spectra of two different lipids: phosphotidylcholine (red) and sphingomyelin (purple).

1240 cm^{-1} and 1080 cm^{-1} (asymmetric and symmetric stretching of phosphate groups) depending on the type of lipid. All of these bands can be useful for monitoring levels of lipids, particularly phospholipids of the cell membranes, in tissue sections.

1.6.8 Analysis of IR Imaging

An IR image consists of individual spectra collected at different points across a heterogeneous sample. The image can be constructed by raster scanning a single detector element across an area, or by using an array of detectors to record spectra over an area all at once. In both cases, the individual spectra represent the composition of the sample at that point in space, and combining the spectra allows a researcher to see how the composition of a sample varies across an area.

The most common method of visualization is to create false colour images based on peak areas of bands of interest, although other methods based on mathematical clustering algorithms and principle component analysis are also possible. Creating false colour images based on peak areas can be done solely based on a single peak, or the area of different bands can be ratioed to determine relative concentrations of different components. Using band ratios instead of areas of single bands helps to offset variations in tissue thickness across a sample, while using single peak areas reduces the chance of spectral anomalies giving false impressions of the data. While the visualization of biological components based on one or two peaks is feasible, it is still important to look at the entire spectrum to confirm that the image is actually representative of the spectral date, and not some byproduct of the analysis.

FTIR imaging is an excellent tool for the exploration of biological tissues. The combination of the synchrotron light source, focal plane array (FPA)

detectors, and better microscopes allow for the analysis of a variety of samples of interest including thin sections of bone and cartilage (Boskey, A. 2007), the localization of creatine deposits in transgenic mice and Alzheimer's brain tissue (Gallant, M. 2006), and of cancerous tumours (Srinivasan, G. 2007). In addition to sections of tissue, technological advancements have provided the ability to probe individual cells undergoing apoptosis and necrosis (Miller, L. M. 2006).

Chapter 2: Materials and Methods

2.1 Surgical Procedures and Treatment

Spinal laminectomies were performed on male Wistar rats (Charles River, Laval, PQ, Canada; body mass ~250g) in accordance with the guidelines set by the Canadian Council on Animal Care and the Animal Resources Center at the University of Saskatchewan. Following surgery, animals were assigned to one of three treatment groups. Group 1 received 3 ml normal saline, started 30 minutes post surgery and repeated every 12 hours, for a total of either 36 hours (animals sacrificed 3 days post surgery, n = 6) or 120 hours (animals sacrificed 21 or 63 days post surgery, n = 6). Group 2 received 1 mmol/kg of OTC, started 30 minutes after surgery and repeated every 12 hours, for either 36 hours (animals sacrificed 3 days post surgery, n = 6) or 120 hours (animals sacrificed 21 or 63 days post surgery, n = 6). Group 3 received 0.025 mmol/kg of quercetin, started 1 hour post surgery and repeated every 12 hours, for 36 hours (animals sacrificed at 3 days, n = 6) or 240 hours (animals sacrificed at 21or 63 days, n = 6).

2.2 Tissue Harvesting and Preparation

Animals were anesthetized by halothane gas and sacrificed by perfusion. The desired scar tissue was isolated from the bone and surrounding musculature, placed in a mold filled with OCT compound (Sakura), and flash frozen in liquid nitrogen cooled isopentane. Sections of scar tissue 10 μm thick were cut using a cryotome. Forty slides were prepared from each animal, with two sections per slide. Most sections were mounted on Superfrost Plus micro slides (VWR Scientific, West Chester, PA) for histochemical or immunocytochemical staining. Four samples from each animal were mounted on reflective MirrIR slides (Kevley Technologies, Chesterland, OH) for FTIR analysis.

Samples of Achilles tendon from age-matched adult male Wistar rats were obtained to serve as controls for oriented collagen fibers. The samples were taken from anaesthetized live animals immediately before sacrifice and frozen as for the scar tissue samples. The samples were stored frozen at -80° C until they were sectioned onto MirrIR slides for FTIR microspectroscopy.

2.3 Immunocytochemistry and Histochemistry

2.3.1 Immunocytochemistry

Activated macrophages were detected with antibodies ED1 and OX42 (Serotec), while OX8 and W3/25 (Serotec) were used to detect CD8+ T-lymphocytes and CD4+ T-lymphocytes, respectively. Detection was performed with the Vectastain ABC kit (Vector Laboratories) visualized with diaminobenzidine (Vector Laboratories).

2.3.2 Histochemistry

Sirius red staining for collagen was performed on sections acquired immediately after the first MirrIR (i.e. slide # 11 from each treatment group). The sections were thawed, fixed with 10% buffered formalin, washed and hydrated with PBS. The sections were stained for 90 minutes in 0.1% Sirius Red (Gurr, C.I 35780; BDH Laboratory Supplies, England) dissolved in saturated aqueous picric acid solution. After staining, sections were washed in 5% glacial acetic acid in sterile distilled water (3 times, 2 min each) followed by washes in 0.001N hydrochloric acid (2 times, 5 min each). Finally, the sections were dehydrated in a graded series of ethanol, cleared with xylene and mounted under glass coverslips in non-aqueous mounting medium (Entellan, EM Science, NJ, USA ;). Serial slides were separately stained with Ehrlich's hematoxylin & eosin (H&E) for general morphology and toluidine blue (pH 3.0) for mast cells and to metachromatically detect glycosaminoglycans (GAGs), using standard methods (Humason, G. L. 1979)

2.3.3 Cell Counting

Entire sections were scanned and contrast of the scanned image increased using Adobe Photoshop 6.0. Images were then imported into ImageJ 1.37G software and ED1-positive profiles counted using the Color Deconvoluter in the ROI function to isolate ED1-positive macrophages followed by the Analyze Particles function. Each section was counted 3 times. The scar tissue on each section was traced and the area measured with ImageJ software. The number of cells/mm^2 of scar tissue was calculated.

2.3.4 Polarized Light Microscopy and Imaging of Picrosirius Red Stained Tissue

Stained slides were observed on an Optiphot.1 light microscope (Nikon, NJ, USA) equipped with two polarizers to yield circularly polarized light. The lower polarizer filter was aligned such that a uniform dark background was obtained in absence of a mounted slide. The entire area of each tissue section was systematically photographed at 4x magnification using a Coolpix 995 digital camera (Nikon, NJ, USA) in a series of contiguous fields of view. The individual digital images were then merged in montage fashion to generate a picture of the entire tissue section.

2.4 Infrared Data Collection and Analysis

2.4.1 Synchrotron FTIR Data Collection

Regions of scar tissue for IR mapping were selected based on a visual examination of the tissue in order to ensure adequate representation over the wide range of heterogeneous conditions present, including:

1) Granulation phase tissue, and

2) Wound healing matrix and evolving fibrillar collagen in:

    a) Open areas,

    b) Around necrotic muscle cells, and

    c) Infiltrating healthy muscle cell regions.

An average of 8 to 10 maps was done per section. Synchrotron FTIR maps were collected at the National Synchrotron Light Source (NSLS) at Brookhaven National Laboratory (Nicolet 860 FTIR with a Continuum Microscope) or at the Synchrotron Radiation Center (SRC) in Stoughton, WI (Nicolet Magna 500 FTIR with a Nic-Plan microscope). All spectra were collected at 4 cm^{-1} spectral resolution, with a 12 x 12 μm aperture and a 10 μm step size. Co-addition of 16 or 32 scans gave spectra with excellent signal to noise ratio without zero-filling; no post-collection smoothing or deconvolution were employed. Some lower spatial resolution maps (20 to 25 μm aperture) were collected on a Bruker Tensor 27 FTIR with Bruker Hyperion microscope with a standard globar

source. Single point spectra of rat Achilles tendon were also collected from sections placed both laterally and longitudinally on the MirrIR substrate at both synchrotrons using the naturally polarized synchrotron light. These spectra were compared with spectra acquired from a benchtop instrument at 0^{o} and 90^{o} orientation, for both the laterally and longitudinally mounted sections, with a polarizer placed between the light source and sample.

2.4.2 FTIR Data Analysis

Spectral analysis procedures were based on methods previously published (Gough, K. M. 2003; Wiens, R. 2006), exploiting numerous well-known spectral markers for tissue components. Maps may be processed in myriad ways; both uni- and bivariate analyses, as well as hierarchical clustering, were used to evaluate our spectral data. Because of the extreme heterogeneity of the developing scar tissue, the simplest and most direct approach (univariate analysis of known spectral markers) was found to be the most useful for revealing the main features of interest. In all cases, the component of interest is displayed by a colour scale from red/white (lowest or nil) to blue (highest).

Collagen: The presence of collagen in tissue can be monitored by the presence of a quartet of bands at 1204, 1240, 1284, and 1338 cm^{-1} (Camacho, N. P. 2001; Fraser, R. D. B. 1950; Gough, K. M. 2003;). The amide III absorbance at 1240 cm^{-1} directly overlaps with an asymmetric stretching mode of the phosphate head group common to lipid bilayers, making it unsuitable for our analysis. Therefore, univariate analyses showing the distribution of collagen throughout a map were created using Nicolet Omnic/Atlus software, by integrating the area of the 1204 cm^{-1} peak from 1198 to 1211 cm^{-1} with a baseline from 1188 to 1214 cm^{-1} and a display range of 0.025 to 0.45.

The type I collagen amide I has a distinct appearance with a maximum around 1670 cm^{-1} and a low frequency shoulder around 1640 cm^{-1}. While the amide I band appears to be a single band, it is actually the sum of many underlying

bands, one from each of the amino acids in the proteins that are present at that particular point in the tissue. Additional dependence on fibril orientation is also apparent with polarized light, such as from the synchrotron source. With polarized light, the relative height of the amide I and II bands of collagen fibers is a function of their orientation. Therefore, in the synchrotron IR maps, the height of the amide I band at 1662 cm^{-1} (baseline 1604-1724 cm^{-1}) was ratioed to the height of the amide II band at 1555 cm^{-1} (baseline 1490 cm^{-1} to 1604 cm^{-1}), to illustrate the orientation of collagen fibres. As the strength of this effect will be dependent on how the sample is placed on the slide, we are using this only as a rough estimate of the development of oriented collagen fibrils during the healing process.

Lipid bilayer: Univariate analysis showing the distribution of cellular membranes was achieved by taking the area of the symmetric CH_2 stretching vibration (Fig 2B) from 2847 to 2855 cm^{-1} with a baseline of 2837 to 2862 cm^{-1} and a display range from 0.0 to 0.4. Although this is the weaker of the two main bands assigned to CH_2 stretch modes, it is free from interference from collagen and sugar bands that are common to the asymmetric CH_2 stretch.

Sugar and Phosphates: The distribution of total sugar and phosphate from cells, glycosylated collagen, glycoproteins and proteoglycans was evaluated by integrating the area from 1014-1130 cm^{-1} with a baseline from 900 to 1145 cm^{-1}. Alternative processing of these maps was intended to show only the localization of phosphate, from the intensity of the symmetric phosphate stretch at 1082 cm^{-1} (integration over 1077-1087 cm^{-1}, baseline 900-1145 cm^{-1}, display limit from 0.6

to 1.6), or of sugars, from the band at 1032 cm^{-1} (integration 1024-1037 cm^{-1}, baseline 1020-1071 cm^{-1}, display limit from 0.02 to 0.2). The detection of phosphate and sugar was complicated by the overlap between the usual phosphate markers at 1235 and 1082 cm^{-1} and between the sugar C-O-C vibrations at 1032 cm^{-1} with collagen bands at the same position. Spectral analyses were carefully evaluated to monitor this circumstance.

Chapter 3: Results

3.1. Initial Findings

Prior to collecting infrared data on the tissue sections, the sections were photographed to facilitate the selection of regions suitable for infrared mapping. These photographs serve an essential function as time at a synchrotron is limited. It is important to have a clear plan for data collection in order to make efficient use of the available time. The tissue sections are very heterogeneous, and it is critical to ensure that data is collected from the different regions of the wound area. This includes scar tissue at the heart of the wound, developing scar tissue near intact muscle cells, and other regions of interest.

Figure 16 shows photomicrographs of sections from:

1) A control animal that had not undergone the surgical procedure (16a),
2) An animal from the three day saline group (16b),
3) An animal from the twenty one day saline group (16c), and
4) An animal from the sixty three day saline group (16d).

Regions of scar tissue have been outlined in red.

In the control animal (16a), most of the tissue section consists of muscle cells. These muscle cells normally look like small irregular ovoids aligned in a densely packed manner (Figure 17a), but in many of the samples, the muscle cells burst upon freezing, giving them the appearance of the cells in Figure 17b. Spectra obtained from the burst cells were not very good due to the thickness and unevenness of the cells. The spectra were often oversaturated. It was possible to

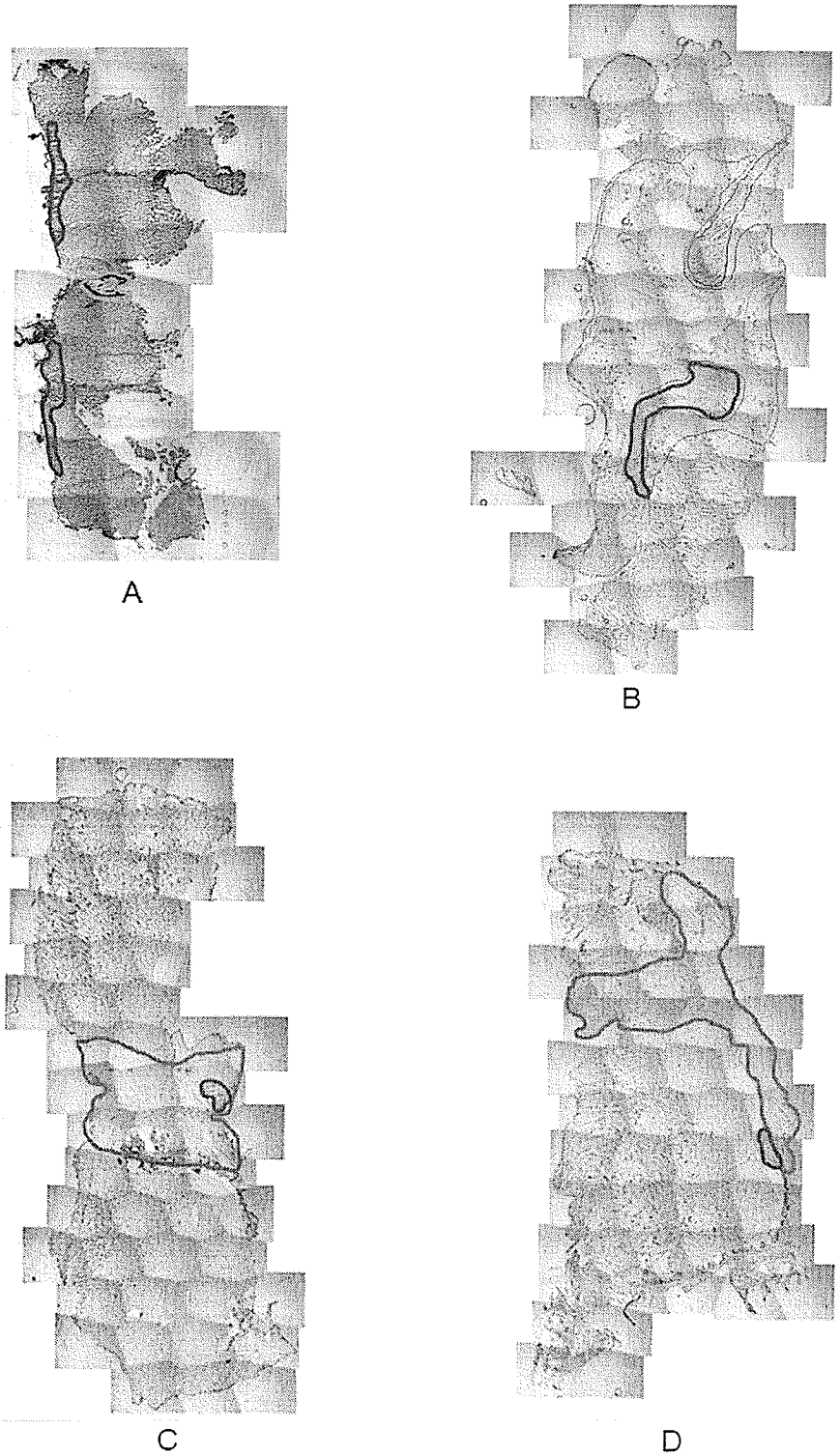

Figure 16: Photomerges of tissue sections from healthy (A), a 21 day saline (B), a 21 day OTC (C), and a 21 Day quercetin (D) rat. Fibrous tendon is outlined in red, scar tissue is outlined in blue, and the green outline denotes bone in the healthy animal.

collect spectra from intact muscle cells in some of the animals that had undergone surgery (17b).

There are two main contributors to the poor quality spectra obtained from the muscle cells. First, if the tissue is very dense, it will absorb most of the incident light, resulting in a very low amount of light being reflected back to the detector. As:

$$Absorbance = \log(\frac{1}{R})$$

Where *R* is the percentage of light reflected back to the detector, for small values of *R* corresponding to dense tissue, there will be large values for the absorbance, and the system will no longer obey Beer's Law. The log function for the calculation of absorbance is approximately linear for absorbance values around 1. This means that the amount of light reflected back to the detector should be about 10%. If only 1% of the light is reflected back to the detector, the resulting absorbance value will be 2, and it begins to stray from the linear portion of the curve.

The second contributor to poor spectra is scattering of light from tissue. Tissue is not perfectly flat or smooth; it has a certain amount of curvature to it. These curved surfaces result in light being scattered, instead of being absorbed or reflected back to the detector. In cases where significant amounts of light are scattered by the sample, the spectra will exhibit an elevated baseline (Figure 17c).

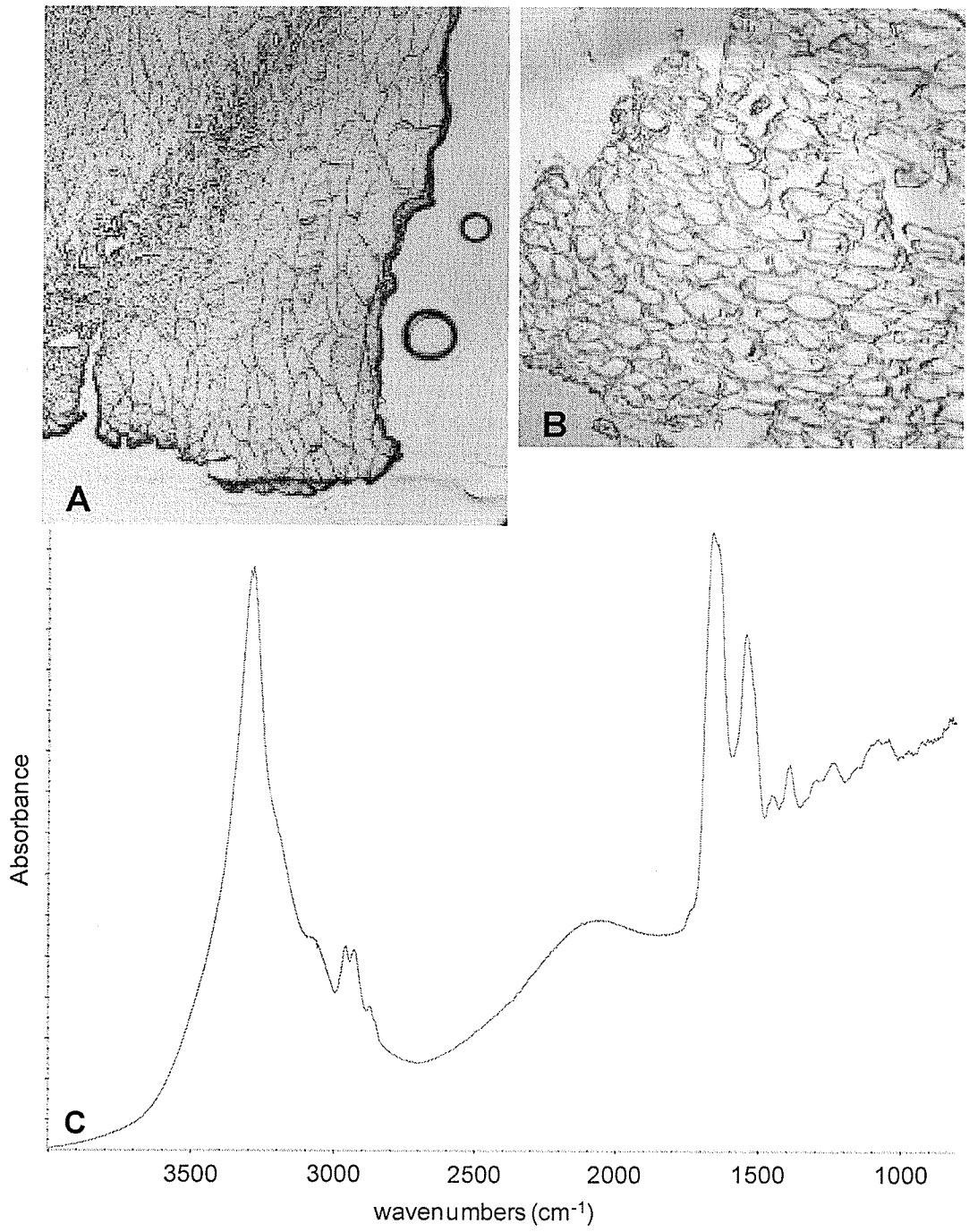

Figure 17: Photomicrographs of intact muscle cells (A), damaged muscle cells (B), and an Infrared spectrum of intact muscle cells

Another feature noticeable in the tissue sections from healthy animals was the presence of a band of connective tissue or tendon that ran along the surface of the tissue section (Figure 16, outlined in blue). Infrared spectra from this connective tissue showed that it was composed mostly of collagen. In some of the sections from animals that had undergone surgery, notably the first group consisting of three animals from the three and twenty one day treatment groups, improper surgical techniques resulted in this connective tissue being folded into the region of developing scar tissue. This artifact was something to be aware of, but the distinctive morphology of the connective tissue allowed it to be distinguished from the developing scar tissue.

The final object to note in the healthy tissue is the region of bone in the centre of the image. This object is the portion of bone that was removed during the laminectomy, and it is around this region that the scar tissue should develop in the animals that have undergone the surgical procedure.

3.2 Three Day Animals

3.2.1 Overview

The 18 animals sacrificed three days after surgery were acquired as two different sets. The first set, consisting of three animals from each treatment group, were mapped at synchrotrons in July and September of 2004. The second set, consisting of another three animals from each treatment group, were mapped at synchrotrons in July and August of 2006 (see Table 1).

Table 1: Summary of IR Mapping Data of Three Day Animals

Set 1: N=1-3				Set 2: N=4-6			
		IR Maps Collected				IR Maps Collected	
Treatment	Animal Number	July 2004	September 2004	Treatment	Animal Number	August 2006	July 2006
OTC	31	5	2	OTC	47	6	3
	32	3	3		50	6	2
	33	6	4		54	6	3
Quercetin	28	6	0	Quercetin	38	6	4
	29	6	0		41	0	3
	30	6	0		44	4	0
Saline	34	6	3	Saline	56	6	2
	35	6	7		59	6	0
	36	3	6		61	4	0

A total of 133 maps were collected, with a minimum of 3 and a maximum of 13 on any given animal. The goal was to acquire at least six maps per animal, but tissue quality, particularly in the animals from Set II, made this goal difficult to achieve for some sections (see discussion). The distribution of components was

similar in animals belonging to a specific treatment group, as well as across an entire age group, encompassing all three treatment regimes. This similarity allows for reasonable confidence that data acquired from a given sample is representative of a particular animal, even if the number of maps collected on a particular sample was less than desired.

3.2.2 Tissue Composition of Three Day Animals

The wound healing area in the three day animals tended to look more disorganized than it did in the animals that had been allowed to heal for a longer period of time. Infrared maps were collected in the central portion, which should represent the developing scar tissue, as well as along the edge of the developing scar tissue, near the healthy muscle cells.

Collagen levels in the three day animals, based on the area of the band at 1240 cm^{-1}, were generally low (Figure 18). This is consistent with what is known about the wound healing process three days post injury.

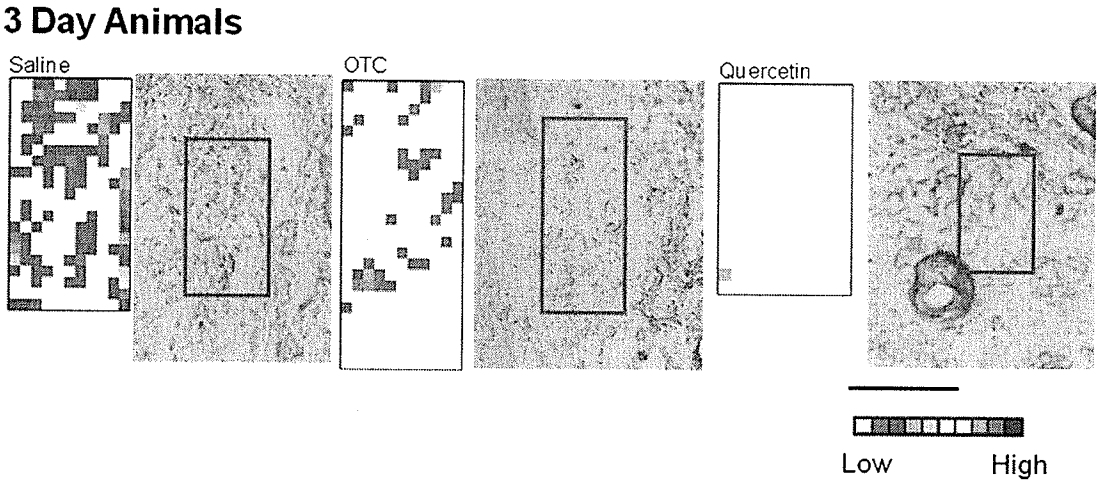

Figure 18: Photomicrographs of wound area from three day animals. Red box represents region mapped with IR microspectroscopy. Adjacent false colour images show the distribution of collagen in the mapped region. Scale Bar = 100 microns.

In addition to looking at collagen levels, infrared maps were also analyzed for sugar levels. In the early stages of the project, the entire region from 1014 to 1130 cm^{-1} was taken to represent sugar levels. This method resulted in maps where the apparent level of collagen was low, while the amount of carbohydrate present was very high. A more detailed examination of the spectra revealed that there were two main maxima in this region of the infrared spectrum (Figure 19). The first maximum was at 1080 cm^{-1} band, representing the symmetric stretching of phosphate groups. A second maximum at 1030 cm^{-1} was also present. This lower band more closely matches the frequencies corresponding to carbohydrate bands. The region from 1014 to 1130 cm^{-1} was then split into two separate regions for analysis. Region 1, encompassing the band at 1030 cm^{-1}, was used to show levels of carbohydrate in the tissue samples. Region 2, centred at the 1080 cm^{-1} band, was used to determine phosphate distribution in the tissue sections.

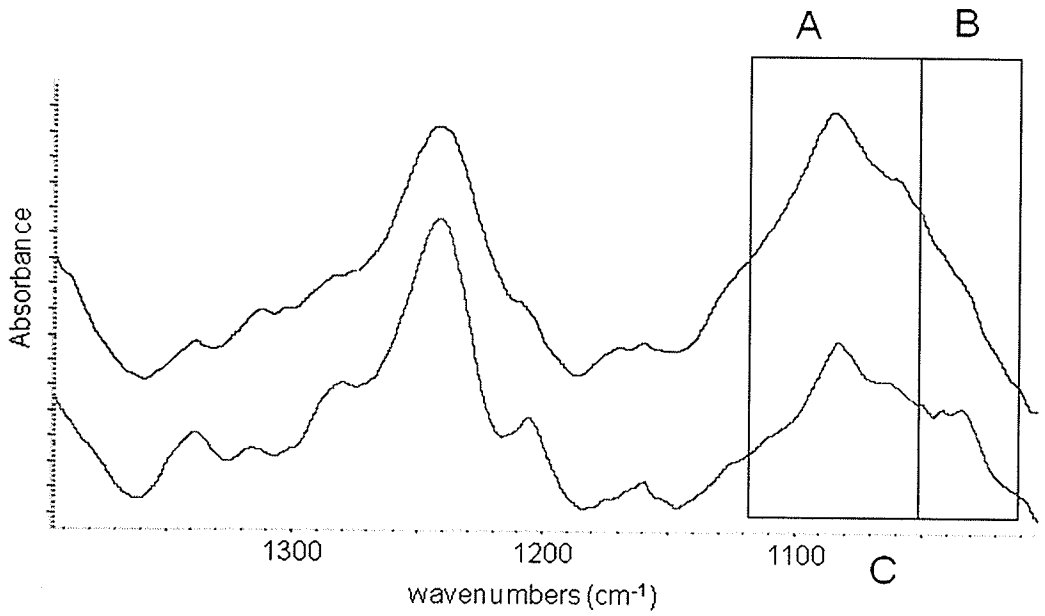

Figure 19: Bands used for Sugar and Phosphate Analysis
Portion of the infrared spectrum indicating two separate bands at 1080 cm^{-1} (A) and 1030 cm^{-1} (B) within the original region encompassing 1014-1130 cm^{-1} (C).

Based on the area of the 1032 cm^{-1} band, the three day animals showed low levels of sugar throughout. Since most of the sugars present in the developing scar tissue will be associated with the collagen fibres, the low amount of sugar present is consistent with the low levels of collagen present in the three day animals.

The increased intensity in the region of the spectrum from 1014-1130 cm^{-1} can be attributed to an increase in the intensity of the 1080 band, indicating an increased level of phosphate groups in the tissue. Comparison of infrared images based on the peak area of the 1080 band with images based on the area of the symmetric CH_2 stretching vibrations (2852 cm^{-1}) showed a good correlation between the intensities of the two bands (Figure 20). This correlation led to the

hypothesis that the increased absorption of the 1080 and 2852 bands were the result of increased cellularity in the three day animals. As mentioned previously, the main processes in early wound healing result in a large influx of cellular material to the site of the wound. The increase in the 1080 band could be from the polar headgroups of the phospholipid bilayers that make up the outer membrane of the cells, while the increase in intensity of the 2852 band would be attributed to the long hydrocarbon tails of the lipid bilayers. Another indicator of increased lipid concentration is the band at 1740 cm^{-1}. This band corresponds to the stretching of the lipid carbonyl, and does not seem to be present in spectra exhibiting the higher intensity of 1080 and 2852 bands. There is a very small band present at 1740 cm^{-1} in most of the spectra from the three day animals, but it does not show the same intensity changes as the 1080 and 2852 vibrations.

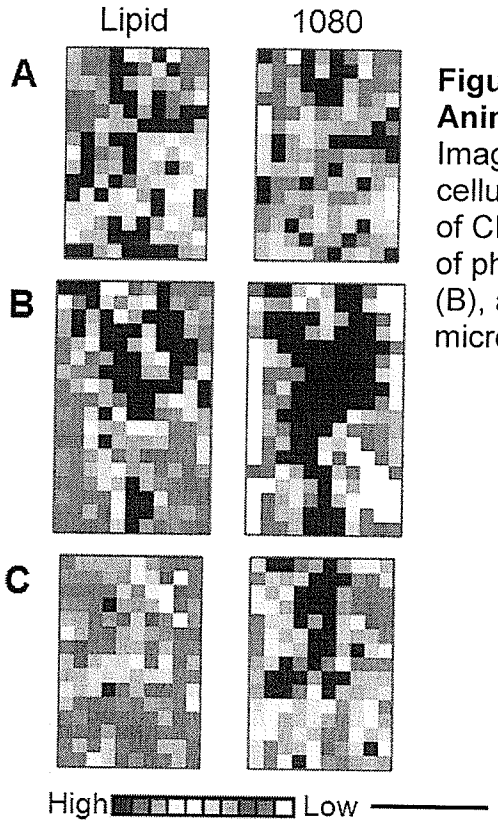

Figure 20: False Colour Images of 3 Day Animals

Images on the left show typical distributions of cellular content, based on symmetric stretching of CH2 groups (lipid) and symmetric stretching of phosphate groups (1080) for saline (A), OTC (B), and Que (C) groups. Scale Bar = 100 microns

Another possibility for the increase in intensity around 1080 cm^{-1} is the presence of DNA and/or RNA in the proliferating cells. DNA shows a group of three bands at 1071 cm^{-1}, 1084 cm^{-1}, and 1095 cm^{-1}, all of approximately equal intensity (Diem, M. 1999). There is also the presence of a band at 1245, corresponding to the phosphodiester stretching vibration. The spectra do not match this model very well. The broad band shows a pronounced maximum at about 1080, instead of a series of three weak bands of relatively similar intensity. RNA has similar spectral features as DNA, but the 1085 band is slightly more intense than the bands on either side. This increased intensity is not great enough to indicate that the 1080 band seen in our data is the result of increased levels of RNA.

The fact that no specific type of spectra matches those from our tissues is not that much of a surprise however. Our tissue spectra are just that, spectra from tissue. The spectra are not IR spectra of DNA, or RNA, or cells, or proteins, but rather a summation of all of those things as well as the other components that make up the complicated and heterogeneous tissue samples. Based on what is known of the wound healing process, it is reasonable to assign the increased intensities of the 1080 and 2852 bands to an increase in the number of cells in three day animals. More cells results in both increased DNA/RNA as well as the increase in lipid content.

3.3 Twenty One Day Animals

3.3.1 Overview

Like the three day animals, the 18 animals making up the group of animals sacrificed twenty one days after surgery were acquired in two sets, at the same time as the two sets that make up the group of three day animals. The first set of twenty one day animals was mapped concurrently with the first set of animals from the three day group, in July, August, and September of 2004. The second set of animals for the twenty one day group was mapped in August 2006 at the Synchrotron Radiation Centre in Madison, Wisconsin. A total of 110 maps were collected. Of these, 66 were from Set I and the remaining 44 from set II.

Table 2: Summary of IR Mapping Data of 21 Day Animals

Set 1: N=1-3					Set 2: N=4-6		
		IR Maps Collected					IR Maps Collected
Treatment	Animal Number	July 2004	August 2004	September 2004	Treatment	Animal Number	August 2006
OTC	21	6	0	0	OTC	73	6
	22	6	0	0		76	3
	23	6	0	0		80	6
Quercetin	17	0	4	2	Quercetin	65	0
	18	0	5	0		69	6
	19	6	0	0		71	6
Saline	25	6	0	4	Saline	84	5
	26	6	0	4		87	5
	27	6	0	5		89	4

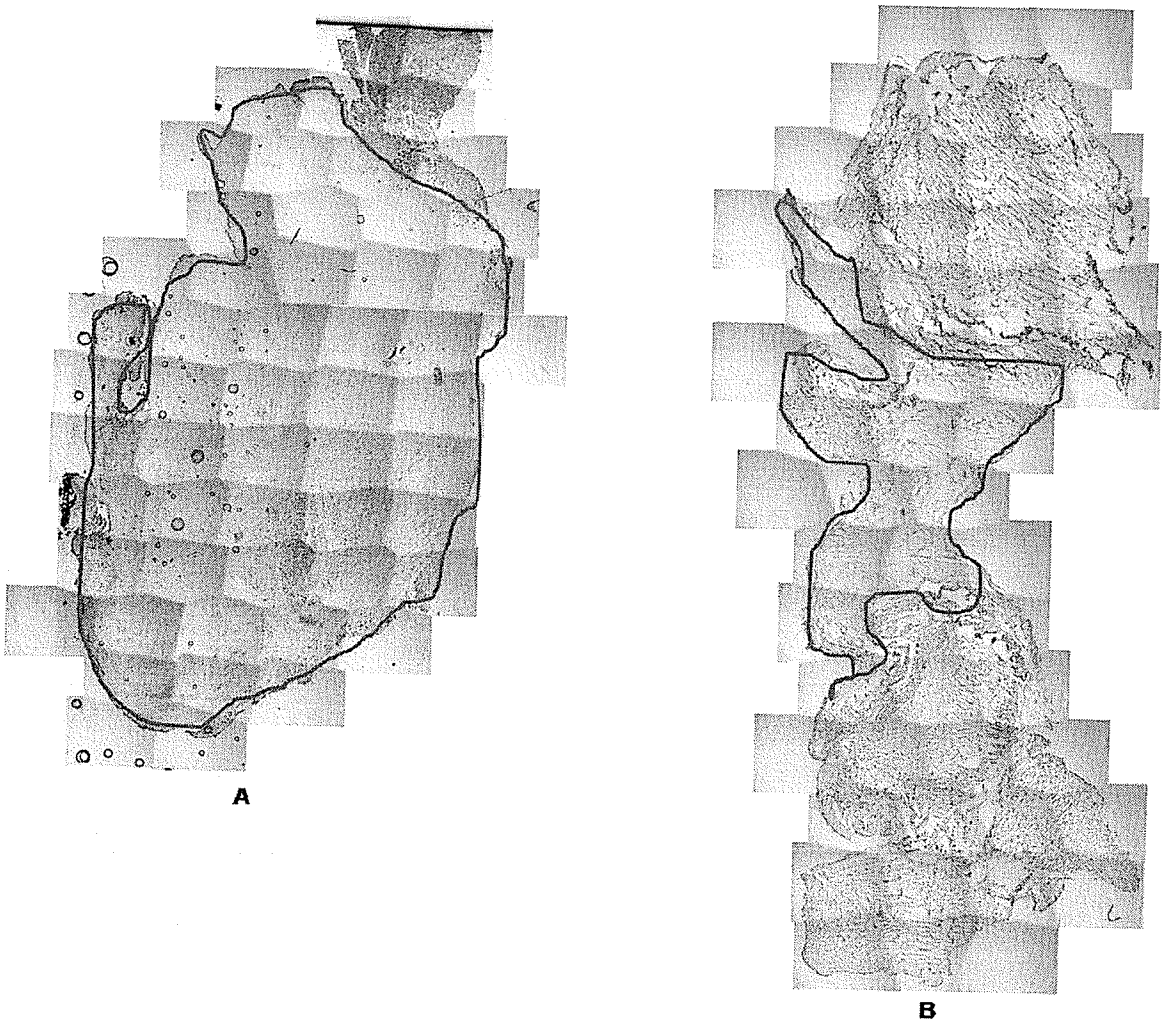

Figure 21: Twenty one day saline controls from Set I (A) and Set II (B).

There was a marked difference in the appearance between the animals comprising Set I and those in Set II (Figure 21). The animals in Set I were characterized by a large amount of scar tissue, relative to the amount of remaining muscle. This characterization held true for all three treatment groups, although the saline control group did seem to have more scar area than the treated groups (Figure 22, also Table 4 on page 115).

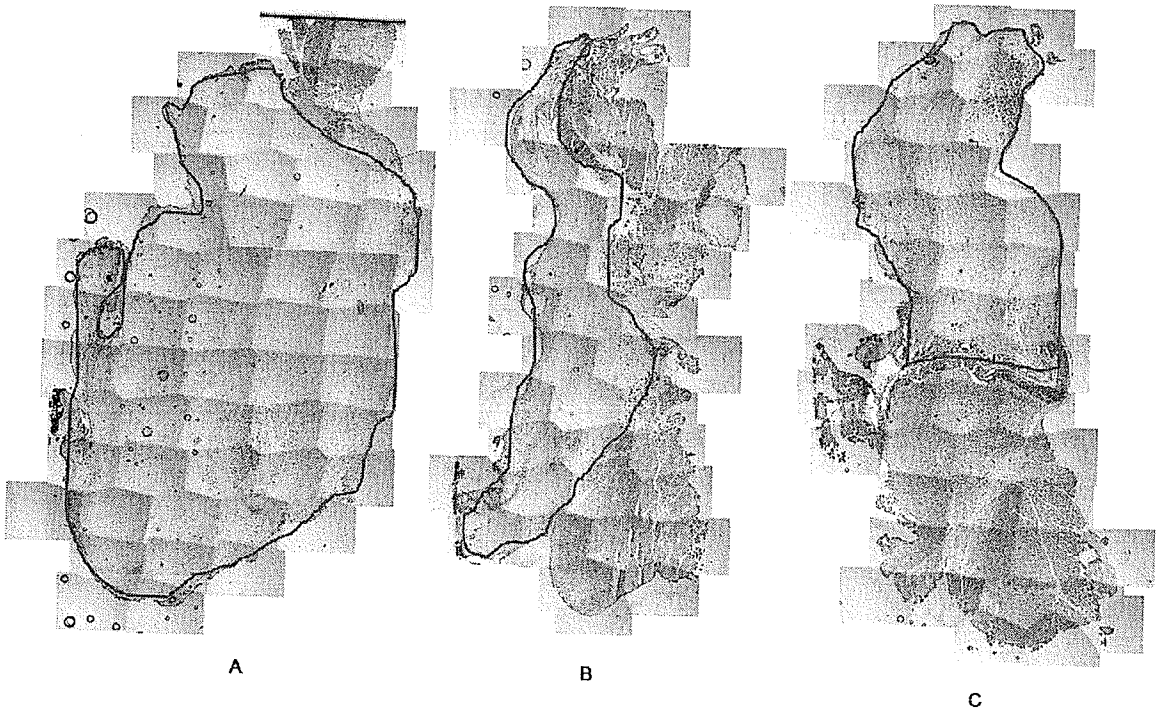

Figure 22: Photomosaics of 21 day saline (A), 21 day OTC (B), and 21 day Que (C) animals from Set I.
Scar tissue is outlined in red.

Even though there was less scar tissue in the 21 day treated animals relative to the controls, there was still a lot more scar tissue in the twenty one day animals than in the three day animals from Set I.

One concern with the animals in set I was the lack of muscle tissue surrounding the scar (See Figure 22). The presence of surrounding muscle tissue confirms that all of the developing scar tissue from the wound area was excised, and the sections are representative of the whole wound healing area. When there is a lack of surrounding muscle tissue, the question arises whether or not there was more scar tissue present that was not excised during the removal of the tissue block.

A follow up project with new animals is planned to determine which of the two sets of 21 day animals is more representative of the group (see Section 5.1: Conclusions and Future Work). The wound area of the animals from Set II is significantly smaller than that of Set I, but there is more surrounding muscle tissue. While the presence of surrounding muscle tissue suggests that all of the scar area was excised, it seems that when the bone was removed from the tissue block some of the scar tissue may have been lost. The animals from Set I show a large amount of developing scar, in an approximately rectangular shape. Upon examination of some of the animals from Set II, it appears that some of the sections are missing portions of tissue, whether that missing tissue is more muscle or scar tissue is unknown.

3.3.2 Distribution of Tissue Components in Twenty One Day Animals

Twenty one days post surgery the granulation tissue has mostly been replaced with Type I collagen, and this is confirmed by my infrared mapping results. Collagen is found throughout the wound area across all three treatment groups and both sets of animals. Figure 23 shows the distribution of collagen in a map from each of the three treatment groups. The false colour images created based on the area of the band at 1204 cm^{-1}, show streaks of collagen running throughout the sampled areas. The heterogeneous nature of the tissue samples is apparent in the IR maps, even though the photomicrographs indicate a mostly homogeneous tissue composition.

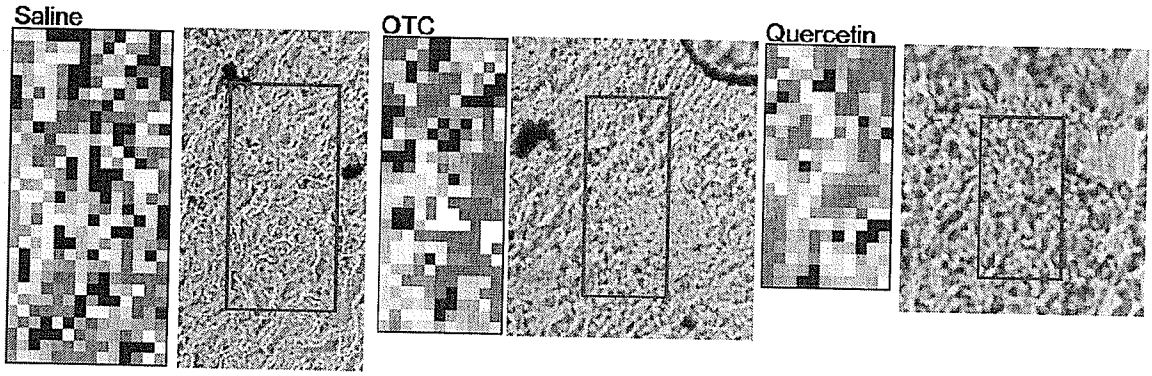

Figure 23: Representative IR images showing collagen distribution in 21 day animals. Scale bar = 100 microns.

The distribution of the collagen varies from map to map. In some maps the collagen seems to be unorganized, existing as pools. In other cases, the collagen can plainly be seen to exist as fibrils running through the map. Figure 24 shows a map from a 21 day saline animal with the collagen fibre (blue streak) running diagonally through the map and visible light image of the tissue showing the collagen fibres.

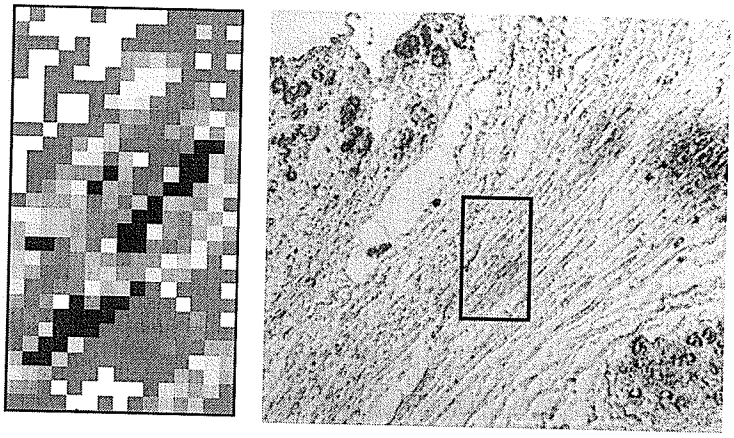

Figure 24 Oriented Fibrillar Collagen in a 21 day saline control.

Like the maps from the 3 day animals, the maps collected from the 21 day animals were also processed for both lipid and sugar. The parameters were initially identical to those for the 3 day animals, using the symmetric CH_2 band for lipid content and the entire region from 1014-1130 for sugar content. Initially, the collagen and sugar seemed to be colocalized, while the general lipid content was significantly lower than it was in the 3 day animals. Upon closer inspection, one of the maps taken from Saline 27 from set 1 showed characteristics similar to the 3 day animals, with the maps based on collagen and sugar not showing similar distribution patterns (Figure 25). The map showed moderate to high levels of

collagen throughout the area, except for a crescent shaped area that had little to no collagen present. The corresponding image constructed using the area of the 1014-1130 cm^{-1} of the spectrum showed a high intensity in the crescent corresponding to a low level of collagen. The more detailed analysis of the spectra from this map led to the change in processing parameters, splitting the analysis of this region into two separate spectral regions, one based on the band at 1030 cm^{-1}, and another based on the band at 1080 cm^{-1}. In the case of low cellular content, both the 1030 and 1080 bands colocalize with the collagen. However, when there is cellular material present, as in the majority of the 3 day animals and occasionally in the 21 day animals, the 1080 band that maps to collagen is dwarfed by the increased phosphate absorbance from the lipid bilayers of the cellular membranes.

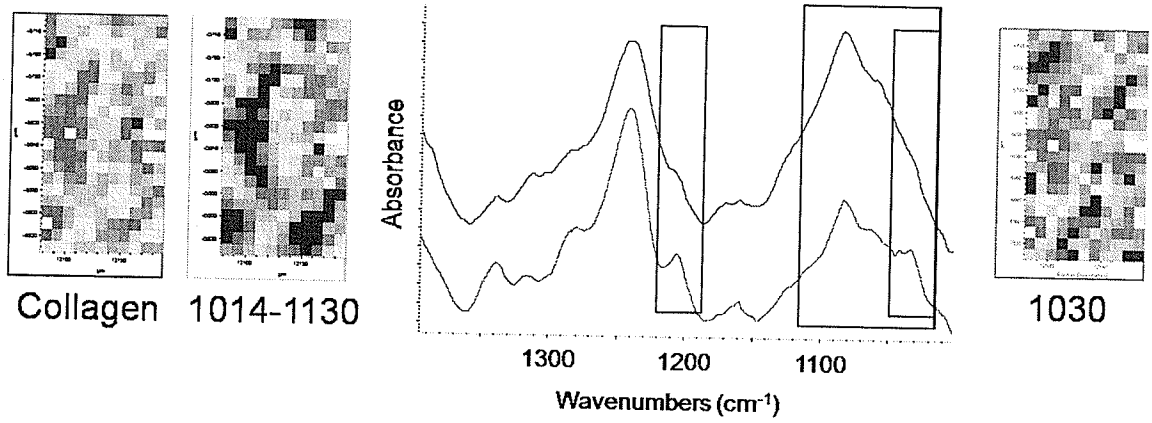

Figure 25: Infrared map from Saline control 27.
Low levels of collagen along with high levels of "sugar" based on 1014 – 1130 band were unusual.
Reprocessing based on the narrower band around1030 excluded the phosphate band at 1080 and yielded more accurate images.

3.4 Sixty Three Day Animals

3.4.1 Overview

The surgeries, treatment, and tissue collection for the 63 day animals were done as one set, as opposed to the 3 and 21 day animals which had been collected in two groups of three animals each. The 63 day animals were sacrificed in late 2005, and preliminary IR mapping was done at the National Synchrotron Light Source in February 2006 on two animals from each of the three treatment groups. Extensive mapping took place in June of 2006 at the Synchrotron Radiation Center, with additional data collected at SRC in April and June of 2007 (see Table 3). A total of 133 maps were collected on the 63 day animals.

Table 3: Summary of IR Mapping for 63 Day Rats

		IR Maps Collected			
Treatment	Animal Number	February 2006	June 2006	April 2007	June 2007
OTC	N13	5	2	0	0
	N15	0	0	0	0
	N17	0	8	2	0
	N19	0	8	0	6
	N21	0	2	0	1
	N23	0	8	2	0
Quercetin	N1	6	2	0	0
	N3	3	3	0	0
	N5	0	7	0	2
	N7	0	6	0	2
	N9	0	5	0	2
	N11	0	6	2	0
Saline	N25	1	0	0	0
	N27	6	0	0	0
	N29	0	8	3	2
	N31	0	8	0	2
	N33	0	6	4	0
	N35	0	8	0	2

The tissue sections from the 63 day animals were similar in appearance to the second set of animals from the 3 and 21 day animals. The 63 day animals had a small area of scar tissue in the center, surrounded on the top and bottom by large areas of muscle tissue. There is concern that some of the scar tissue was lost due to poor techniques, either at the time the tissue was harvested from the animal or during sectioning. If scar tissue was lost during sectioning, it is highly unlikely that the serial sections from an individual animal would continue to look as alike as they do. Since there is not a large difference in serial sections, even those that are 100 or more microns apart (10 sections), it is much more likely that the problems lie in the harvesting of tissue from the wound area.

Figure 26 shows sections from a 63 day saline, 63 day OTC, and a 63 day quercetin animal illustrating some of the deficiencies in the sections.

For the 63 day saline section, it appears that only half of the wound area may have been excised. One can clearly see the fibrous tendon, also present in normal, healthy tissue; running along the left hand side of the section, until it reaches the scar tissue at the lower end of the section. At the bottom of the scar tissue, the end of the tendon can be seen to have curved into the developed scar tissue, but there is no continuation of the tendon, and there are no intact muscle cells below the scar tissue.

The section from the OTC treated animal does not have a clearly defined tendon, making it more difficult to determine which side is the skin side of the section. The bottom portion of the section is comprised of muscle cells, many of which are still intact, and have not burst as they did in most of the other tissue sections. The dark region near the centre of the image may represent bone regrowth, although the collection of infrared spectra from this region is not possible. The tissue surrounding the possible regrown bone is then most likely the mature scar tissue. While there is an intact block of muscle tissue below the scar area, the tissue section does not have that same amount of intact muscle above the scar area.

Finally, in the tissue section from the 63 day quercetin animal, there are a large number of muscle cells above and below the scar tissue, although unlike the OTC sample the vast majority of these cells have burst upon freezing. One can also see a fairly intact tendon, denoting the skin side of the section.

However, there does seem to be tissue that was lost in the central portion of the section. Whether this tissue was scar or muscle is difficult to tell.

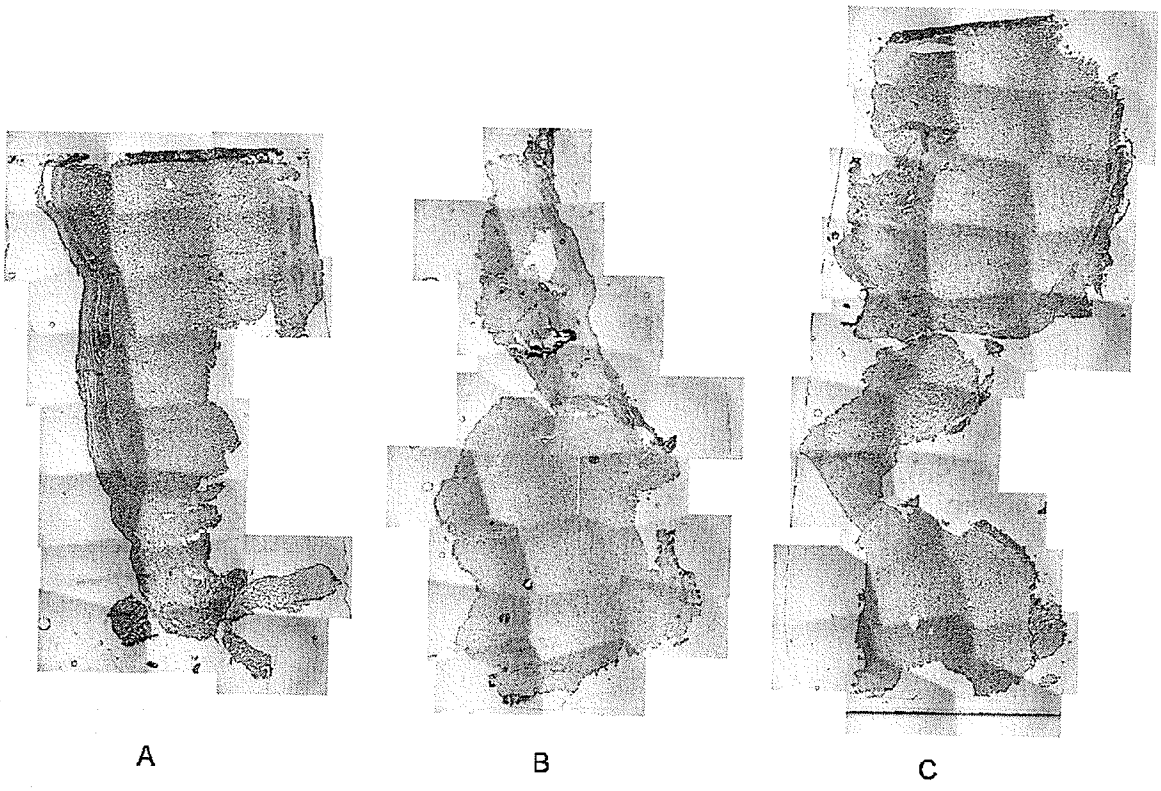

Figure 26 – Photomosaics of 63 Day Saline (A), OTC (B), and Quercetin (C) animals.

3.4.2 Tissue Composition of 63 Day Animals

Nine weeks after injury, there has been significant remodeling of the initial wound area. The remodeling predominantly involves contraction of the collagen fibres that make up the developing scar tissue, resulting in a decrease in wound area. Visual inspection of the tissues show that there is indeed a smaller area of scar tissue in the 63 day animals relative to the 21 day animals, but there do not seem to be any major differences among the three different treatment types within the 63 day age group.

While the wound area itself had contracted, infrared maps collected from the mature scar tissue showed similar spectral features to that of the developing scar tissue in the 21 day animals. The main difference in the 63 day animals was that the intensities of the bands used to construct the false colour images were greater in the 63 day animals than in the 21 day animals. These intensities resulted in a saturation of the display limits and that translated into a false impression of tissue homogeneity in the processed maps (Fig 27a). Increasing the maximum value in the display limits allows for the differences in the top and bottom portions of the map to become apparent (Figure 27b). Increasing the maximum value too high, however, results in the map once more appearing homogeneous (27c).

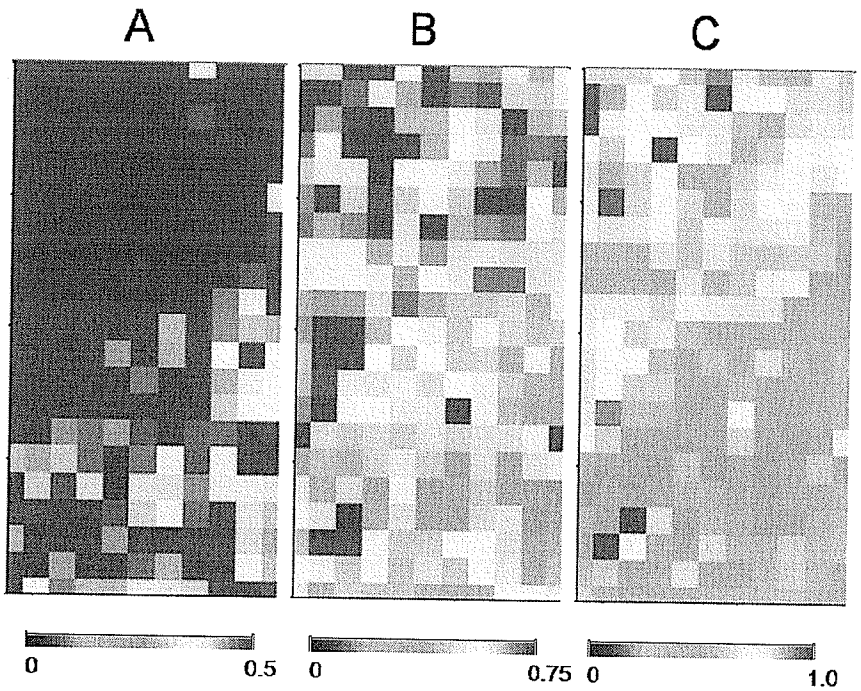

Figure 27: Infrared Images showing distribution of collagen based on different display limits.

Two possible explanations for the increased intensity of the collagen signature in the 63 day animals are:

1) The increase in formation of ordered fibrils, and
2) Differences in tissue thickness.

The IR spectrum of ordered, well-oriented, collagen fibres are affected by the relationship of their axis of vibrations with the orientation of the electromagnetic field of the incident IR light (See section 3.5 for more on the effects of polarized radiation on oriented molecules). It is also possible that the area of mature scar tissue is more or less uniform, and the minor differences in intensity seen by altering the display limits are the result of slight changes in tissue thickness. While tissue sections are all theoretically 10 microns thick, in practice there are minute variations in tissue thickness across a large section like those from the rat

samples. While it is difficult to determine the amount of variation in tissue thickness, an estimate can be made. In the past, some tissues sectioned at 10 microns proved to be too thick, resulting in acquisition of poor spectra. When the same tissue was resectioned at 8 microns in thickness, the spectra were noticeably better. This leads to the conclusion that the variation in tissue thickness is probably not much worse than 2 microns, or 20%.

The levels of sugar and phosphate in the mature scar tissue were similar to those in the 21 day animals. Both the 1030 and 1080 bands mapped to collagen, as they did in the 21 day animals.

This correlation did not hold true for regions of mature scar observed to contain irregular, globular artifacts. These artifacts are either on top of, or embedded within, the tissue. Figure 28 shows photomicrograph of a group of these artifacts, along with the IR map from the same region, processed for carbonyl (1740), lipid (CH_2 symmetric stretch), and collagen (1204). The IR spectra from tissue surrounding the artifacts (green spectrum) are consistent with collagen rich spectra from developing and mature scar tissue. These spectra show normal Amide I profiles, and the characteristic set of bands at 1204, 1240, 1284, and 1338 cm^{-1}. They also have the normal doublet at 1030 and 1080, with little carbonyl (>1700 cm^{-1}) and the characteristic set of bands in the CH stretch region of the spectrum. The dense, curved bodies scatter light, making it difficult to get good quality spectra from them, but it is possible. The red spectrum is fairly normal, corresponding to spectra from regions with increased lipid content. The band at 1740 cm^{-1} corresponds to the lipid carbonyl, and the increased intensity

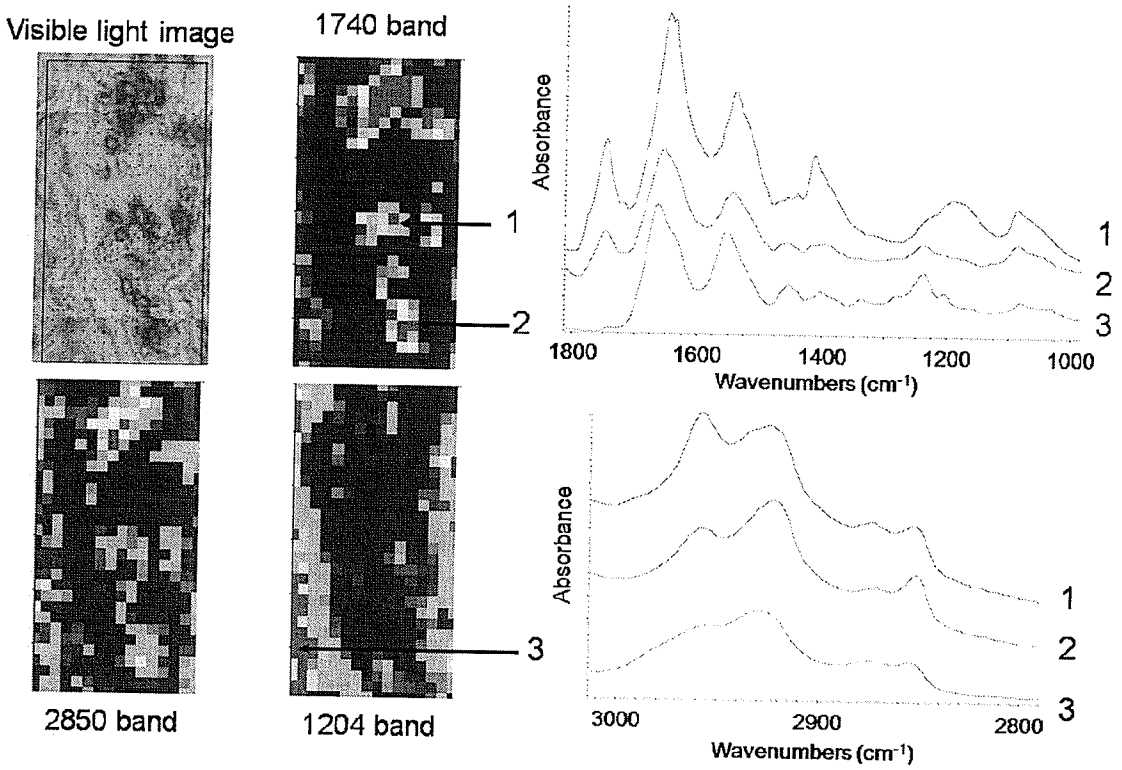

Figure 28: Tissue artifacts present in 63 day animals.
These artifacts show unusual spectra, and may be necrotic cells.

of the symmetric CH_2 band and the 1080 band are likely due to the aliphatic chains and phosphate headgroups of lipid bilayers. The purple spectrum displays spectral features that do not correspond with standard known tissue components. First, there is a very intense band at 1740 but there is little to no increase in the intensity of the symmetric CH_2 band, as seen in spectra of white matter in brain tissue. Hence, the 1740 cm^{-1} band is not the result of lipid carbonyl. In addition to this peculiarity, the bands below 1500 cm^{-1} are distorted. There is a very intense band at 1400 cm^{-1}, and the normal phosphate band at 1240 is dwarfed by a broad band centred around 1180 cm^{-1}. Finally, the shape of the 1080 is unusual. The band rises linearly starting around 1000 cm^{-1} to its maximum around 1080, and then drops off precipitously, resulting in a very unusual band shape.

3.5 Effects of Polarized Light on Oriented Samples

3.5.1 Overview

The light from a synchrotron is inherently polarized. Oriented samples can exhibit drastic changes in their infrared spectrum based on the polarization of the light source. In order to investigate the effects of polarized light on the scar tissue, samples we first examined sections of tissue from the Achilles tendon of a rat. These samples were highly oriented, and by placing some sections with the fibres running vertically and others with the fibres running horizontally we were able to examine the two extreme orientations at synchrotrons. In addition, by using a benchtop FTIR microscope equipped with a polarizer we were able to collect spectra at the same point in the tissue at ~ 22.5 degree intervals. After examining the Achilles tendon data, regions of oriented collagen fibres were sought in the developing wound area of the rats.

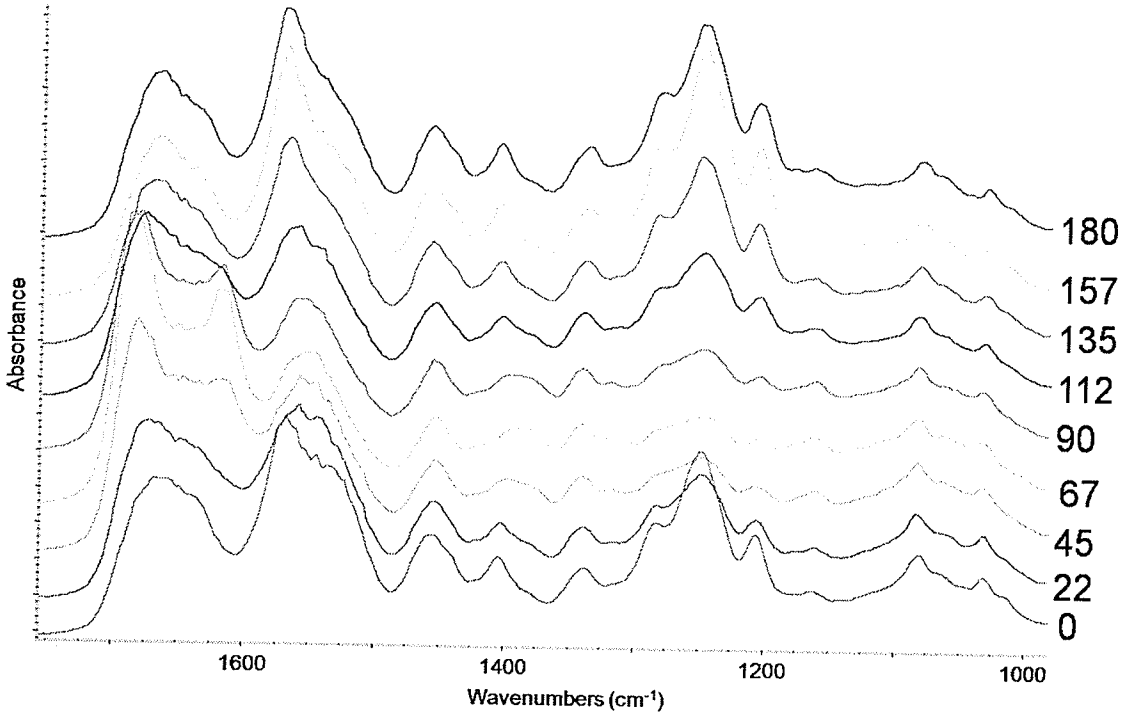

Figure 29: Polarized Spectra of rat Achilles Tendon taken at intervals of ~22.5 degrees polarization.

3.5.2 Infrared Spectra of Achilles Rat Tendon

Figure 29 shows a visible light image from vertically aligned rat Achilles tendon, as well as a group of three spectra. The red spectrum is from non oriented collagen, the blue spectrum if from vertically oriented collagen with the light polarized perpendicular to the axis of the fibres, and the purple spectrum is from vertically oriented collagen with light polarized parallel to the axis of the fibres.

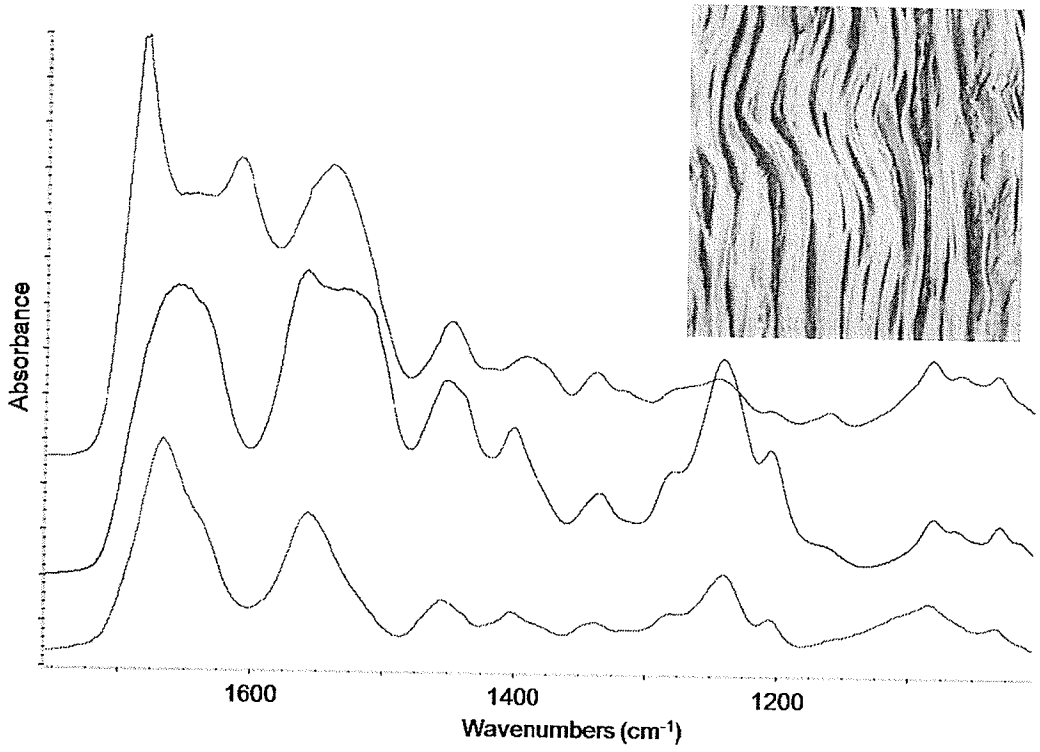

Figure 30: Infrared spectra of unoriented collagen (red), and oriented collagen in Achilles tendon parallel (purple) and perpendicular (blue) to the infrared light.

The spectra show marked differences in their band shapes. The unoriented collagen shows the characteristics expected. The most intense band is the Amide I, with a maximum around 1670 cm^{-1}, and a shoulder at 1655 cm^{-1}. Next in intensity is the Amide II, with a maximum at 1558 cm^{-1}. The collagen fingerprint consisting of the four bands at 1338, 1284, 1240, and 1204 cm^{-1} is present, with the 1240 band being more intense than the others. Finally, there is the broad band arising from the C-O-C, C-OH, and C-C ring vibrations with the two maxima at 1030 and 1080 cm^{-1}.

In the oriented sample, with the light polarized parallel to the fibres (blue), the spectral changes can be classified in two ways. First, changes in relative intensity of bands. The Amide II and Amide III bands (1560 and 1240) are now almost as intense as the Amide I band. Second, there are changes in the shape of both the Amide I and Amide II bands. The Amide I band has lost its shoulder, and is more or less symmetrical around the maximum at 1655 cm^{-1}. In addition to the changes in the Amide I band, the maximum for the Amide II band has shifted very slightly (to 1560) and it now has a broad plateau before dropping off around 1515 cm^{-1}.

When the orientation of the light is rotated by 90 degrees, there are again marked differences from both the unoriented spectrum and the oriented spectrum with the opposite polarization. The Amide band has split into two separate maxima, one local maximum occurs at 1683 cm^{-1}, the other at 1611 cm^{-1}. The Amide II band is back to a more normal appearance, although still different from that of unoriented collagen. The Amide II maximum occurs at 1540 cm^{-1}. The

other major change in this spectrum is in the region surrounding the Amide III vibration at 1240 cm^{-1}. The intensity of the 1240 cm^{-1} band has dropped drastically, and the three noticeable peaks that existed at 1284, 1240 and 1204 are now brought, not well defined series of shoulders.

When spectra were collected from horizontally aligned fibres, the results were reversed. The polarized light that had been perpendicular to the fibres was now parallel, and the light that had been parallel was now perpendicular. The two spectra collected at 0 and 90 degrees for the horizontal tissue looked the same as the ones collected at 90 and 0 degrees for the vertically aligned tendon. Spectra taken on vertically aligned tendons at SRC indicated that the light from the synchrotron was oriented perpendicularly to the vertical tendons. This orientation is characteristic of the synchrotron at SRC and may not be the same for other synchrotrons.

3.5.3 Evidence for Oriented Fibres in Wound Healing Areas

After determining the effects of polarized light on oriented fibres, maps collected from the rat scar tissue were re-examined to look for spectroscopic evidence of oriented fibres. Serial sections stained with Picrosirius red, a dye that binds to interstitial fibrillar collagen. Fibres stained with Picrosirius red will display a birefringence under polarized light. Once suitable fibres had been found in the serial sections, the sections mapped by IR spectroscopy were examined to see which sections had maps collected near fibrillar collagen shown by the stained serial sections. By taking the ratio of the Amide I and II bands, it was possibly to map out the oriented collagen fibres. Figure 31 shows a photomicrograph taken with visible light, the Picrosirius red stained serial section, as well as the infrared map processed for collagen and the Amide I to II ratio showing the collagen fibre running through the map. Since the fibre is not running precisely along an axis, the spectral differences are not nearly as pronounced as they are in the model system of the rat Achilles tendon. While the Picrosirius red stain clearly reveals the presence of well-developed, well-oriented collagen fibres, the IR data provides additional information on the presence of less developed, non fibrous collagen. IR spectroscopy indicates low levels of collagen, of a less oriented nature as shown by the high Amide I to Amide II ratio, throughout the tissue that the Picrosirius red stain does not reveal.

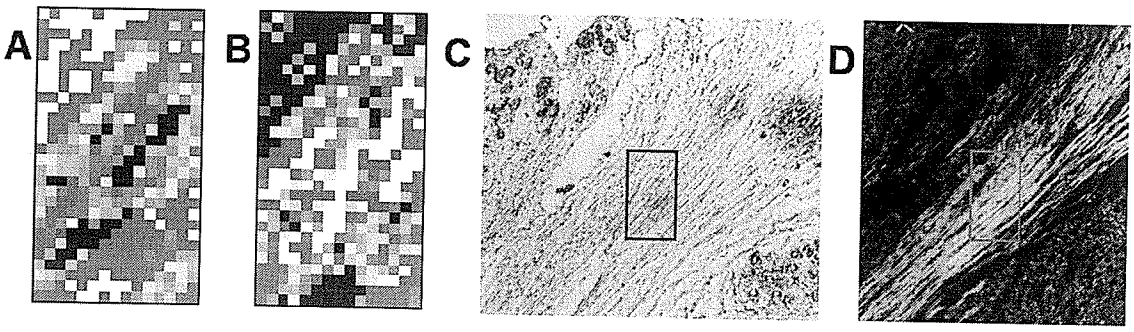

Figure 31: Oriented Collagen Fibres in Rat Wound Healing areas.

IR images showing collagen (A), Amide I to Amide II ratio (B), visible light image (C), and Picrosirius red stained image (D).

Chapter 4: Discussion

4.1 Overview

The discussion is broken up in two main sections: 1) Tissue Morphology and Visual Differences, and 2) Infrared Data Analysis.

The wound healing process can be divided into three overlapping stages (Section 1.3). The tissue making up the wound area undergoes significant alterations in its composition and morphology throughout the wound healing process. Chronologically, the three stages of wound healing are:

1) The inflammatory stage, lasting from 0-3 days post injury,
2) The granulation stage, lasting from 2-6 days post injury, and
3) The remodelling phase, continuing until 21 days post injury, or even longer.

In the initial proposal, we had planned to investigate animals sacrificed 1 day (beginning of inflammatory phase), 3 days (end of inflammatory stage, beginning of granulation phase), 21 days (remodelling phase), and 63 days (end of remodelling) after surgery. In practice, the 1 day animals had not healed sufficiently to facilitate the differentiation of wound area from surrounding muscle tissue, and the harvesting of tissue proved problematic. This issue resulted in only three time points (3, 21, and 63 days post surgery), but these three time points still provide a reasonable timeline of the wound healing process.

The first section deals with the visual appearance of the sections based on age, treatment type, and acquisition period. The second section discusses the IR results in the context of the wound healing process.

The animals were acquired in three different batches. The first batch of animals consisted of a total of 12 animals, 6 three day animals (two of each treatment type), and 6 twenty-one day animals. These animals were acquired in 2003, and are designated Set 0. Unfortunately, the serial sections of these animals were lost at the University of Saskatchewan, and no immunohistochemistry was ever done on them. Visually and spectroscopically these animals were similar to the Set I animals.

The second batch of animals consisted of 18 animals, 9 three day animals (three of each treatment type) and 9 twenty-one day animals. These animals were acquired in 2004, and mapped extensively at synchrotrons (SRC and NSLS) during that year. These animals were designated as Set I animals.

The final batch of animals was the largest, consisting of 36 animals. These animals included 9 three day animals and 9 twenty-one day animals, to bring the total number of animals at each of these age/treatment combinations to 6. In addition, this batch contained all 18 of the sixty-three day animals (six for each treatment group). The three and twenty-one day animals from this batch were designated as Set II animals, and deviated a lot in appearance from the Set I animals.

In addition to these two larger sections, there are smaller sections discussing the observed effects of the treatment types on the wound healing process, possible future work including additional data collected on a new Varian IR FPA microscope, and a brief discussion of some immunohistochemistry of Smad proteins conducted at the University of Manitoba.

4.2 Visual Appearance of Control and Treated Animals

4.2.1 Three Day Animals

The 3 day animals represent a time point encompassing the end of the inflammation phase and the beginning of the granulation phase (Singer, A. J. 1999). At this point, there should be a large amount of cellular material (neutrophils, monocytes, and macrophages) involved in cleaning out the wound, as well as by-products of cellular necrosis. There should be little collagen present in the 3 day animals, and what collagen there is in the wound healing area will likely be found in small pools, instead of oriented fibres (see section 1.4).

One potential feature, observed in a morphological examination of the tissue sections, is the presence of a band of fibrous tendon penetrating through the middle of the wound. This fibrous tendon runs along the surface side of the section, just under the skin, in healthy tissue (Figure 16a). Prior to suturing the wound closed, the flaps of skin were folded into the wound, and the wound was then closed. This procedure introduced a collagen rich tendon into the middle of our wound healing area. While the tendon itself is usually easily visible, it is possible that small parts of the tendon might break off from the larger portion, and lose their visual distinctiveness, resulting in regions showing collagen in their IR spectra, even though the collagen is not strictly speaking from the wound healing process.

Set I vs Set II Animals: In the three day animals, there were some minor differences between the Set I and Set II animals. The primary difference is that the Set II animals have more surrounding intact muscle tissue than do the Set I animals. The wound healing area in both animals appeared disorganized, and the contrast between wound healing area and surrounding muscle tissue was less obvious, especially in the Set I animals.

One concern with the Set I and Set II animals is the length of time between their acquisition. In an ideal situation, the animals comprising one age group would all come from the same litter, to minimize the effects of genetic variability on the healing process. Given the size of the groups, it would be difficult, but having a group of animals born around the same time, having their surgeries performed at the same time, and healing at the same time, is more controllable than having two groups of animals separated by 2 years.

Treatment Groups: There is little to visually differentiate a saline control from an OTC or quercetin treated animal. While the major inflammatory processes occur during the early days of wound healing (Park, J. E., 2004), it is possible that the treatments require more time to provide noticeable changes, either because of metabolism or the chance that any decrease in inflammatory effects at this stage is felt more acutely later in the wound healing. In retrospect, it would have been interesting to include another time point between the 3 and 21 day animals (e.g. 10 or 12 days post surgery) to see if there were any changes later in the early stages of the wound healing process.

4.2.2 Twenty-One Day Animals

The animals sacrificed 21 day days after surgery should have been in the remodelling phase of the wound healing process (Singer, A. J. 2004). At this point, the initial cellularity should have decreased, as the inflammatory cells in charge of cleaning out the wound complete their functions and die off, and the initial granulation tissue composed primarily of type III collagen and various sugar molecules should have been replaced by type I collagen (see section 1.4).

From a visual inspection of the tissue, there are three main points to be addressed:

1) The marked difference between the Set I and Set II animals,
2) There is evidence that tissue harvesting may have been poorly done, leading to incomplete sections, and
3) There are the differences between age groups and treatment types to be discussed.

Set I and Set II animals: The differences between the Set I and Set II animals 21 days post surgery were obvious. The animals from Set II showed a significantly lower proportion of wound area.

Table 4: Percentage of Scar Area in Set I and II Animals at 21 Days

	Saline	OTC	Quercetin
Set I	75-90%	30-60%	33-60%
Set II	25-33%	25-30%	25-30%

The 21 day animals from Set I were almost entirely wound area, consisting of broad swaths of collagen, with only small amounts of intact muscle cells along the edges. In contrast, the saline control sections from Set II did not have the same large areas of scar tissue, being only about 30% scar, and having a large amount of surrounding muscle cells on either side of the wound healing area.

The story is similar for both the OCT and quercetin treated animals. For both treatment subgroups, 30-60% of their sectioned area consisted of scar tissue in the Set I animals, and only 25-30% of the Set II animals consisted of scar tissue.

Incomplete Tissue Harvesting: There are two concerns with the tissue harvesting. First, for the Set I animals, there is little to no muscle tissue surrounding the wound healing area. Without surrounding muscle tissue to delineate the wound healing area, it becomes very difficult to make accurate comparisons between the animals. There is no way of knowing if all the wound healing area was harvested from the animal or if some of it was left behind.

The animals from Set II also showed signs of incomplete tissue harvesting. While there was plenty of surrounding muscle tissue, the sections looked incomplete, especially around the central portion of the section (i.e. the wound healing area). Figure 22B shows an image of a Saline control animal from Set II, and the section narrows dramatically in the wound healing area. The narrowing may have resulted from the method in which tissue was harvested. According to N. Cox (M. Sc., University of Saskatchewan, 2008), the rat was placed on its

back, and an incision was made in the stomach. The interior organs were removed, and the scar tissue was separated from the spine by excision with a scalpel. According to our collaborators in Saskatchewan, separating the tissue from the spine was difficult, and it is hypothesized that some of scar tissue from the wound area remained attached to the spine and was lost. The incompleteness of tissue sections is also apparent in the 63 day animals, and since tissues from the 63 day animals were all acquired by the same person, one of the variables is removed and it is possible to look at some sections that seem intact and others that are not (Section 4.2.3).

Treatment Groups: Based on the visual assessment, there is some evidence for the reduction of scar tissue in the treated animals from Set I (see Table 4), but without surrounding muscle cells to delineate the wound area, there is insufficient evidence to draw any meaningful conclusions. The Set II animals show similar amounts of scar tissue across all three treatment types, but the appearance of the tissue suggests that not all the scar tissue from the wound area is present in the sections. The difference between the two sets of animals, and the animal to animal variation within a set and treatment group, make it difficult to determine whether there are significant differences between the treatment groups.

4.2.3 Sixty Three Day Animals

The animals sacrificed 63 days post-surgery were in the final stages of the wound healing process (Singer, A. J. 2004). From 21 days onwards, the major change in the wound area will be contraction of the wound. This should result in a smaller wound area, and more oriented collagen fibrils (section 1.4).

Unlike the 3 and 21 day animals, the 63 day animals were all obtained at one time, which eliminates any variability caused by having different personnel involved in tissue harvesting. While having all the surgeries, tissue harvesting, and sectioning performed by one person removed the variability inherent in having these tasks performed by multiple personnel, problems arise if the tissue is not harvested properly. The main problem in the 63 day animals is the incompleteness of some of the sections. In addition to the incompleteness of sections, there are the irregular ovoid shapes in the tissue, not seen in the 3 or 21 day animals.

Incomplete Tissue Harvesting: Figure 32 shows photomicrographs of all 18 animals in the 63 day age group. Some of the sections, including Saline 31, OTC N17 and N19, and Quercetin N7 and N11 look complete. They have a small scar area relative to the 21 day animals, and it is shaped somewhat like a butterfly (outlined in blue). The scar area is concentrated in the centre, but also branches out along the outer surface (underneath the skin) of the animal. There is some muscle on either side of the scar, although the amount varies. These are

good, intact sections. However, some of the sections are missing entire regions of the tissue. Looking at Saline N27, there is a large amount of muscle on one side of the scar, and a small amount of scar, but there is no muscle on the other side of the scar. It is impossible in a situation like this to say whether or not all the wound area was harvested. Even worse is a situation like OTC N15, where there is sufficient muscle tissue, but a blank hollow where one would expect the scar tissue to be. The two halves of muscle are not even connected. It is apparent that important regions of scar tissue are missing and were likely destroyed during the tissue harvesting procedure. Intra-group variations were as great or greater than inter-group variations, preventing the formation of conclusions on the efficacy of the treatment groups.

Irregular Ovoids: Visual inspection of the 63 day animals revealed the presence of irregular ovoids in some of the sections. These anomalies were not present in any of the 3 or 21 day animals, but they were also not present in every 63 day animal. They are likely necrotizing cells, and will be discussed in the context of their IR spectra in Section 4.3.3.

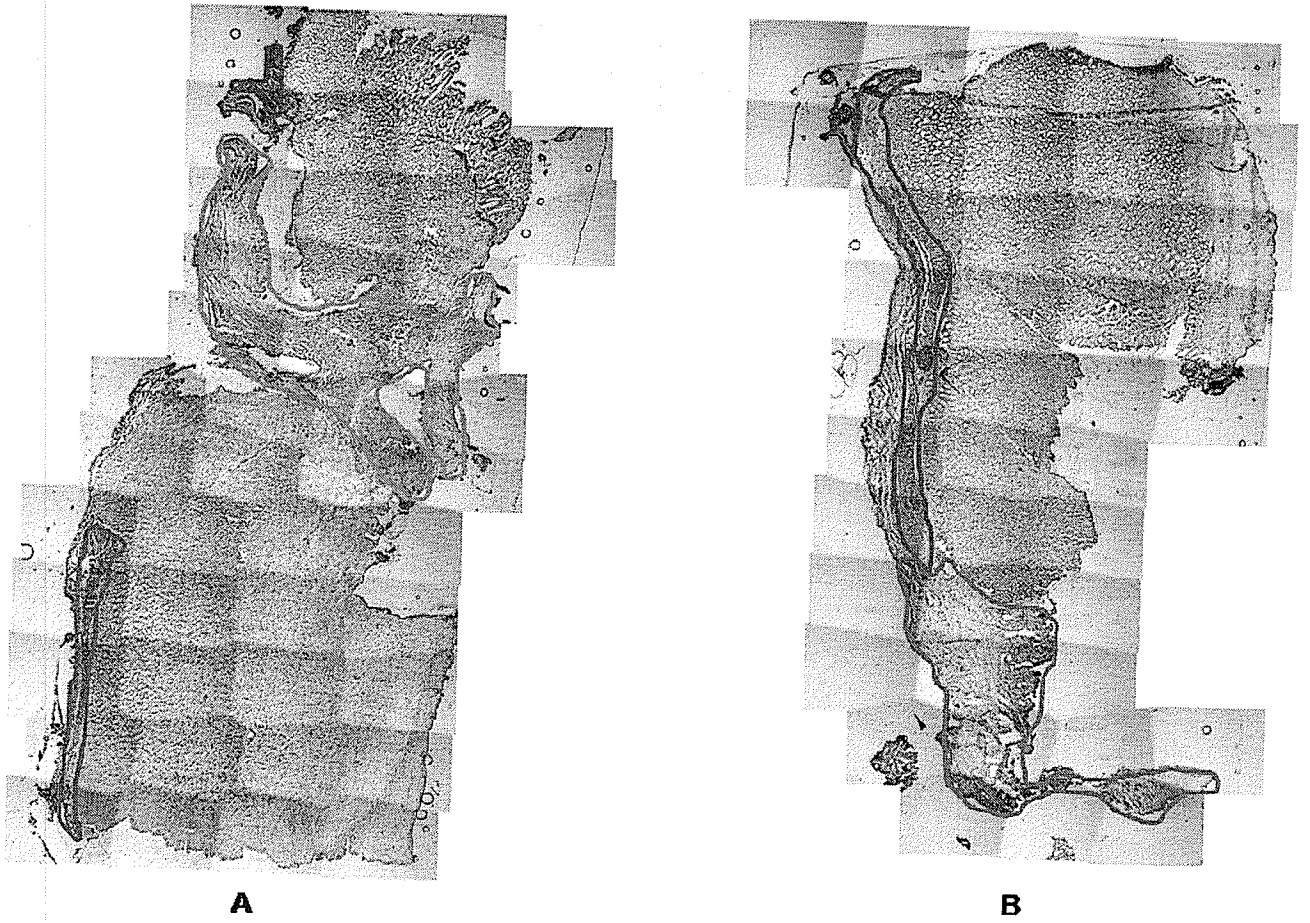

Figure 32.1: 63 Day Saline N25 (A) and N27 (B). Scar Tissue outlined in blue. Red outlines denote fibrous tendon present in healthy animals.

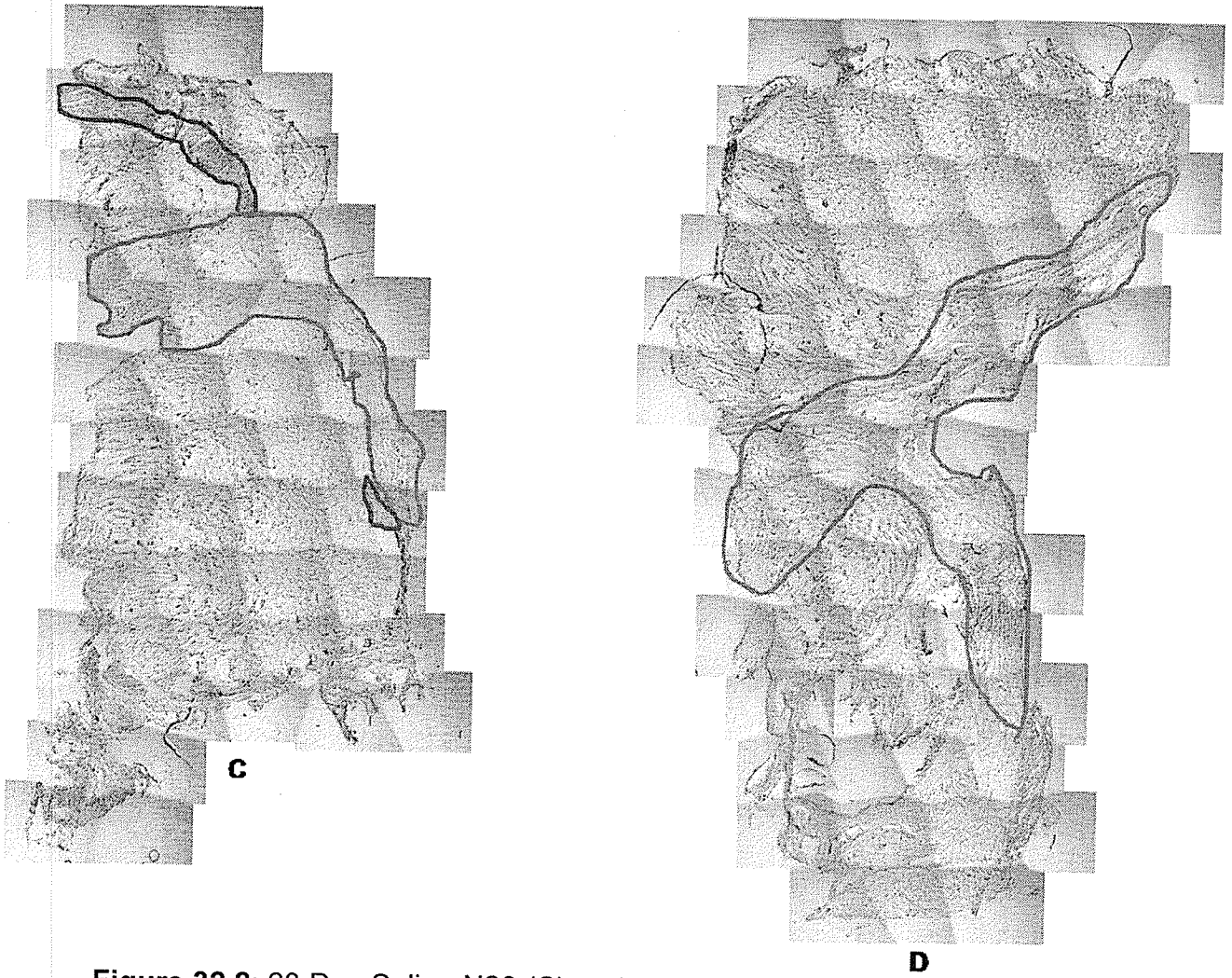

Figure 32.2: 63 Day Saline N29 (C) and N31 (D). Scar Tissue outlined in blue. Red outlines denote fibrous tendon present in healthy animals.

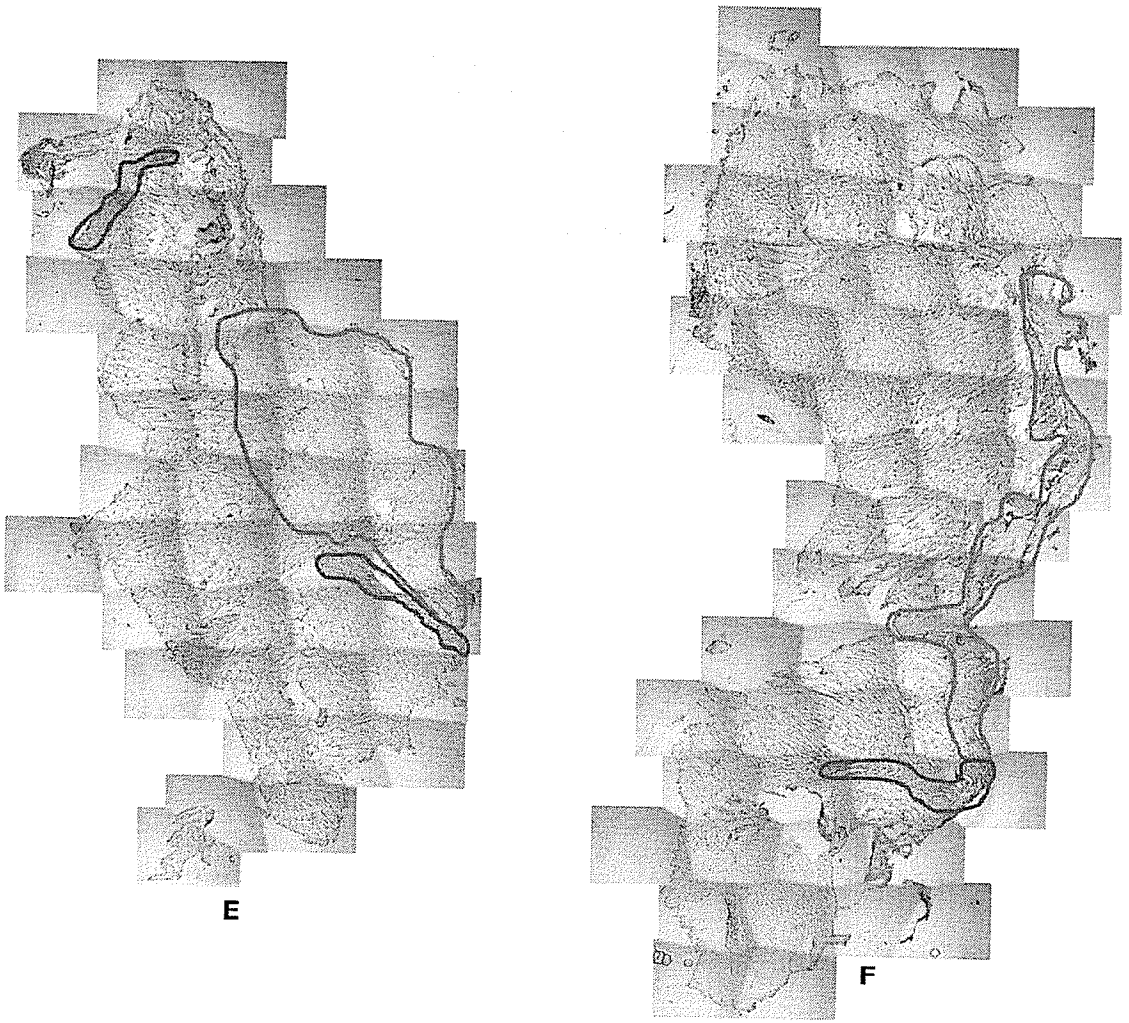

Figure 32.3: 63 Day Saline N33 (E) and N35 (F). Scar Tissue outlined in blue. Red outlines denote fibrous tendon present in healthy animals.

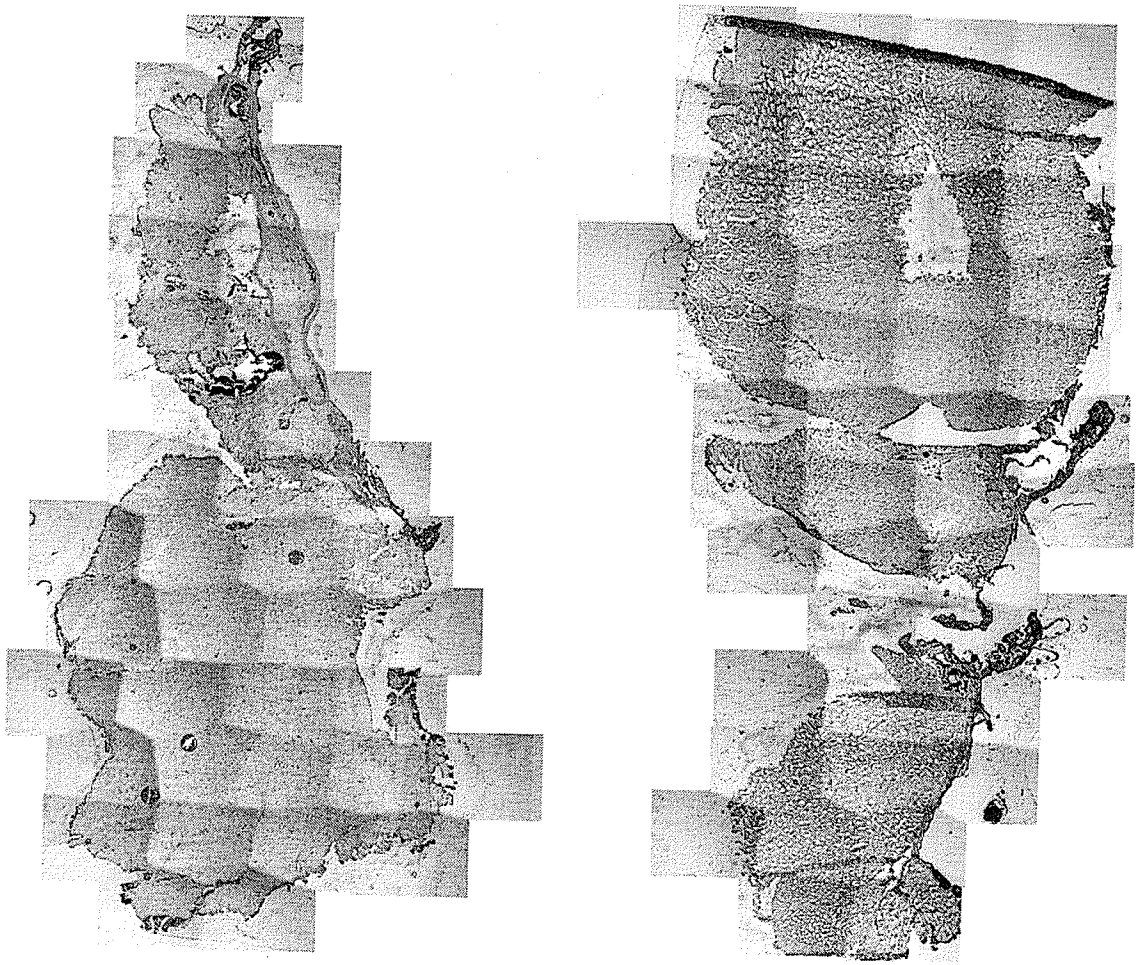

G H

Figure 32.4: 63 Day OTC N13 (G) and N15 (H). Scar Tissue outlined in blue. Red outlines denote fibrous tendon present in healthy animals.

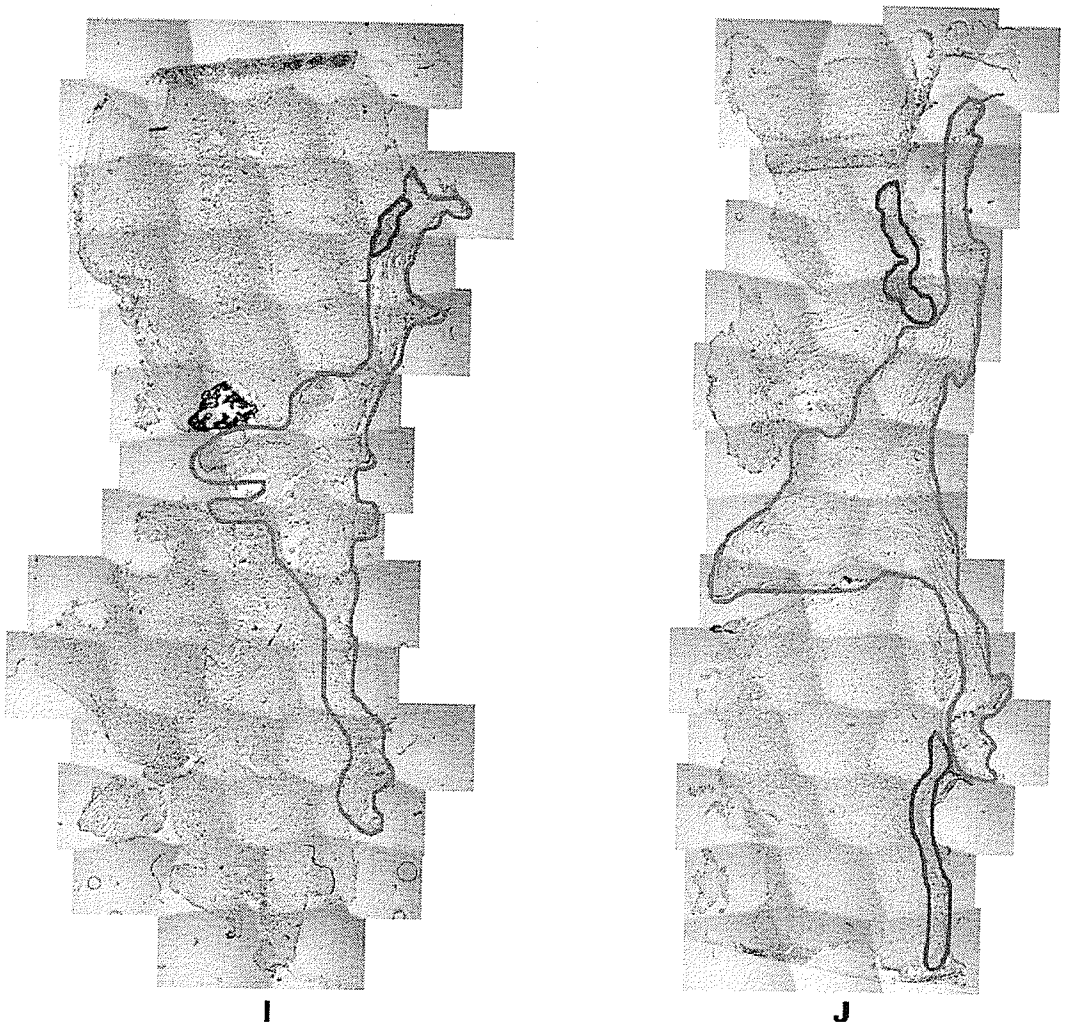

I J

Figure 32.5: 63 Day OTC N17 (I) and N19 (J). Scar Tissue outlined in blue. Red outlines denote fibrous tendon present in healthy animals.

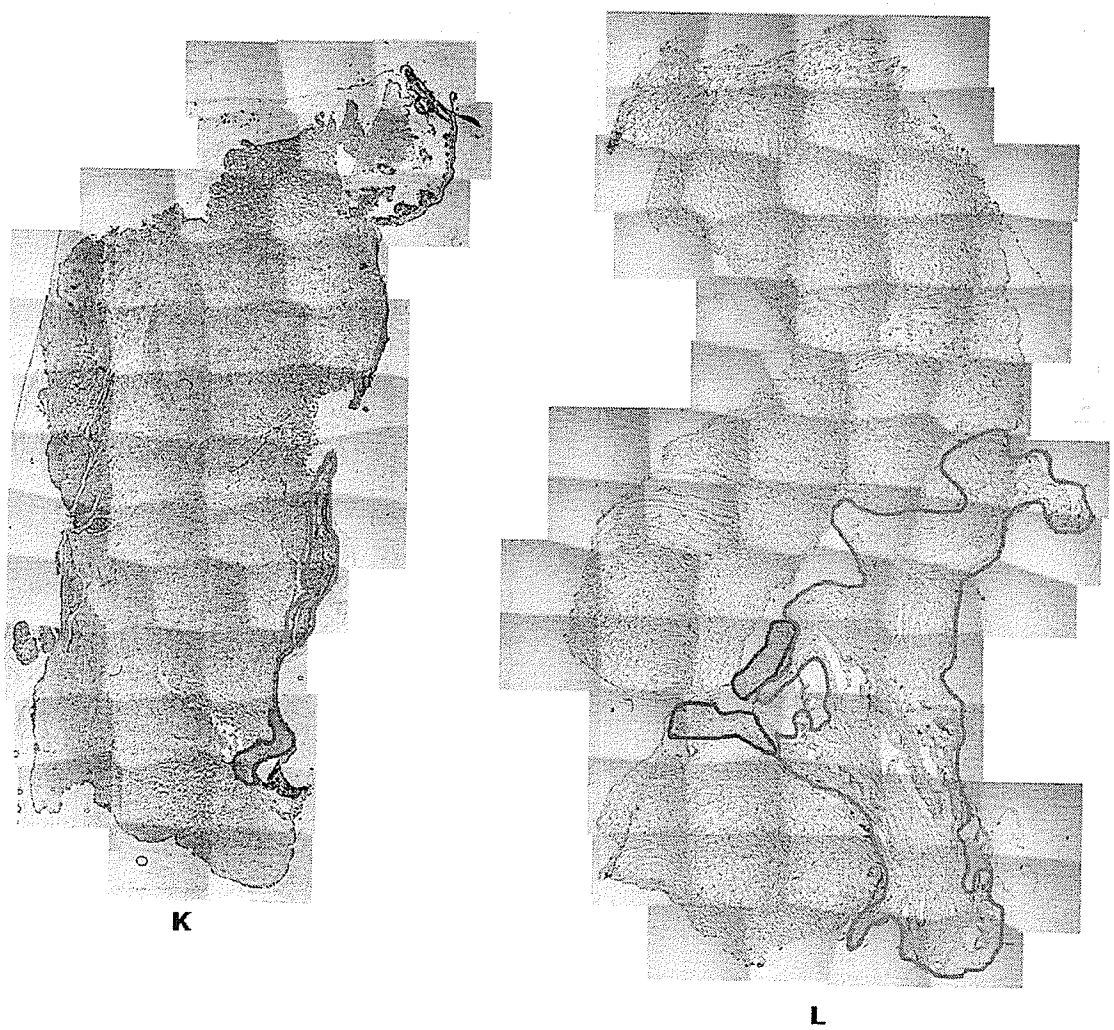

Figure 32.6: 63 Day OTC N21 (K) and N23 (L). Scar Tissue outlined in blue. Red outlines denote fibrous tendon present in healthy animals.

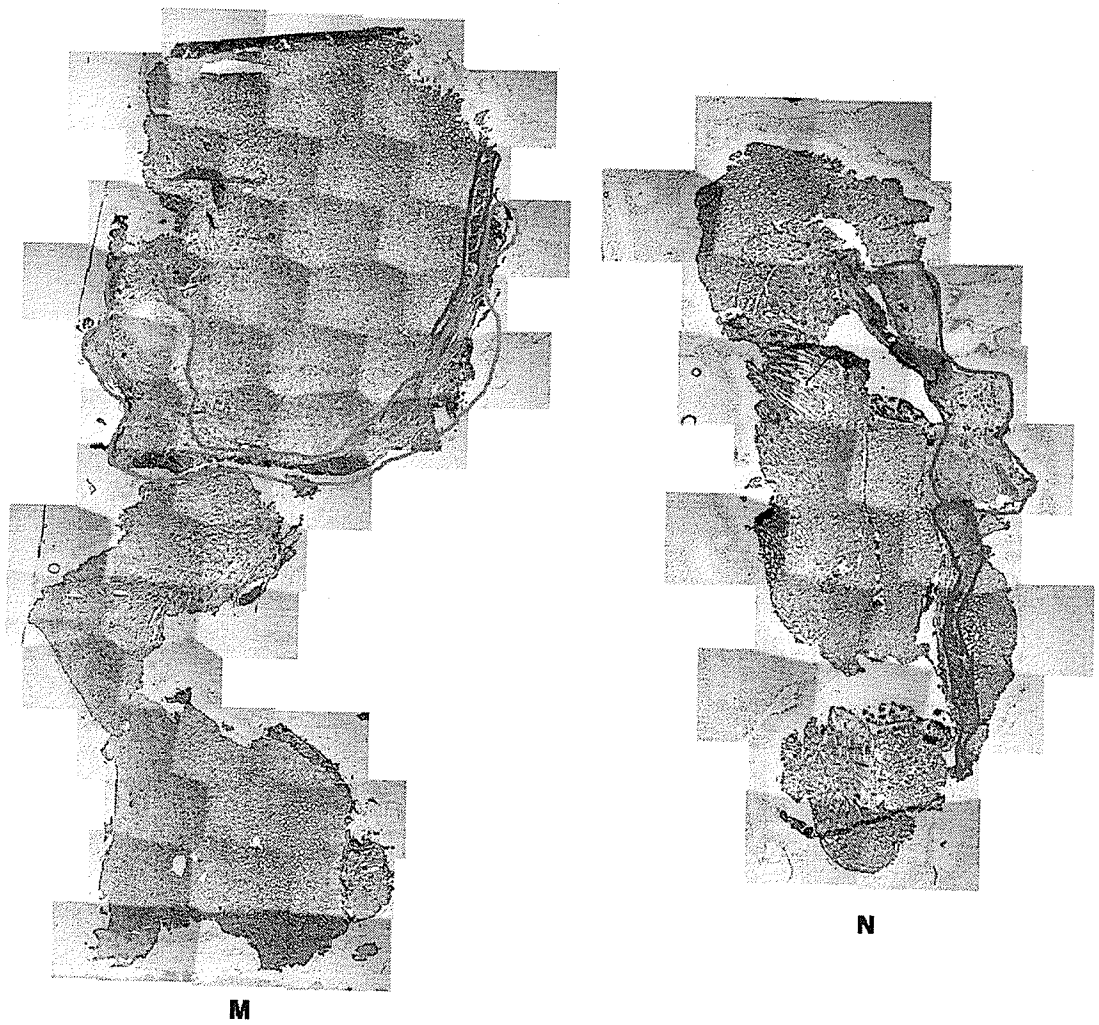

Figure 32.7: 63 Day quercetin N1 (M) and N3 (N). Scar Tissue outlined in blue. Red outlines denote fibrous tendon present in healthy animals.

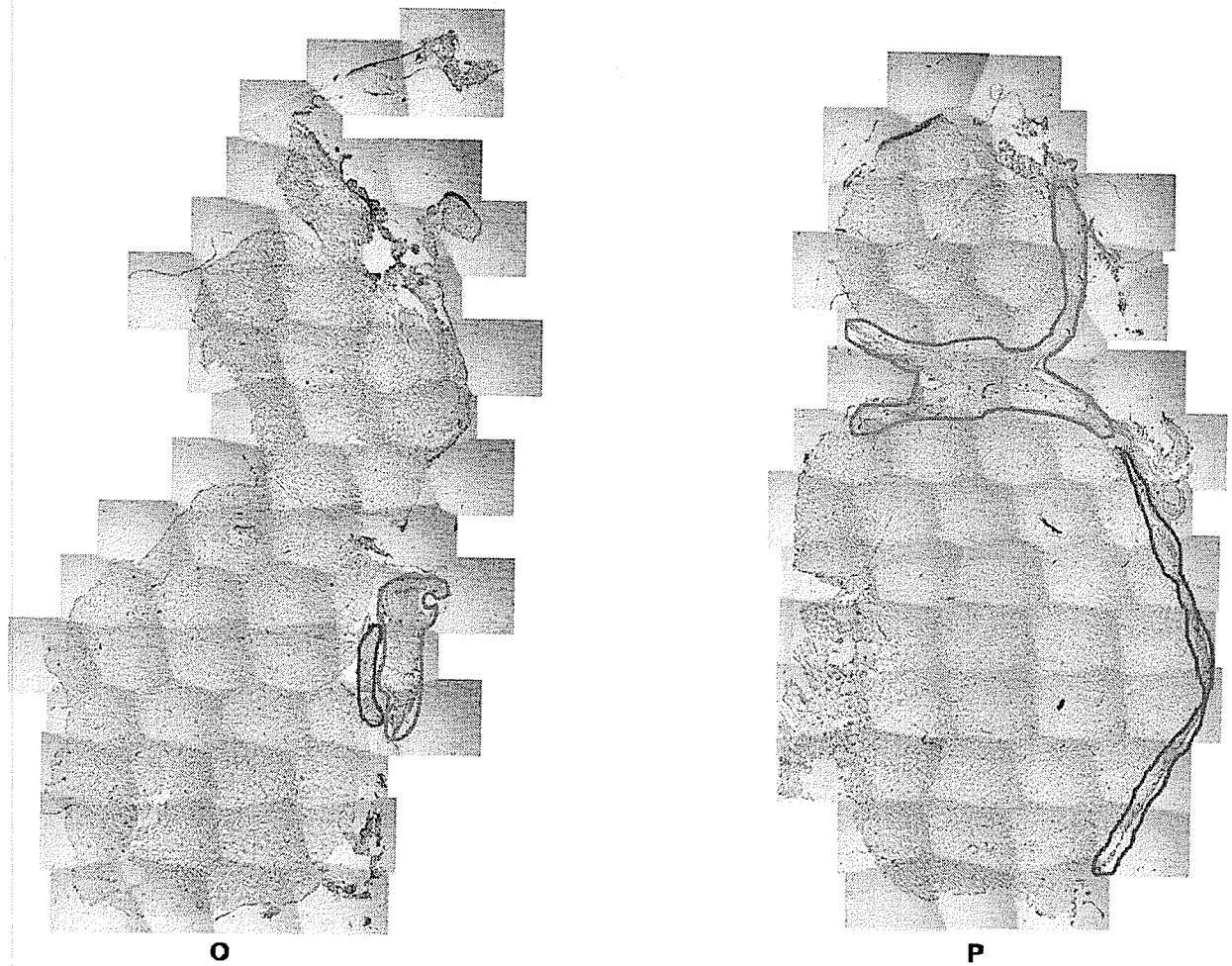

Figure 32.8: 63 Day quercetin N5 (O) and N7 (P). Scar Tissue outlined in blue. Red outlines denote fibrous tendon present in healthy animals.

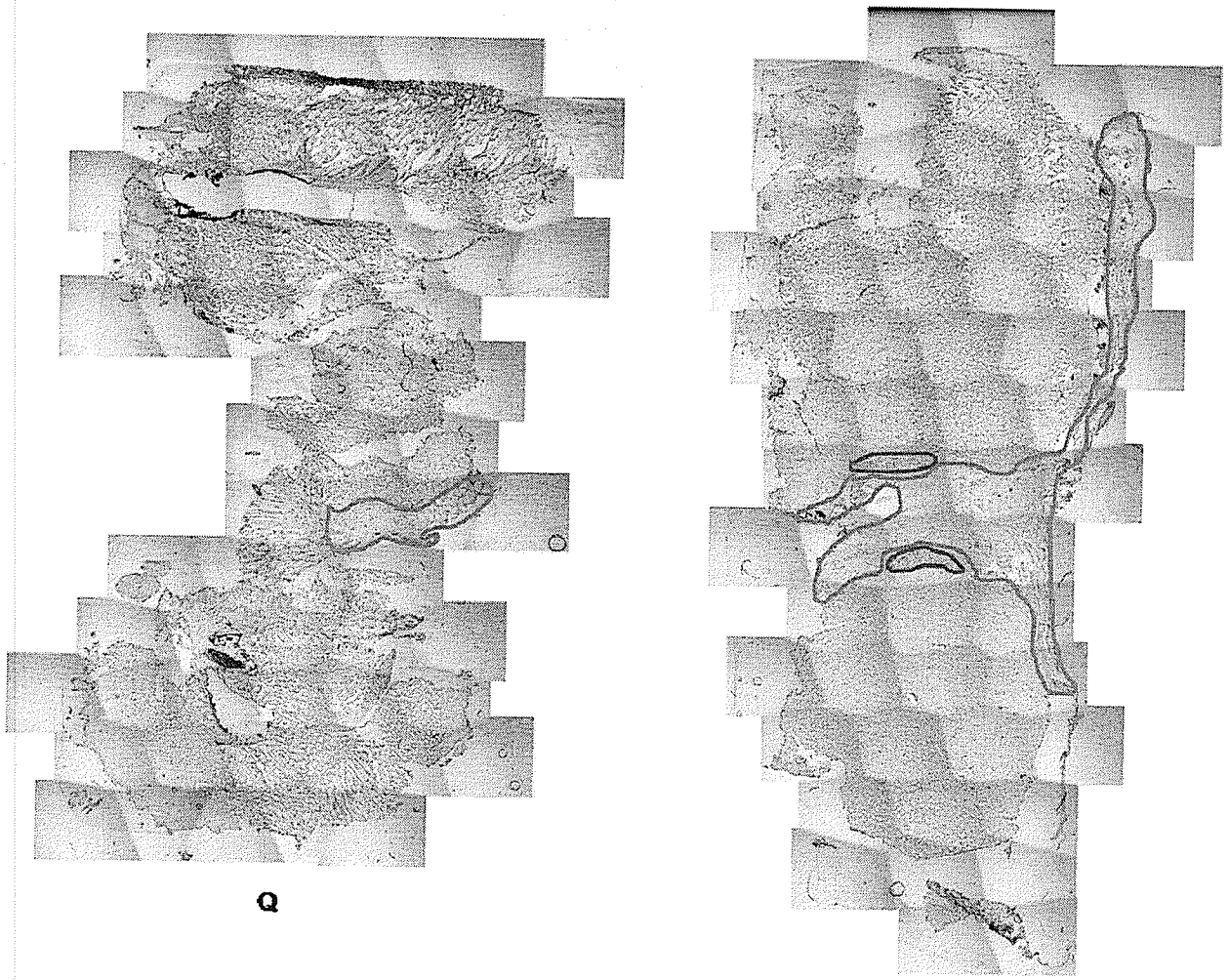

Figure 32.9: 63 Day quercetin N9 (Q) and N11 (R). Scar Tissue outlined in blue. Red outlines denote fibrous tendon present in healthy animals.

4.3 Infrared Data and Its Correlation with the Wound Healing Process

4.3.1 Three Day Animals

The infrared data from the 3 day animals indicated an increase in the number of CH_2 groups relative to CH_3 groups, as well as an increase in the intensity of the symmetric phosphate vibration at 1080 cm^{-1}. There were isolated amounts of collagen in the nascent wound area.

The 3 day animals represent a time point encompassing the end of the inflammation phase and the beginning of the granulation phase. At this point, there should be a large amount of cellular material (neutrophils, monocytes, and macrophages) involved in cleaning out the wound, as well as by-products of cellular necrosis (Monaco, J. L. 2003, O'Leary, R. 2002). The increased intensities of the CH_2 and symmetric phosphate vibrations are likely the result of the increased cellularity present in the early stages of wound healing. The phospholipids that make up the lipid bilayer of the cellular membrane have a high CH_2 to CH_3 ratio as a result of their long hydrocarbon tails, and their phosphate headgroups could account for the increased intensity of the symmetric phosphate stretch at 1080 cm^{-1}.

The presence of collagen in the 3 day animals has two possible explanations. First, the 3 day animals fall right at the beginning of the granulation phase, during which type III collagen is deposited along with many other molecules including proteoglycans (O'Leary, R. 2002). Type III collagen is a homotrimer of three α1(III) chains (Kadler, K. 1994). The differences between the amino acid sequences of the α1(III) chains that make up type III collagen and the

two α1(I) and α2(I) chains that make up type I collagen are insufficient to allow for spectroscopic differentiation between the two (Figure 13). Some of the animals may have healed faster than others. These animals would be further along in the wound healing process, resulting in the formation of some type III collagen. The phases of wound healing are not absolutely separate: the granulation phase can begin as early as two days after injury and persists for up to a week after injury (O'Leary, R. 2002, Singer, A. J. 1999). Human beings certainly show variability in the time required to recover from an injury. For example, an athlete may be given a progress of 4-6 weeks to recover from a broken leg. The variation in individual healing rates among a group of animals is of particular concern given that the three day animals were acquired in two separate groups, almost two years apart. The animals were not littermates, and thus the two sets of animals have the potential for greater variations in individual healing rates.

The other potential explanation for finding collagen lies in the post surgical techniques used to close the wound. As mentioned in Section 4.2.1, the skin was folded into the wound, leading to part of the collagen rich, fibrous tendon being introduced into the wound area. While this feature is usually visible and could be identified in mapped areas showing collagen, it is possible that smaller pieces of the tendon could break off the main portion and lose their distinctive appearance.

4.3.2 Twenty One Day Animals

The infrared spectra from 21 day animals show a significant amount of collagen throughout the wound area in all treatment groups. The IR spectrum of collagen is diagnostic for the protein conformation and structure at many levels of organization. The primary structure of a protein is given by the sequence of amino acids that make up the protein. In the case of collagen, this would be the amino acid sequence of one of the three individual helices that make up the collagen triple helix. Secondary structure refers to the general three dimensional shape formed by a sequence of amino acid sequence. For collagen in scar tissue, this would be the left handed helical secondary structure. The tertiary structure of a protein is similar to secondary structure, but includes specific coordinates in three dimensional space for the individual atoms that make up the protein. Quaternary structure is the aggregation of secondary structures into a super structure. In the case of collagen, the quaternary structure consists of three left handed helices wound around each other and stabilized by hydrogen bonds to form a right handed super helix. The formation of large collagen fibres, composed of individual collagen molecules joined by crosslinks (See Section 1.1.2), is another level in the structural pyramid, and it is this level of structure that begins to become noticeable in the 21 day animals. In the 21 day animals, there was a noticeable tendency for the collagen to form localized clusters of parallel fibres running through the tissue. These fibres can be seen in the false colour images generated from the infrared data, where bands of high collagen content can be seen to traverse a map in a linear fashion (Figures 23 and 30).

Due to the similarity of many functional groups, most biomolecules will have similar, and overlapping, spectra. It is important to look at the entire spectrum to deduce which components are present in the mapped area. In the case of our tissue, where the major components are collagen, cellular material, and a variety of extracellular matrix molecules, there are subtle ways of distinguishing the major components of an individual spectrum. Both collagen and cells have bands around 1240 cm^{-1}. In cells this is the result of an asymmetric stretching of the phosphate group, while the collagen band is the result of vibrations from the peptide backbone. The spectra will differ in the CH stretching region of the spectrum. This provides us a valuable tool in separating regions rich in cellular material from those composed primarily of collagen. In addition, if the spatial resolution is sufficient, one can determine which part of a cell is being imaged. The nucleus of a cell will have significant IR contributions from the DNA and RNA in the fingerprint region, but only minor absorptions in the CH stretching region of the spectrum. A spectrum recorded of the cellular membrane will have a significantly greater absorption in the CH stretching region of the spectrum, as result of the long hydrophobic chains making up the phospholipid bilayer of the cell. The amount of cellular material, as monitored by the area of the CH_2 band and the symmetric phosphate band, has decreased relative to that of the 3 day animals. There are still pockets of cellular material, indicated by localized increases in the intensity of the CH_2 and 1080 bands. With the reduced cellularity in the 21 day animals, images created of the total area from 1014 to 1130 cm^{-1} (our initial parameters for sugar) look similar to the

images created based on the 1024 band. This suggests that outside of localized regions of high cellularity, the level of phosphate is mostly constant throughout the wound area, and changes in this region of the spectrum are the result of glycosylation of maturing collagen fibres. Collagen contains both mono and disaccharides covalently linked to hydroxylysyl residues (Section 1.1). The role of these glycosyl groups is not well understood, but they are thought to play a role in modulating the diameter of collagen fibrils.

4.3.3 Sixty Three Day Animals

The absorbance of the 1204 band, used to evaluate collagen levels, is increased in the 63 day animals relative to that in the 21 day animals. This increase is presumably the result of the maturation of the collagen fibres in the scar tissue. More mature fibres could be thicker and/or more oriented, increasing the total absorbance, and the area under the band.

The levels of lipid and phosphate remained about the same as they were in the 21 day animals, and showed little variation among treatment groups at 63 days post surgery, but these conclusions are limited by the variability of the samples, and the likelihood of missing tissue from the wound area, as described in section 4.2.3.

A major point of interest in the 63 day animals was the presence of irregular ovoid shapes found in the tissue. These objects are likely the remains of cells (probably collagen producing fibroblasts) that have died via necrosis.

The cellular debris is likely the remains of fibroblasts, since if they were the remains of cells involved in the early stages of wound healing, they would presumably have been found in the 21 day animals as well.

The hypothesis that they are the result of necrosis, instead of apoptosis, comes from the fact that they are still present in the tissue. If cells undergo apoptosis (programmed and regulated cell death), the debris left by the dead cells would normally be removed by phagocytosis (Alberts, B. 2002). Necrosis is the premature death of cells, and is caused by outside factors such as infection,

cancer, infarction, poisons or inflammation. Unlike cells that undergo apoptosis, necrotic cells do not release the same chemical signals, and thus are not normally found by phagocytes, leading to a build up of dead tissue and cellular debris at the site of cell death.

There is little evidence in the infrared spectra for a dramatic increase in the degree of orientation of collagen fibres in the 63 day animals. While it is expected that the fibres become more oriented during contraction of the wound during the remodelling phase (O'Leary, 2002), the fibres will still be less oriented than those in the Achilles tendon, which was used as a model for orientation studies. It is also more difficult to align any potentially oriented fibres in the wound area with the synchrotron light. The stage of the IR microscope at SRC, where most of the data was collected, provides limited rotational capabilities making it difficult to align to align fibres that are not vertically or horizontally oriented relative to the microscope slide. Oriented fibres in unstained tissue are also not usually visible under white light microscopy. Only once the IR data has been collected, can one see the collagen fibres present in the IR maps.

4.4 Effects of OTC or Quercetin Treatment on Wound Healing

My goals were a) the determination of the effects, if any, of OTC and quercetin treatments on the wound healing process, and, b) to compare the effects between treatment groups and over time. These goals have been complicated by the variability among animals within the individual groups and the variations among the Set I and II animals from the 3 and 21 day groups. The three techniques used to evaluate the treatments were infrared spectroscopy (this thesis), the generation of RNA probes by in-situ hybridization methods (Suraj Abraham, Ph. D Thesis, University of Saskatchewan), and conventional immunohistochemical methods (Nicole Cox, M. Sc Thesis, University of Saskatchewan).

While there are noticeable differences in the IR spectra among animals sacrificed at different time points, there is little spectroscopic evidence of differentiation between the animals of any one of the time points on the basis of treatment groups. Tissue sections for each of the different animals have regions that yield infrared spectra similar to those from another region in an animal that has undergone a different treatment. Among the 21 day animals in Set I, there seems to be some evidence for less scar tissue present in the OTC and quercetin treated animals compared with the saline controls, but the lack of surrounding muscle tissue in the saline animals makes confident assessments of the amount of scar tissue present in the individual sections difficult. There does not seem to be a corresponding difference in the 21 day animals from set 2, although the state of the tissue sections again makes it difficult to make this statement with a large degree of confidence.

4.5 Immunohistochemistry

4.5.1 Introduction

Immunohistochemistry (IHC) is the localization of proteins in tissue sections using the principle of antibodies binding to antigens (Ramos-Vara, 2005). IHC is used in the diagnosis of abnormal cells such as those found in cancerous tumours, and in research in chemistry, biochemistry, and microbiology to investigate the distribution of proteins in different types of tissue.

IHC is performed on thin sections (~10 micron thickness) of tissue that are cut from either frozen tissue blocks or tissue blocks embedded in paraffin, using a microtome. The first step in an IHC protocol usually involves fixation of the tissue by either chemical or physical methods. Fixation of tissue sections results in the stabilization of the sections by halting enzymatic decay and formation of crosslinks among protein molecules, leading to hardening of the tissue (Hayat, MA. 2002). Following fixation, tissues are treated with a detergent to rupture the cellular membranes and allow the antibodies easier access to the targets of interest. Treatment with a detergent also reduces hydrophobic interactions between the tissue and reagent proteins. After rupturing the cellular membranes, the sections may be treated with a blocking antibody to prevent non specific binding of the antibody. The blocking agent, typically skim milk, or a generic protein such as bovine serum albumin, will bind to the available sites, but its affinity for the antigens of interest will be less than that of the antibody. This lower

affinity allows the antibody to displace the blocking agent from the targeted antigen.

There are two possible methods for IHC (Ramos-Vana, 2005). The direct method is a one step procedure where the antibody is directly linked to the method of visualization, typically a fluorescent dye molecule. The antibody binds to the antigen of interest and the complex can be visualized using a microscope equipped with fluorescent filters. Because it involves a single step the procedure is relatively simple and quick to conduct, but the method can suffer from sensitivity issues due to the lack of signal amplification.

The indirect method is a two step process in which a primary antibody binds to the antigen of interest. A secondary antibody conjugated with a method for visualization (either a fluorescent dye or an enzyme) then binds to the primary antibody allowing for visualization of the antigen of interest. A common method of visualization in indirect IHC involves a biotinylated secondary antibody that is coupled to streptavidin-horseradish peroxidise (HRP). The tissue section is then covered with 3,3'-Diaminobenzidine (DAB). DAB reacts with the HRP to form a brownish pigment allowing for the visualization of the antigen of interest. The indirect method is more sensitive than the direct method because of the potential for multiple secondary antibodies to bind at different sites on the primary antibody. The use of a colorimetric (DAB) technique for antibody visualization over a fluorescence (fluorescent labelled primary or secondary antibodies) technique has the advantage of permanence. Fluorophores will fade over time, and images must be taken shortly after staining for best results. If the DAB visualization

method is employed, stained sections can be re-examined in the future. The ability to re-examine sections is a benefit if new data becomes available.

4.5.2 Immunohistochemistry of Smad Proteins

Immunohistochemistry was initially used to detect activated macrophages, CD4+ T-lymphocytes, and CD8+ T-lymphocytes (Section 2.3, and Cox, 2008). Additionally, it was decided to attempt to use IHC methods to determine the presence of three different SMAD proteins: Smad3, phosphorylated Smad3 (p-Smad3), and Smad7.

Smad proteins are a family of receptor substrates involved in the signalling of the TGF-β superfamily of proteins (Massagué, 2000a). The Smad proteins are divided into three different groups. The three subgroups are the receptor (R) Smads (Smad1, Smad2, Smad3, Smad5, and Smad8), the cooperative (co) Smads (Smad 4), and the inhibitory (I) Smads (Smad6 and Smad7) (Massagué, 2000b). Of the five R-Smads, three (1, 5, 8) are involved in the signalling pathways of bone morphogenetic protein, and are not of interest in this study. The other two R-Smads are recognized by TGF-β and activin receptors.

Signalling begins when an extracellular TGF-β ligand binds to a transmembrane type II serine/threonine kinase receptor (Cohen Jr. 2003, Wrana 2000). This binding allows for the formation of a heteromeric receptor complex including the ligand and a type I and type II receptor. Upon formation of this complex, the type II receptor phosphorylates the type I receptor, activating the type I receptor and allowing it to propagate the signal. The targets for this activated receptor are the R-Smad proteins. SARA (Smad anchor for receptor activation) recruits unphosphorylated R-Smads to the membrane where the type

I receptor is able to phosphorylate the R-Smad. Upon phosphorylation, the R-Smad is freed from SARA, which can then go on to recruit other unphosphorylated R-Smads. The phosphorylated R-Smad forms a heteromeric complex with the co-Smad (Smad4) and this complex translocates into the nucleus of a cell where it can regulate gene expression. The last group of Smad proteins, the inhibitory Smads, have a negative impact on signalling by competing for phosphorylation sites of the type I receptor and interfering with the formation of R-Smad/co-Smad complex.

Once inside the nucleus the R-Smad/co-Smad complex, along with a co-activator or co-repressor and a DNA binding cofactor, regulate transcription of target genes. The association with different DNA-binding partners allows for the formation of complexes of specific composition and geometry. These different complexes can achieve high-affinity and selective interactions with DNA.

4.5.3 Protocols for Smad Staining

Two protocols were attempted to localize the distribution of Smad proteins in the control and treated rats. The first method used fluorophores as a method of detection while the second used a commercially available DAB visualization kit.

Protocol for Fluorescence Staining:

1) Sections were fixed in 4% paraformaldehyde in doubly distilled water for 15 minutes.
2) Sections were rinsed three times for 5 minutes, in 1 x PBS.
3) Sections were permeabilized with 0.1% Triton X-100 in 1x PBS for 15 minutes.
4) Slides were washed three times for one minute in 1 PBS, dried with gentle vacuum and placed in a humidity chamber.
5) Slides were covered with a 1:20 solution of primary antibody in PBS with 1% BSA and incubated for one hour at room temperature.
6) Slides were washed three times in 1x PBS for 5 minutes and carefully dried.
7) Slides were covered with a 1:1000 solution of the secondary antibody in PBS with 1% BSA and incubated for one hour at room temperature.
8) Slides were rinsed three times for five minutes in 1x PBS.
9) Slides were placed in Hoechst stain for one minute to stain nuclei.
10) Slides were washed three times in 1x PBS for five minutes.
11) Slides were carefully dried and cover slipped.

Protocol for DAB Visualization:

1. Sections were hydrated twice in PBS for 5 minutes to remove bound IgGs, thus decreasing background.
2. Sections were fixed in 3.7% formaldehyde buffered with PBS for 30 minutes.
3. The sections were washed in two changes of PBS.
4. The epitope was retrieved in 70% formic acid for 30 minutes.
5. The sections were washed in three changes of PBS.
6. The sections were blocked in 1% BSA in PBS for 30 minutes.
7. Excess buffer was tapped off and sections were covered with 0.6% hydrogen peroxide in methanol for 5 minutes.
8. Sections were rinsed with distilled water and placed in PBS for 5 minutes.
9. Sections were blocked with 20% nonimmune goat serum in 1% BSA in PBS for 30 minutes.
10. Excess blocking buffer was tapped off, and 50-100 µL of primary antibody diluted in 1% BSA in PBS was applied and incubated for an hour.
11. The sections were rinsed with PBS and placed in PBS bath twice for 5 minutes.
12. The sections were covered with biotinylated goat antibody to mouse/rabbit immunoglobulins diluted in PBS, and incubated for 20 minutes.
13. The sections were rinsed with PBS and placed in PBS bath twice for 5 minutes.

14. The sections were covered with StreptABComplex/HRP diluted in PBS, and incubated for 20 minutes.
15. The sections were rinsed with PBS and placed in PBS bath twice for 5 minutes
16. Sections were incubated with diluted DAB+ (Dako) solution for 1 minute.
17. The sections were rinsed with distilled water and placed in a distilled water bath for 1 minute.
18. Sections were counterstained for 3 minutes in Mayer's hematoxylin.
19. The sections were rinsed in tap water and incubated in a tap water bath for 1 minute to develop the counter stain.
20. The sections were dehydrated by being placed for 2 minutes in 70% ethanol, 2 minutes in absolute ethanol, and 2 minutes in xylene.

The sections were mounted with Permount (Fisher) and cover slipped.

4.5.4 Results and Discussion of Smad Staining

The fluorescence imaging of Smad proteins was unsuccessful. Initial attempts at staining resulted in high levels of background fluorescence, and attempts to reduce the background fluorescence were unsuccessful.

With the fluorescence staining being unsuccessful, it was hoped that the change to a colorimetric staining with the DAB visualization would provide better results. Unfortunately, the DAB staining was also unsuccessful. The formation of the DAB compound was indiscriminate and occurred to similar degrees even when one of the steps in the staining protocol was omitted.

It is believed that the epitope that is the target of the Smad antibody had degraded to a point where the antibodies were unable to bind specifically to that series of amino acids and the staining was indiscriminate. At the time of the staining the three and twenty one day animals from Set I were four years old, and the three and twenty one day animals from Set II, as well as the 63 day animals, were two years old. There is the potential for acquisition of new animals, to be stained shortly after surgery, either in conjunction with the IR data from the old animals, or new IR data from serial sections taken from the new animals.

4.6 Focal Plane Array Mapping

The data presented in this thesis has been collected at synchrotrons, collected one pixel at a time, raster scanning across a section of tissue to create images.

In May of 2009, an IR spectrometer coupled to an infrared microscope equipped with a focal plane array (FPA) detector was installed at the University of Manitoba. This instrument opens up a whole new avenue for collection of IR data. The FPA is a 64 x 64 array of detectors, enabling the simultaneous acquisition of 4096 spectra, covering an area 350 x 350 microns, for a nominal spatial resolution of 5.5 microns.

Figure 33 shows an entire tissue section from 21 day Saline 27. The boxes outlined in red denote maps collected at synchrotrons. A typical synchrotron map will consist of 231 spectra covering an area 110 by 210 microns. This map would take ~1.5 hours to collect. Also on the section is an overnight map, consisting of 976 spectra, covering an area 160 x 610 microns. This map took approximately 7 hours to record.

Outlined in blue is a map collected on the new Varian FTIR spectrometer, equipped with a FPA detector at the University of Manitoba. This map encompassed an area 1750 x 1750 microns, contained over 100,000 spectra, and yet took only 1.5 hours to collect. With the new FPA detector, it would be possible to map entire sections of tissue, and data acquisition is much more accessible than it is at synchrotrons. The on site microscope is accessible 24

hours a day, seven days a week, 52 weeks a year. By mapping entire sections, there is much less cause for concern that the sample heterogeneity will result in misrepresentation of the tissue components as a result of local anomalies.

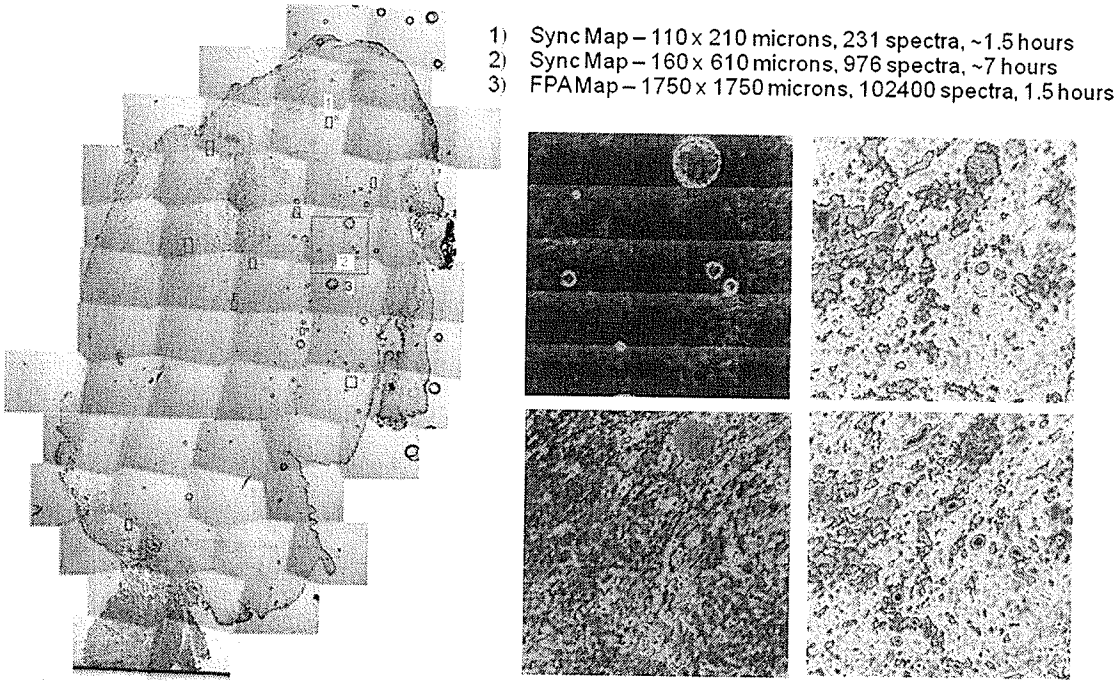

Figure 33: FPA Maps collected using a benchtop FTIR microscope

Visible light section of 21 day scar section showing maps collected at synchrotrons (red and orange rectangles) and map collected in house using FPA detector (blue box). False colour images (clockwise from upper left) show signal intensity, collagen distribution, sugar distribution, and lipids.

Chapter 5: Conclusions and Future Work

5.1 Conclusions and Future Work

Based on the infrared data, there are noticeable changes in the composition of the scar tissue as the wound healing process progresses, but there is little find evidence in the IR data to support the hypothesis that systemic administration of OTC and quercetin reduced the level of inflammation and oxidative stress leading to better wound healing. The visual and immunohistochemical methods used by our collaborators at the University of Saskatoon provide evidence of improved wound healing in the quercetin treated animals, but the animal to animal variation within a treatment group, age group, or set of animals makes it difficult to draw robust conclusions.

While the IR data may not provide evidence of improved wound healing, it does provide a large amount of information at one time. The IHC methods used to stain serial sections are usually capable of only looking at one specific analyte, while infrared spectroscopy can provide information on a wide variety of biomolecules including proteins, lipids, and sugars all at the same time. The information rich nature of the IR spectrum is both a blessing and a curse. It is important to look at the entire infrared spectrum to confirm that evidence in one part of the spectrum is supported by the rest of the spectrum. Along with the rich amount of information contained in one spectrum, synchrotron FTIR microspectroscopy has the added advantage of not adding anything to the tissue sections or taking anything away from them. As can be seen in Appendix A,

protocols for IHC involve many steps, some of which use harsh chemicals. These steps can alter the tissues, as well as preventing the sections from being reused. Sections placed on MirrIR slides for IR mapping are fairly stable, and be reanalyzed years in the future to take advantage of constantly evolving and improving technology.

Two of the disadvantages of FTIR microspectroscopy are the time required to collect a map, and the size of a map that can be collected. A typical scar tissue sections is ~ 2 cm x 3 cm, and we were only able to map a very small fraction of that. With access to Focal Plane Array (FPA) detectors, it becomes possible to image much larger portions of a tissue section, perhaps even the entire section, in a reasonable amount of time. The acquisition of data from a larger portion of the section would help to remove some of the assumptions that tissue that looks the same under a microscope will have a similar IR profile.

The greatest source of uncertainty in the analysis of the 3 and 21 day animal groups is the difference between the animals in Set I and II. Everything begins with the tissue sections themselves, and it is extraordinarily important to have intact tissue sections in order to be able to draw meaningful conclusions. There is an opportunity, with the acquisition of a new IR microscope equipped with a FPA detector at the University of Manitoba, to acquire new sets of 3, 21, and 63 day animals which would all be sectioned at the same time, by the same person. These new sections could be promptly stained with the Smad antibodies to provide complementary information to the IR data, and serial sections could be mapped extensively using the new IR microscope with a FPA.

References

Alberts, B., Johnson, A., Lewis, J., Raff, M., Roberts, K.. and Walter, P. Molecular Biology of the Cell, 4th Ed. Garland Science, 2002.

Anderson, M.E. Glutathione: an overview of biosynthesis and modulation. Chemico-Biological Interactions, 111-112, 1, 1998.

Anderson, V. C. and Burchiel, K. J. A prospective study of long term intrathecal morphine in the management of chronic non-malignant pain. Neurosurgery, 44: 289, 1999.

Anderson, V.C. and Israel, Z. Failed Back Surgery Syndrome. Current Review of Pain 4(5), 105. 2000.

Atkins, P. W. Physical Chemistry, 6th Edition. New York, Freeman, 1998.

Barditch-Crovo, P., Noe, D., Skowron, G., Lederman, M., Kalayjian, R. C., Borum, P., Buier, R., Rowe, W. B., Goldberg, D. and Lietman, P. A phase I/II evaluation of L-2-oxothiazolidine-4-carboxcylic acid in asymptomatic patients infected with human immunodeficiency virus. Journal of Clinical Pharmacology, 38 (4), 357, 1998.

Bender, E., Silver, F. H., Hayashi, K. and Trelstad, R. L. Type I collagen segment longspacing banding patters. Evidence that the alpha 2 chain is in the reference or A position. Journal of Biological Chemistry, 257 : 9653, 1982

Boskey, A., and Camacho, N. P. FT-IR imaging of native and tissue-engineered bone and cartilage. Biomaterials, 28, 2465, 2007.

Brod, S. A. Unregulated inflammation shortens human functional longevity. Inflammation Research, 49:561, 2000.

Burton, C. V., Kirkaldy-Willis, W. H., Yong-Hing, K. and Heithoff, K. B. Causes of Failure of Surgery on the Lumbar Spine. Clinical Orthopaedics and Related Research, 157, 191 (1981).

Byers, P. H., Click, E. M., Harper, E. and Bornstein, P. Interchain disulfide bonds in procollagen are located in a large nontriple helical COOH terminal domain. Proceedings of the National Academy of Sciences, USA, 72 (8) 3009, 1975.

Camacho, N. P., West, P., Torzilli, P. A. and Mendelsohn, R. FTIR microscopic imaging of collagen and proteoglycans in bovine cartilage. Biopolymers, 62, 1, 2001.

Cohen, I. K., Diegelman, R. F., Doren, R. Y., et al. Wound healing. Surgery: scientific principles and practice, 3rd ed. Philadelphia: Lippincort-Raven; 86, 1993.

Cohen Jr., M. M. TGF-β/Smad signalling system and its pathologic correlates. American Journal of Medical Genetics 116A, 1, 2003.

Conigliaro, D.A.: Opioids for chronic non-malignant pain. Journal of the Florida Medical Association, 83:708, 1999

Cooley, J. W. and Tukey, T. W. An Algorithm for the machine computation of complex Fourier series. Mathematics of Computation, 19, 297, 1965.

Coskun, E., Suzer, T. K., Topuz, O., Zencir, M., Pakdemirli, E. and Tahta, K. Relationships between epidural fibrosis, pain, disability, and psychological factors after lumbar disc surgery. European Spine Journal, 9, 218, 2000.

Cox, Nicole. The Anti-inflammatory potential of quercetin and L-2-oxothiazolidine-4-carboxylate in developing scar tissue. Ms Thesis, 2008.

Crock, H. V. Observations on the management of failed spinal operations. Journal of Bone and Joint Surgery, 58B, 193, 1976.

Cudkowicz, M. E., Sexton, P. M., Ellis, T., Hayden, D. L., Gwilt, P. R., Whalen, J. and Brown, R. H. Jr. The pharmacokinetics and pharmacodynamics of Procysteine in amyotrophic lateral sclerosis. Neurology 52 (7), 1492, 1999.

Davidson, J. M. and Berg, R. A. Posttranslational events in collagen biosynthesis. Methods in Cell Biology, 23, 119, 1981

Devulder, J., Deene, P., De Laat, M., Van Bastelaere, M., Brusselmans, G. and Rolly, G. Nerve root sleeve injections in patients with failed back surgery syndrome: a comparison of three solutions. Clinical Journal of Pain, 15:132, 1999.

Diem, M., Boydston-White, S., and Chiriboga, L. Infrared spectroscopy of cells and tissues: Shining light on a novel subject. Applied Spectroscopy, 53 (4), 148A, 1999.

Engel, J. and Prockop, D. J. The zipper-like folding of collagen triple helices and the effects of mutations that disrupt the zipper. Annual Review of Biophysics and Biophysical Chemistry. 20, 137. 1991

Erlund, I. Review of the flavonoids quercetin, hespretin, and naringenin. Dietary sources, bioactivities, bioavailability, and epidemiology. Nutrition Research 24, 851, 2004.

Fraser, R. D. B. Infrared microspectrometry with a 0.8 N. A. reflecting microscope. Discussions of the Faraday Society, 9, 378, 1950.

Fredman, B., Nun, M. B., Zohar, E., Iraqi, G., Shapiro, M., Gepstein, R. and Jedeikin, R. Epidural steroids for treating "Failed Back Surgery Syndrome": Is fluoroscopy really necessary? Anesthesia and Analgesia, 88, 367, 1999.

Fridovich, I. Biological effects of the superoxide radical. Archives of Biochemistry and Biophysics, 247, 1, 1986.

Fritsch, E. K., Heisel, J., and Rupp, S. The Failed Back Surgery Syndrome, Reasons, Intra-operative Findings, and Long-Term Results: A Report of 182 Operative Treatments. Spine 21 (5), 626, 1996.

Gallant, M., Rak, M., Szeghalmi, A., Del Bigio, M. R., Westaway, D., Yang, J., Julian, R., and Gough, K. M. Focally elevated creatine detected in amyloid precursor protein (APP) transgenic mice and Alzheimer's disease brain tissue. Journal of Biological Chemistry, 281 (1), 5, 2006.

Georges, C., Lefaix, J. L., and Delanian, S. Resolution of symptomatic epidural fibrosis following treatment with combined pentoxifylline–tocopherol. British Journal of Radiology, 77, 885, 2004.

Glagov S., Weisenberg E., Zarins C. K., Stankunavicius R., and Kolettis G. J. Compensatory enlargement of human atherosclerotic coronary arteries. New England Journal of Medicine, 316, 1371, 1987.

Gough, K. M., Zielinski, D., Wiens, R., Rak, M., and Dixon I. M. C. Fourier transform infrared evaluation of microscopic scarring in the cardiomyopathic heart: Effect of chronic AT1 suppression. Analytical Biochemistry, 316, 232, 2003.

Griffiths, P. R. Chemical Infrared Fourier Transform Spectroscopy, 1-59, 1975.

Hasler P. Biological therapies directed against cells in autoimmune disease. Springer Seminars in Immunopathology 27 (4): 443, 2006.

Hayat, M. A. Fixation and Embedding. In: Microscopy, Immunohistochemistry, and Antigen Retrieval Methods for Light and Electron Microscopy. PP 71-93. Kluwer Academic, New York, New York. 2002.

Hazard, R. G. Failed Back Surgery Syndrome: Surgical and Nonsurgical Approaches. Clinical Orthopaedics and Related Research. 443, 228, 2006.

Hojima, Y., McKenzie, J. A., van Der Rest, M., and Prockop D.J. Type I procollagen N-proteinase from chick embryo tendons. Purification of a new 500 kDa form of the enzyme and identification of the catalytically active polypeptides. Journal of Biological Chemistry, 264, 11336, 1989

Humason, G. L. Animal tissue techniques, 4th Edition, Freeman, San Francisco. 1979.

Jamison, R. N., Raymond, S. A., Slawsby, E. A., Nedeljkovic, S. S. And Katz, N. P. Opioid therapy for chronic noncancer back pain. A randomized prospective study. Spine, 23, 2591, 1998.

Juurlink, B. H. J. Therapeutic potential of dietary phase 2 enzyme inducers in ameliorating diseases that have an underlying inflammatory component. Canadian Journal of Pharmacology, 79, 1, 2001.

Kadler, K. Protein Profile: Extracellular Matrix 1: Fibril Forming Collagens. Vol 1, Issue 5, 1994

Kamencic, H., Griebel, R.W., Lyon, A.W., Paterson, P.G., and Juurlink, B.H.J. Promoting glutathione synthesis after spinal cord trauma decreases secondary damage and promotes retention of function. The FASEB Journal, 15, 243, 2001.

Kohn, L. D., Isersky, C., Zupnik, J., Lenners, A., Lee, G., and Lapiere, G. M. Calf tendon procollagen peptidase: Its purification and endopeptidase mode of action. Proceedings of the National Academy of Sciences, USA. 71, 40, 1974.

Kumar, K., Malik, S., and Demeria, D. Treatment of chronic pain with spinal cord stimulation versus alternative therapies: Cost Effectiveness Analysis. Neurosurgery 51 (1), 106, 2002.

Kunitomo M. Oxidative stress and atherosclerosis. Yakugaku Zasshi. 127 (12), 1997, 2007

Lazarev, Y. A., Grishkovsky, B. A. and Khromova, T. B. Amide I band of IR spectrum and Structure of Collagen and related polypeptides. Biopolymers, 24, 1449, 1985.

Levi-Schaffer, F., Garbuzenko, E., Rubin A., Reich, R., Pickholz, D., Gillery, P., Emanard, H., Nagler, A. and Maquart, F.A. Human eosinophils regulate human lung and skin derived fibrblast properties in vitro: A role for transforming growth factor β (TGF-β). Proceedings of the national Academy of Sciences USA, 96, 9660, 1999;

Massagué, J. How cells read TGF-β signals. Nature Reviews Molecular Cell Biology, 1(3), 169, 2000a.

Massagué, J. and Wotton, D. Transcriptional control by the TGF-β/Smad signaling system. The EMBO Journal, 19 (8), 1745, 2000.

Majithia V. and Geraci S. A. Rheumatoid arthritis: Diagnosis and Management. American Journal of Medecine, 120 (11), 936, 2007

Melzack R. and Wall, P. Pain mechanisms: A New Theory. Science 150, 971, 1965.

Miller, E. J. and Gay, S. Collagen: An Overview. Methods in Enzymology, 82, Pt. A: 3, 1982

Miller, L. M. And Dumas, P. Chemical imaging of biological tissue with synchrotron infrared light. Biochimica and Biophysica Acta – Biomembranes, 1758 (7), 846, 2006.

Monaco, J. L. and Lawrence, W. T. Acute Wound Healing: An Overview. Clinical Plastic Surgery, 30, 1, 2003.

Myhrstad, M. C. W., Carlsen, H., Nordstrom, O., Blumhoff, R., and Moskaug, J. O. Flavonoids increase the intracellular glutathione level by transactivation of the glutamylcysteine synthase catalytical subunit promoter. Free Radical Biology and Medicine, 32 (5), 386, 2002.

Myllyla, R. Studies on the Mechanism of Collagen Galactosyltransferase Reaction. European Journal of Biochemistry, 70, 225, 1976.

Myllyla, R., Ristell, L. and Kivirikko, K. Glucosylation of galactosylhydroxylysyl residues in collagen in vitro by collagen glucosyltransferase. European Journal of Biochemistry, 58, 517, 1975.

O'Leary, R., Wood, E. J. and Guillou, P. J. Pathological Scarring: Strategic Interventions. European Journal of Surgery, 168, 523, 2002.

O'Dell J. Therapeutic strategies for rheumatoid arthritis. New England Journal of Medecine, 350 (25), 2591, 2004.

Onesti, S. T. Failed Back Syndrome. The Neurologist. 10(5), 259, 2004.

Park, J. E. and Barbul, A. Understanding the role of immune regulation in wound healing. The American Journal of Surgery, 187 (supp to May 2004), 11s, 2004

Ramachandran, G. N. and Chandrasekharan, R. Interchain hydrogen bonds via bound water molecules in the collagen triple helix. Biopolymers 6, 1649, 1968

Ramachandran, G. N., Bansal, M. and Bhatnagar, R. S. A hypothesis on the role of hydroxyproline in stabilizing collagen structure. Biochimica et Biophysica Acta, 322, 166. 1973

Ramos-Vara, JA. Technical Aspects of Immunohistochemistry. Veterinary Pathology, 42, 405, 2005.

Rich, A. and Crick, F. H. The molecular structure of collagen. Journal of Molecular Biology, 3, 483, 1961.

Robertson, J. T. Role of peridural fibrosis in the failed back: a review. European Spine Journal, (5 (supp 1)), S2, 1996.

Rosati G. The prevalence of multiple sclerosis in the world: an update. Neurological Sciences, 22 (2), 117, 2001.

Rother, K. I. Diabetes Treatment - Bridging the Divide. New England Journal of Medicine, 356 (15), 1499 -1501, 2007.

Rowlingson, J. Epidural steroids in treating failed back surgery syndrome. Anaesthesiology and Analgesics, 8, 240, 1999.

Savage, S.R. Opioid use in the management of chronic pain. Medical Clinic of North America, 83, 761, 1999.

Schultke, E., Kendall, E., Kamencic, H., Ghong, Z., Griebel, R.W. and Juurlink, B.H.J. Quercetin Promotes Functional Recovery Following Acute Spinal Cord Injury. Journal of Neurotrauma, 20 (6), 583, 2003.

Singer, A. J. and Clark, R. A. F. Cutaneous Wound Healing. The New England Journal of Medicine, 341 (10), 738, 1999.

Slipman, C. W., Shin, C. H., Patel, R. K., Isaac, A., Huston, C. W., Lipetz, J. S., Lenrow, D. A., Braverman, D. L. and Vresilovic Jr., E. J. Etiologies of Failed Back Surgery Syndrome. Pain Medicine 3 (3), 200, 2002.

Smith, T. I. The source issue in infrared microspectroscopy. Nuclear Instruments and Methods in Physics Research A, 483, 565, 2002.

Srinivasan, G. and Bhargava, R. Fourier transform-infrared spectroscopic imaging: the emerging evolution from a microscopy tool to a cancer imaging modality. Spectroscopy, 22 (7), 30, 2007)

Turesson, C., O'Fallon, W. M., Crowson, C. S., Gabriel, S. E. and Matteson E. L. Extra-articular disease manifestations in rheumatoid arthritis: incidence trends and risk factors over 46 years. Annals of the Rheumatic Diseases. 62 (8), 722, 2003.

Wiens, R., Rak, M., Cox, N., Abraham, S., Juurlink, B. H. J., Kulyk, W. M., and Gough, K. M. Synchrotron FTIR microspectroscopic analysis of the effects of anti-inflammatory therapeutics on wound healing in laminectomized rats. Analytical and Bioanalytical Chemistry, 387, 1679, 2007.

Wrana, J. L. and Attisano, L. The Smad Pathway. Cytokine and Growth Factor Reviews 11, 5, 2000.

Zhang, Z., Juurlink, B.H.J., Lyon, A. W. and Paterson, P.G. Effects of dietary protein and L-2-oxothiazolodine-4-carboxylate on rat brain glutathione concentration. Nutrition Research, 22, 1475, 2002.

Appendix A: Infrared Mapping Data

Notes on Presentation:

The following pages contain false colour images for all infrared maps collected at synchrotrons during this research.

The data is organized by age and treatment group, and within these groups the data is organized by collection time.

Synchrotron time is a limited resource, and thus it is important to use the time as efficiently as possible. For this reason, data would be collected on different samples, from different projects, during one trip. While I was present for the majority of data collection on the scar tissue sections, I was not there for all of them. At the beginning of each set of data, there is a preliminary slide indicating who was present at the synchrotron for data collection, both for our records and to make it easier to determine whose lab book contains records on data collection from that particular trip.

The majority of data was collected using Omnic 6.x software. For these maps, the colour scheme goes from white (none) to red (low) through orange, yellow, green, and blue (high).

Some of the more recent data on the 63 day animals was collected using Omnic 7.x software, which inverted the colour scheme (blue is now low and red is high) as well as removing white from the colour palette.

Detailed parameters including the peak ranges, baselines, and display limits can be found in the Materials and Methods section.

Table 5: Processing Parameters for Scar Tissue

Function	Peak (cm^{-1})	Baseline (cm^{-1})	Display Limits
Collagen	1198-1211	1188-1214	0.0 to 0.45
Phosphate + Sugar	1014-1130	900-1145	4 to 11
Phosphate	1077-1087	900-1145	0.6 to 1.6
Sugar	1024-1037	1020-1041	0.02 to 0.2
Symmetric CH_2	2847-2855	2837-2862	0.0 to 0.45

3 Day OTC

June 2003 SRC

Kathy Gough
Meghan Gallant
Vincent Okoli

4 YH OTC 43B_01.MAP

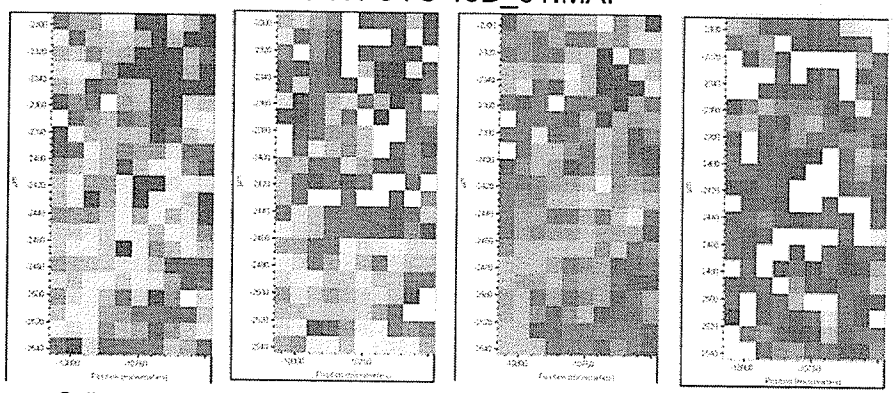

Collagen 1014-1130 Sugar Sym CH2

4 YH OTC 43B_02.MAP

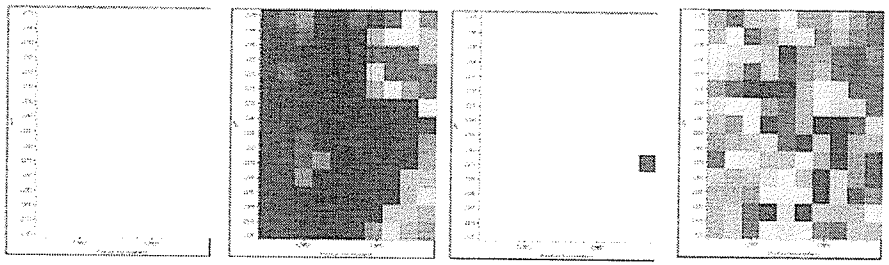

Collagen 1014-1130 Sugar Sym CH2

4 YH OTC 43B_03.MAP

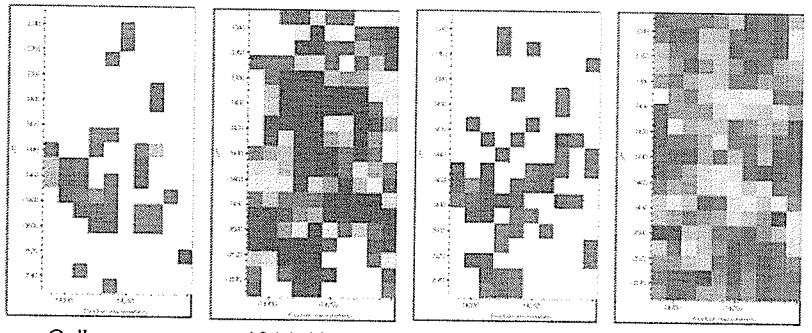

Collagen 1014-1130 Sugar Sym CH2

4 YH OTC 43B_04.MAP

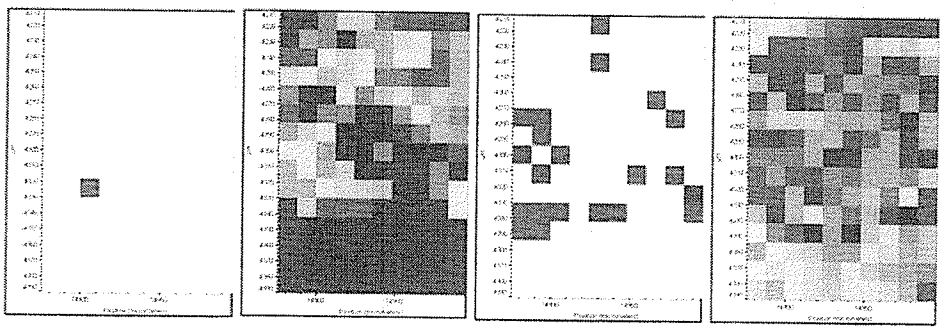

Collagen 1014-1130 Sugar Sym CH2

4 YH OTC 43B_05.MAP

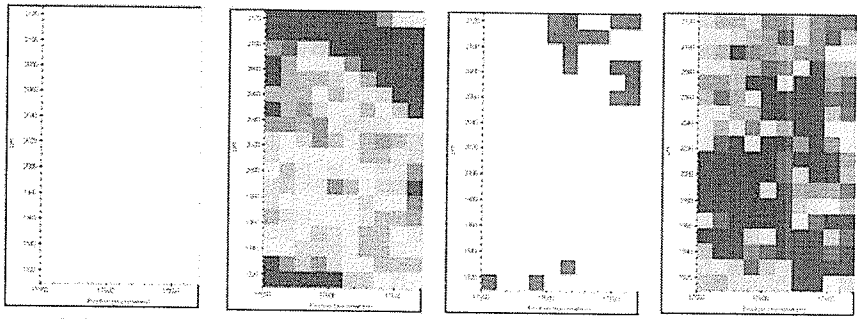

Collagen 1014-1130 Sugar Sym CH2

4 YH OTC 43B_06.MAP

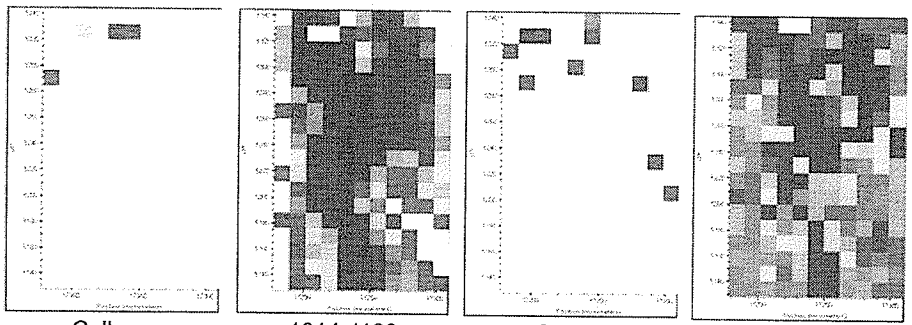

Collagen 1014-1130 Sugar Sym CH2

4 YH OTC 43B_07.MAP

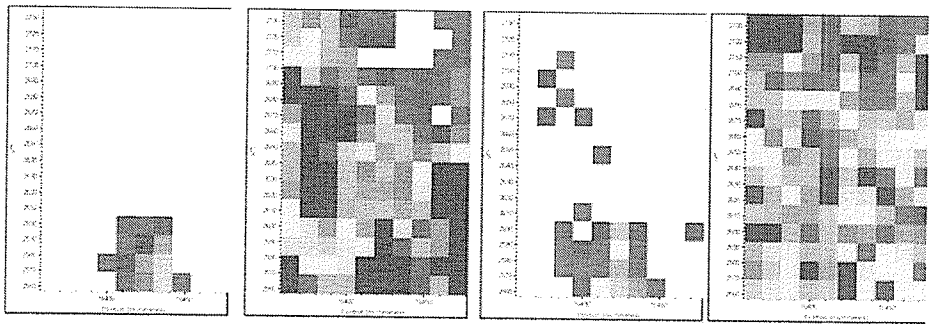

Collagen 1014-1130 Sugar Sym CH2

4 YH OTC 43B_08.MAP

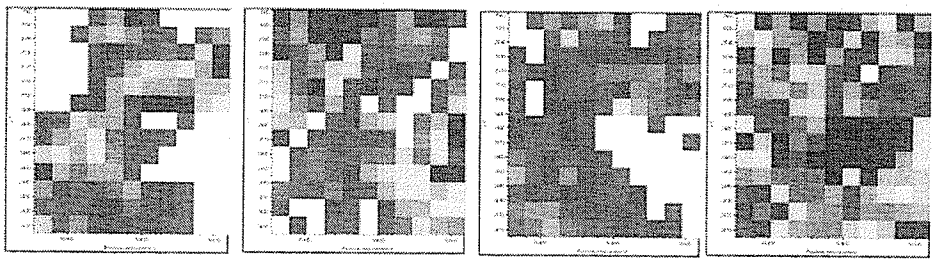

Collagen 1014-1130 Sugar Sym CH2

4 YH OTC 43B_09.MAP

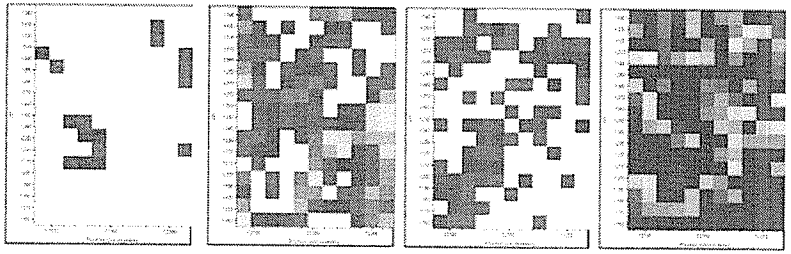

Collagen 1014-1130 Sugar Sym CH2

4 YH OTC 44A_01.MAP

No Liquid N_2 means bad spectra

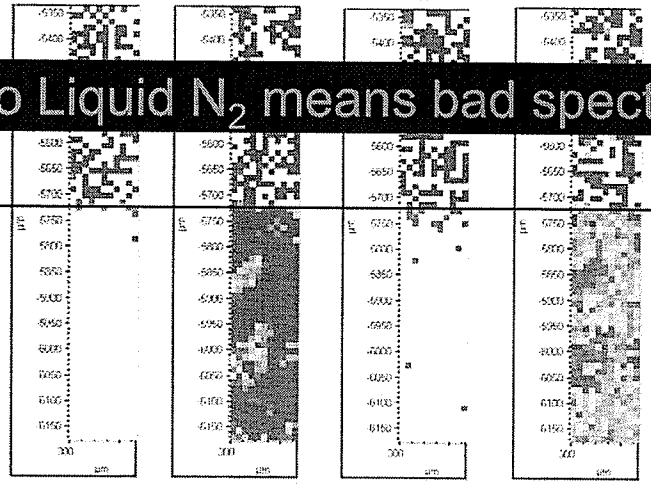

Collagen 1014-1130 Sugar Sym CH2

4 YH OTC 44A_02.MAP

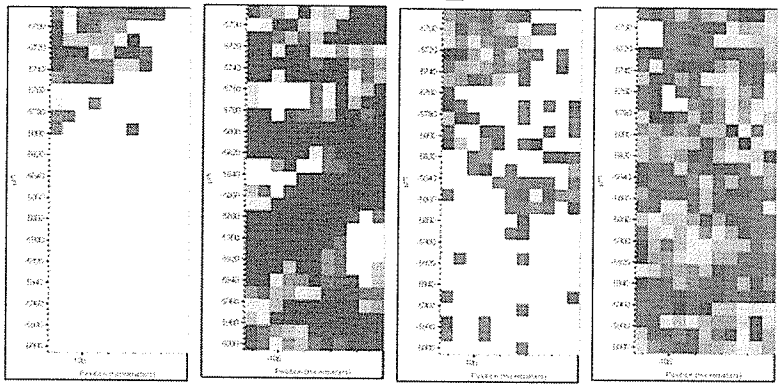

Collagen 1014-1130 Sugar Sym CH2

4 YH OTC 44A_03.MAP

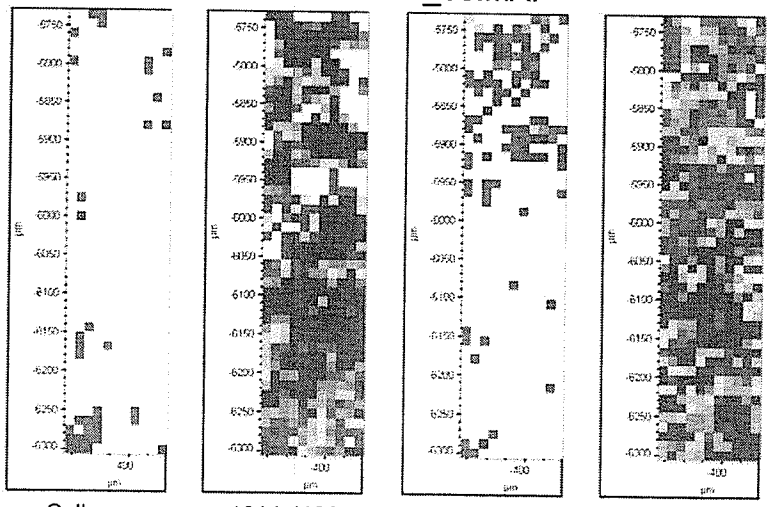

Collagen 1014-1130 Sugar Sym CH2

4 YH OTC 44A_04.MAP

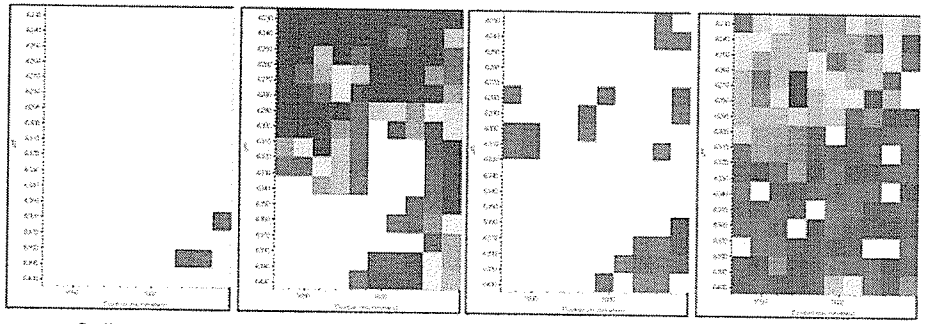

Collagen 1014-1130 Sugar Sym CH2

4 YH OTC 44A_05.MAP

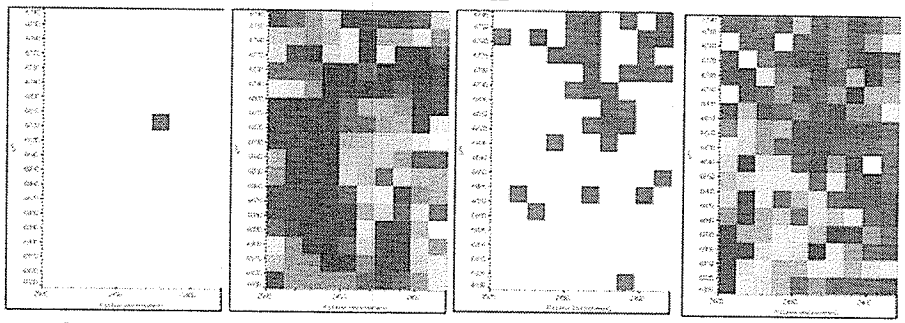

Collagen 1014-1130 Sugar Sym CH2

4 YH OTC 44A_06.MAP

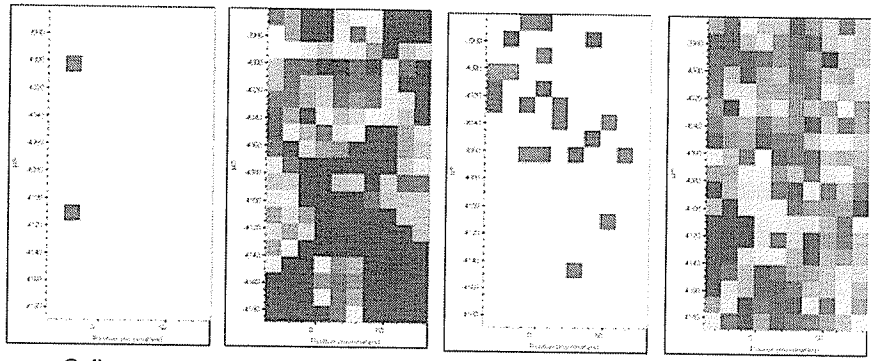

Collagen 1014-1130 Sugar Sym CH2

4 YH OTC 44A_07.MAP

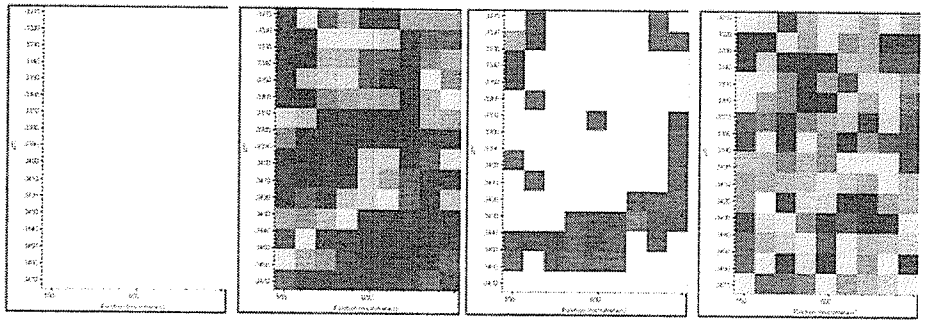

Collagen 1014-1130 Sugar Sym CH2

4 YH OTC 44A_08.MAP

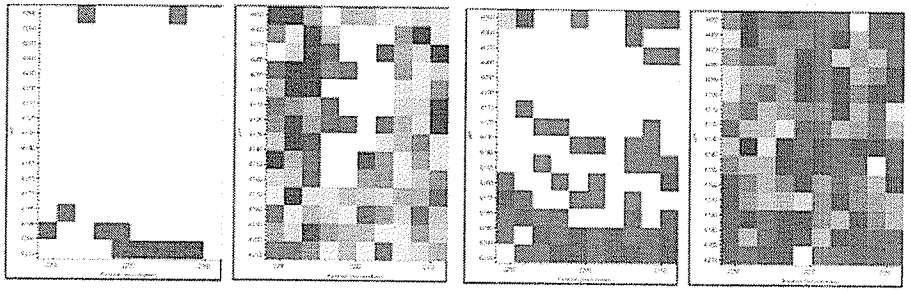

Collagen 1014-1130 Sugar Sym CH2

4 YH OTC 44A_09.MAP

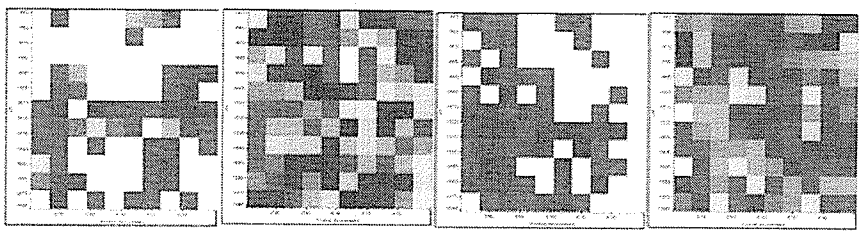

Collagen 1014-1130 Sugar Sym CH2

4 YH OTC 44A_10.MAP

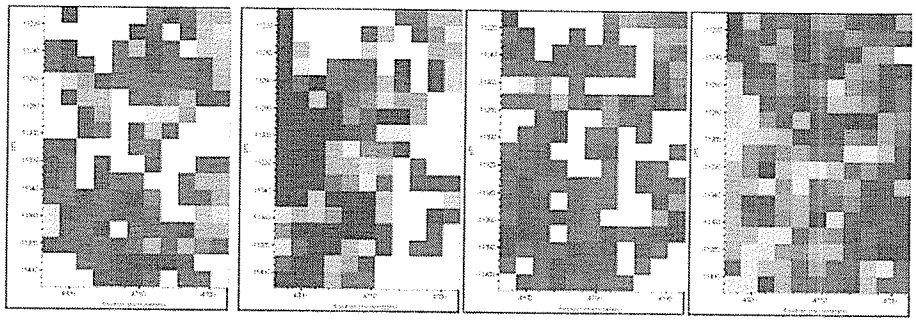

Collagen 1014-1130 Sugar Sym CH2

3 Day OTC

SRC July 2004

Fred Zeiler
Richard Wiens
Margaret Rak

3 day OTC animal 31 slide 10 map1

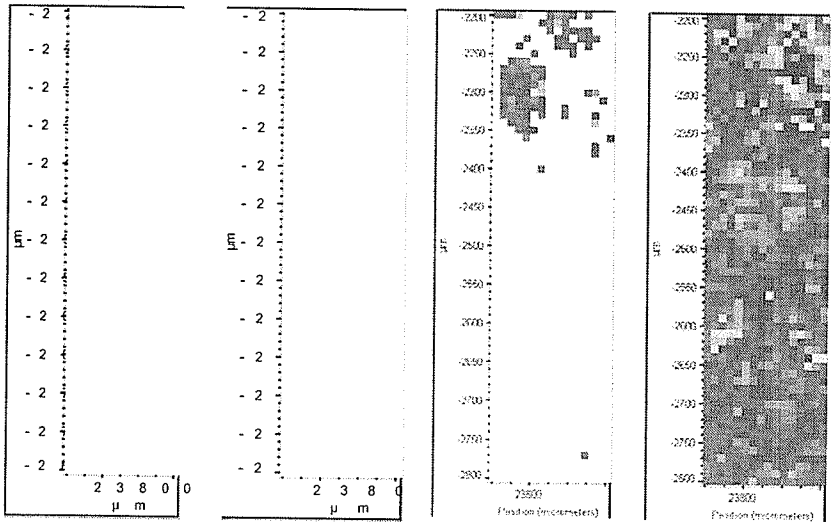

Collagen 1014-1130 Sugar Sym CH2

3 day OTC animal 31 slide 10 map 2

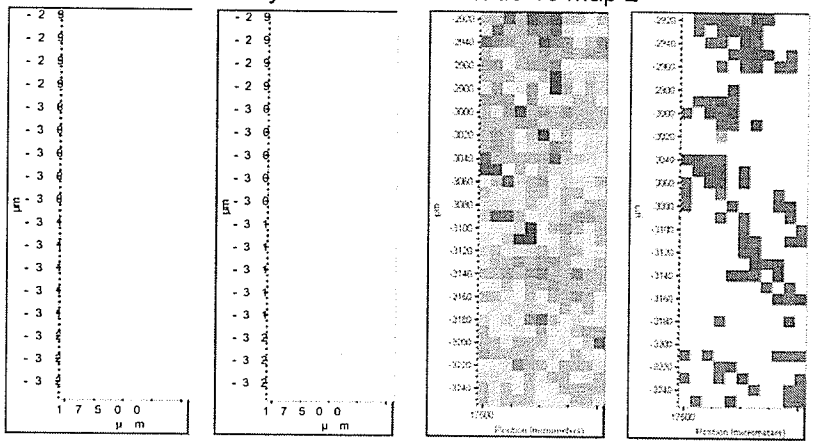

Collagen 1014-1130 Sugar Sym CH2

Map is located at what appears to be surface side of tissue.
Tissue looks folded as well.
We suspect that this is skin-associated collagen.

3 day OTC animal 31 slide 10 map 3

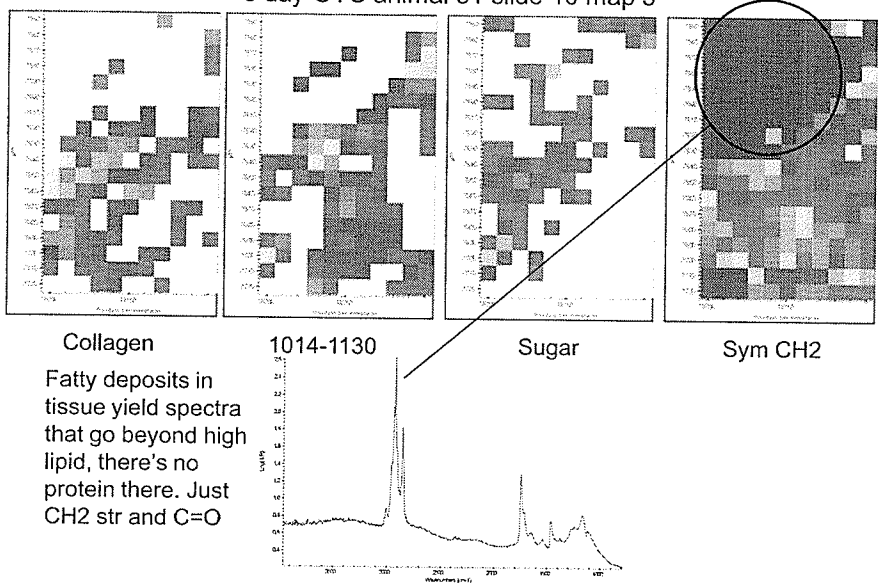

Collagen 1014-1130 Sugar Sym CH2

Fatty deposits in tissue yield spectra that go beyond high lipid, there's no protein there. Just CH2 str and C=O

3 day OTC animal 31 slide 10 map 4

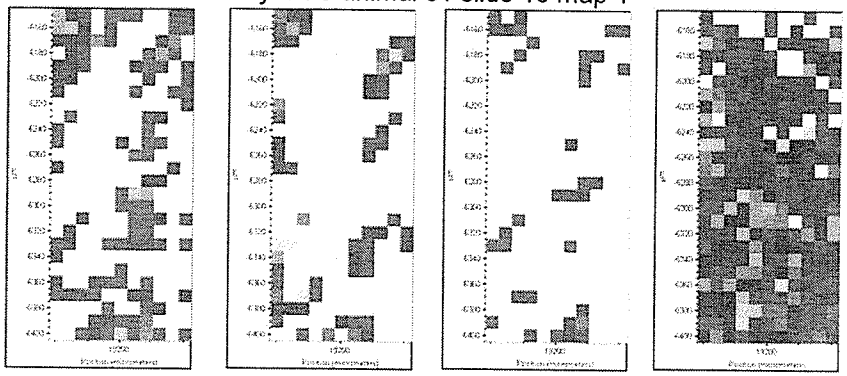

Collagen 1014-1130 Sugar Sym CH2

- Tissue seems to be very thin.
- Again, very high lipid in some places

3 day OTC animal 31 slide 10 map 5

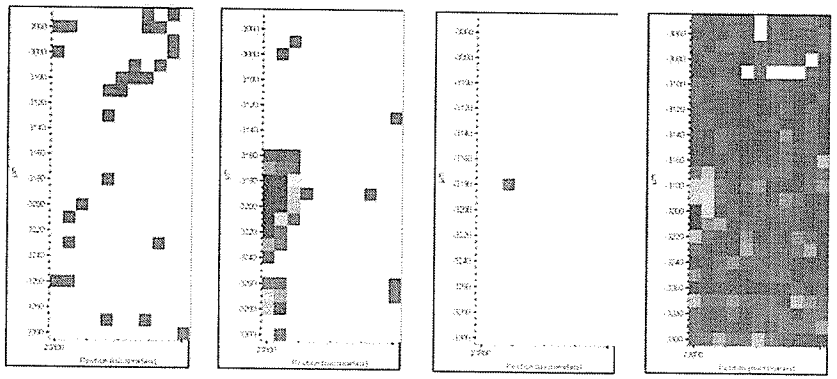

Collagen 1014-1130 Sugar Sym CH2

3 day OTC animal 32 slide 10 map1

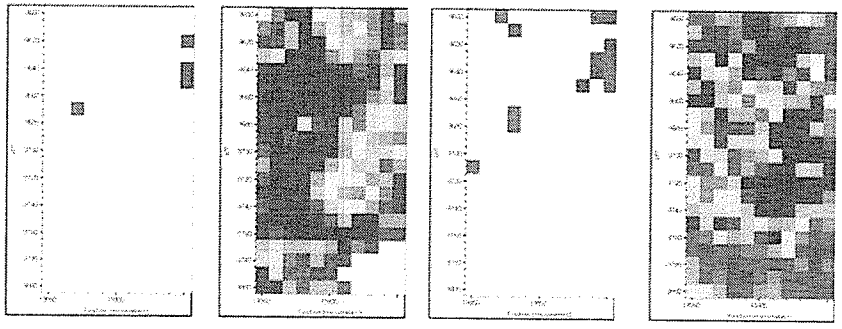

Collagen 1014-1130 Sugar Sym CH2

3 day OTC animal 32 slide 10 map 2

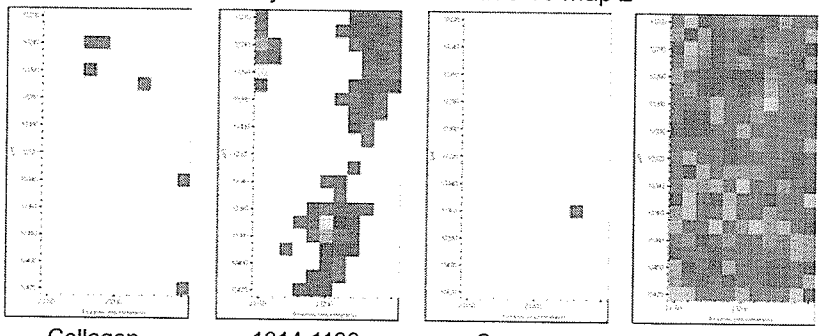

Collagen 1014-1130 Sugar Sym CH2

Pretty thin tissue throughout, Amide I frequently < 1

3 day OTC animal 32 slide 10 map 3

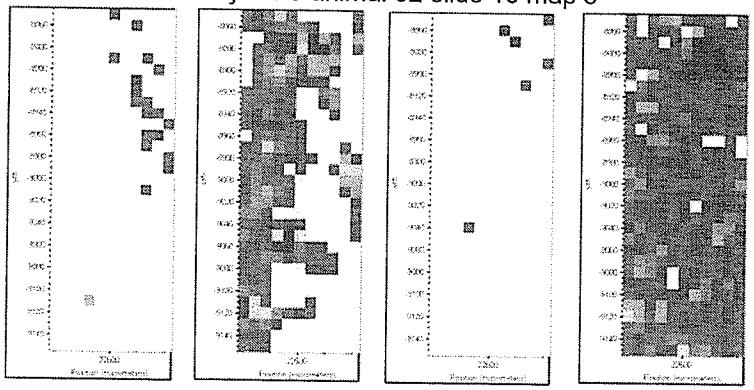

Collagen 1014-1130 Sugar Sym CH2

3 day OTC animal 33 slide 10 map 1

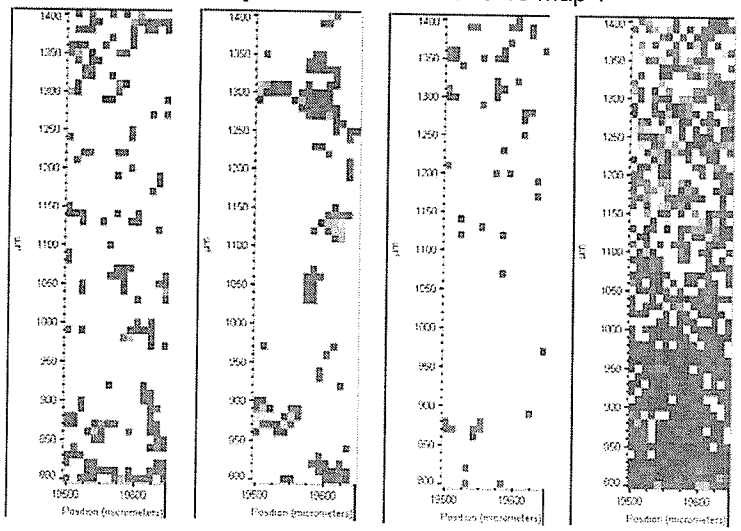

Collagen 1014-1130 Sugar Sym CH2

Not a lot of meaning in this map. Very out of focus.

3 day OTC animal 33 slide 10 map 2

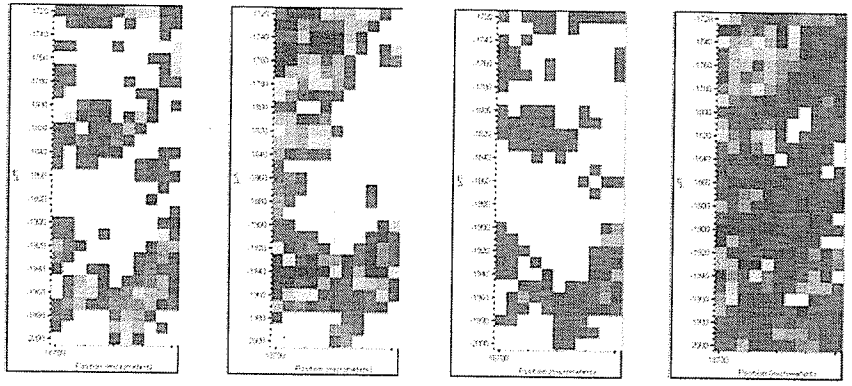

Collagen 1014-1130 Sugar Sym CH2

3 day OTC animal 33 slide 10 map 3

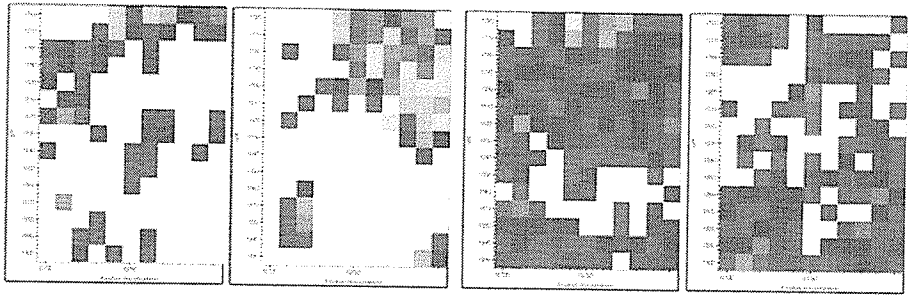

Collagen 1014-1130 Sugar Sym CH2

3 day OTC animal 33 slide 10 map 4

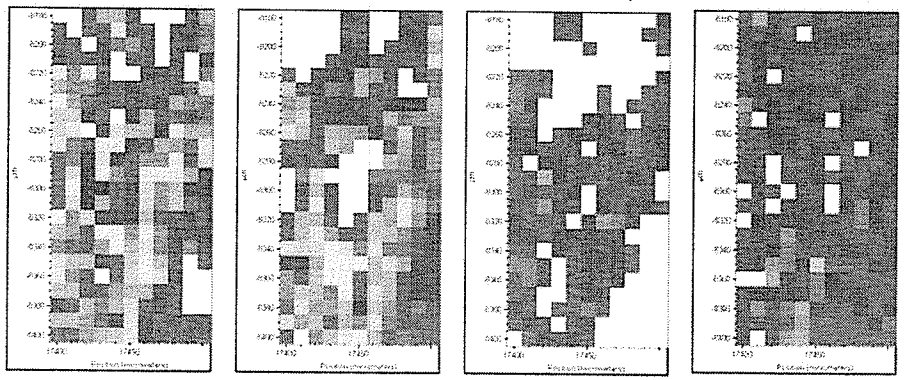

Collagen 1014-1130 Sugar Sym CH2

3 day OTC animal 33 slide 10 map 5

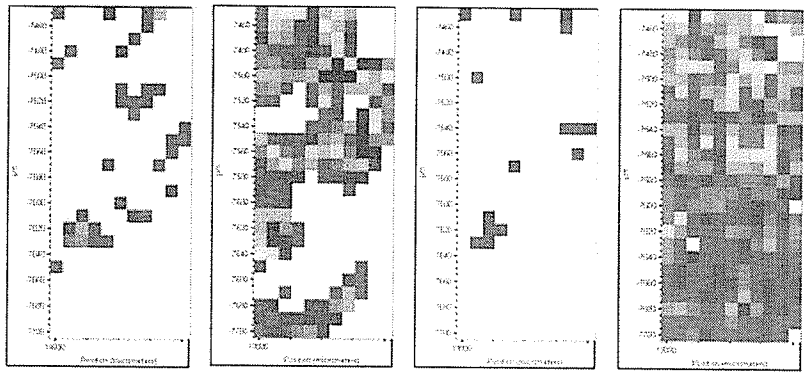

Collagen 1014-1130 Sugar Sym CH2

3 day OTC animal 33 slide 10 map 6

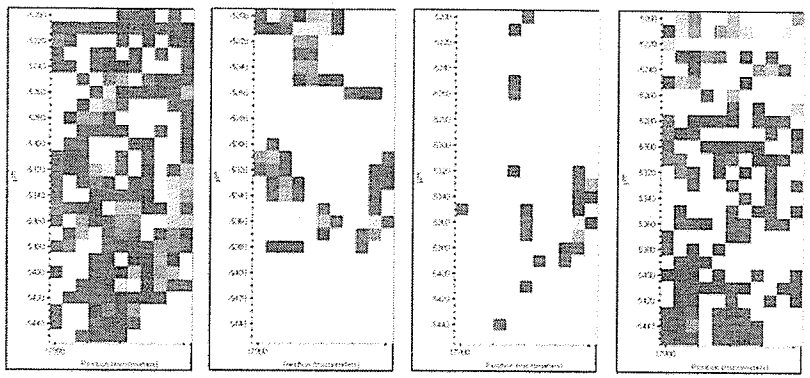

Collagen 1014-1130 Sugar Sym CH2

-Top quarter or so of map is really noisy and looks like garbage

3 Day OTC

SRC September 2004
Margaret Rak

SRC Sept 2004 3 Day OTC 31 Map 1

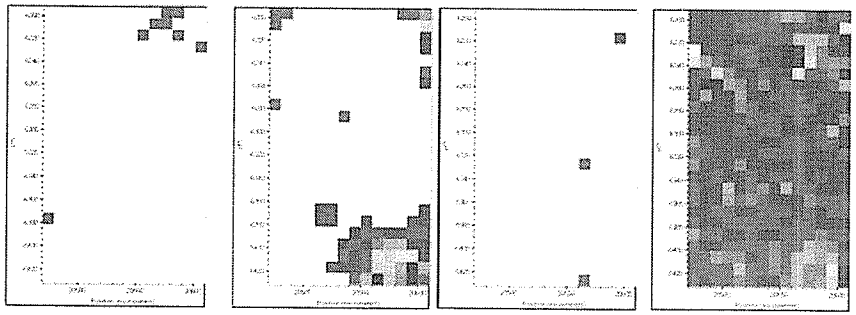

Collagen 1014-1130 Sugar Sym CH2

SRC Sept 2004 3 Day OTC 31 Map 2

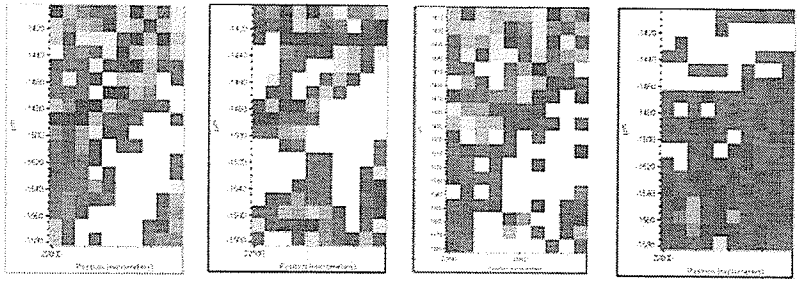

Collagen 1014-1130 Sugar Sym CH_2

SRC Sept 2004 3 Day OTC 32 Map 1

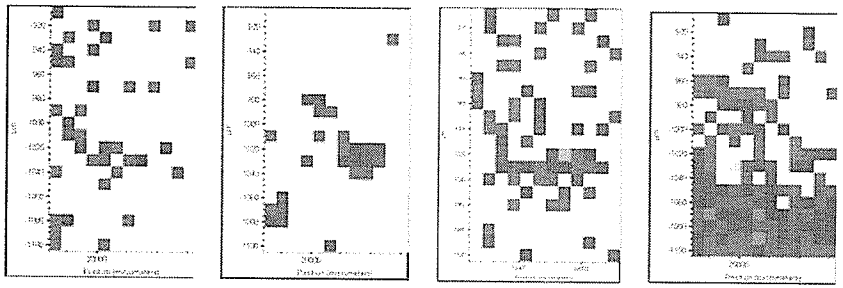

Collagen 1014-1130 Sugar Sym CH_2

SRC Sept 2004 3 Day OTC 32 Map 2

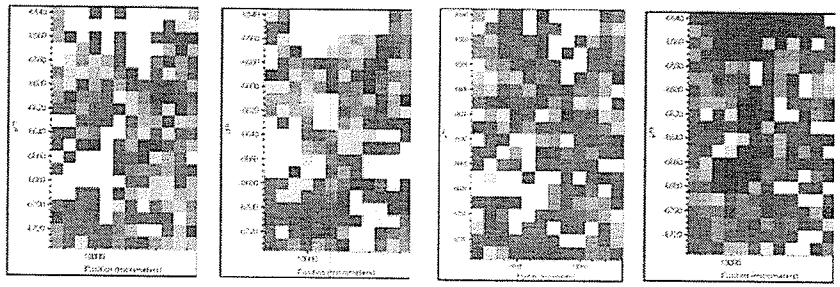

Collagen 1014-1130 Sugar Sym CH_2

SRC Sept 2004 3 Day OTC 32 Map 3

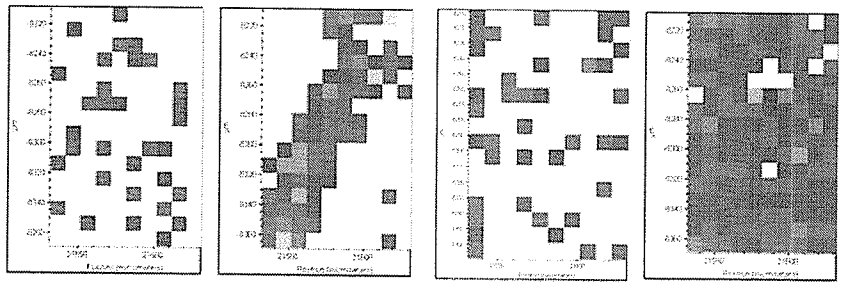

Collagen 1014-1130 Sugar Sym CH_2

SRC Sept 2004 3 Day OTC 33 Map 1

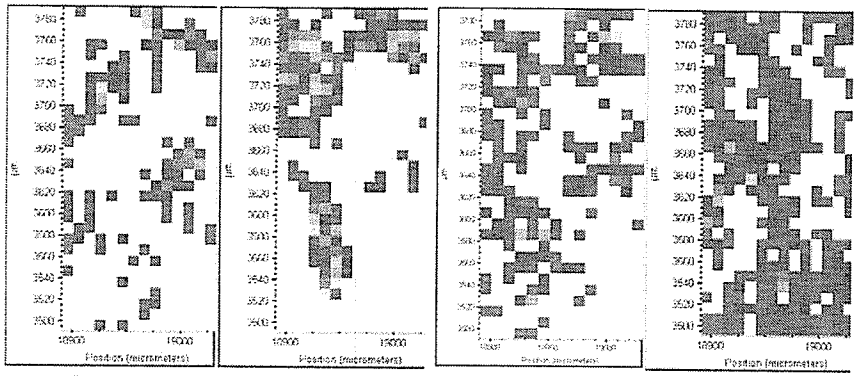

Collagen 1014-1130 Sugar Sym CH_2

SRC Sept 2004 3 Day OTC 33 Map 2

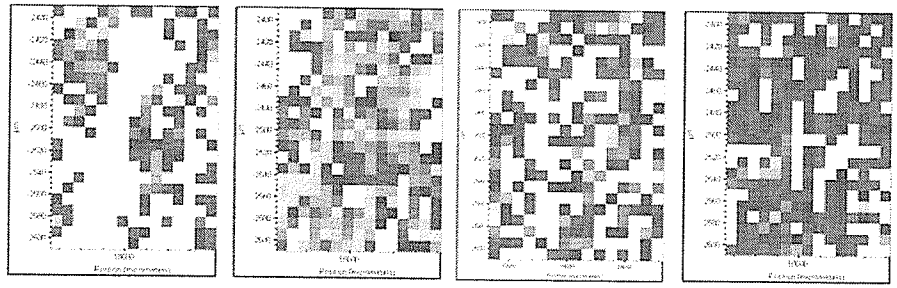

Collagen 1014-1130 Sugar Sym CH_2

SRC Sept 2004 3 Day OTC 33 Map 3

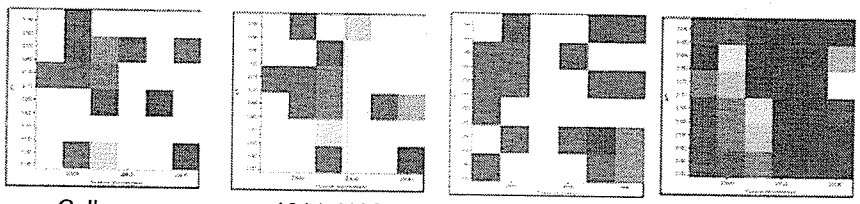

Collagen 1014-1130 Sugar Sym CH_2

SRC Sept 2004 3 Day OTC 33 Map 4

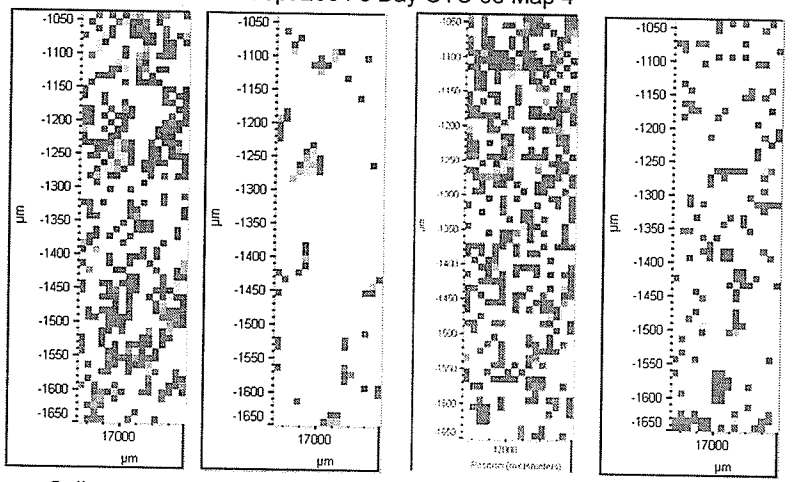

Collagen 1014-1130 Sugar Sym CH_2

3 Day OTC

SRC August 2006

Richard Wiens

3 Day OTC N47 Map 1

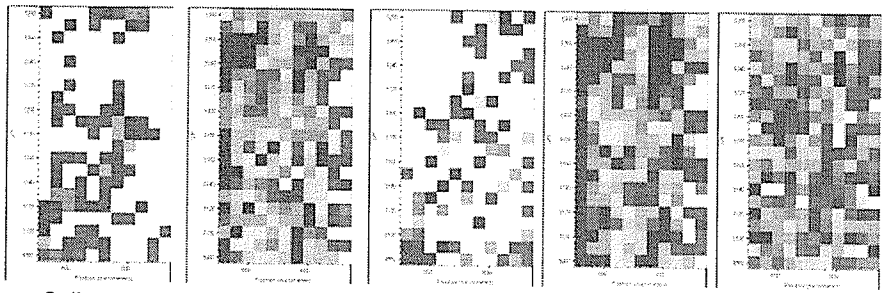

3 Day OTC N47 Map 2

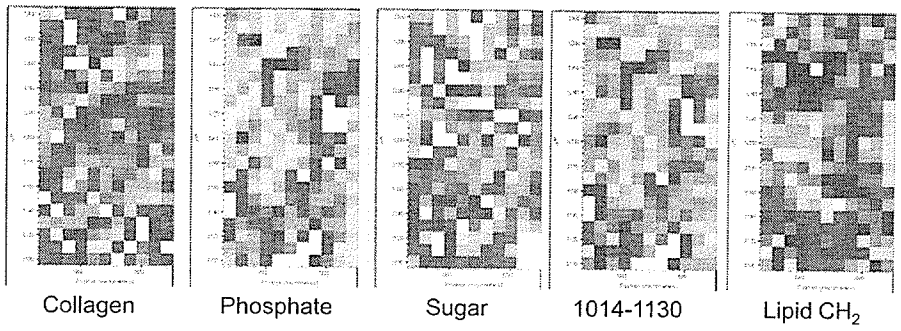

3 Day OTC N47 Map 3

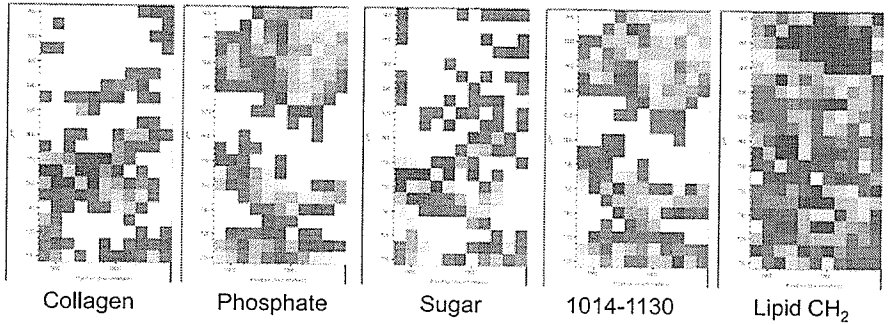

3 Day OTC N47 Map 4

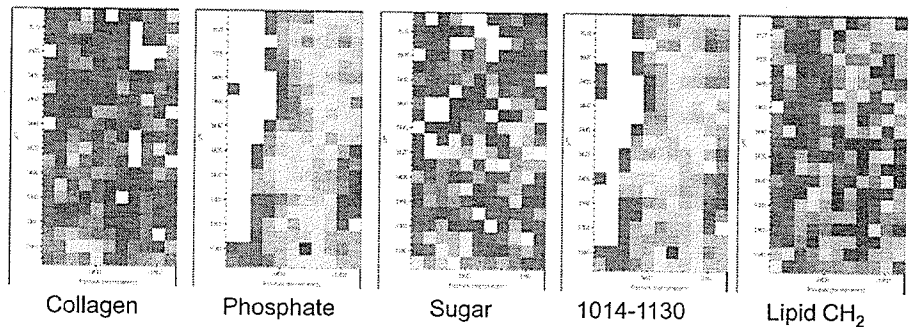

3 Day OTC N47 Map 5

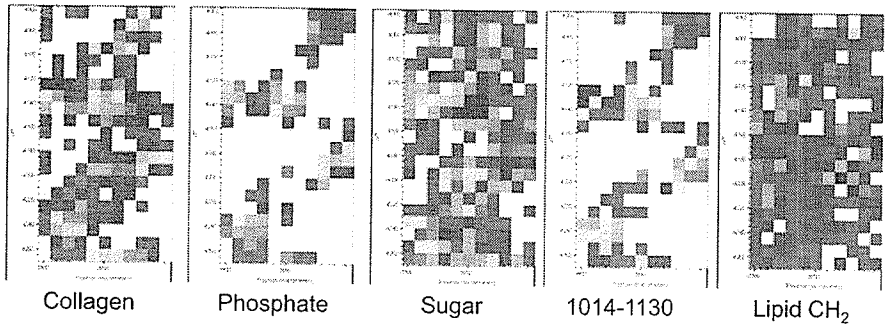

3 Day OTC N47 Map 6

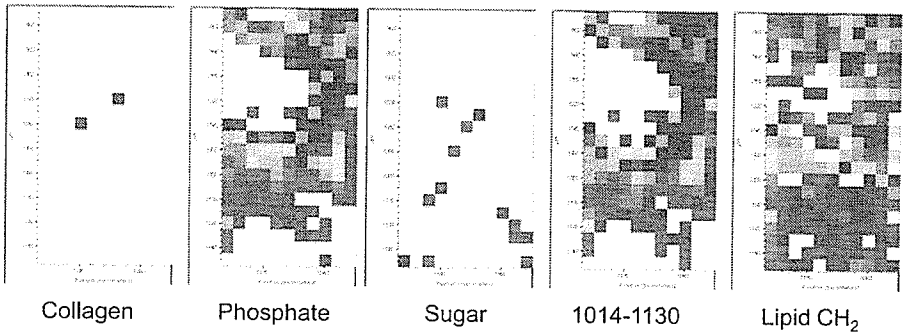

3 Day OTC N50 Map 1

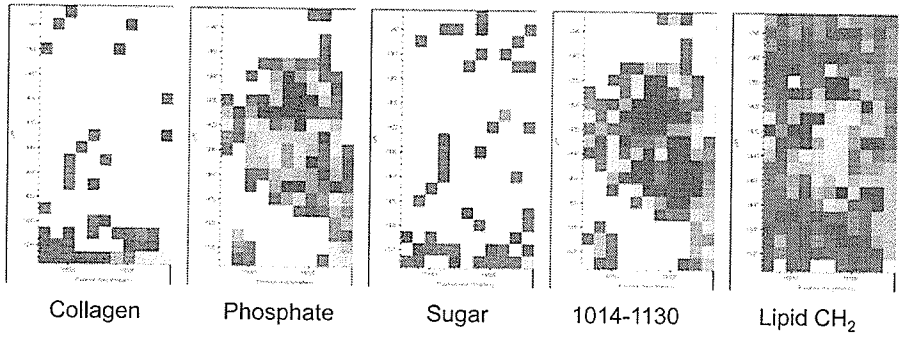

3 Day OTC N50 Map 2

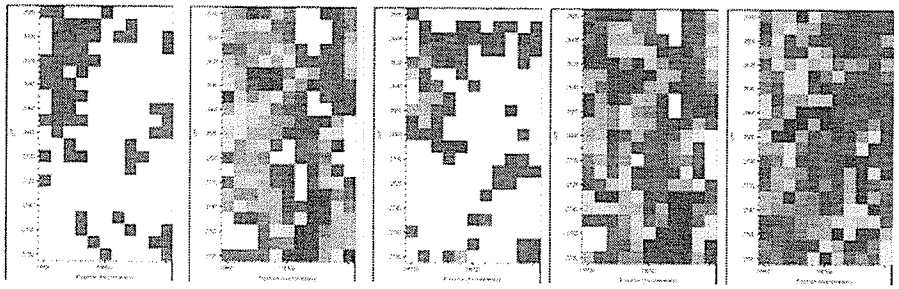

Collagen Phosphate Sugar 1014-1130 Lipid CH_2

3 Day OTC N50 Map 3

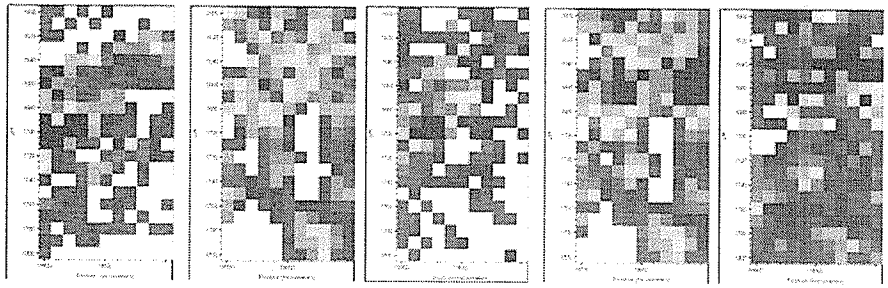

Collagen Phosphate Sugar 1014-1130 Lipid CH_2

3 Day OTC N50 Map 4

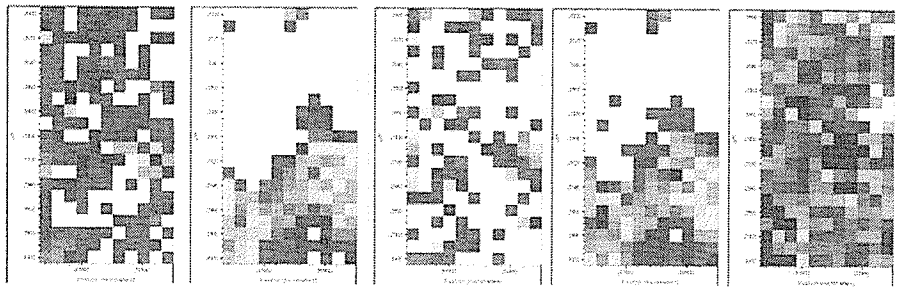

Collagen Phosphate Sugar 1014-1130 Lipid CH_2

3 Day OTC N50 Map 5

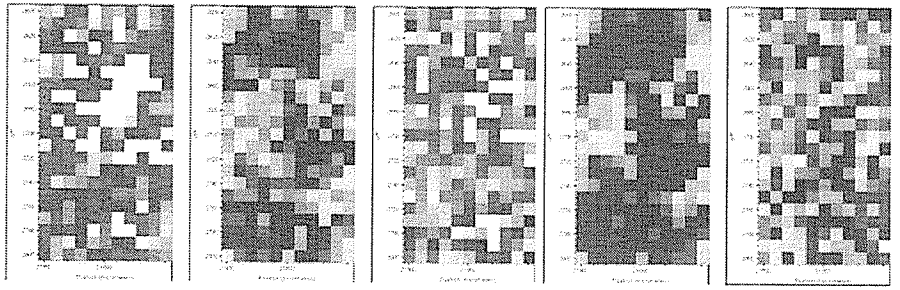

Collagen Phosphate Sugar 1014-1130 Lipid CH_2

3 Day OTC N50 Map 6

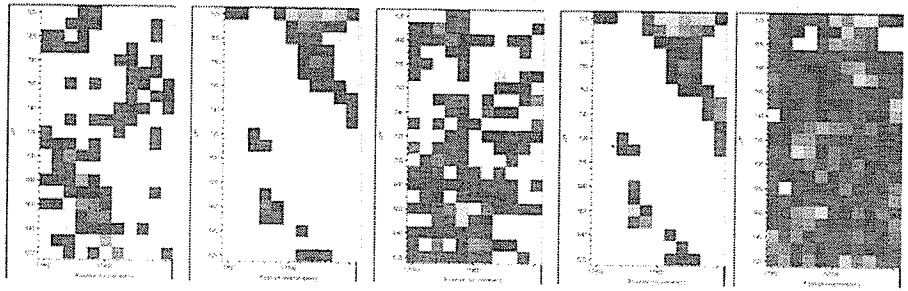

3 Day OTC N54 Map 1

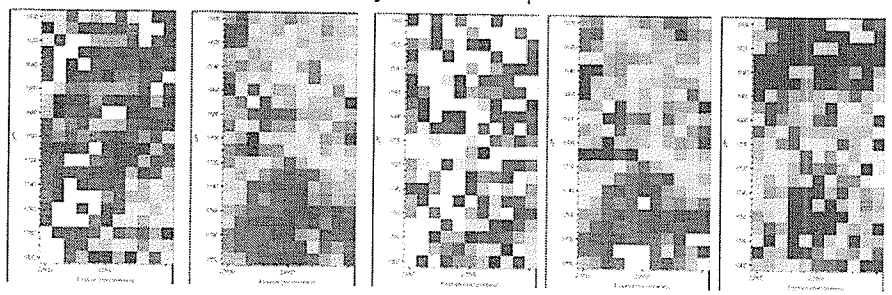

3 Day OTC N54 Map 2

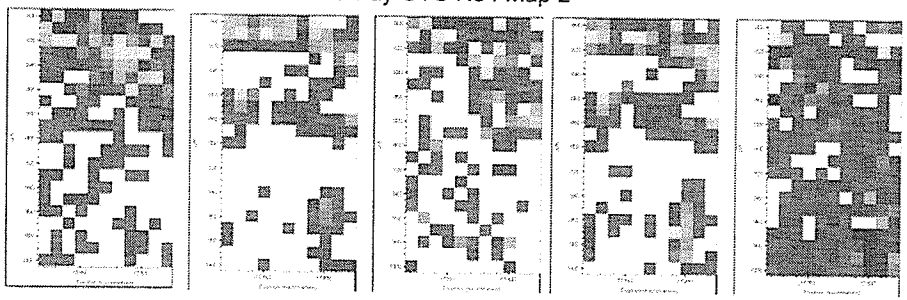

3 Day OTC N54 Map 3

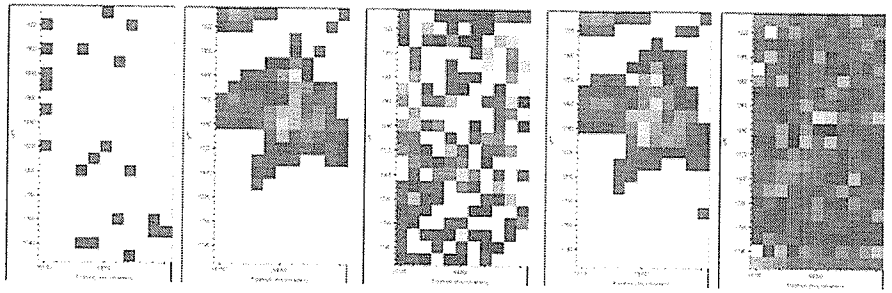

3 Day OTC N54 Map 4

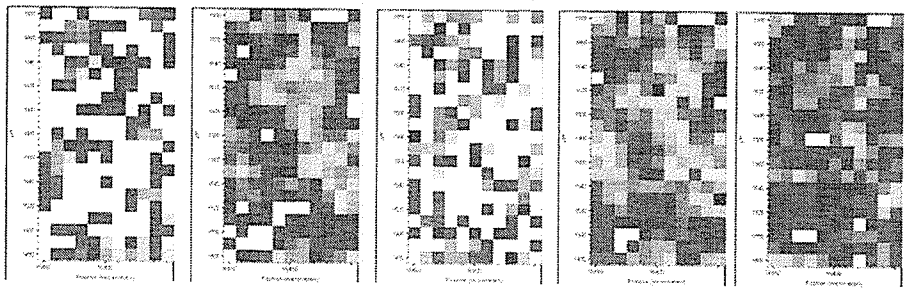

Collagen Phosphate Sugar 1014-1130 Lipid CH_2

3 Day OTC N54 Map 5

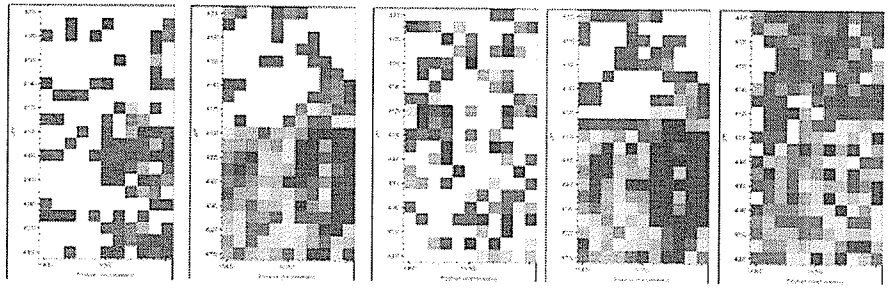

Collagen Phosphate Sugar 1014-1130 Lipid CH_2

3 Day OTC N54 Map 6

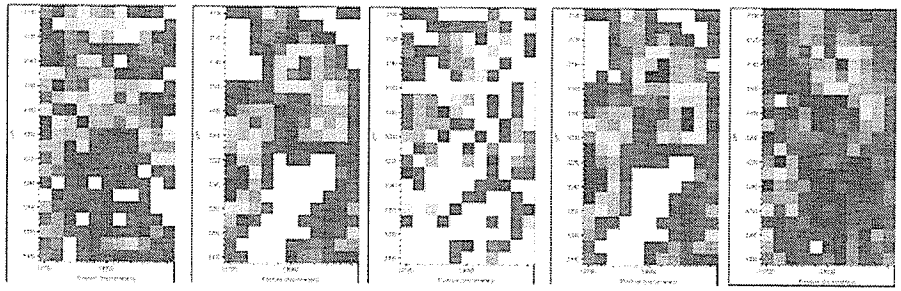

Collagen Phosphate Sugar 1014-1130 Lipid CH_2

3 Day Quercetin

SRC June 2003

Kathy Gough
Meghan Gallant
Vincent Okoli

4 YH QU 41A_01.MAP

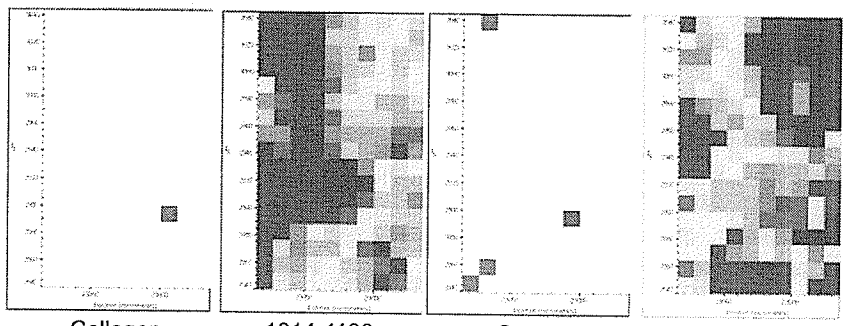

Collagen 1014-1130 Sugar Sym CH2

4 YH QU 41A_02.MAP

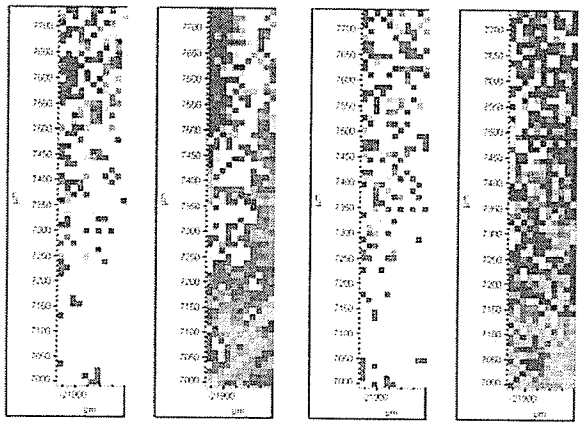

Collagen 1014-1130 Sugar Sym CH2

Most of the map is thick tissue/out of focus
and doesn't provide real information.

4 YH QU 41A_03.MAP

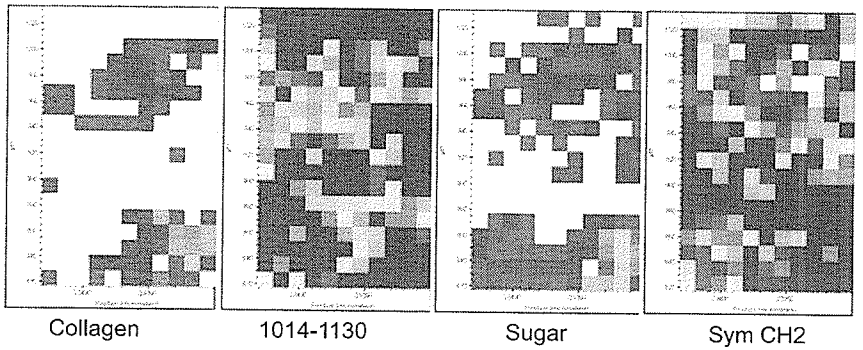

Collagen 1014-1130 Sugar Sym CH2

This map is pretty out of focus

4 YH QU 41A_04.MAP

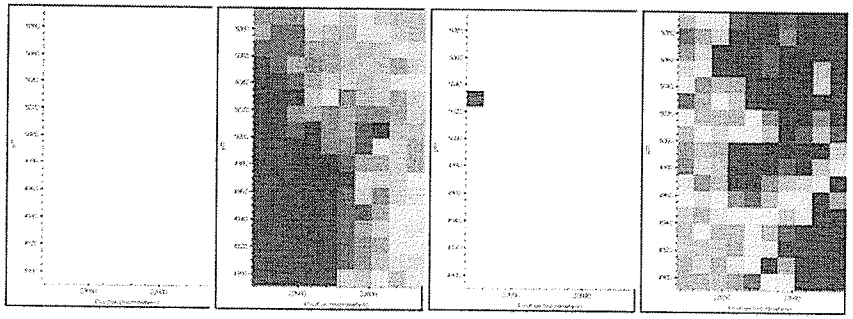

Collagen 1014-1130 Sugar Sym CH2

4 YH QU 41A_05.MAP

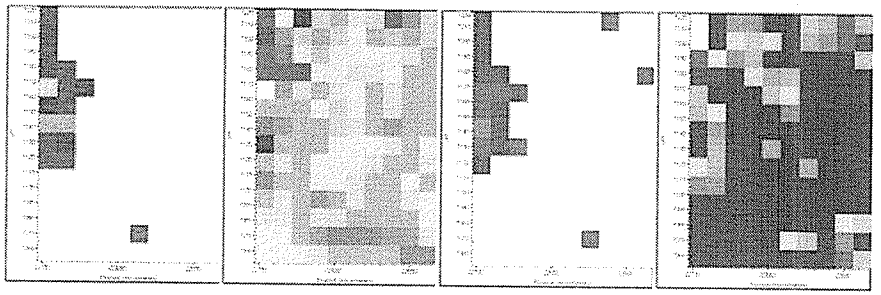

Collagen 1014-1130 Sugar Sym CH2

8 YH QU 42A_01.MAP

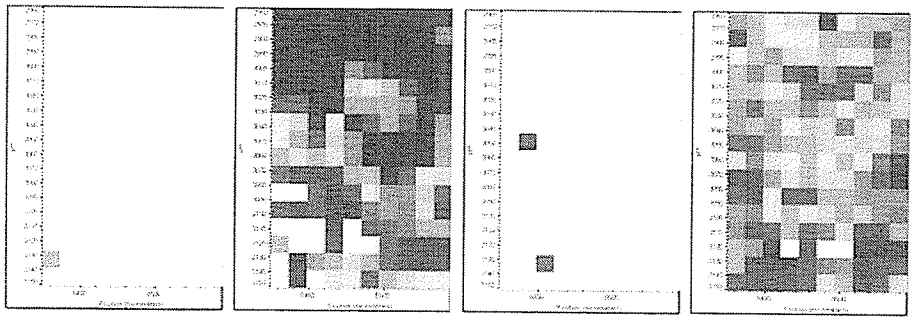

Collagen 1014-1130 Sugar Sym CH2

8 YH QU 42A_02.MAP

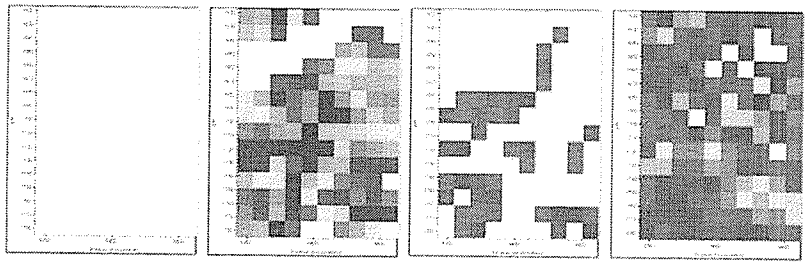

Collagen 1014-1130 Sugar Sym CH2

8 YH QU 42A_03.MAP

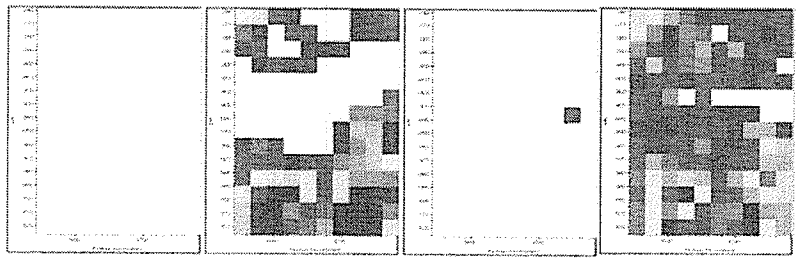

Collagen 1014-1130 Sugar Sym CH2

8 YH QU 42A_04.MAP

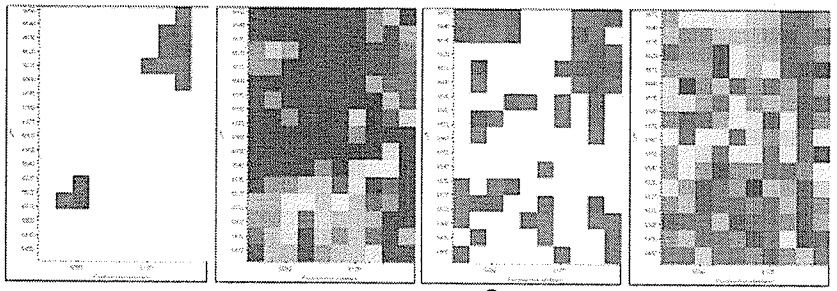

Collagen 1014-1130 Sugar Sym CH2

8 YH QU 42A_05.MAP

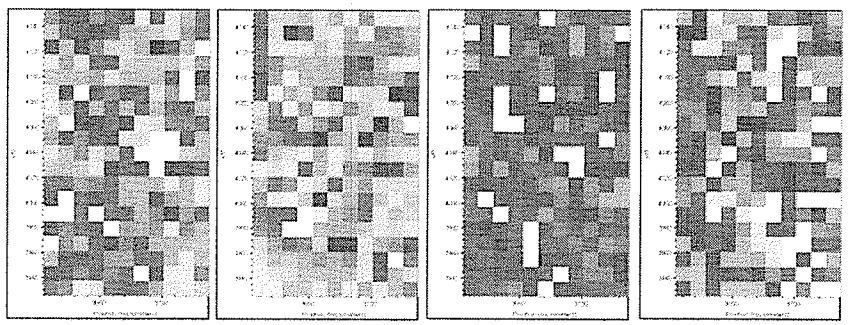

Collagen 1014-1130 Sugar Sym CH2

8 YH QU 42A_06.MAP

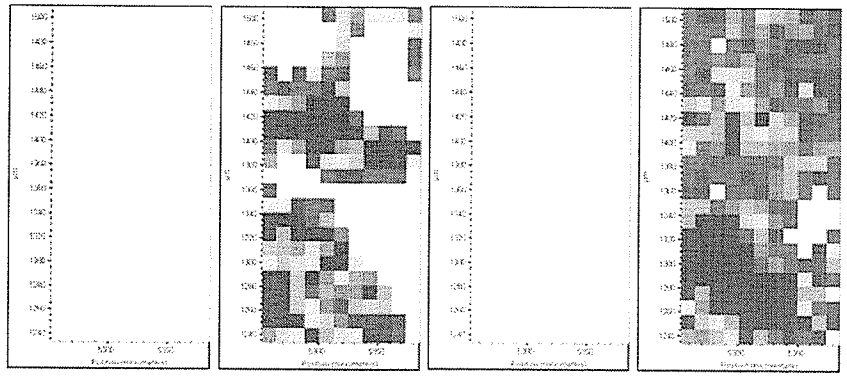

Collagen 1014-1130 Sugar Sym CH2

8 YH QU 42A_07.MAP

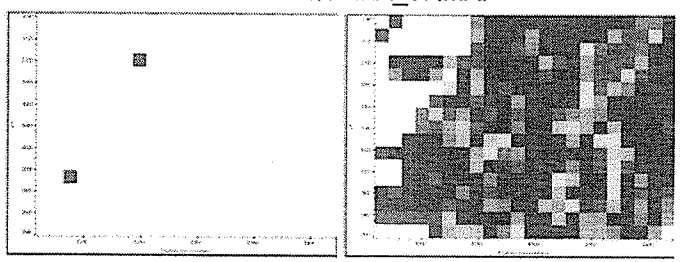

Collagen

1014-1130

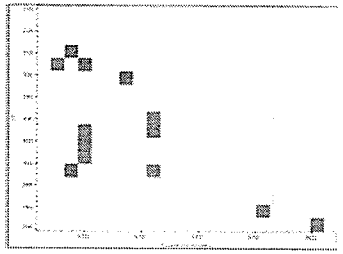

Sugar

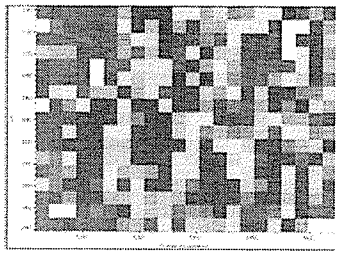

Sym CH2

3 Day Quercetin

SRC July 2004

Fred Zeiler
Richard Wiens
Margaret Rak

3 day Quercetin Animal 28 slide10 map 1

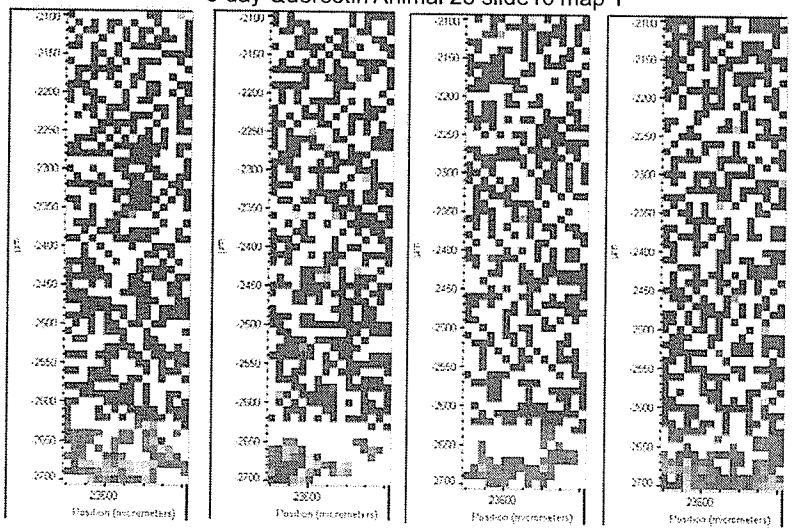

Collagen 1014-1130 Sugar Sym CH2

3 day Quercetin Animal 28 slide10 map2

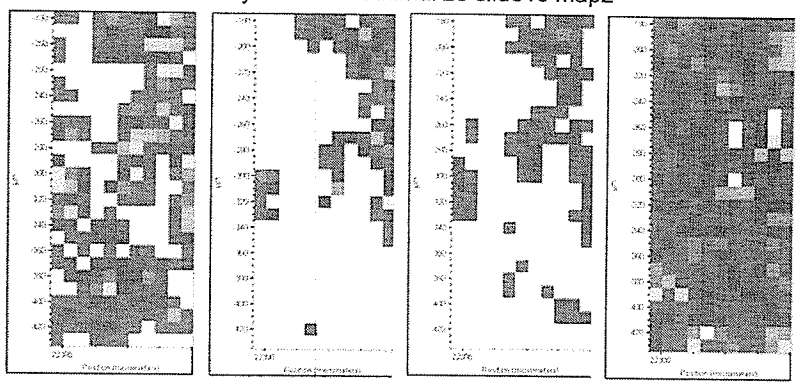

Collagen 1014-1130 Sugar Sym CH2

3 day Quercetin Animal 28 slide10 map 3

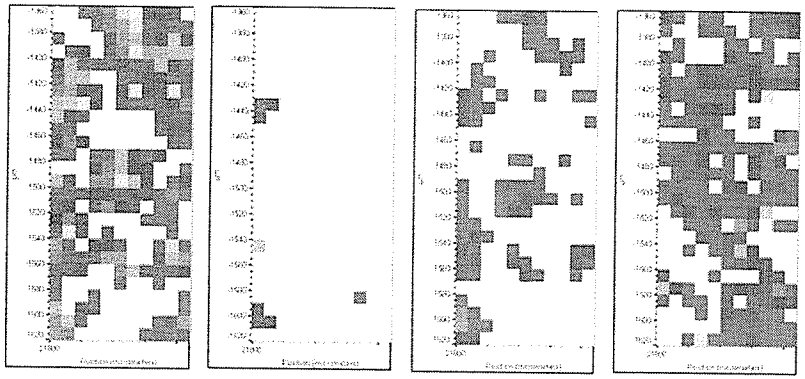

Collagen 1014-1130 Sugar Sym CH2

3 day Quercetin Animal 28 slide10 map 4

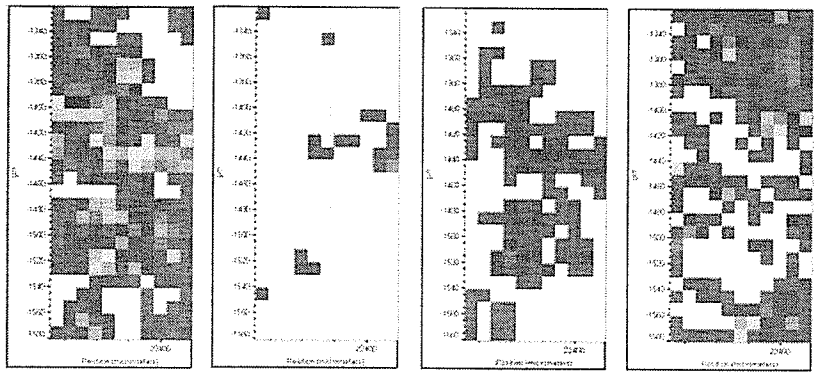

Collagen 1014-1130 Sugar Sym CH2

3 day Quercetin Animal 28 slide10 map 5

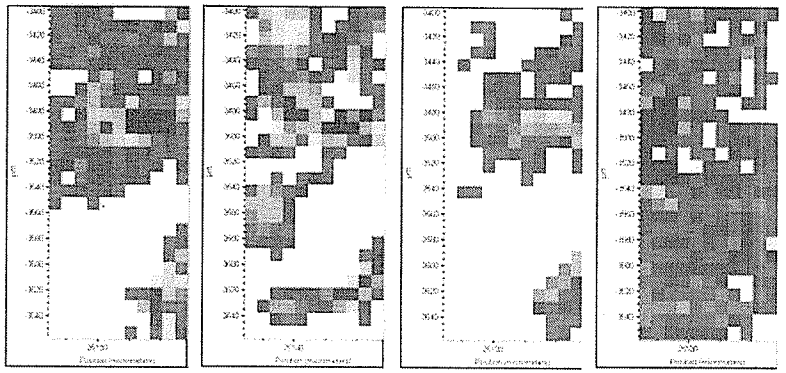

Collagen 1014-1130 Sugar Sym CH2

3 day Quercetin Animal 28 slide10 map 6

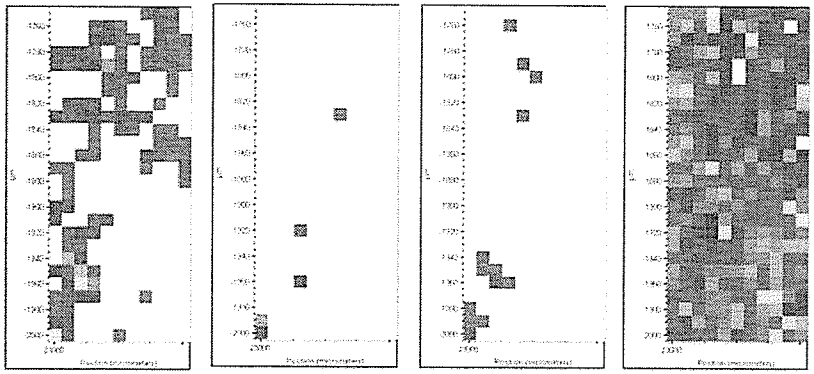

Collagen 1014-1130 Sugar Sym CH2

3 day Quercetin Animal 29 slide10 map 1

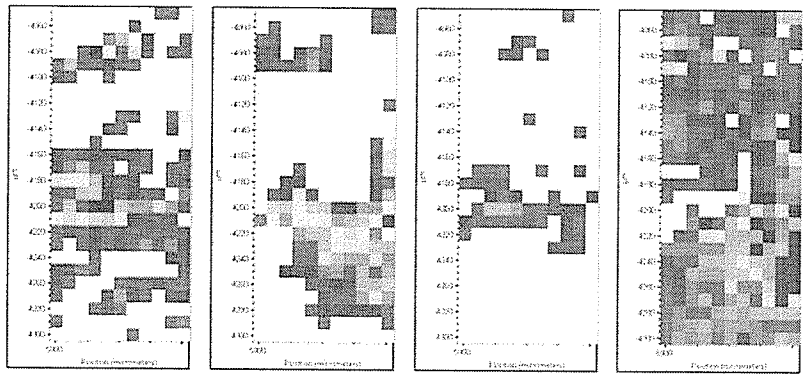

Collagen 1014-1130 Sugar Sym CH2

Top half of map is out of focus

3 day Quercetin Animal 29 slide10 map 2

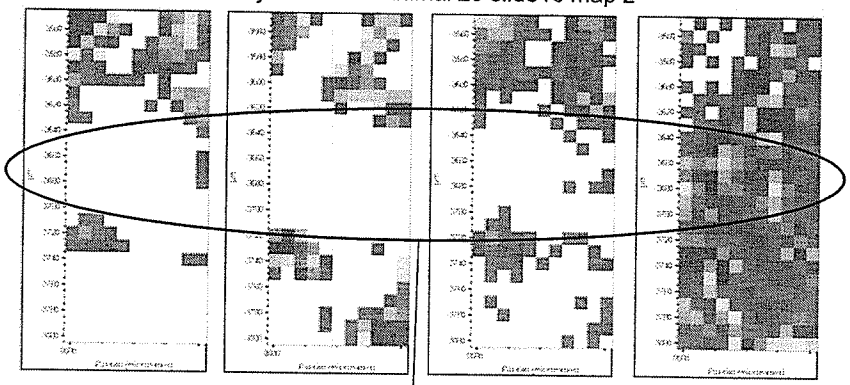

Collagen 1014-1130 Sugar Sym CH2

Tissue is quite thin in places (amide I < 0.6)

3 day Quercetin Animal 29 slide10 map 3

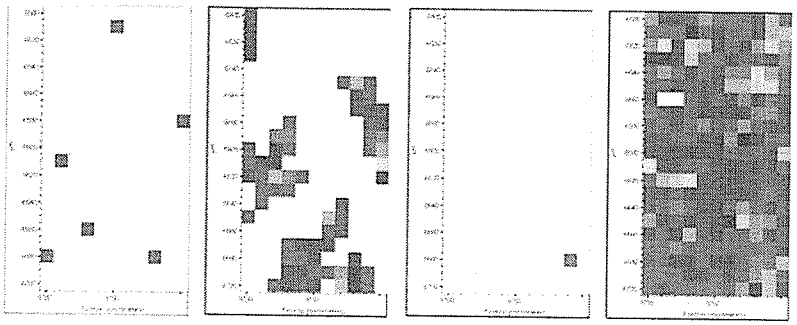

Collagen 1014-1130 Sugar Sym CH2

3 day Quercetin Animal 29 slide10 map 4

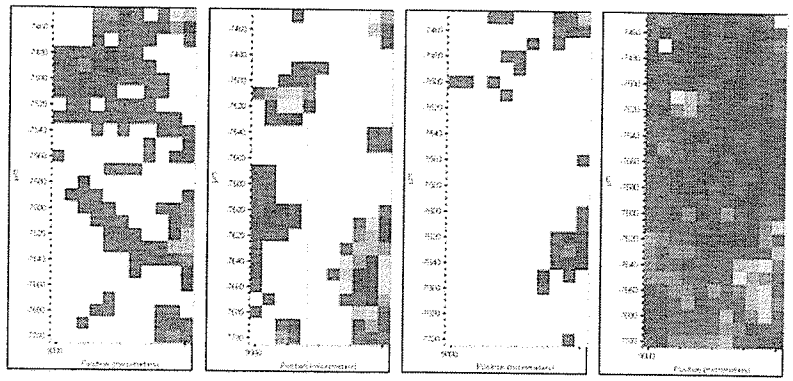

Collagen 1014-1130 Sugar Sym CH2

3 day Quercetin Animal 29 slide10 map 5

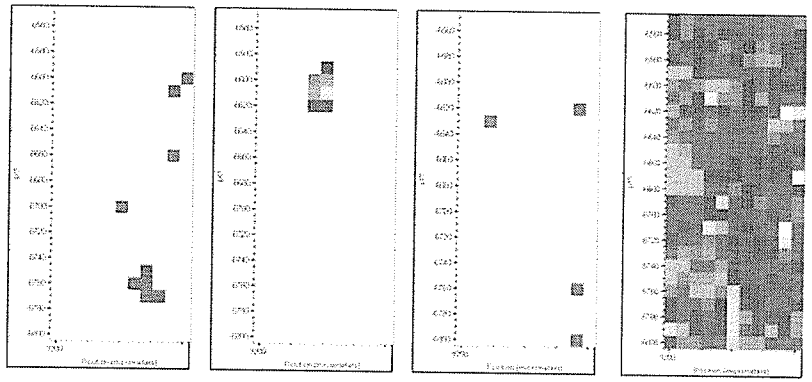

Collagen 1014-1130 Sugar Sym CH2

Thin Tissue (amide I < 0.6)

3 day Quercetin Animal 29 slide10 map 6

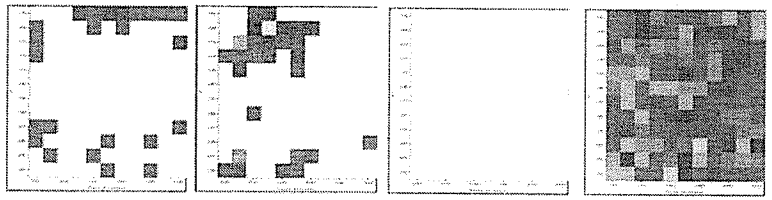

Collagen 1014-1130 Sugar Sym CH2

3 day Quercetin Animal 30 slide10 map 1

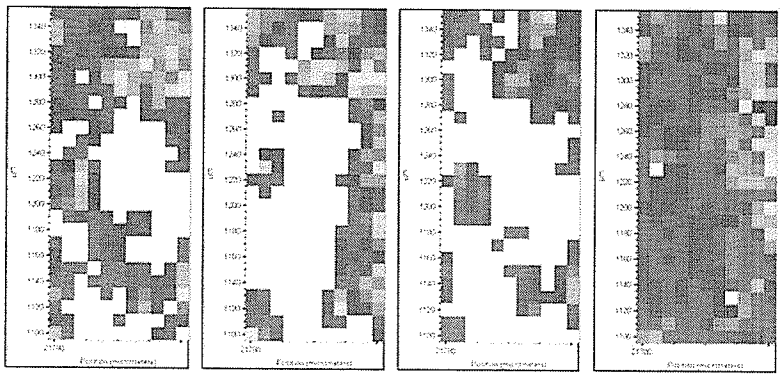

Collagen 1014-1130 Sugar Sym CH2

3 day Quercetin Animal 30 slide10 map 2

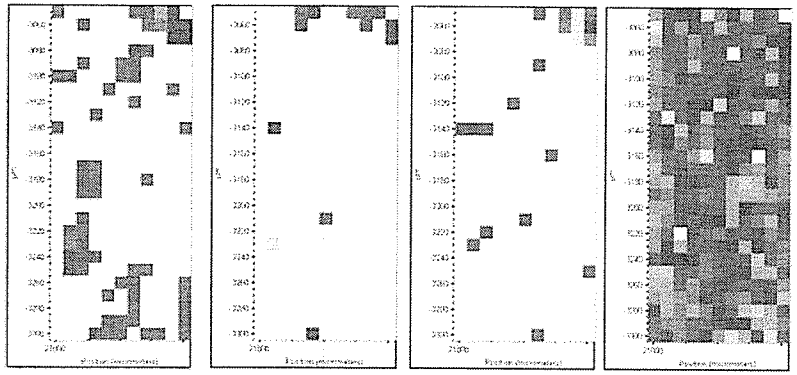

Collagen 1014-1130 Sugar Sym CH2

Very Uneven Tissue. Some places are thick (Amide I > 2) and others are thin (Amide I < 0.6)

3 day Quercetin Animal 30 slide10 map 3

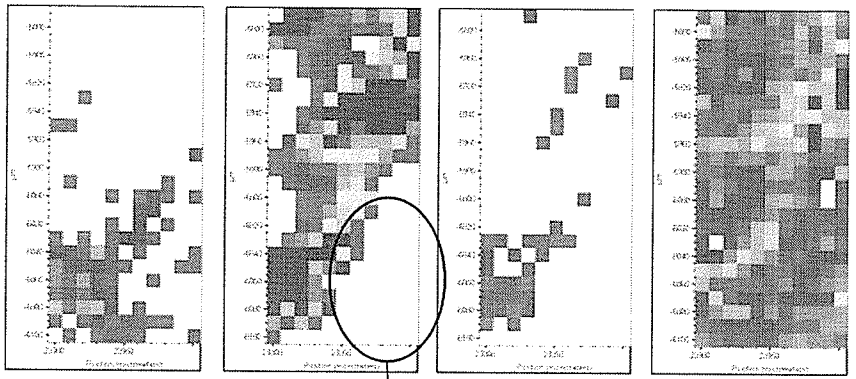

Collagen 1014-1130 Sugar Sym CH2

Thin Tissue (Amide I < 0.6)

3 day Quercetin Animal 30 slide10 map 4

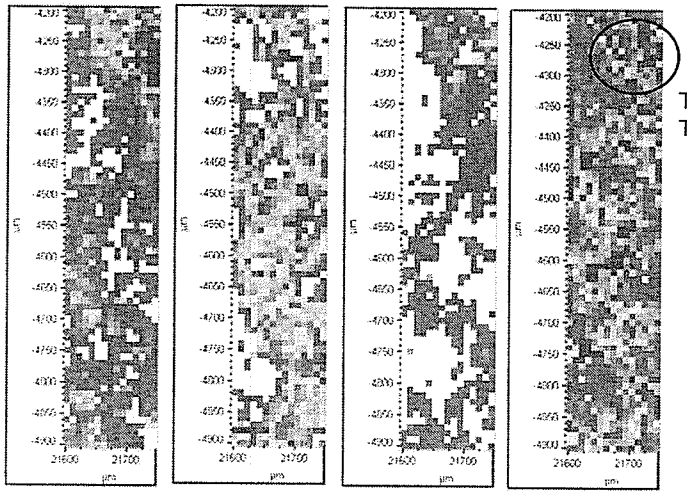

Thick Tissue

Collagen 1014-1130 Sugar Sym CH2

3 day Quercetin Animal 30 slide10 map 5

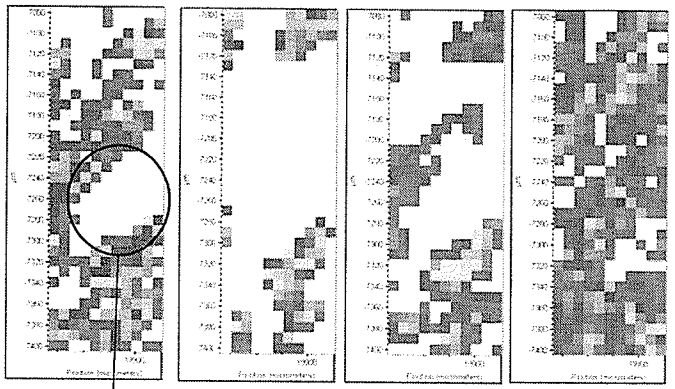

Collagen 1014-1130 Sugar Sym CH2

Yet more thin tissue

3 day Quercetin Animal 30 slide10 map 6

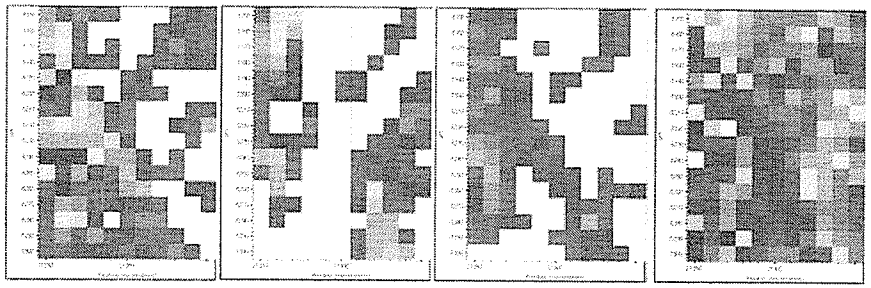

Collagen 1014-1130 Sugar Sym CH2

3 Day Quercetin

SRC August 2006

Richard Wiens

3 Day Que N38 Map 1

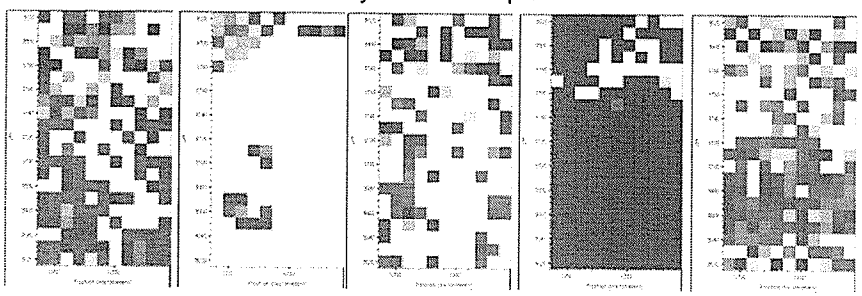

Collagen Phosphate Sugar 1014-1130 Lipid CH_2

3 Day Que N38 Map 2

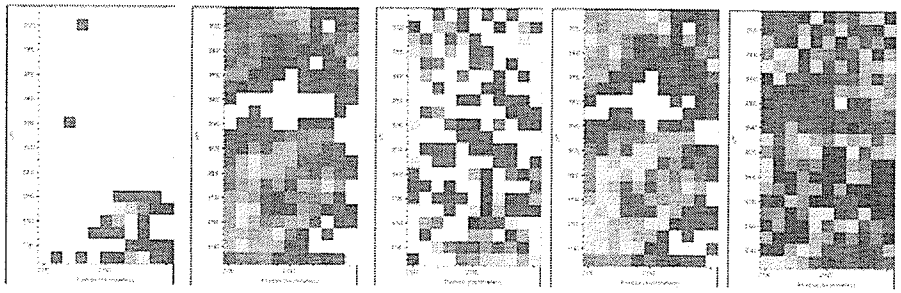

Collagen Phosphate Sugar 1014-1130 Lipid CH_2

3 Day Que N38 Map 3

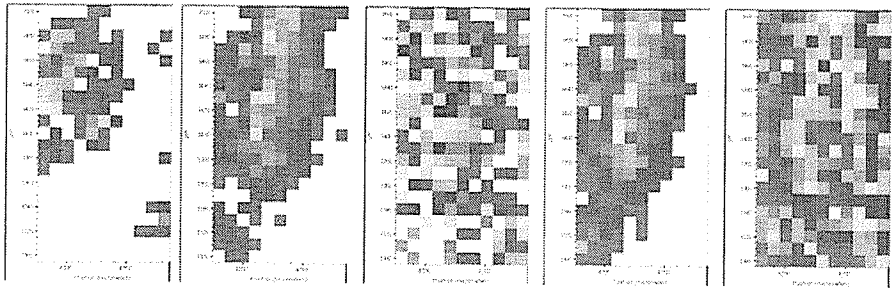

Collagen Phosphate Sugar 1014-1130 Lipid CH_2

3 Day Que N38 Map 4

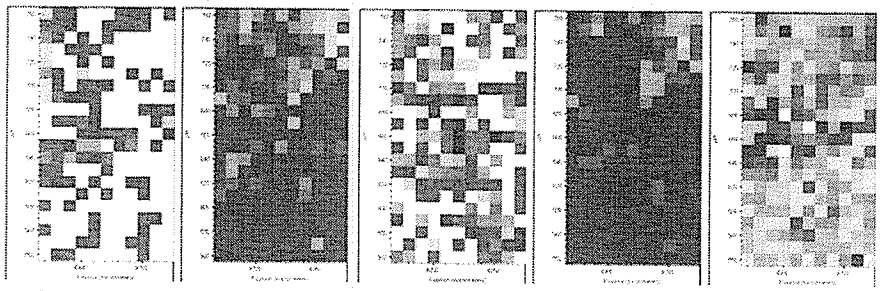

3 Day Que N38 Map 5

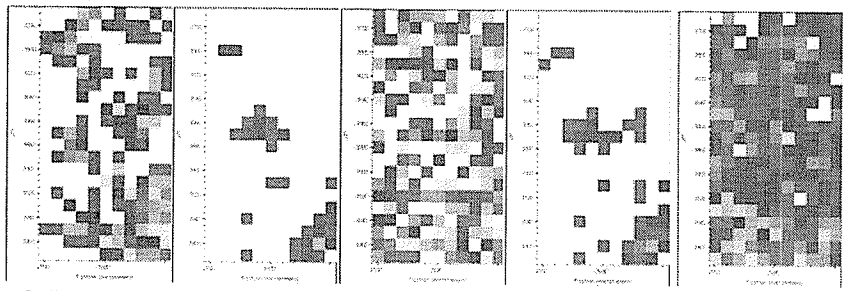

3 Day Que N38 Map 6

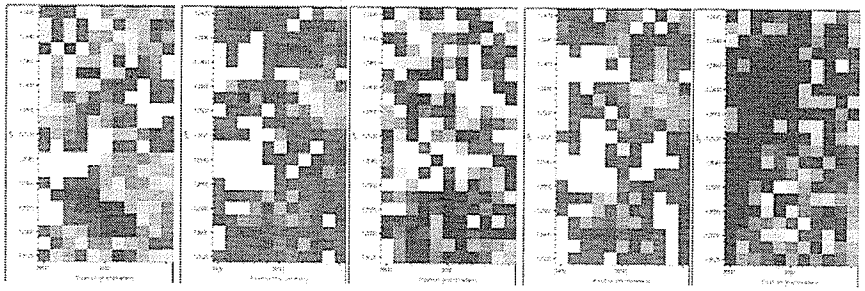

3 Day Que N44 Map 1

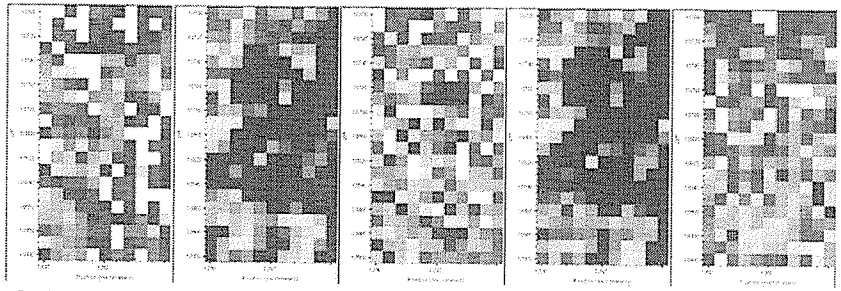

3 Day Que N44 Map 2

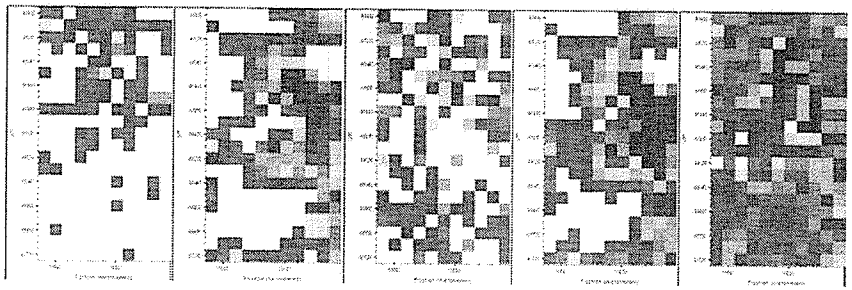

Collagen Phosphate Sugar 1014-1130 Lipid CH_2

3 Day Que N44 Map 3

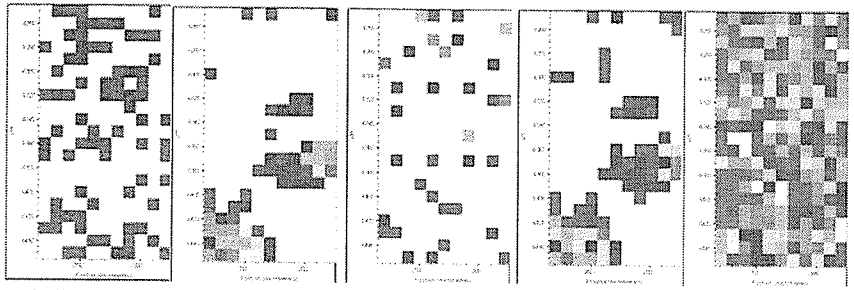

Collagen Phosphate Sugar 1014-1130 Lipid CH_2

3 Day Que N44 Map 4

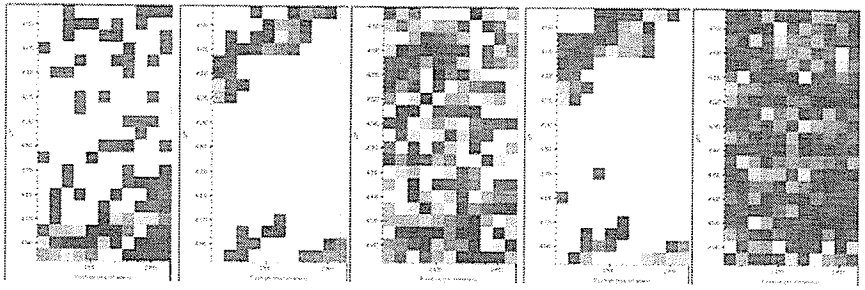

Collagen Phosphate Sugar 1014-1130 Lipid CH_2

3 Day Saline

June 2003

Kathy Gough
Meghan Gallant
Vincent Okoli

4 YH C45 A Map 1

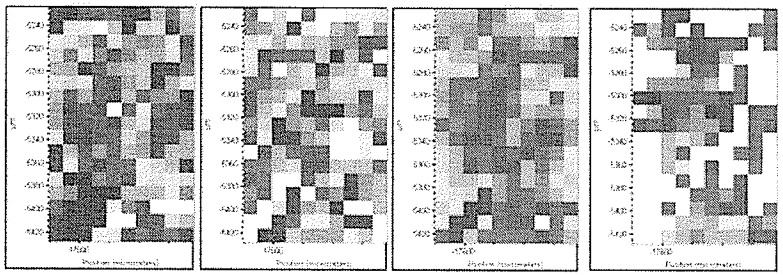

Collagen 1204 | 1014-1130 | Sugar 1024 – 1037 BL: 1020 – 1041 DL: 0.0 to 0.4 | CH_2 Symmetric

4 YH C45 A Map 2

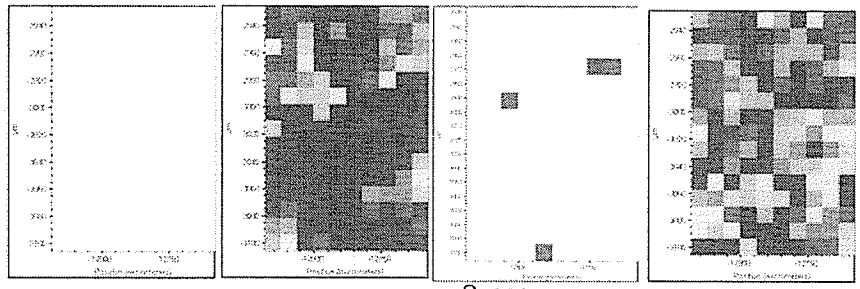

Collagen 1204 | 1014-1130 | Sugar 1024 – 1037 BL: 1020 – 1041 DL: 0.05 to 0.4 | CH_2 Symmetric

4 YH C45 A Map 3

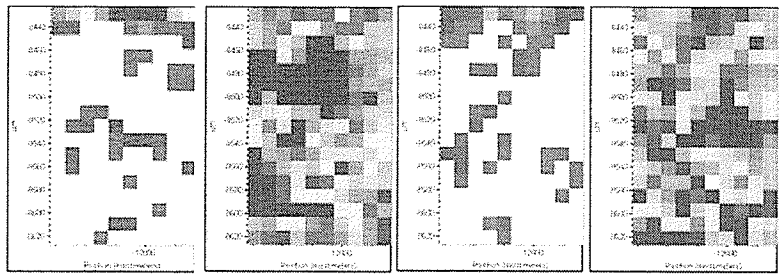

Collagen | 1014-1130 | Sugar 1024 – 1037 BL: 1020 – 1041 DL: 0.05 to 0.4 | CH_2 Symmetric

This map is a bit of an oddity. The top row of spectra has collagen, and lipid (according to CH2), but it has very low sugar/phosphate region compared to the rest of the map. **Collagen + cellular lipid = Myofibroblast?**

4 YH C45 A Map 4

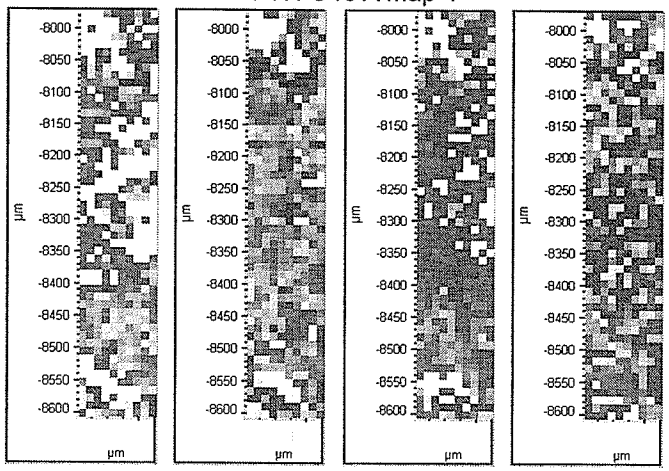

Collagen 1204 | 1014-1130 | Sugar 1024 – 1037 BL: 1020 – 1041 DL: 0.0 to 0.4 | CH_2 Sym

4 YH C45 A Map 5

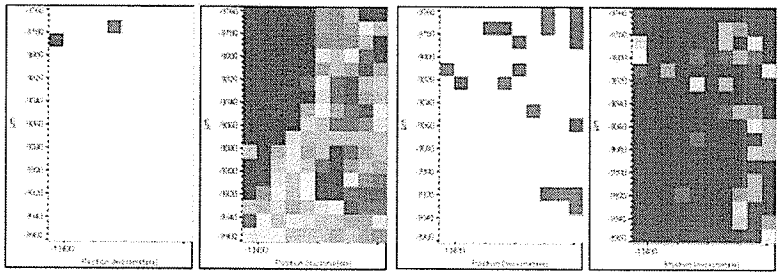

Collagen | 1014-1130 | Sugar 1024 – 1037 BL: 1020 – 1041 DL: 0.0 to 0.4 | CH2 Sym

4 YH C45 A Map 6

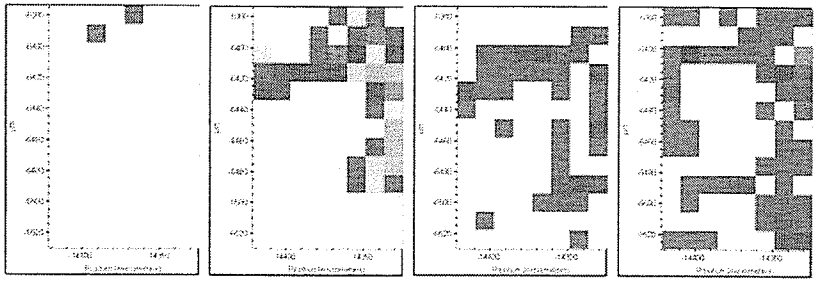

Collagen | 1014-1130 | Sugar 1024 – 1037 BL: 1020 – 1041 DL: 0.05 to 0.4 | CH2 Sym

4 YH C45 A Map 7

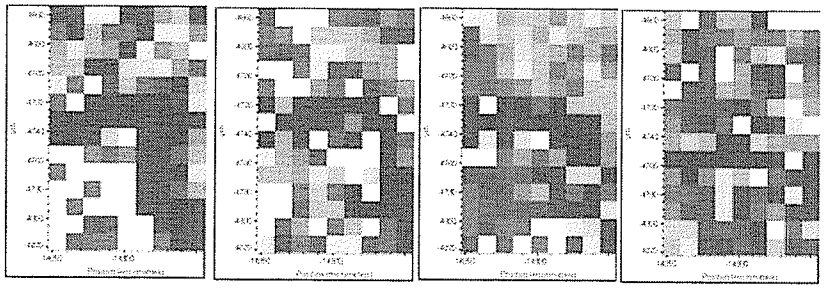

Collagen | 1014-1130 | Sugar 1024 – 1037 BL: 1020 – 1041 DL: 0.05 to 0.4 | CH2 Sym

4 YH C45 A Map 8

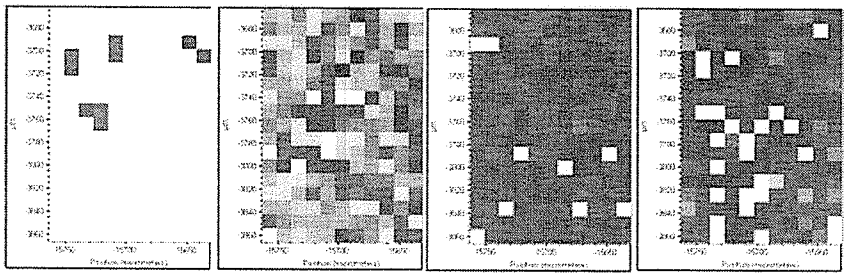

Collagen | 1014-1130 | Sugar 1024 – 1037 BL: 1020 – 1041 DL: 0.0 to 0.4 | CH2 Sym

A lot of the high absorbances in the 1014-1130 map is due to a long period rolling baseline. The other possibility is that we've finally found a region of HA/CS matrix. High sugar, low collagen, low lipid.

4 YH C45 A Map 9

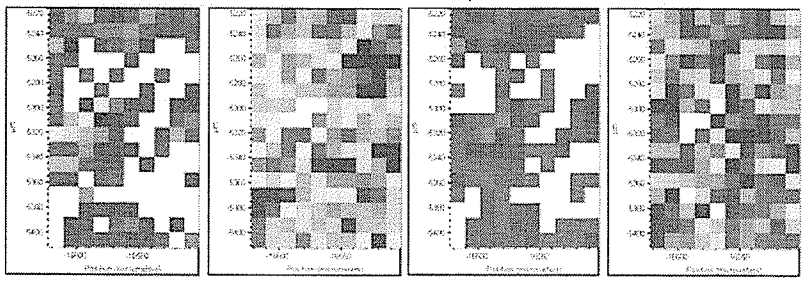

Collagen | 1014-1130 | Sugar 1024 – 1037 BL: 1020 – 1041 DL: 0.05 to 0.4 | CH2 Sym

4 YH C45 A Map 10

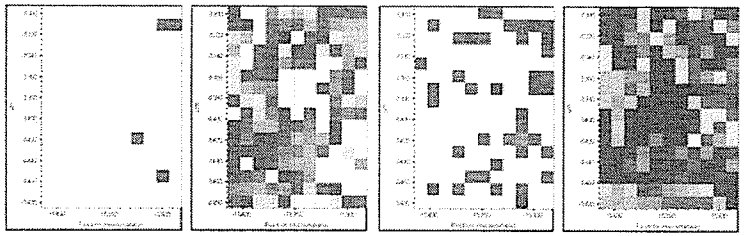

Collagen | 1014-1130 | Sugar 1024 – 1037 BL: 1020 – 1041 DL: 0.05 to 0.4 | CH2 Sym

4 YH C45 A Map 11

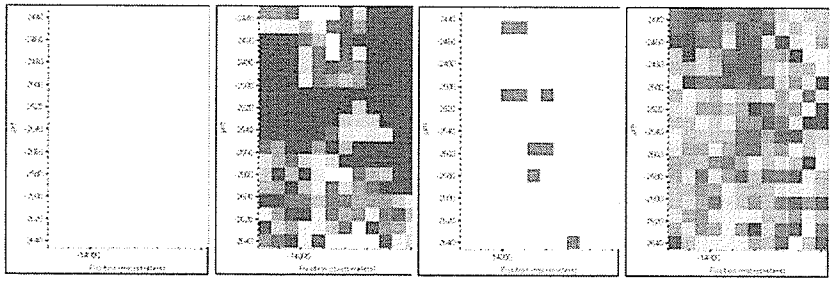

Collagen | 1014-1130 | Sugar 1024 – 1037 BL: 1020 – 1041 DL: 0.05 to 0.4 | CH2 Sym

8 YH C46A Map 1

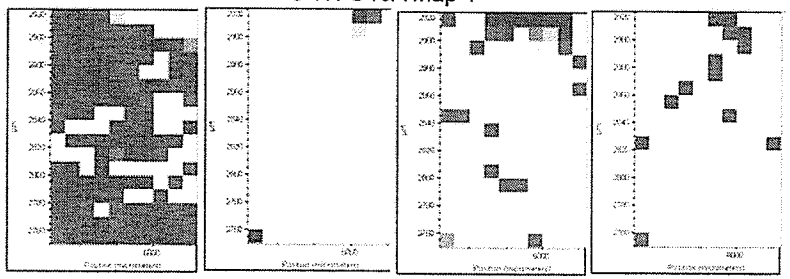

Collagen | 1014-1130 | Sugar 1024 – 1037 BL: 1020 – 1041 DL: 0.05 to 0.4 | CH2 Sym

Something odd with the data collection. Spectra look normal but units are "single beam" and this really messes up display with the normal display limits.

8 YH C46A Map 5

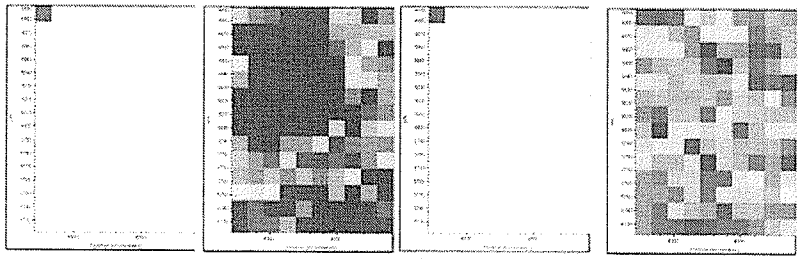

Collagen | 1014-1130 | Sugar 1024 – 1037 BL: 1020 – 1041 DL: 0.05 to 0.4 | CH2 Sym

8 YH C46A Map 6

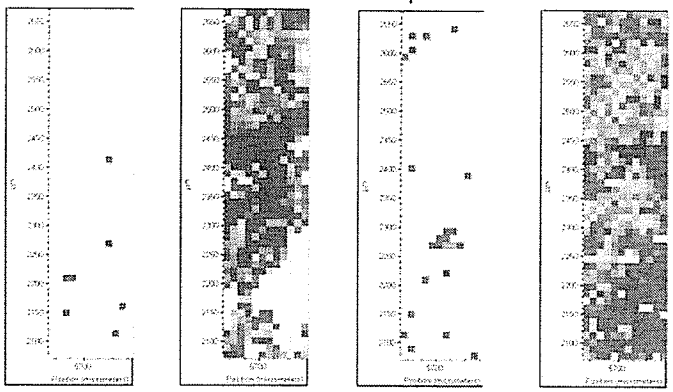

Collagen | 1014-1130 | Sugar 1024 – 1037 BL: 1020 – 1041 DL: 0.05 to 0.4 | CH2 Sym

3 Day Saline

July 2004

Fred Zeiler
Richard Wiens
Margaret Rak

3 Day Saline Animal 34 Slide 10 map1

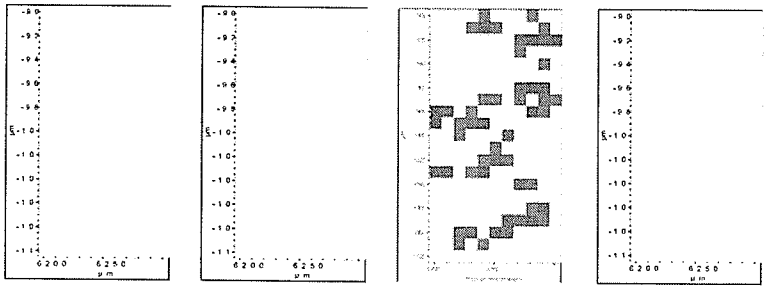

Collagen | 1014-1130 | Sugar 1024 – 1037 BL: 1020 – 1041 DL: 0.05 to 0.4 | Sym CH_2

3 Day Saline Animal 34 Slide 10 map 2

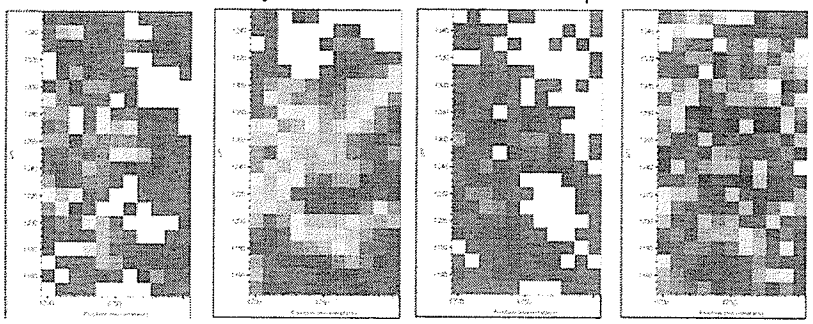

Collagen | 1014-1130 | Sugar 1024 – 1037 BL: 1020 – 1041 DL: 0.05 to 0.4 | Sym CH_2

3 Day Saline Animal 34 Slide 10 map3

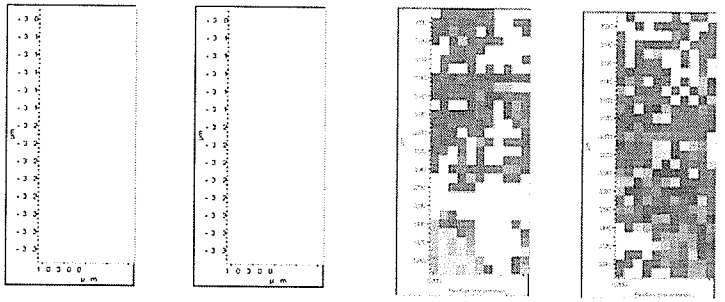

Collagen | 1014-1130 | Sugar 1024 – 1037 BL: 1020 – 1041 DL: 0.05 to 0.4 | Sym CH_2

3 Day Saline Animal 34 Slide 10 map4

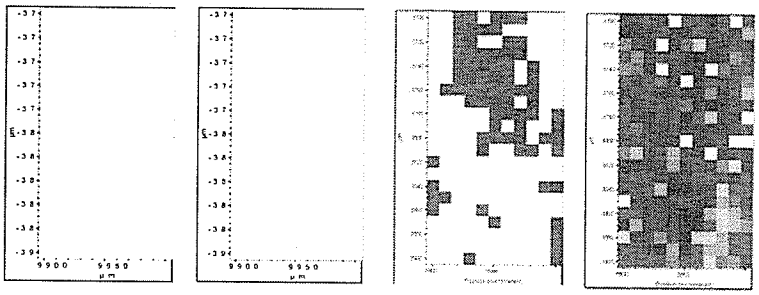

Collagen | 1014-1130 | Sugar | Sym CH_2

Sugar
1024 – 1037
BL: 1020 – 1041
DL: 0.05 to 0.4

3 Day Saline Animal 34 Slide 10 map5

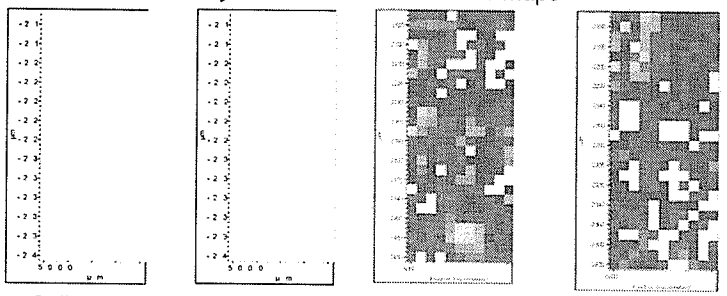

Collagen | 1014-1130 | Sugar | Sym CH_2

Sugar
1024 – 1037
BL: 1020 – 1041
DL: 0.05 to 0.4

3 Day Saline Animal 34 Slide 10 map6

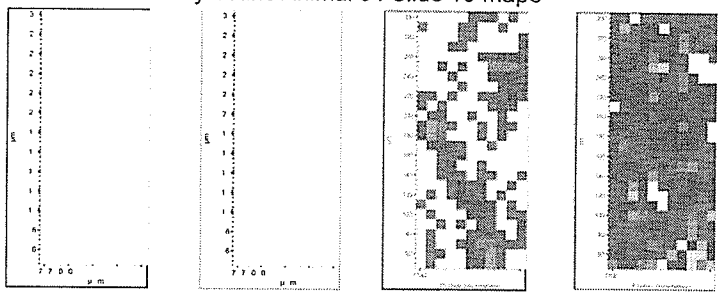

Collagen | 1014-1130 | Sugar | Sym CH_2

Sugar
1024 – 1037
BL: 1020 – 1041
DL: 0.05 to 0.4

3 Day Saline Animal 35 Slide 10 map1

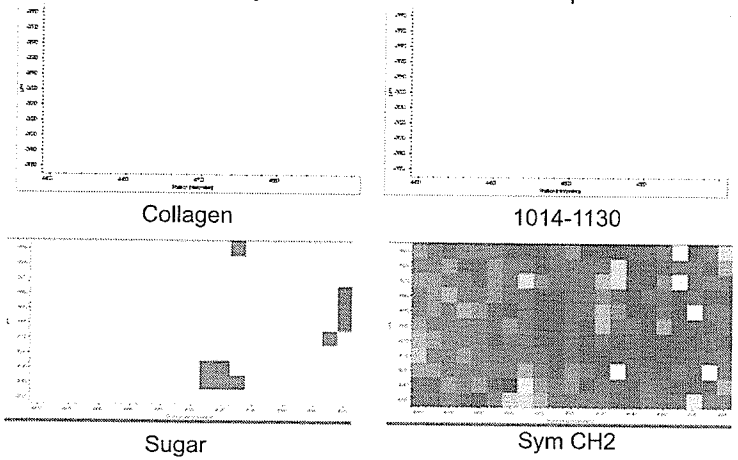

Collagen | 1014-1130 | Sugar | Sym CH2

-top of map is out of focus,
while the bottom is very thin.

3 Day Saline Animal 35 Slide 10 map2

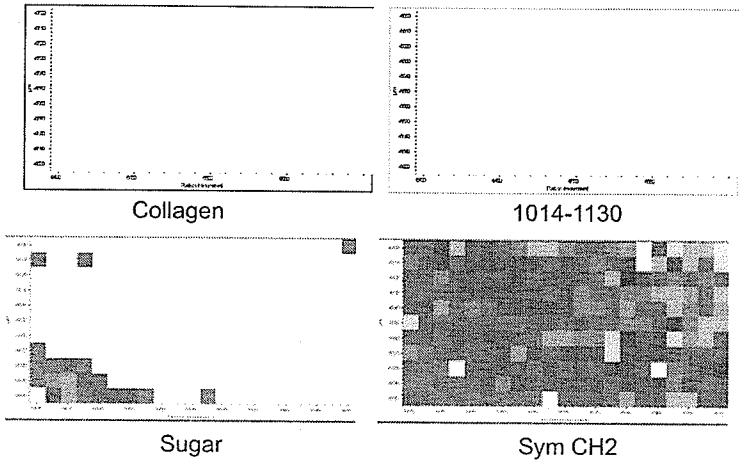

Collagen 1014-1130

Sugar Sym CH2

3 Day Saline Animal 35 Slide 10 map3

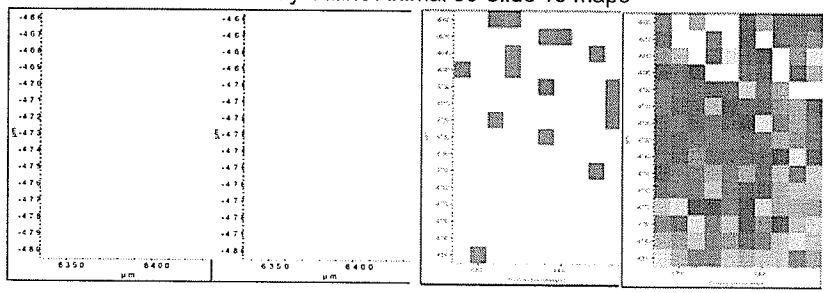

Collagen 1014-1130 Sugar Sym CH_2

1024 – 1037
BL: 1020 – 1041
DL: 0.05 to 0.4

3 Day Saline Animal 35 Slide 10 map4

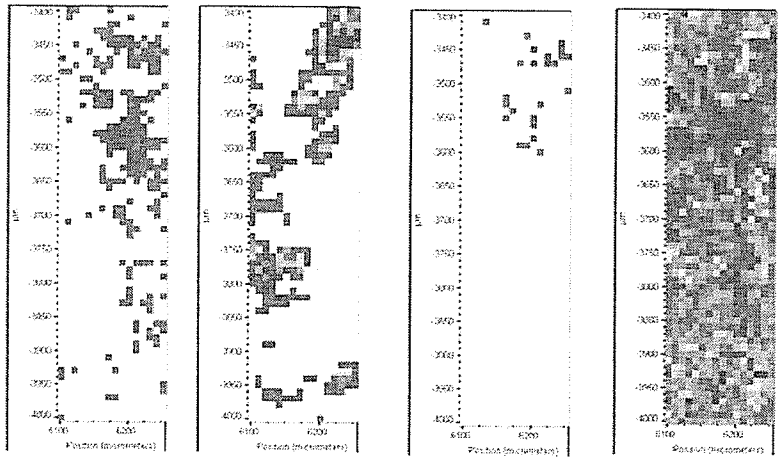

Collagen 1014-1130 Sugar Sym CH_2

1024 – 1037
BL: 1020 – 1041
DL: 0.05 to 0.4

3 Day Saline Animal 35 Slide 10 map5

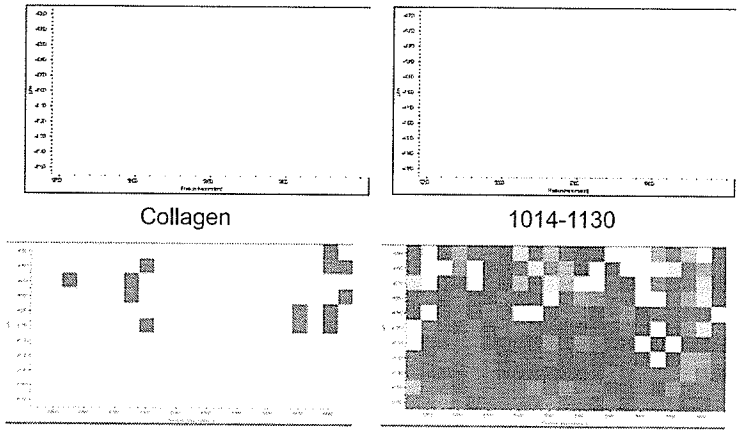

Collagen 1014-1130

Sugar Sym CH2

3 Day Saline Animal 35 Slide 10 map6

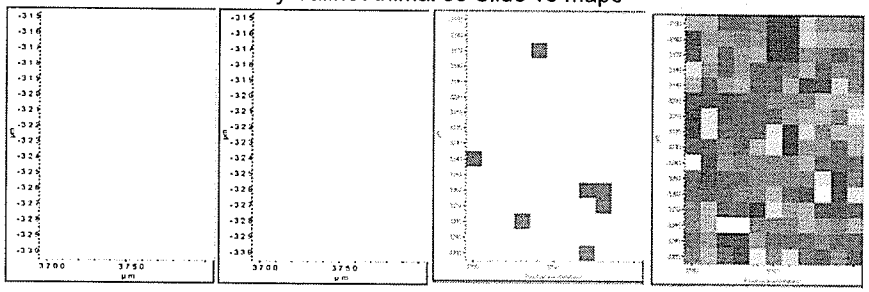

Collagen | 1014-1130 | Sugar | Sym CH_2

Sugar
1024 – 1037
BL: 1020 – 1041
DL: 0.05 to 0.4

3 Day Saline Animal 36 Slide 10 map 1B

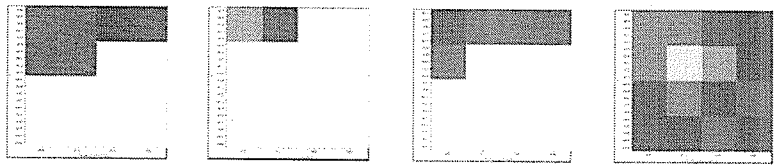

Collagen | 1014-1130 | Sugar | Sym CH2

3 Day Saline Animal 36 Slide 10 map2

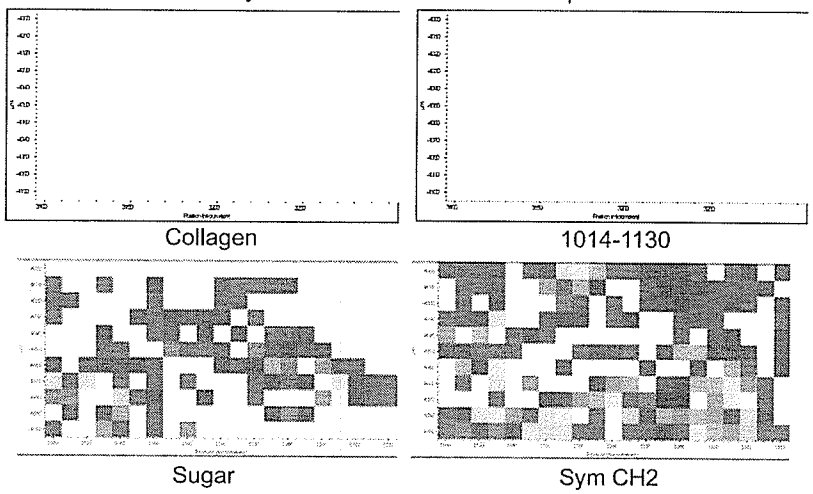

Collagen | 1014-1130

Sugar | Sym CH2

3 Day Saline Animal 36 Slide 10 map3

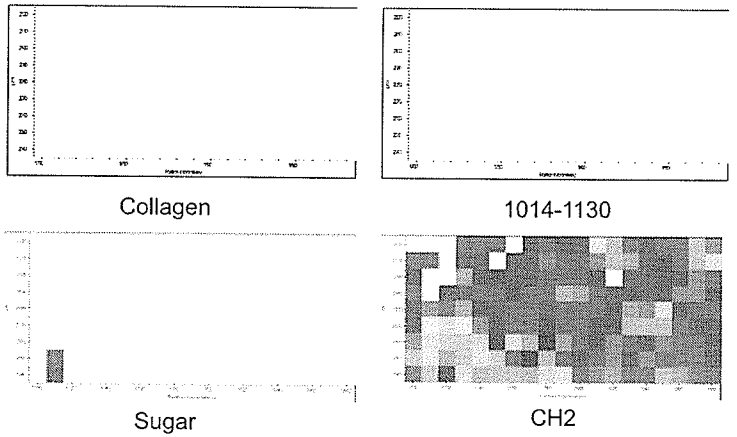

Collagen | 1014-1130

Sugar | CH2

3 Day Saline Rats

Data Collected at SRC in Sept 2004

Margaret Rak

3 day saline 34 Map 1

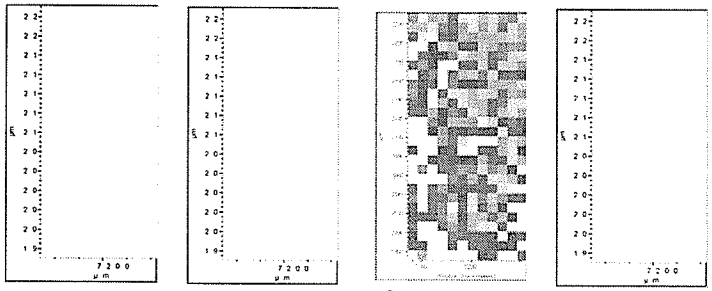

Collagen | 1014-1130 | Sugar 1024 – 1037 BL: 1020 – 1041 DL: 0.05 to 0.4 | Sym CH_2

3 day saline 34 Map 2

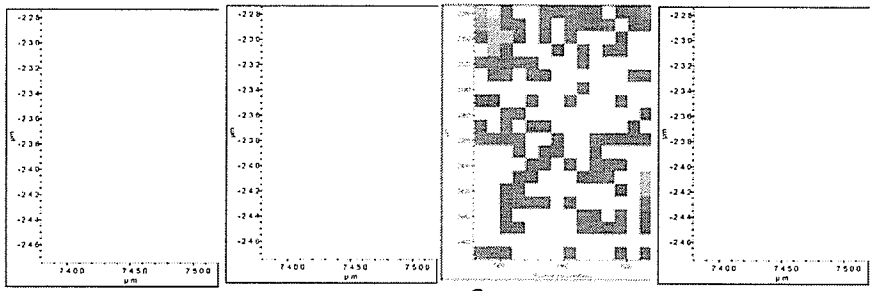

Collagen | 1014-1130 | Sugar 1024 – 1037 BL: 1020 – 1041 DL: 0.05 to 0.4 | Sym CH_2

3 day saline 34 Map 3

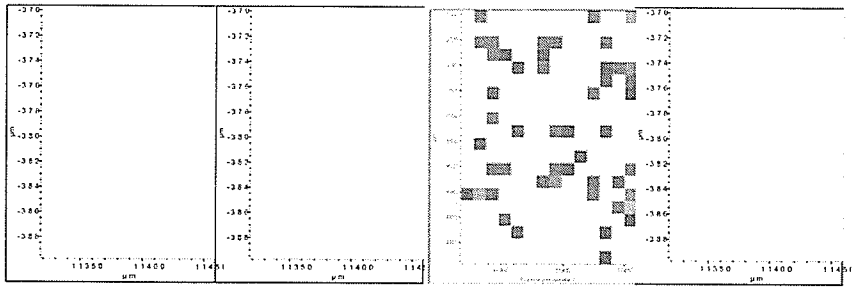

Collagen | 1014-1130 | Sugar 1024 – 1037 BL: 1020 – 1041 DL: 0.05 to 0.4 | Sym CH_2

3 day saline 35 Map 1

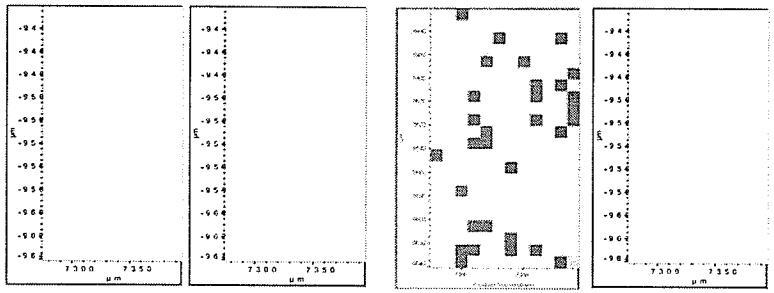

Collagen | 1014-1130 | Sugar | Sym CH_2

Sugar
1024 – 1037
BL: 1020 – 1041
DL: 0.05 to 0.4

3 day saline 35 Map 2

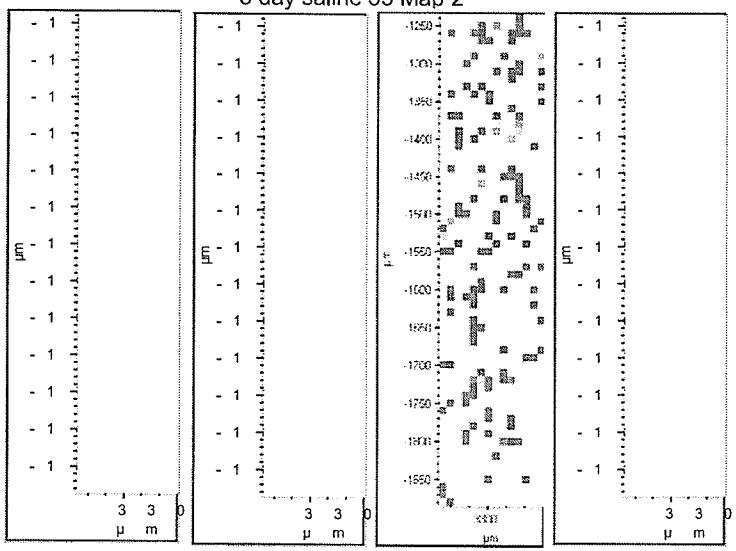

Collagen | 1014-1130 | Sugar | Sym CH_2

Sugar
1024 – 1037
BL: 1020 – 1041
DL: 0.05 to 0.4

3 day saline 35 Map 3

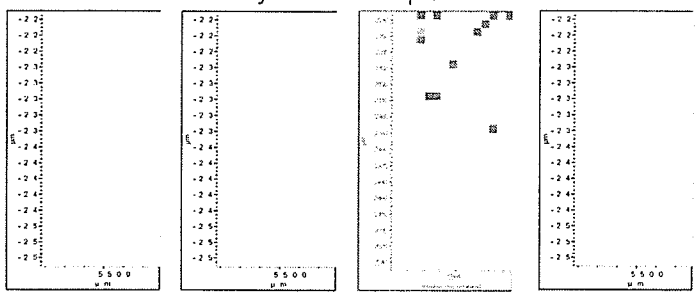

Collagen | 1014-1130 | Sugar | CH_2 Sym

Sugar
1024 – 1037
BL: 1020 – 1041
DL: 0.05 to 0.4

3 day saline 35 Map 4 redone

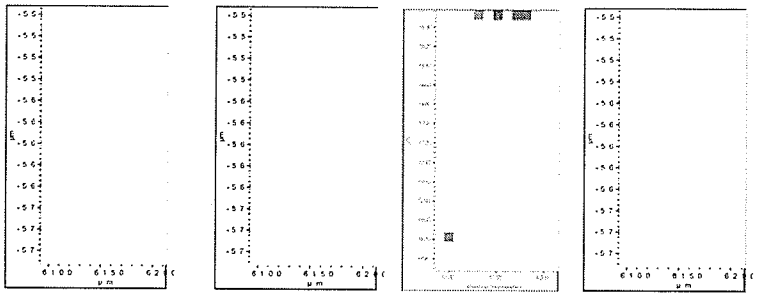

Collagen | 1014-1130 | Sugar | CH_2 Sym

Sugar
1024 – 1037
BL: 1020 – 1041
DL: 0.05 to 0.4

- Somewhat noisy data, but there is collagen there
- White Pixels in lipid processing don't give relevant results
- Very Thin tissue throughout the sample

3 day saline 35 Map 5

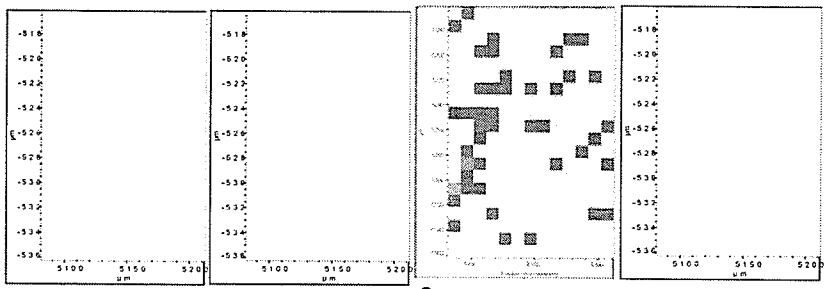

Collagen | 1014-1130 | Sugar 1024 – 1037 BL: 1020 – 1041 DL: 0.05 to 0.4 | Sym CH_2

Spectra below 1400 cm-1 tend to be noisy

3 day saline 35 Map 6

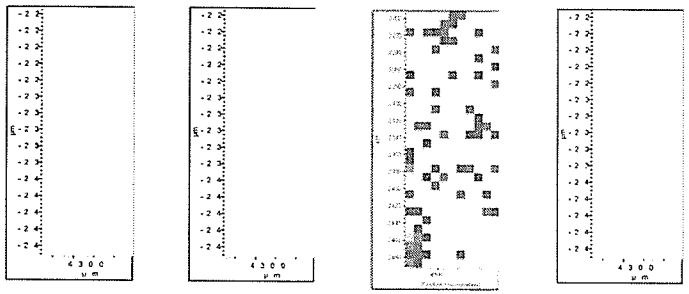

Collagen | 1014-1130 | Sugar 1024 – 1037 BL: 1020 – 1041 DL: 0.05 to 0.4 | Sym CH_2

3 day saline 35 Map 7

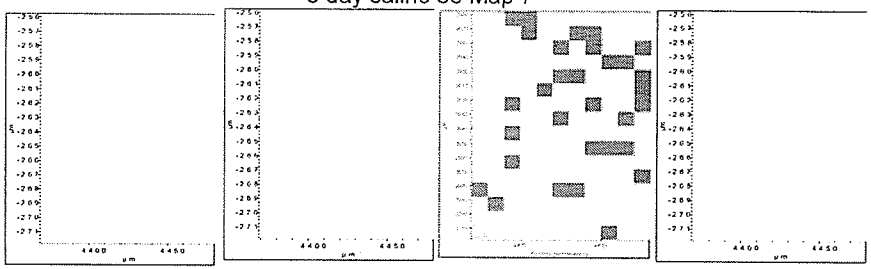

Collagen | 1014-1130 | Sugar 1024 – 1037 BL: 1020 – 1041 DL: 0.05 to 0.4 | Sym CH_2

3 day saline 36 Map 1

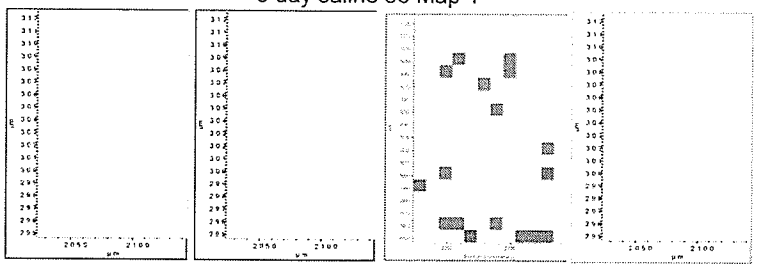

Collagen | 1014-1130 | Sugar 1024 – 1037 BL: 1020 – 1041 DL: 0.05 to 0.4 | Sym CH_2

3 day saline 36 Map 2

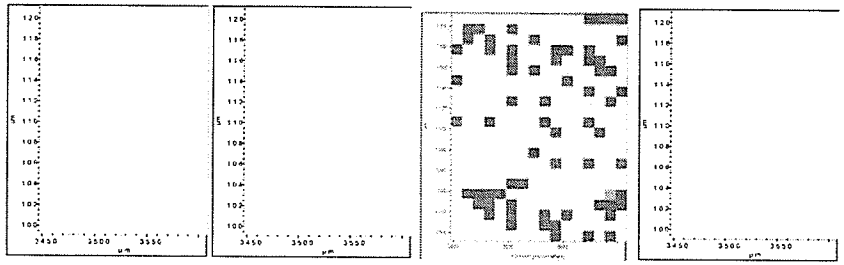

Collagen | 1014-1130 | Sugar 1024 – 1037 BL: 1020 – 1041 DL: 0.05 to 0.4 | Sym CH_2

3 day saline 36 Map 3

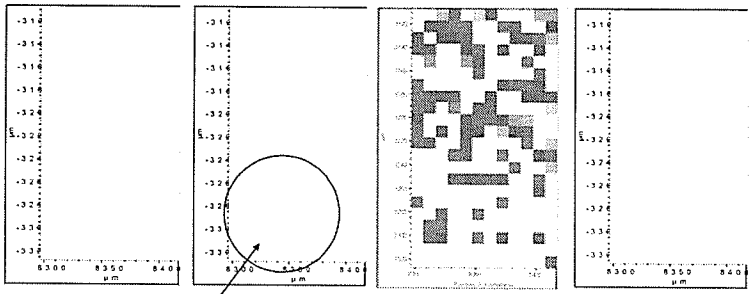

Collagen | 1014-1130 | Thin Tissue | Sugar 1024 – 1037 BL: 1020 – 1041 DL: 0.05 to 0.4 | Sym CH_2

3 day saline 36 Map 4

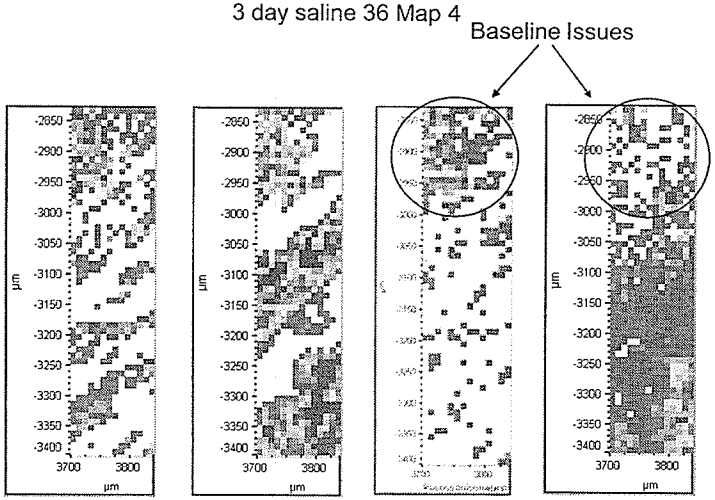

Collagen | 1014-1130 | Sugar 1024 – 1037 BL: 1020 – 1041 DL: 0.05 to 0.4 | Sym CH_2

3 day saline 36 Map 5

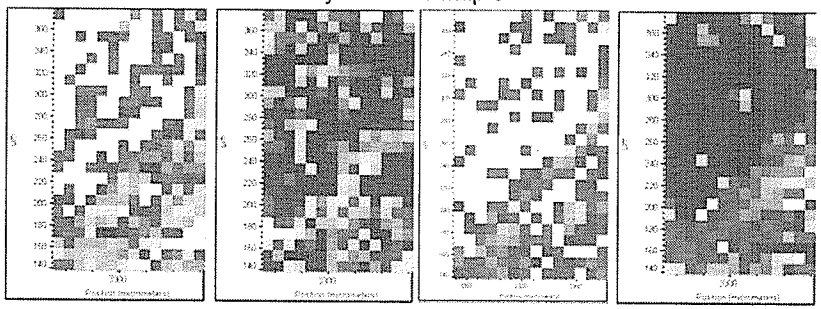

Collagen | 1014-1130 | Sugar 1024 – 1037 BL: 1020 – 1041 DL: 0.05 to 0.4 | Sym CH_2

3 day saline 36 Map 6

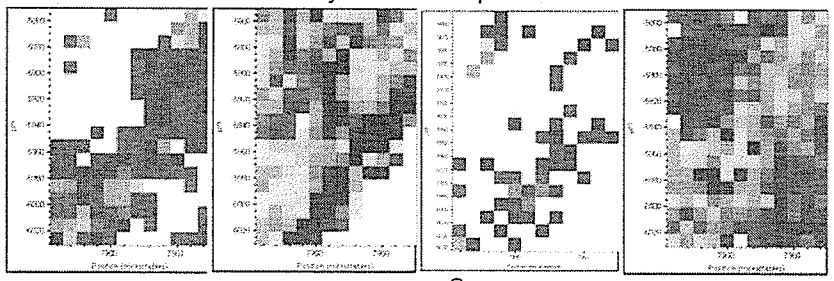

Collagen | 1014-1130 | Sugar | Sym CH_2

Sugar
1024 – 1037
BL: 1020 – 1041
DL: 0.05 to 0.4

3 Day Saline

SRC August 2006

Richard Wiens

3 Day Saline N56 Map 1

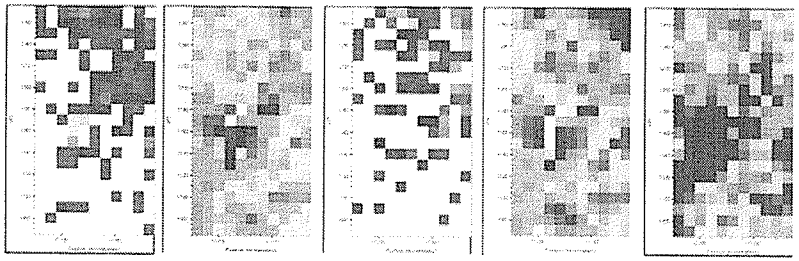

Collagen | Phosphate | Sugar | 1014-1130 | Lipid Sym CH_2

3 Day Saline N56 Map 2

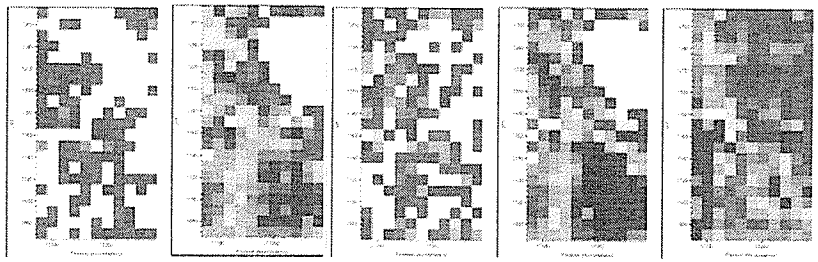

Collagen | Phosphate | Sugar | 1014-1130 | Lipid Sym CH_2

3 Day Saline N56 Map 3

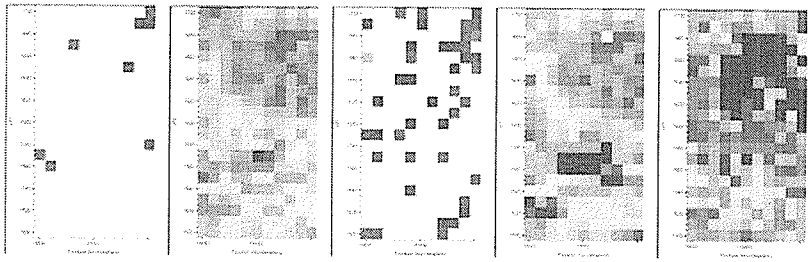

Collagen | Phosphate | Sugar | 1014-1130 | Lipid Sym CH_2

3 Day Saline N56 Map 4

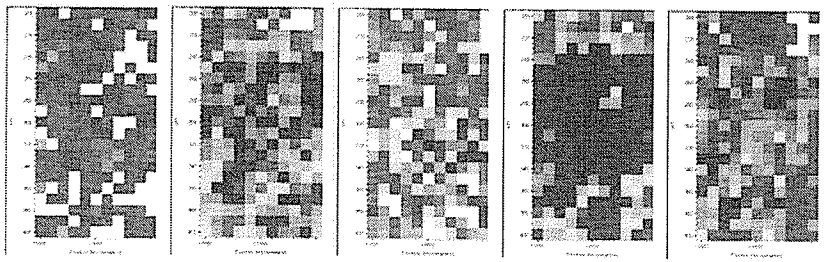

Collagen Phosphate Sugar 1014-1130 Lipid Sym CH_2

3 Day Saline N56 Map 5

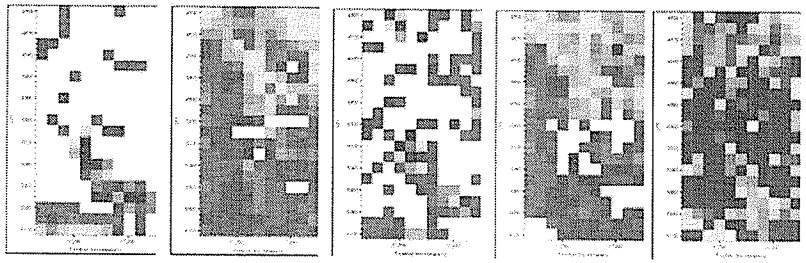

Collagen Phosphate Sugar 1014-1130 Lipid Sym CH_2

3 Day Saline N56 Map 6

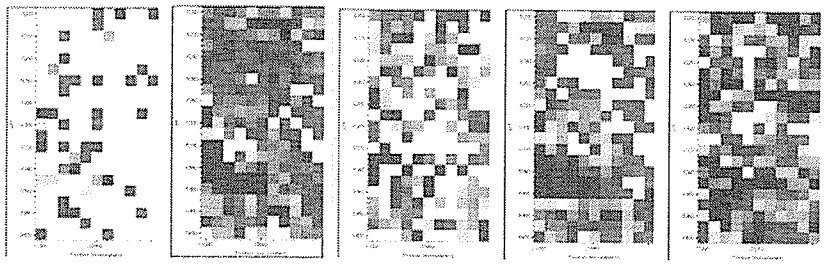

Collagen Phosphate Sugar 1014-1130 Lipid Sym CH_2

3 Day Saline N59 Map 1

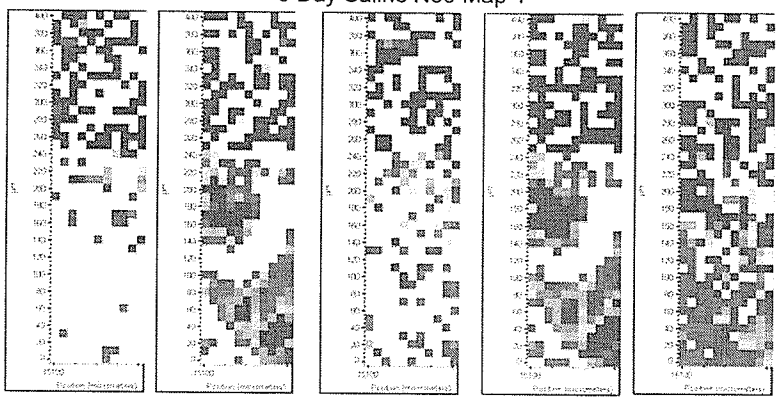

Collagen Phosphate Sugar 1014-1130 Lipid Sym CH_2

3 Day Saline N59 Map 2

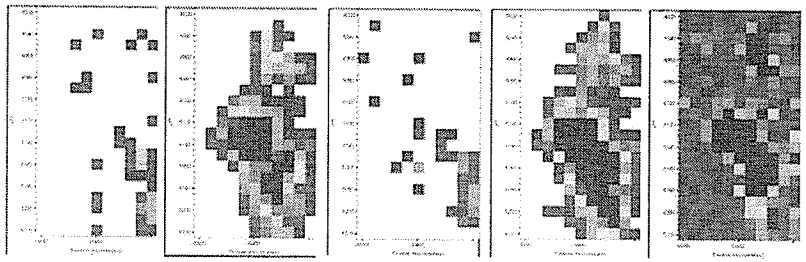

Collagen Phosphate Sugar 1014-1130 Lipid Sym CH_2

3 Day Saline N59 Map 3

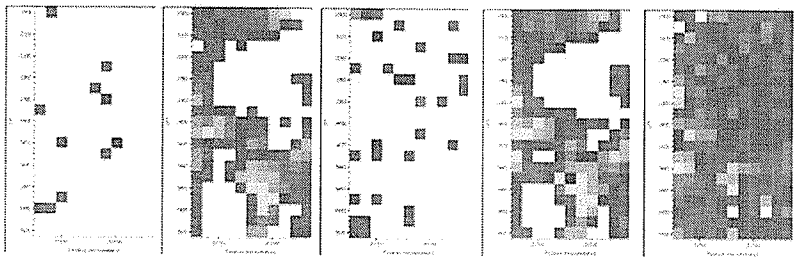

Collagen Phosphate Sugar 1014-1130 Lipid Sym CH_2

3 Day Saline N59 Map 4

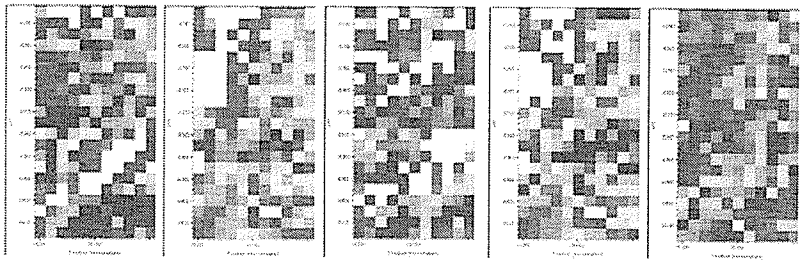

Collagen Phosphate Sugar 1014-1130 Lipid Sym CH_2

3 Day Saline N59 Map 5

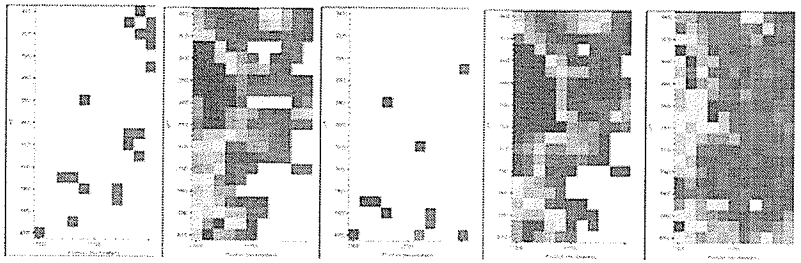

Collagen Phosphate Sugar 1014-1130 Lipid Sym CH_2

3 Day Saline N59 Map 6

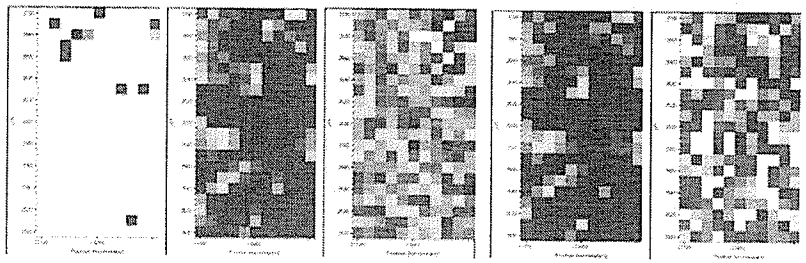

Collagen Phosphate Sugar 1014-1130 Lipid Sym CH_2

3 Day Saline N61 Map 1

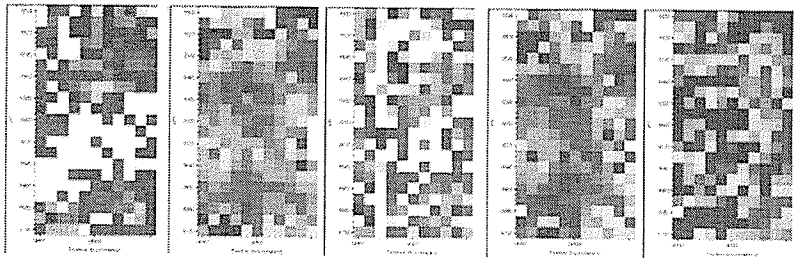

Collagen Phosphate Sugar 1014-1130 Lipid Sym CH_2

3 Day Saline N61 Map 2

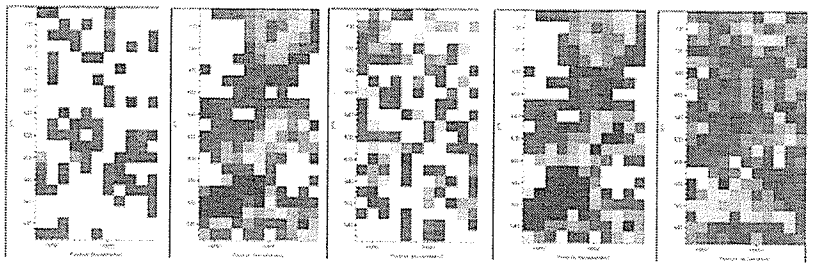

Collagen Phosphate Sugar 1014-1130 Lipid Sym CH_2

3 Day Saline N61 Map 3

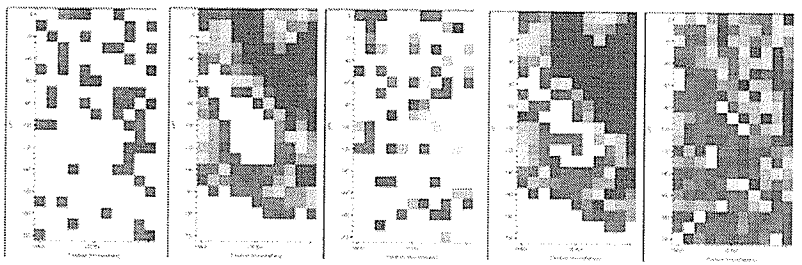

Collagen Phosphate Sugar 1014-1130 Lipid Sym CH_2

3 Day Saline N61 Map 4

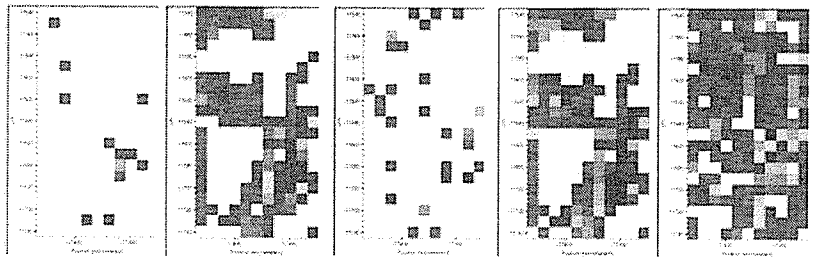

Collagen | Phosphate | Sugar | 1014-1130 | Lipid Sym CH_2

21 Day OTC

October 2003

Margaret Rak

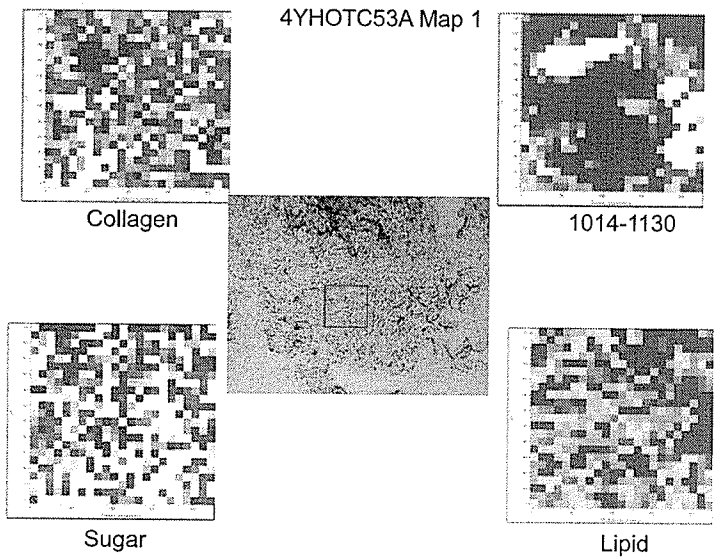

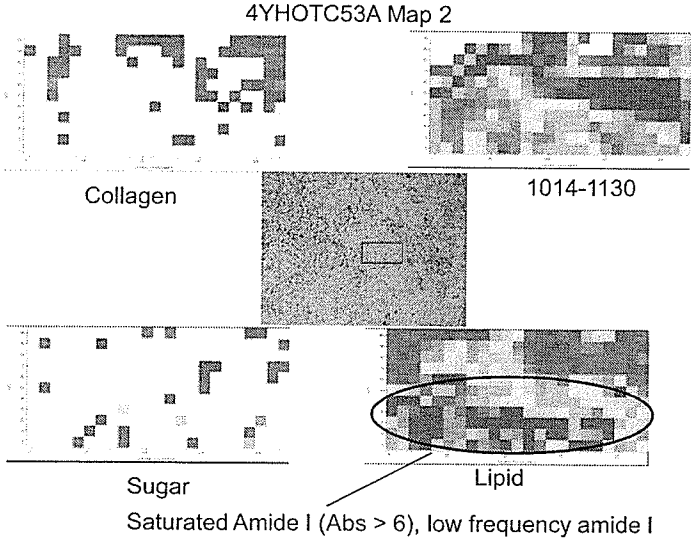

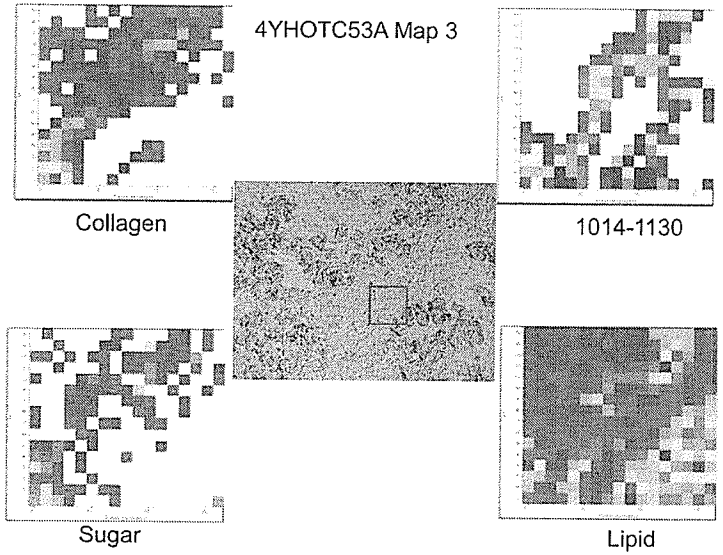

4YHOTC53A Map 4

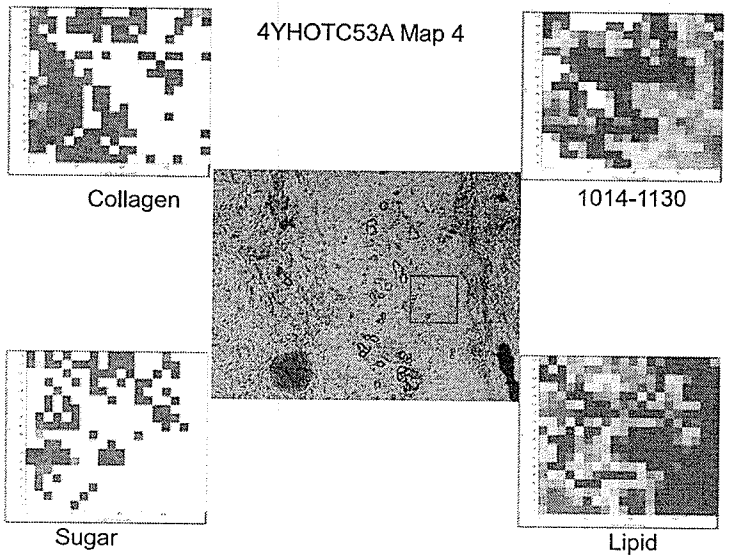

8YHOTC53A Map 1

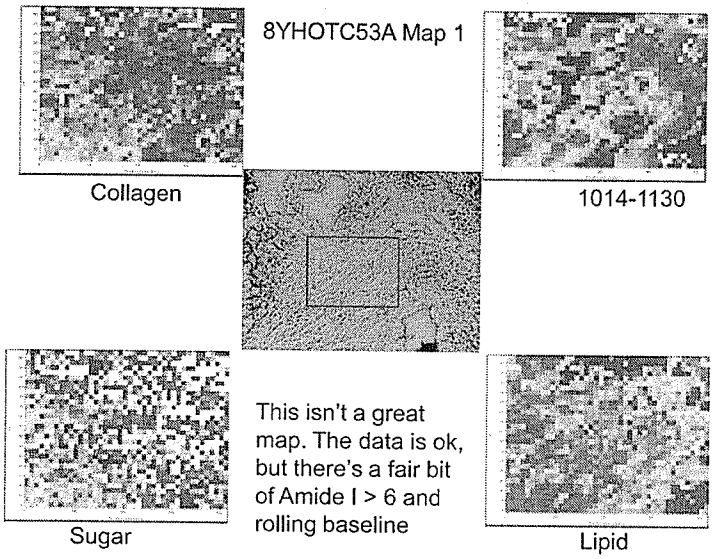

This isn't a great map. The data is ok, but there's a fair bit of Amide I > 6 and rolling baseline

4YHOTC54A Map 1

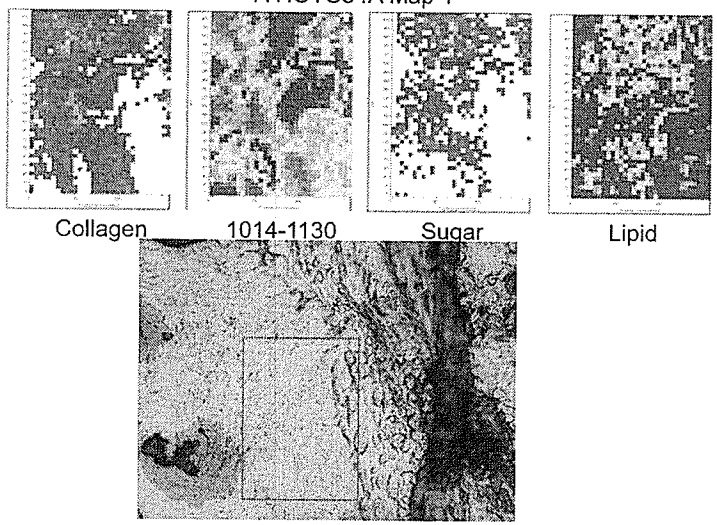

4YHOTC54A Map 2

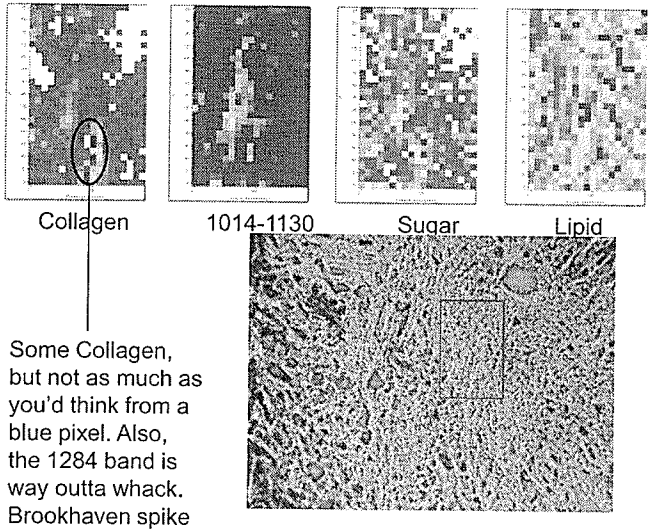

Some Collagen, but not as much as you'd think from a blue pixel. Also, the 1284 band is way outta whack. Brookhaven spike maybe?

4YHOTC54A Map 3

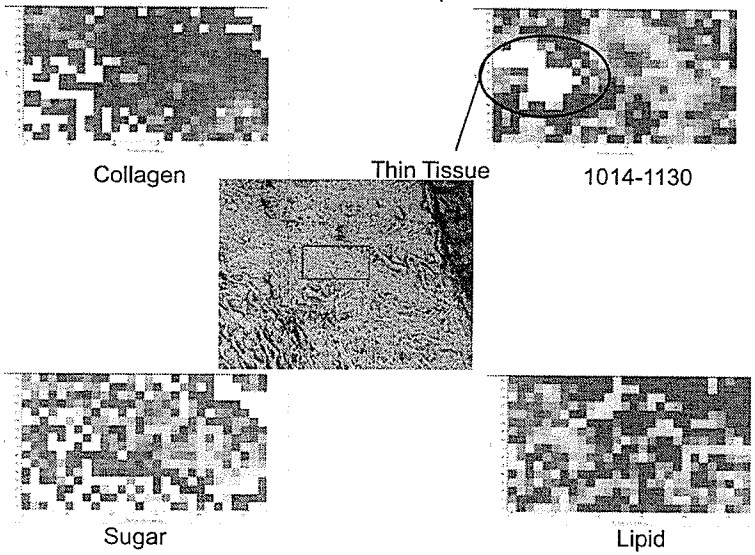

4YHOTC54A Map 4

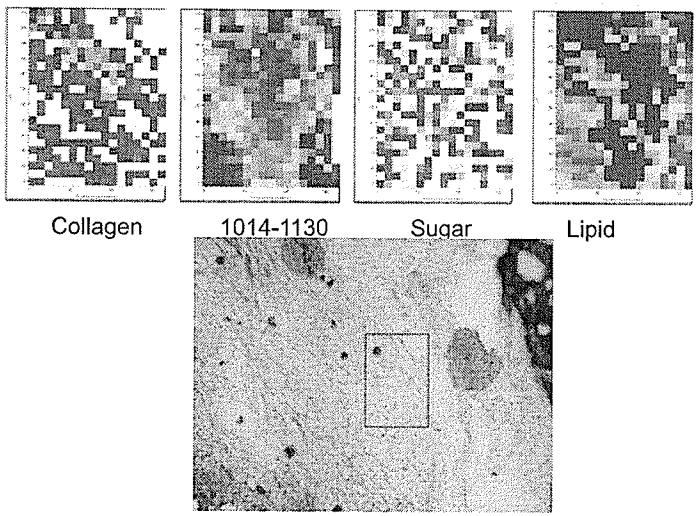

8YHOTC54A Map 1

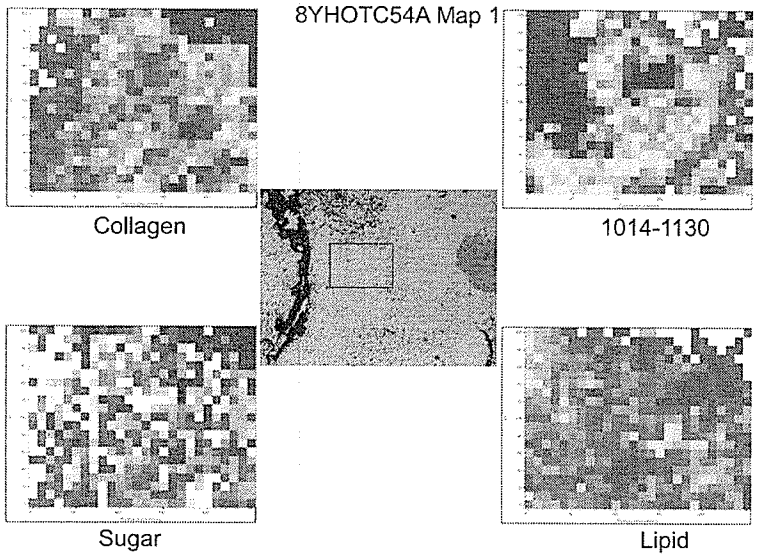

8YHOTC54A Map 1

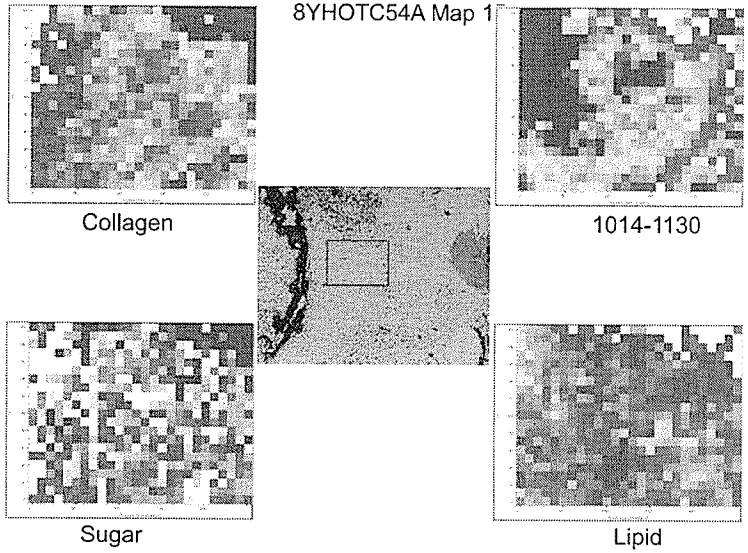

8YHOTC54A Map 2

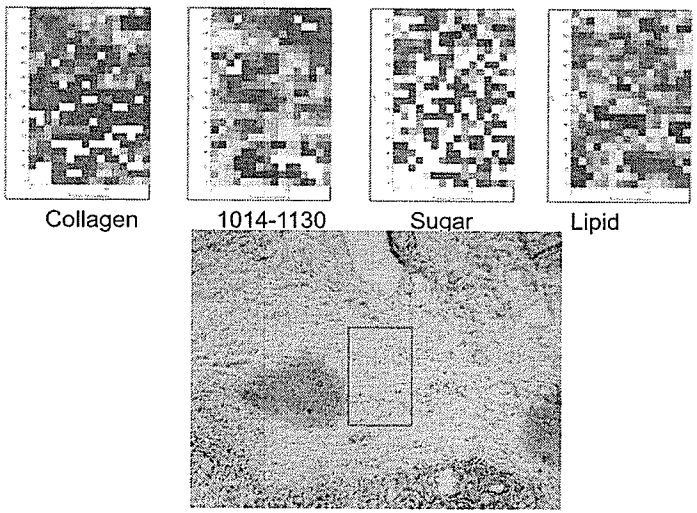

8YHOTC54A Map 3

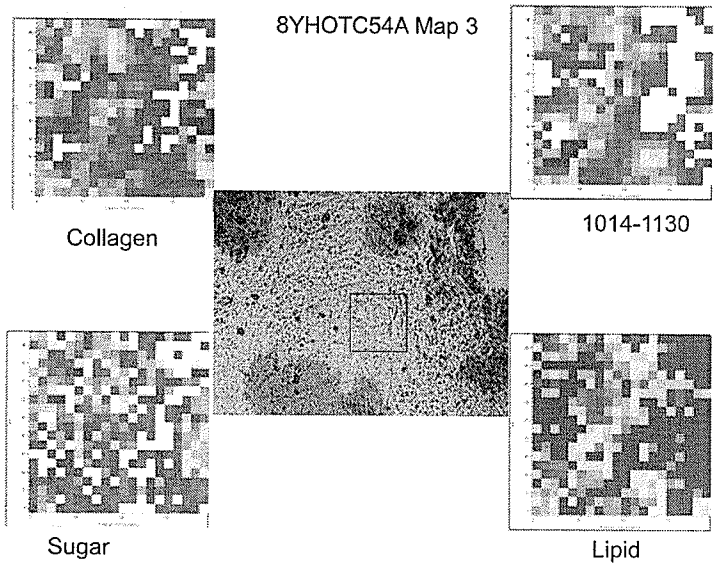

21 Day OTC

SRC July 2004

Fred Zeiler
Richard Wiens
Margaret Rak

21 Day OTC 21 Map 1 Section 10 original

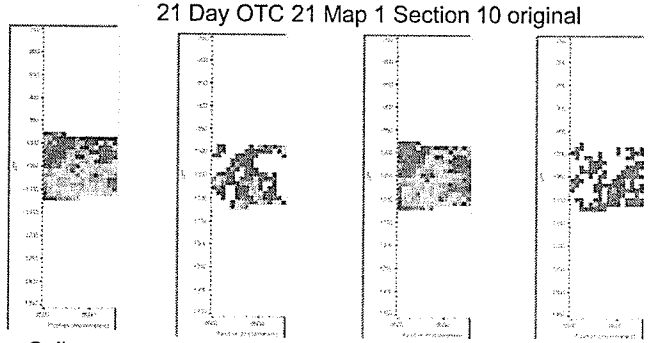

This is the weirdo map of doom. The top half in omnic shows as nonexistant, while the bottom part is ok, but when you try and copy it into ppt the bottom part vanishes too.

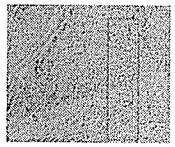

21 Day OTC 21 Map 1 Section 10 stopped

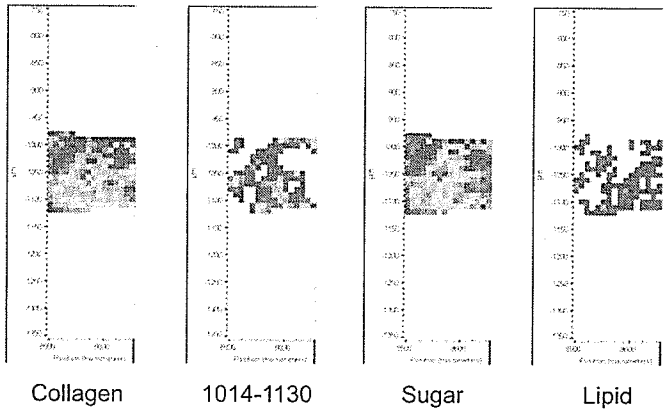

This is the weirdo map of doom. The top half in omnic shows as nonexistant, while the bottom part is ok, but when you try and copy it into ppt the bottom part vanishes too.

21 Day OTC 21 Map 2 Slide 10

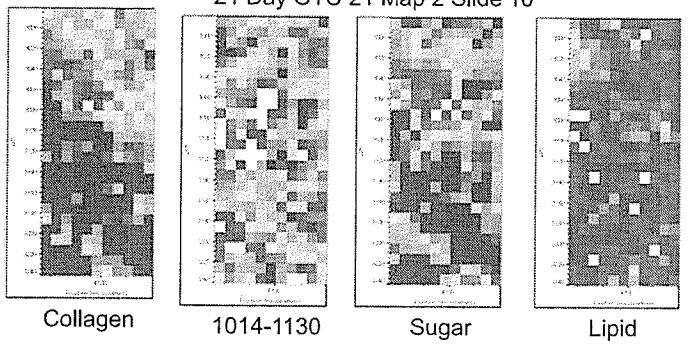

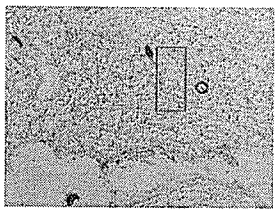

21 Day OTC 21 Map 3 Slide 10

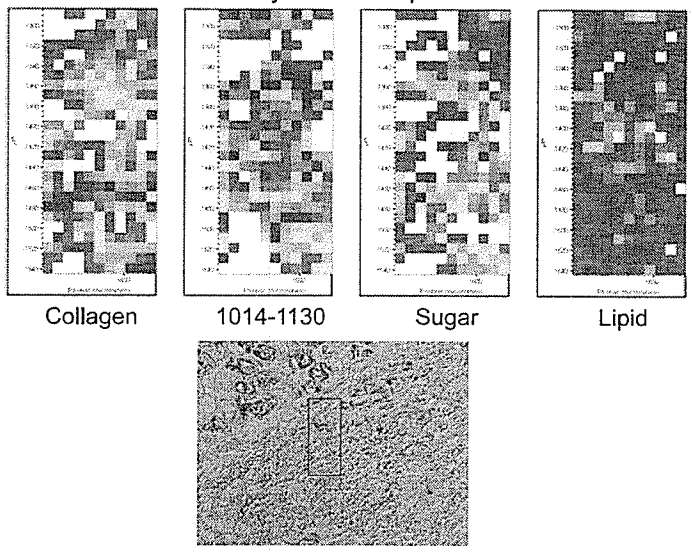

Collagen 1014-1130 Sugar Lipid

21 Day OTC 21 Map 4 Slide 10

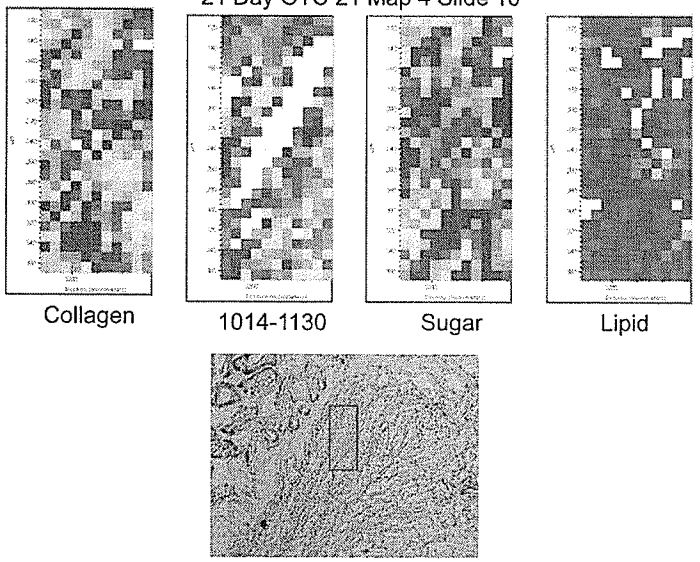

Collagen 1014-1130 Sugar Lipid

21 Day OTC 21 Map 5 Slide 10

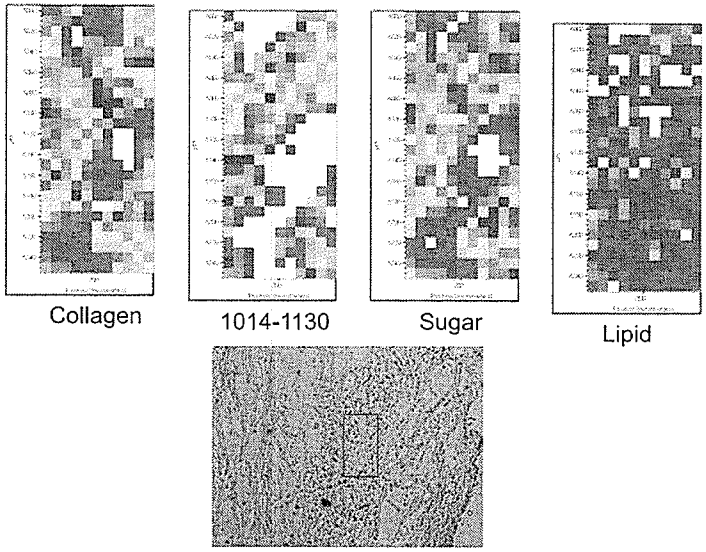

Collagen 1014-1130 Sugar Lipid

21 Day OTC 21 Map 6 Slide 10

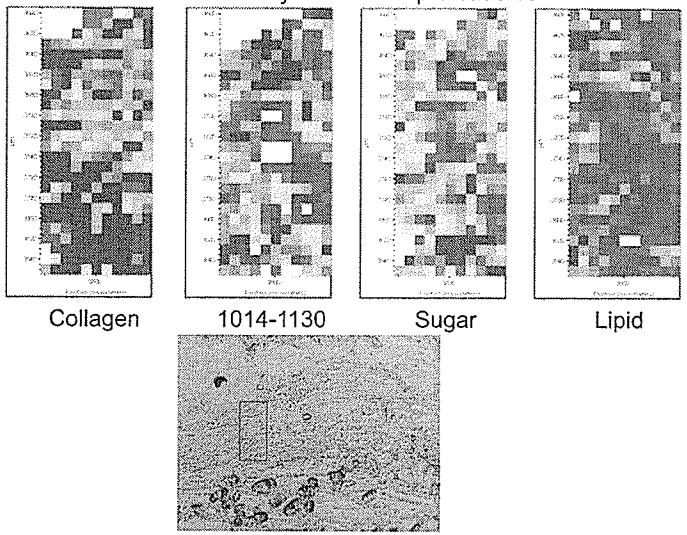

Collagen 1014-1130 Sugar Lipid

21 Day OTC 22 Map 1 Section 10

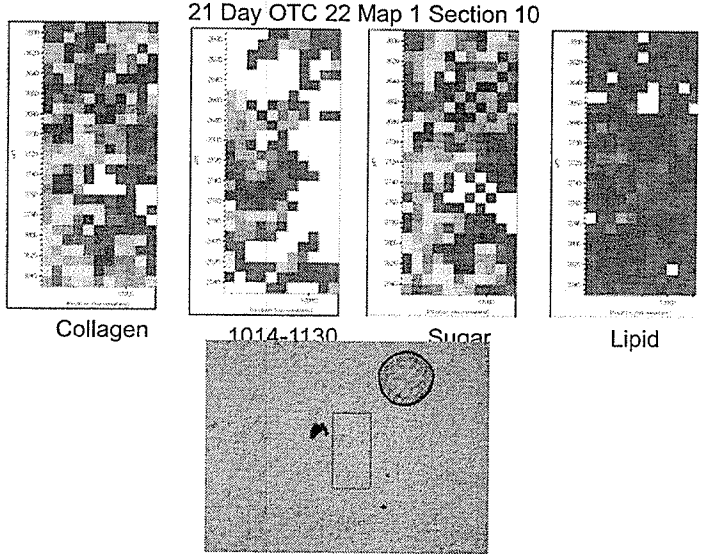

21 Day OTC 22 Map 2 Section 10

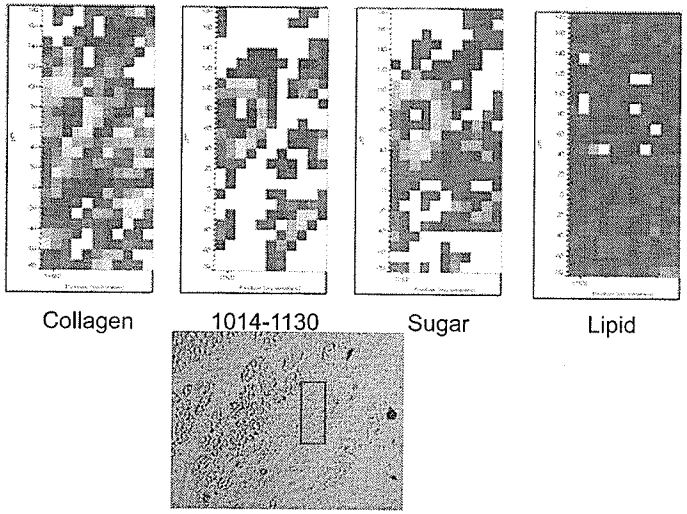

21 Day OTC 22 Map 3 Section 10

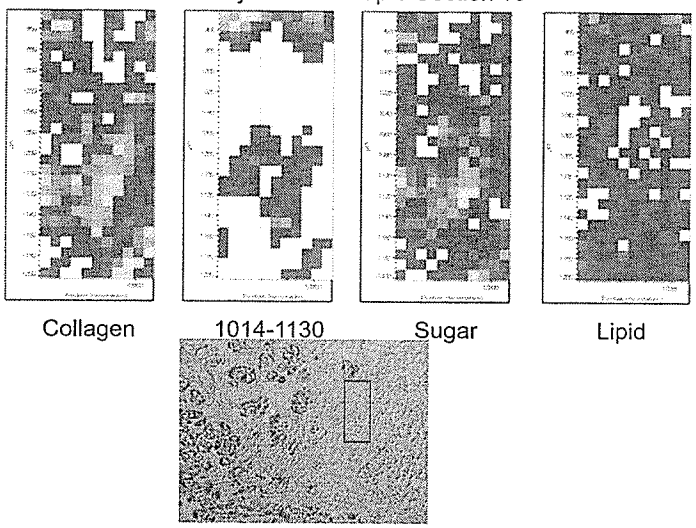

21 Day OTC 22 Map 4 Section 10

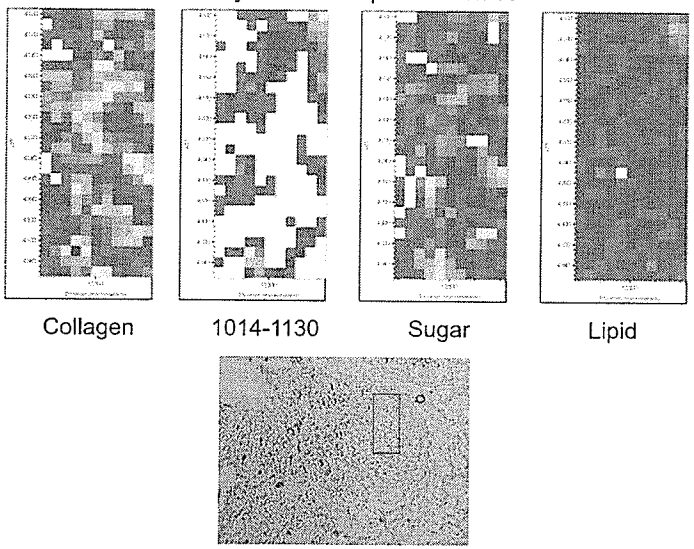

21 Day OTC 22 Map 5 Section 10

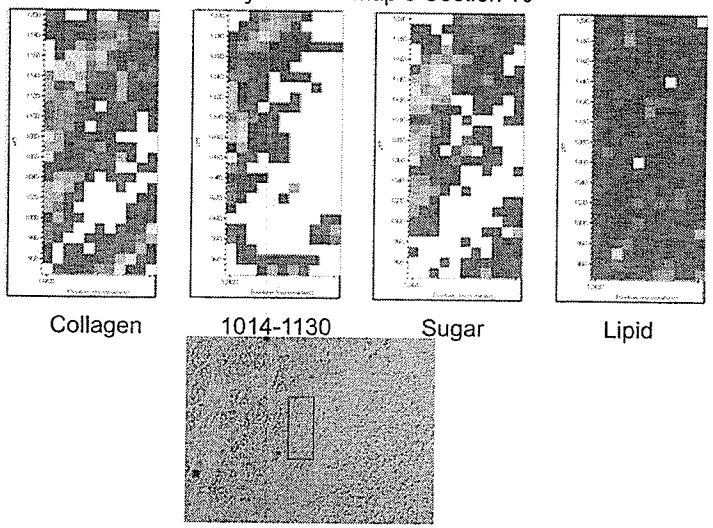

Collagen 1014-1130 Sugar Lipid

21 Day OTC 22 Map 6 Section 10

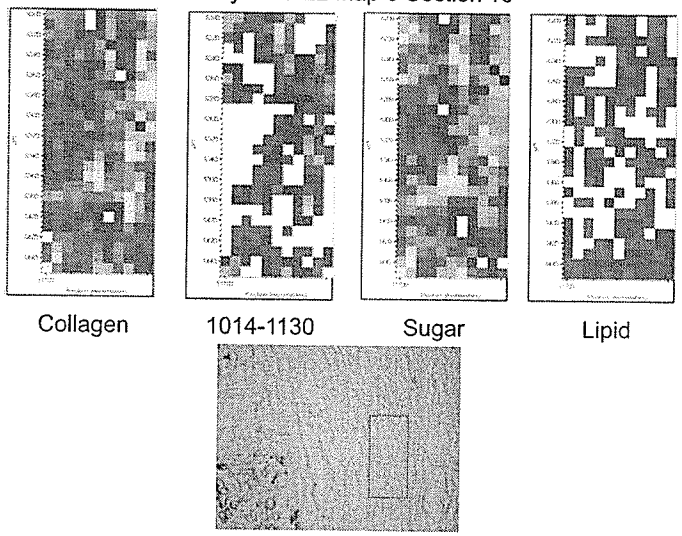

Collagen 1014-1130 Sugar Lipid

21 Day OTC 23 Map 1 Section 10

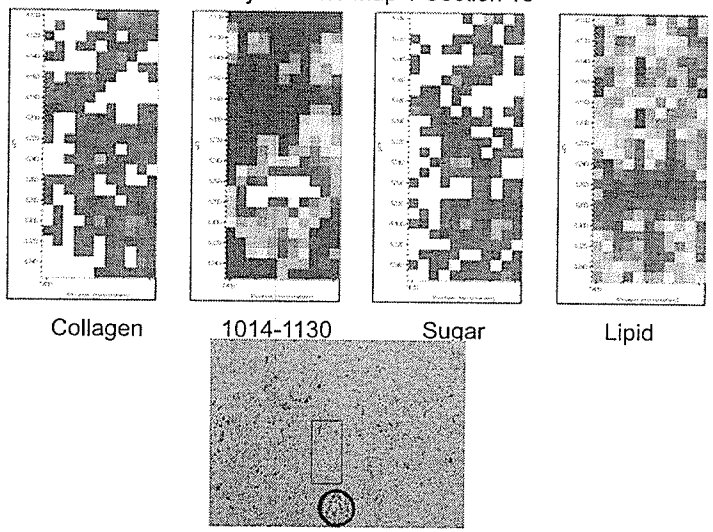

Collagen 1014-1130 Sugar Lipid

21 Day OTC 23 Map 2 Section 10

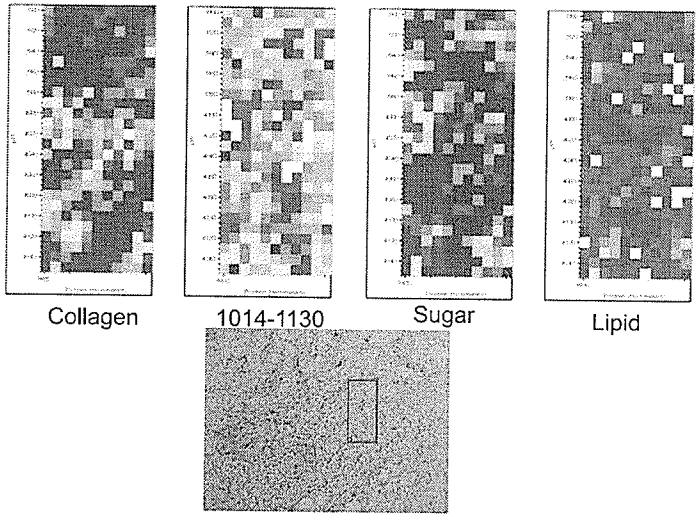

Collagen 1014-1130 Sugar Lipid

21 Day OTC 23 Map 3 Section 10

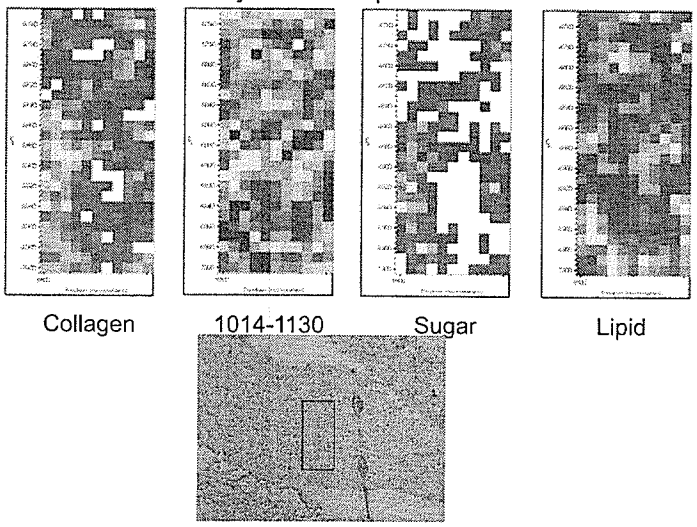

21 Day OTC 23 Map 4 Section 10

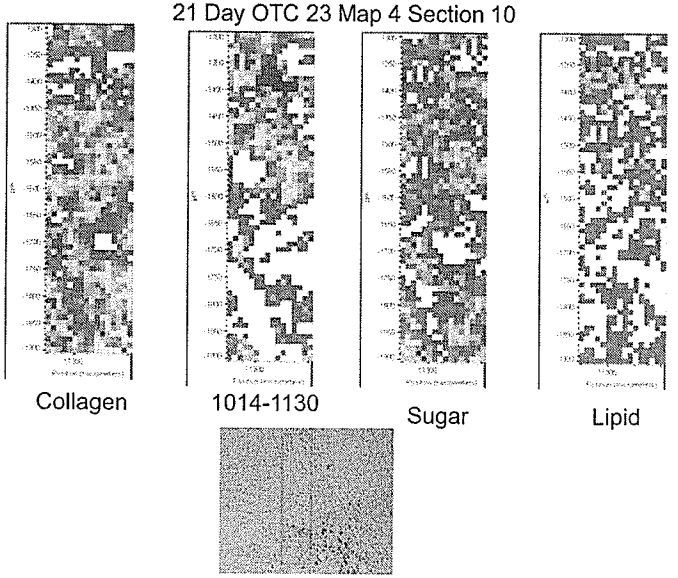

21 Day OTC 23 Map 5 Section 10

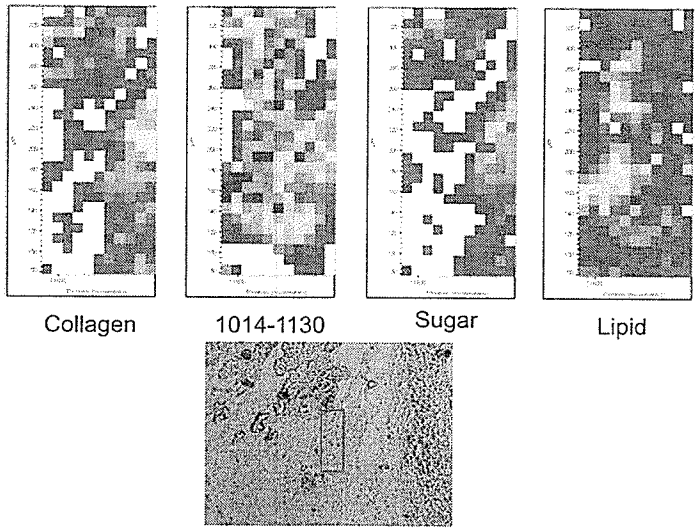

21 Day OTC 23 Map 6 Section 10

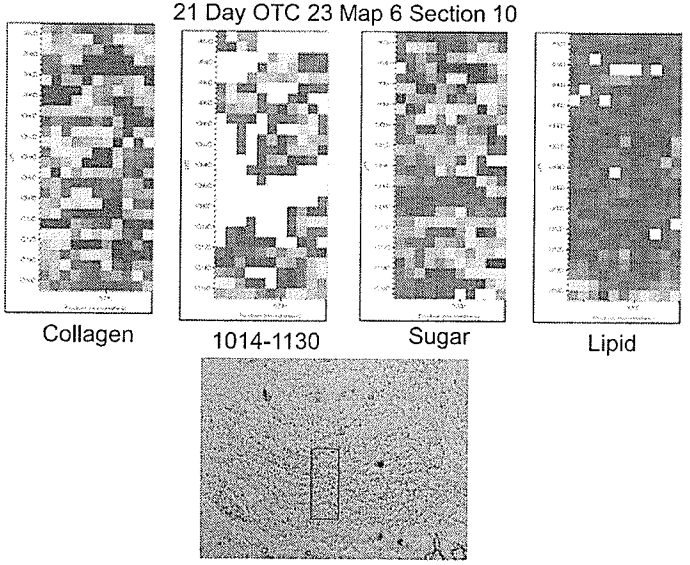

21 Day OTC

NSLS July 2005

Kathy Gough
Margaret Rak

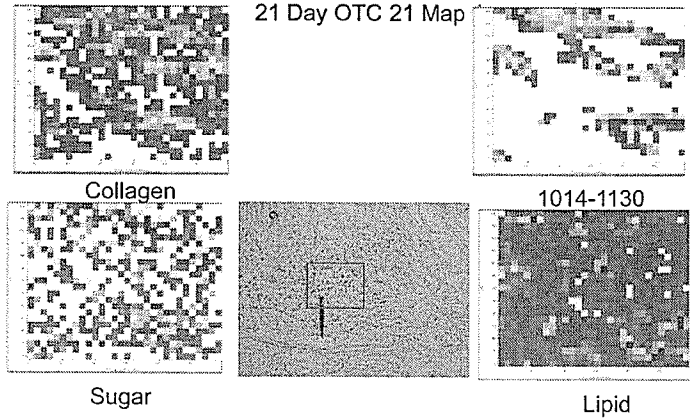

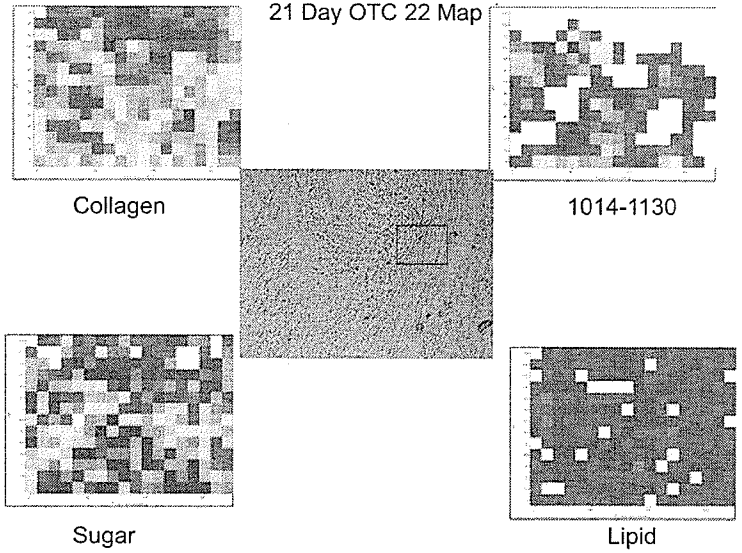

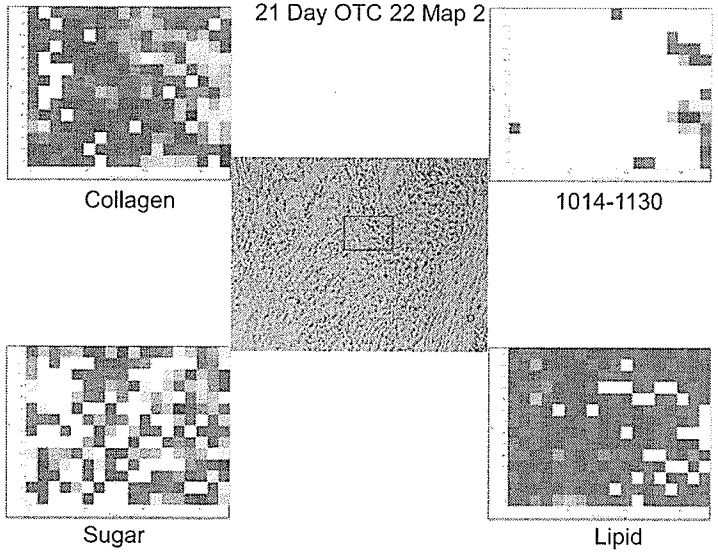

21 Day Quercetin

October 2003

Margaret Rak

4 YH Qu 51B Map 1

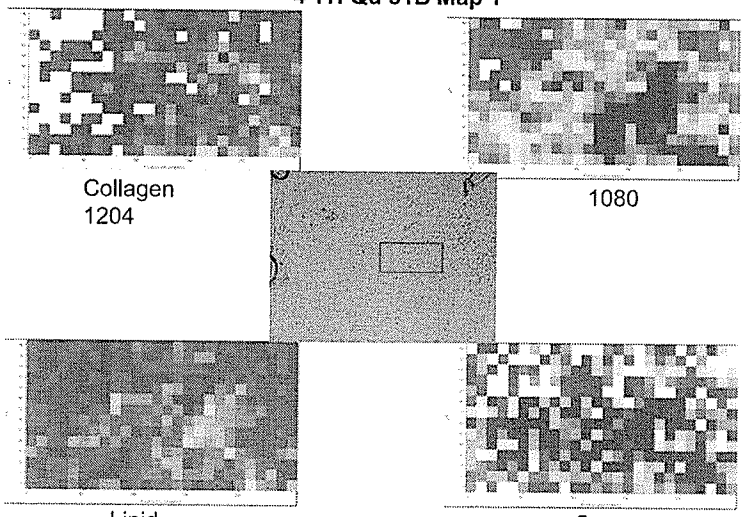

4 YH Qu 51B Map 2

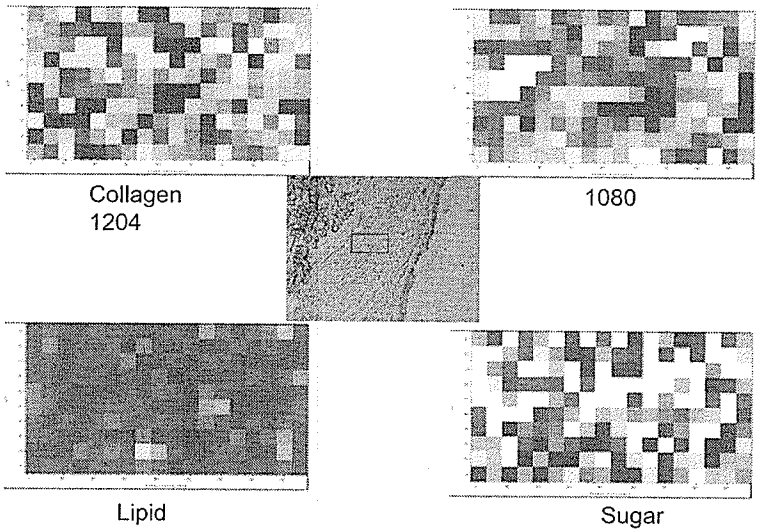

4 YH Qu 51B

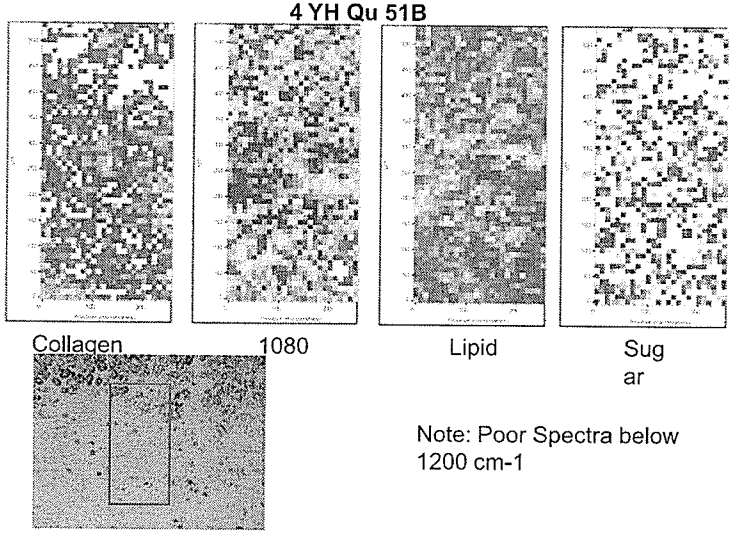

Note: Poor Spectra below 1200 cm-1

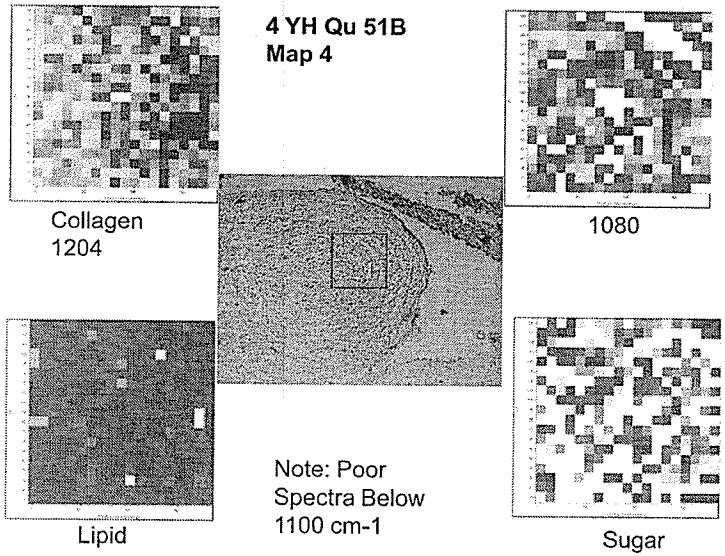
4 YH Qu 51B
Map 4
Collagen
1204
1080
Lipid
Note: Poor
Spectra Below
1100 cm-1
Sugar

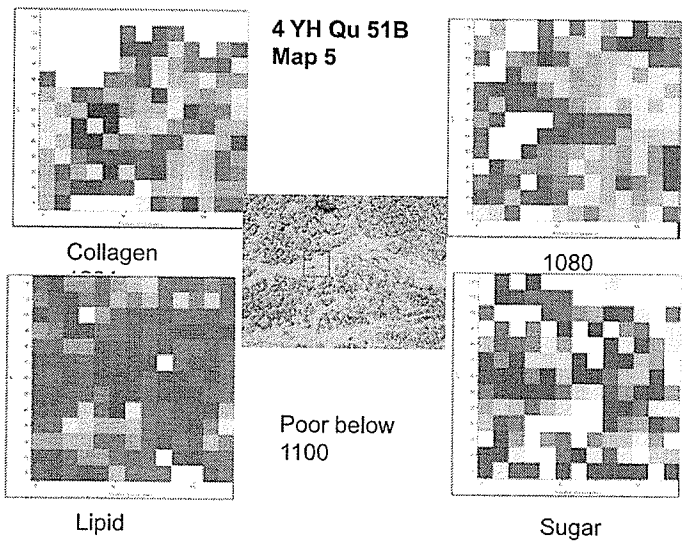
4 YH Qu 51B
Map 5
Collagen
1080
Poor below
1100
Lipid
Sugar

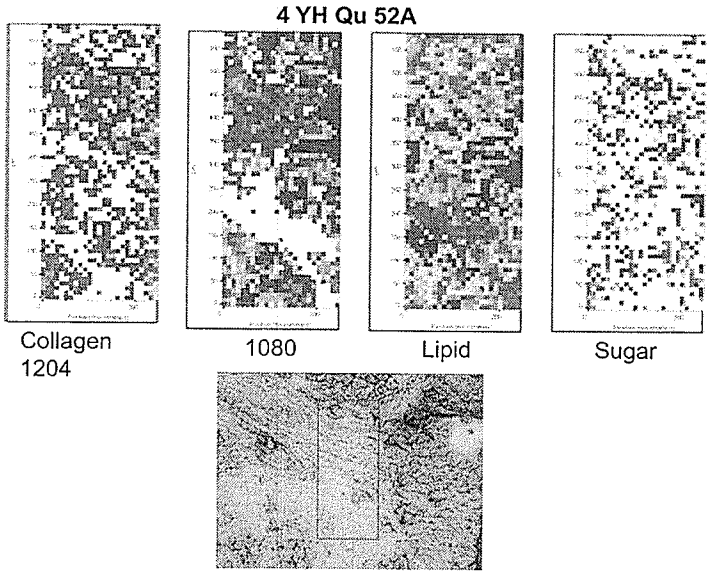
4 YH Qu 52A
Collagen
1204
1080
Lipid
Sugar

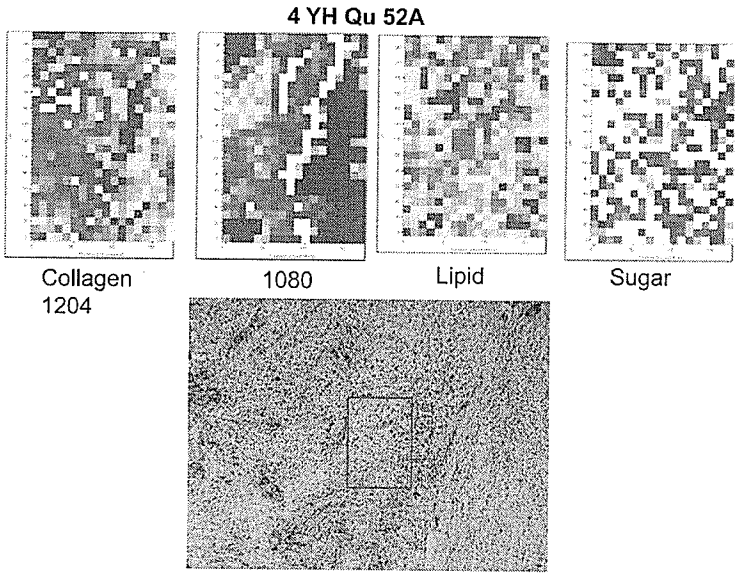
4 YH Qu 52A
Collagen
1204
1080
Lipid
Sugar

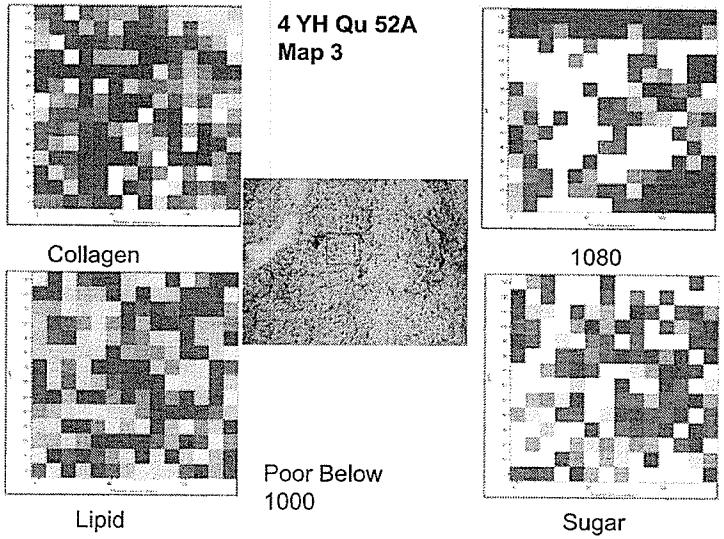
4 YH Qu 52A
Map 3
Collagen
1080
Poor Below
1000
Lipid
Sugar

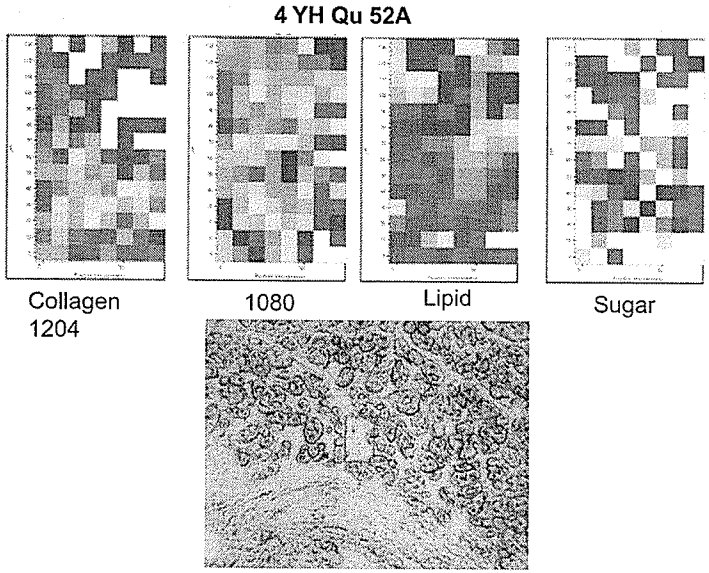
4 YH Qu 52A
Collagen
1204
1080
Lipid
Sugar

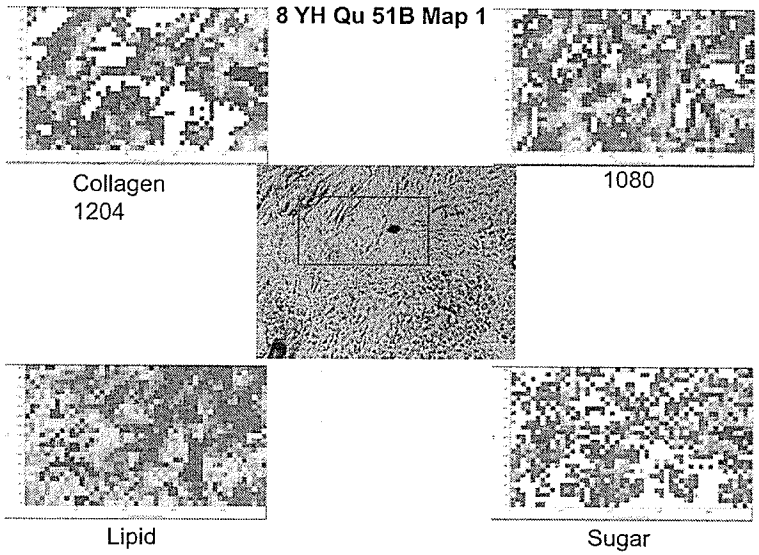
8 YH Qu 51B Map 1
Collagen
1204
1080
Lipid
Sugar

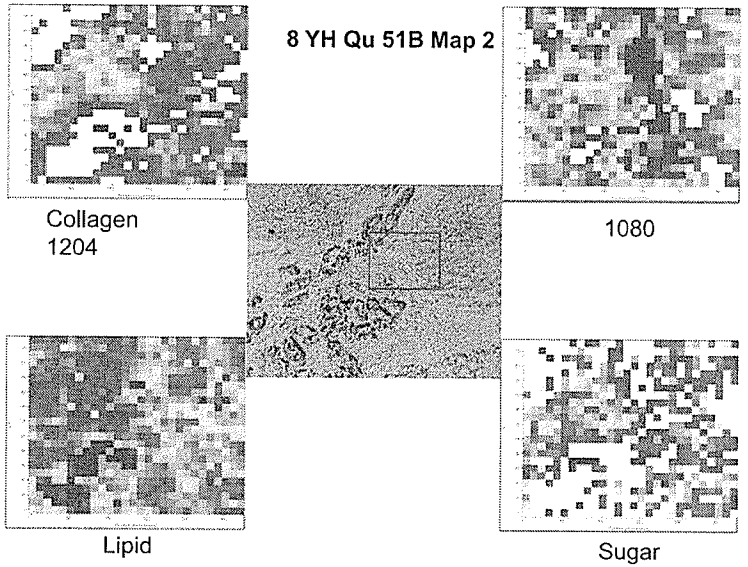
8 YH Qu 51B Map 2
Collagen
1204
1080
Lipid
Sugar

8 YH Qu 51B Map 3

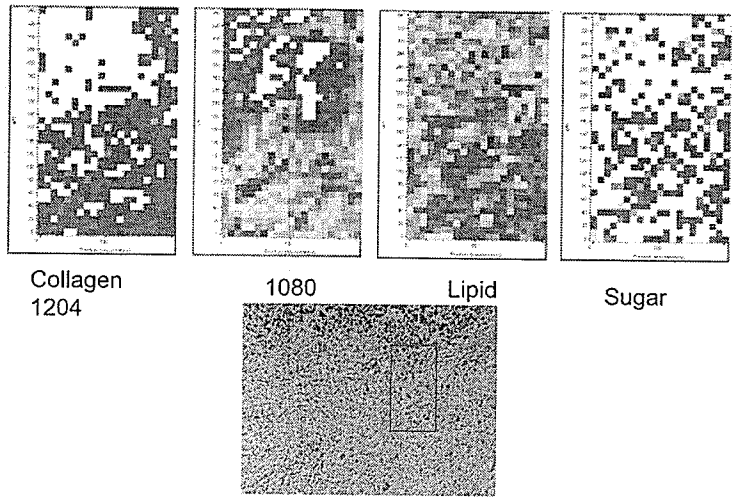

Collagen 1204 | 1080 | Lipid | Sugar

8 YH Qu 52A Map 1

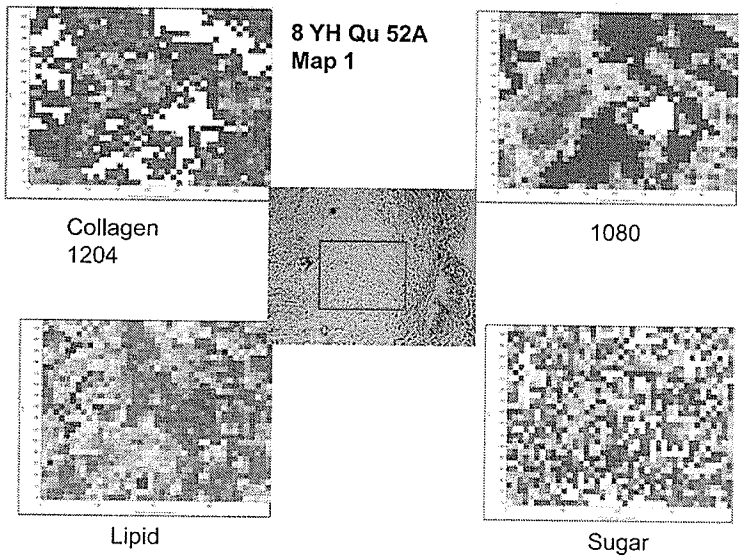

Collagen 1204 | 1080 | Lipid | Sugar

21 Day Quercetin

July 2004

Fred Zeiler
Richard Wiens
Margaret Rak

21 day Que 19 Map 1

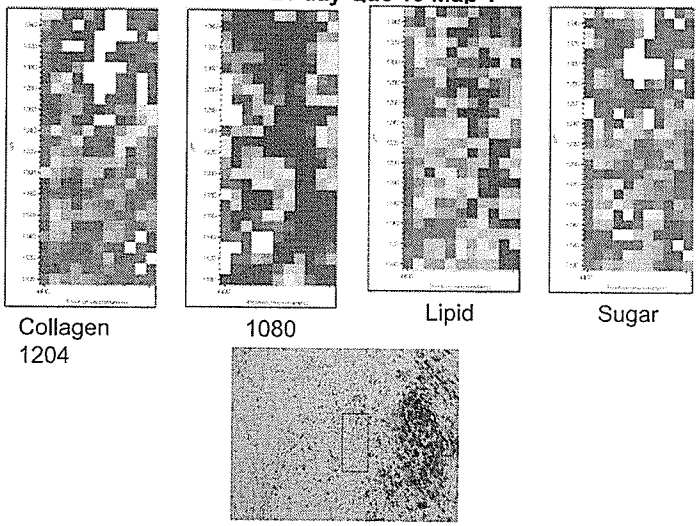

21 day Que 19 Map 2

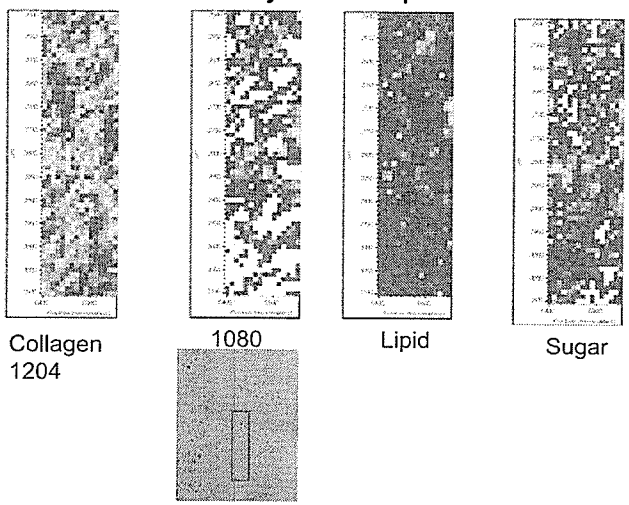

21 day Que 19 Map 3

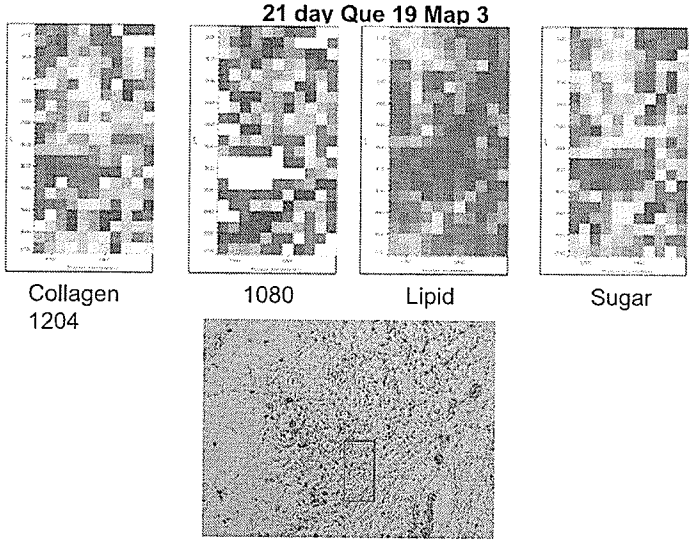

21 day Que 19 Map 4

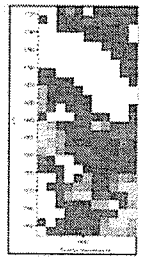
Collagen
1204

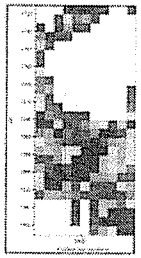
1080

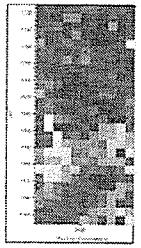
Lipid

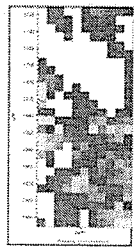
Sugar

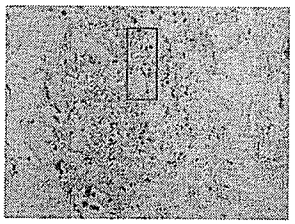

21 day Que 19 Map 5

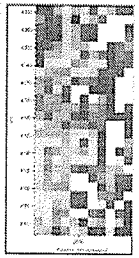
Collagen
1204

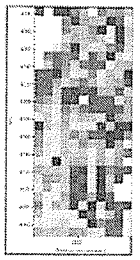
1080

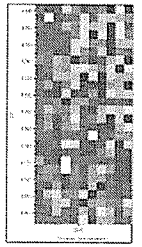
Lipid

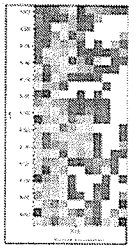
Sugar

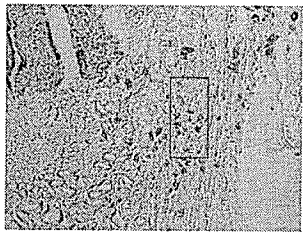

21 day Que 19 Map 6

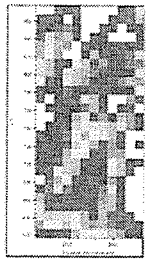
Collagen
1204

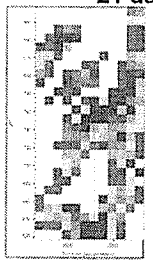
1080

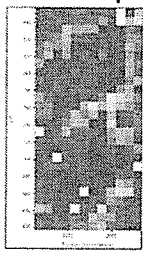
Lipid

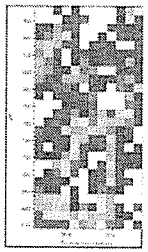
Sugar

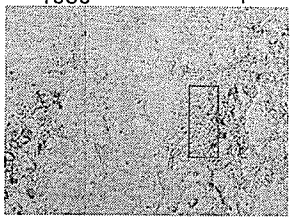

21 Day Quercetin

August 2004

Margaret Rak

21 day Que 17 Map 1

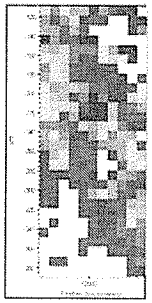

Collagen
1204

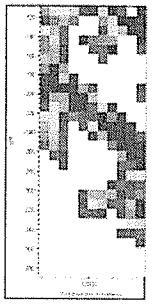

1080

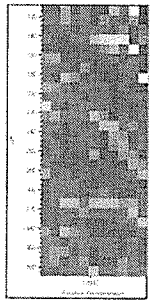

Lipid

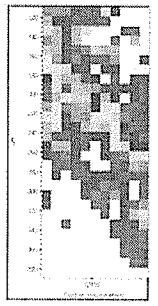

Sugar

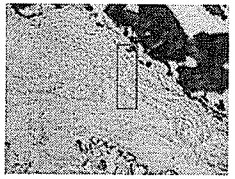

21 day Que 17 Map 2

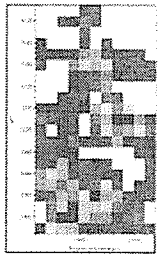

Collagen
1204

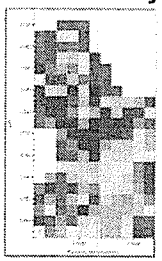

1080

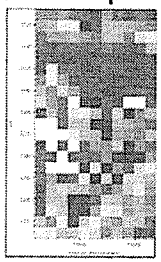

Lipid

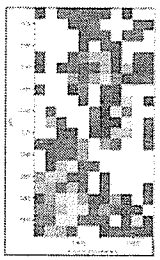

Sugar

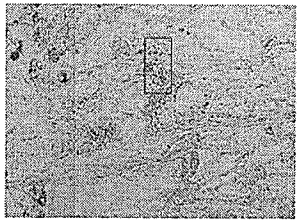

21 day Que 17 Map 3

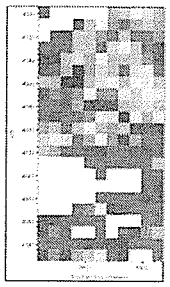

Collagen
1204

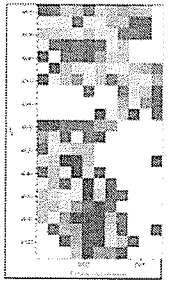

1080

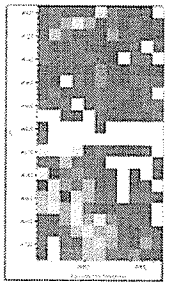

Lipid

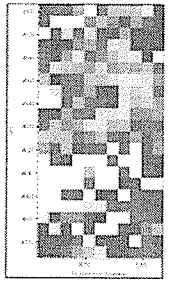

Sugar

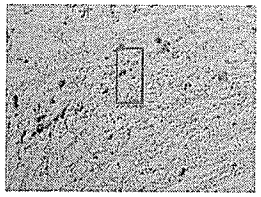

21 day Que 17 Map 4

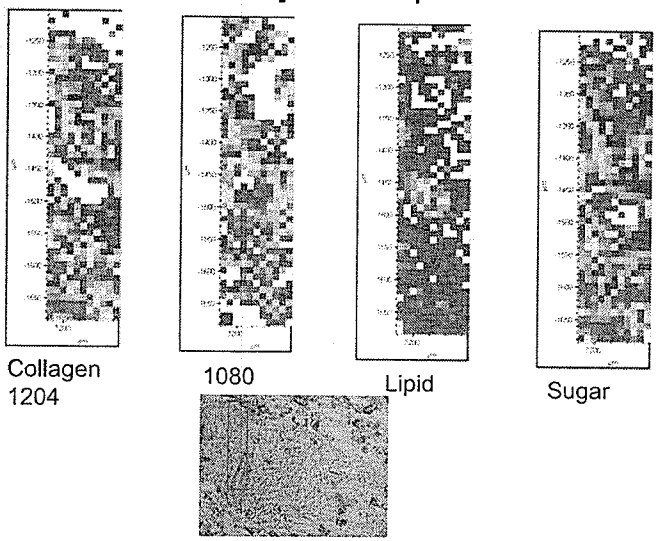

21 day Que 18 Map 1

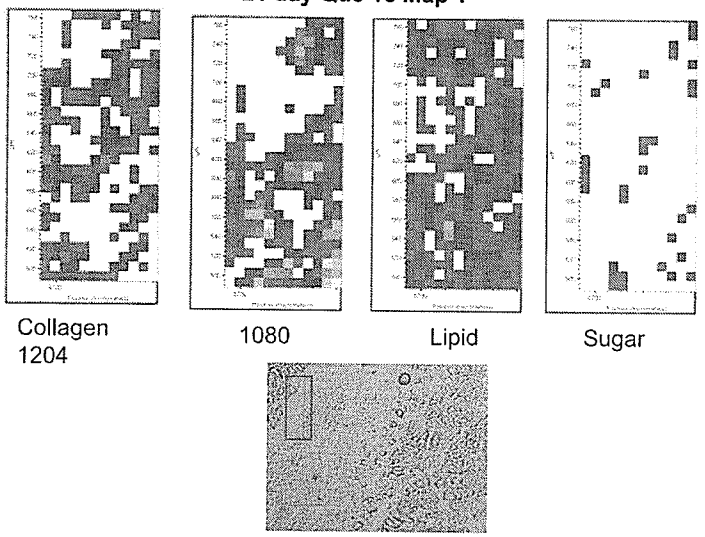

21 day Que 18 Map 2

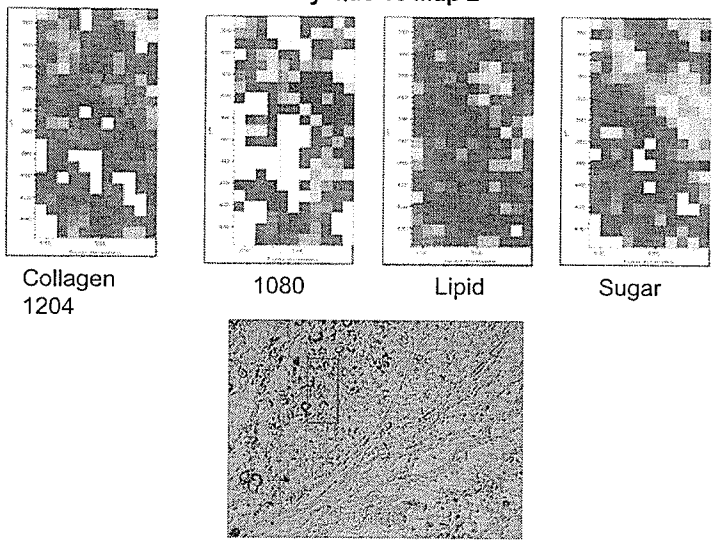

21 day Que 18 Map 3

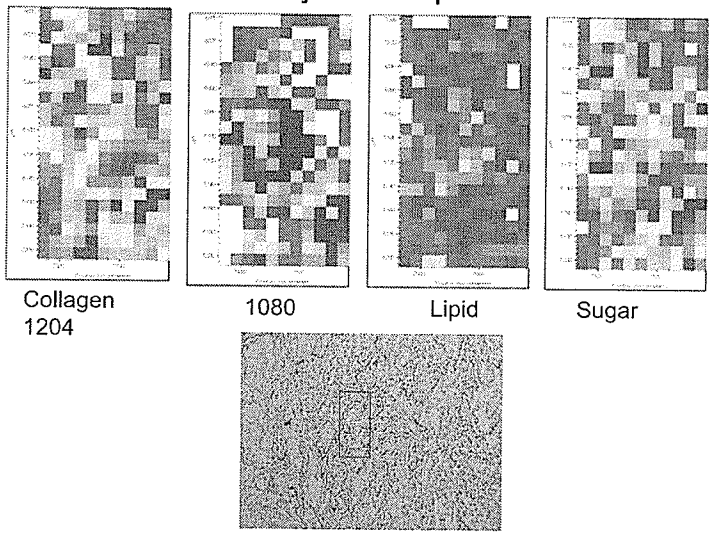

21 day Que 18 Map 4

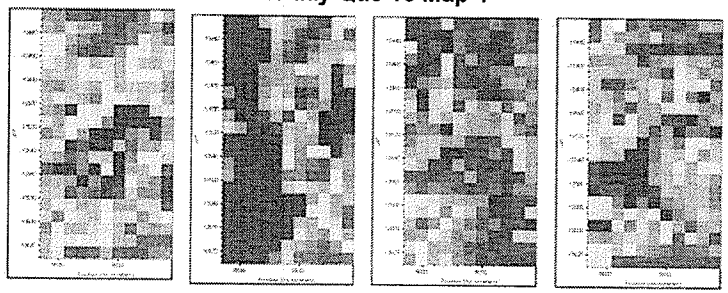

Collagen 1204 | 1080 | Lipid | Sugar

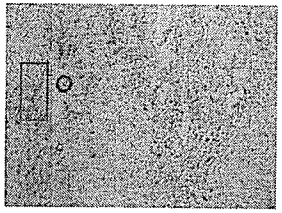

21 day Que 18 Map 5

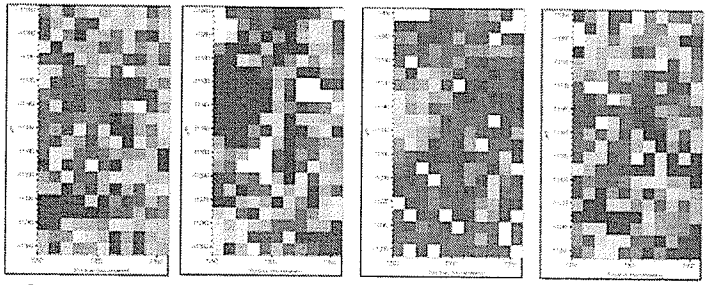

Collagen 1204 | 1080 | Lipid | Sugar

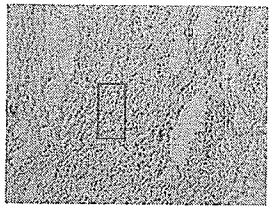

21 Day Quercetin

September 2004
Margaret Rak
Nicky Cox

21 day Que 17 Map 1

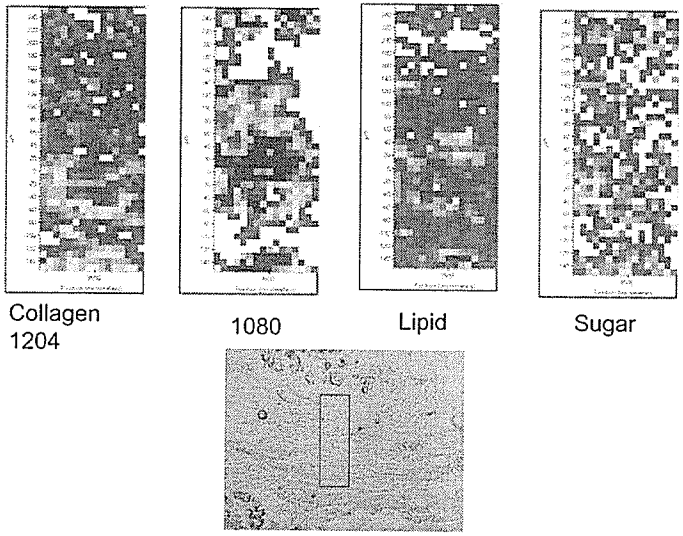

Collagen 1204 | 1080 | Lipid | Sugar

21 day Que 17 Map 2

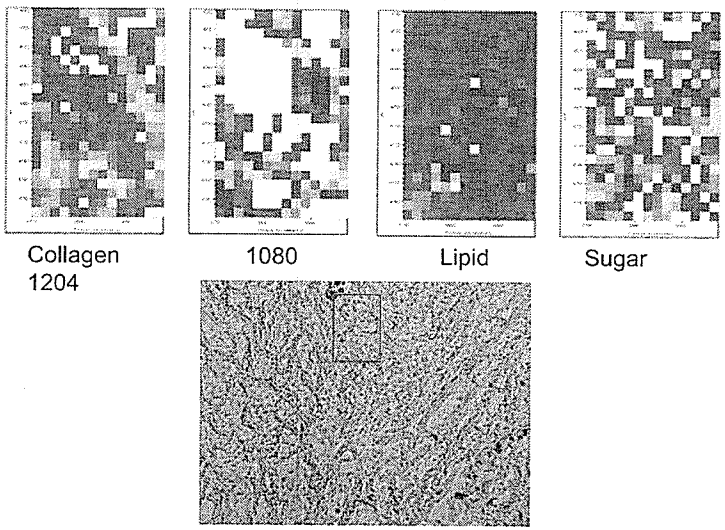

Collagen 1204 | 1080 | Lipid | Sugar

21 Day Quercetin

July 2005
Kathy Gough
Margaret Rak

21 day Que 17 Map 1

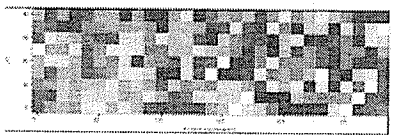

Collagen
1204

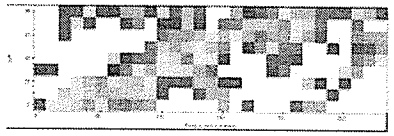

1080

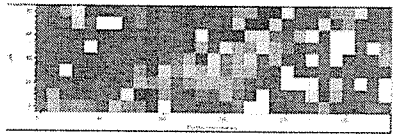

Lipid

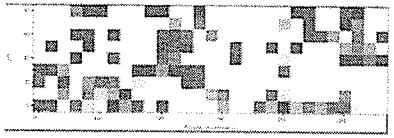

Sugar

Poor spectra below 1000

NO MATCHING MOSAIC

Map is not marked on image

21 day Que 17 Map 1a

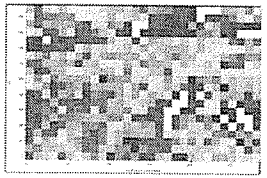

Collagen 1204

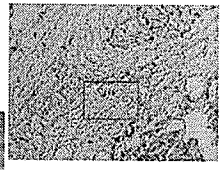

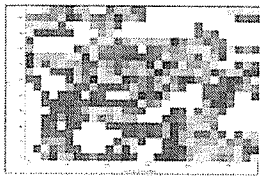

1080

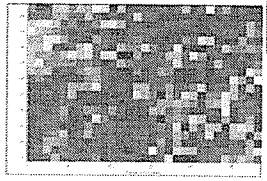

Lipid

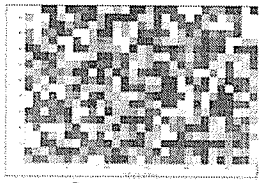

Sugar

21 day Que 17 Map 2

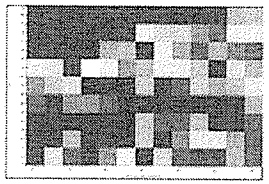

Collagen 1204

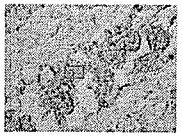

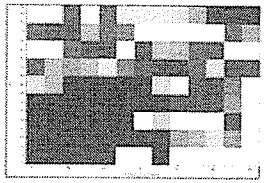

1080

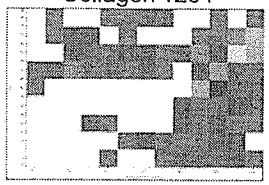

Lipid

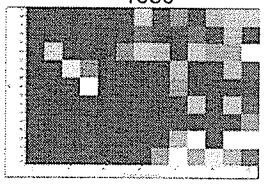

Sugar

21 day Que 17 Map 3

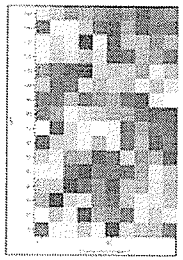

Collagen
1204

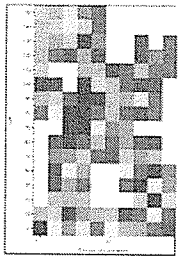

1080

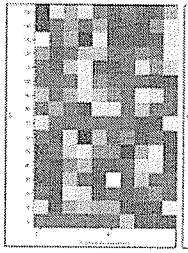

Lipid

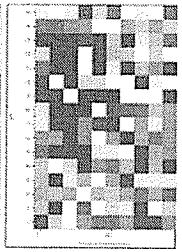

Sugar

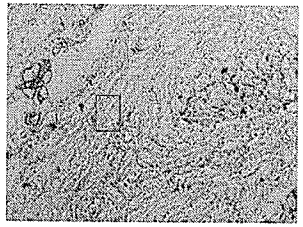

21 day Que 17 Map 4

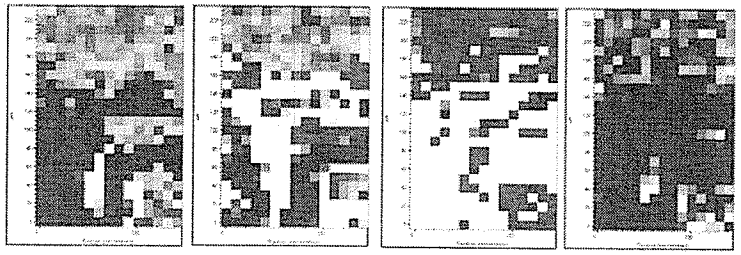

Collagen 1204 | 1080 | Lipid | Sugar

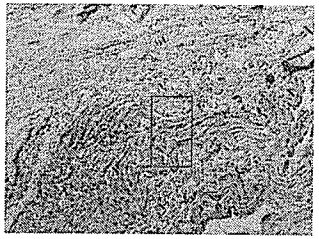

21 day Que 17 Map 5

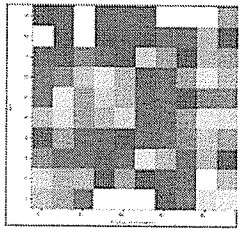

Collagen 1204

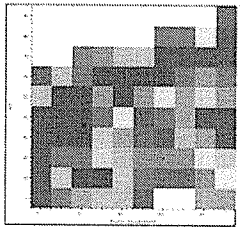

1080

Poor Below 1000

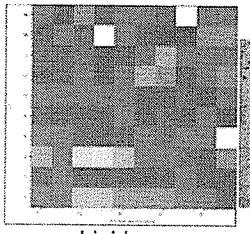

Lipid

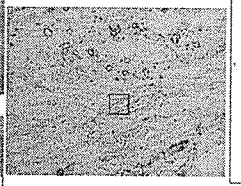

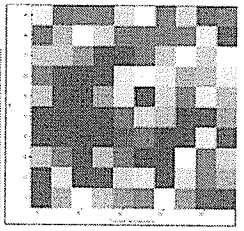

Sugar

21 day Que 18 Map 1

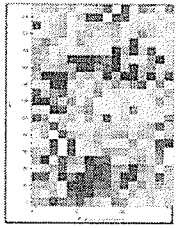

Collagen 1204

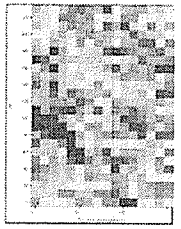

1080

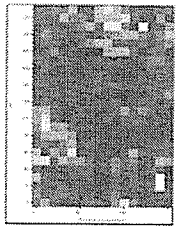

Lipid

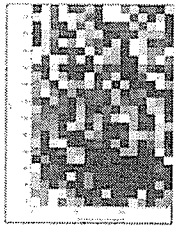

Sugar

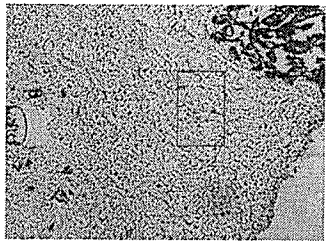

Poor Below 1000

21 day Que 18 Map 2

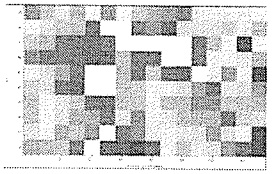

Collagen 1204

Poor Below 1000

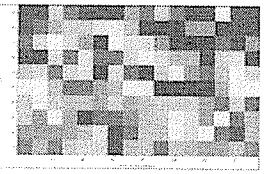

1080

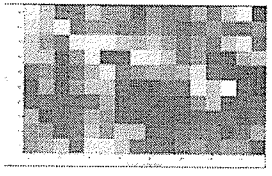

Lipid

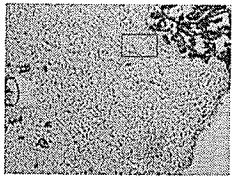

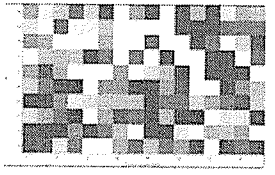

Sugar

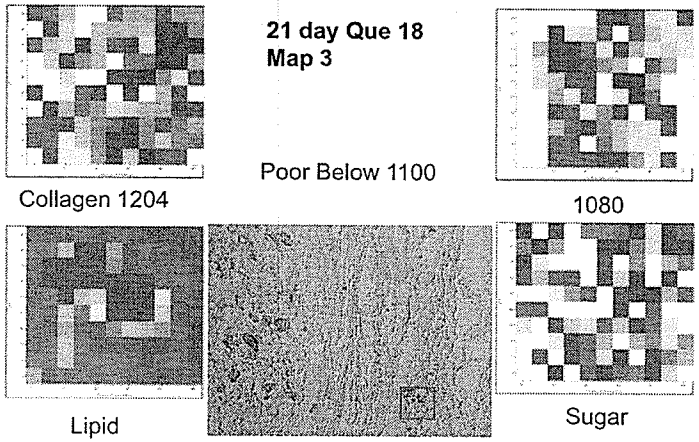

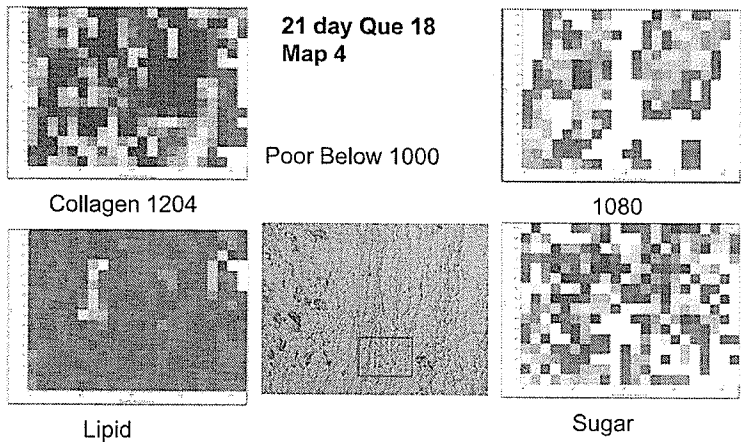

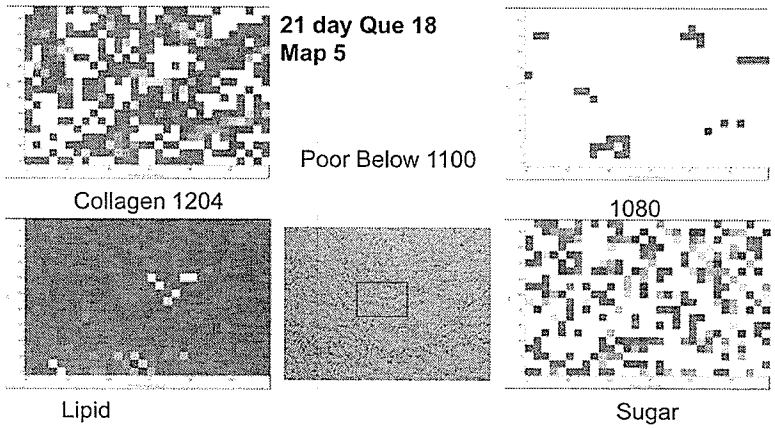

21 Day Quercetin

August 2006

Richard Wiens

21 Day Que N69 Map 1

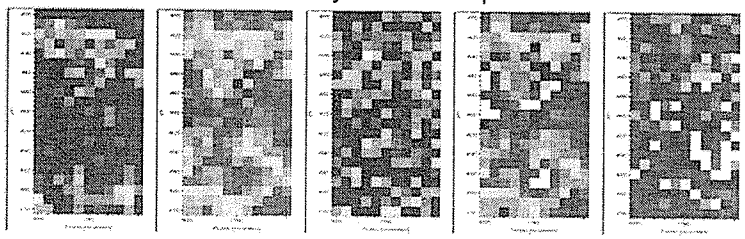

Collagen Phosphate Sugar 1014-1130 Sym CH_2

21 Day Que N69 Map 2

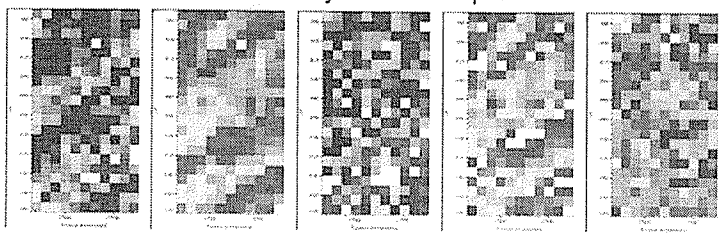

Collagen Phosphate Sugar 1014-1130 Sym CH_2

21 Day Que N69 Map 3

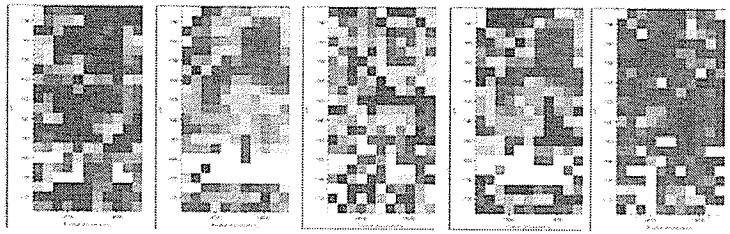

Collagen Phosphate Sugar 1014-1130 Sym CH_2

21 Day Que N69 Map 4

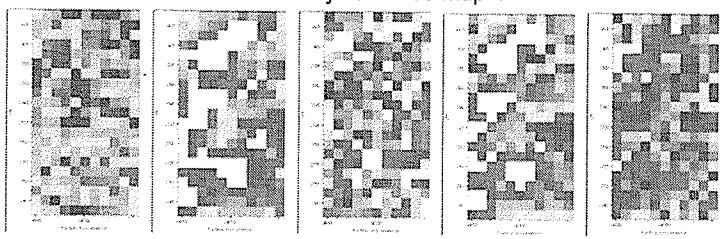

Collagen Phosphate Sugar 1014-1130 Sym CH_2

21 Day Que N69 Map 5

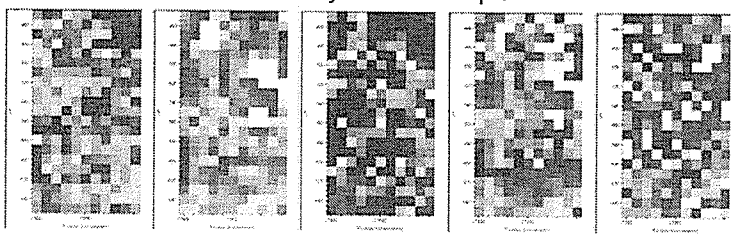

Collagen Phosphate Sugar 1014-1130 Sym CH_2

21 Day Que N69 Map 6

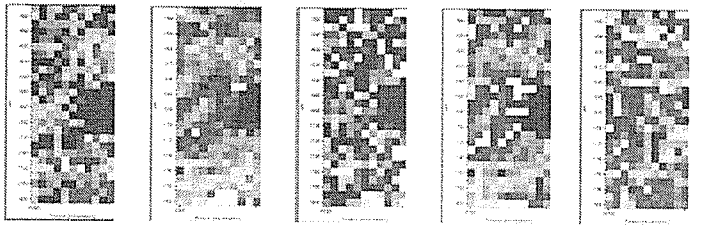

Collagen Phosphate Sugar 1014-1130 Sym CH_2

21 Day Que N71 Map 1

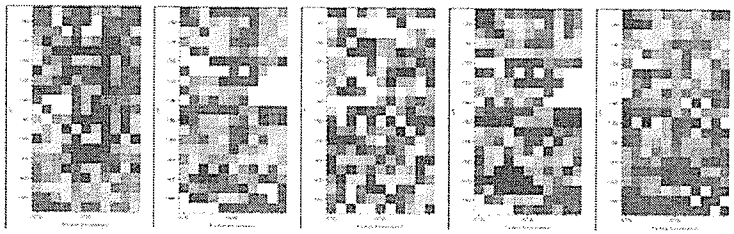

Collagen Phosphate Sugar 1014-1130 Sym CH_2

21 Day Que N71 Map 2

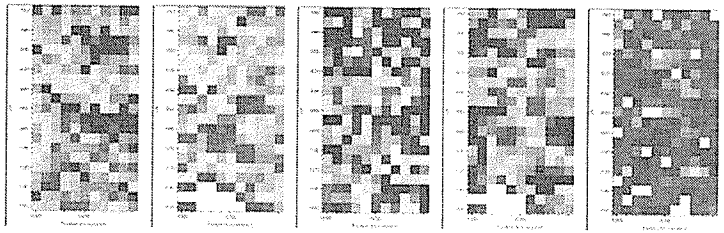

Collagen Phosphate Sugar 1014-1130 Sym CH_2

21 Day Que N71 Map 3

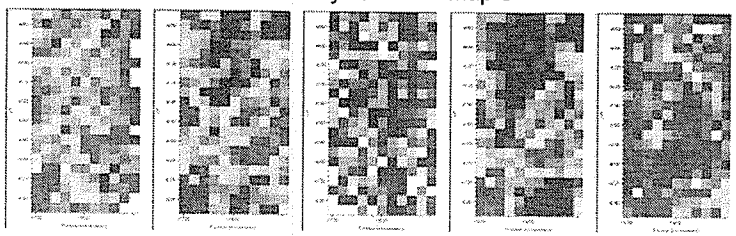

Collagen Phosphate Sugar 1014-1130 Sym CH_2

21 Day Que N71 Map 4

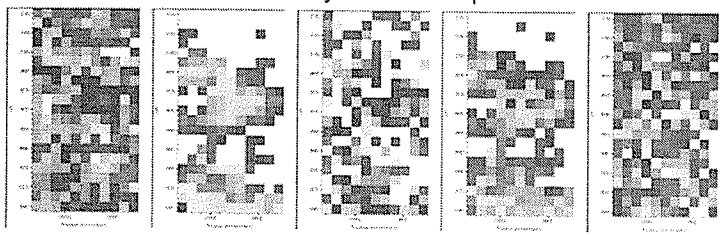

Collagen Phosphate Sugar 1014-1130 Sym CH_2

21 Day Que N71 Map 5

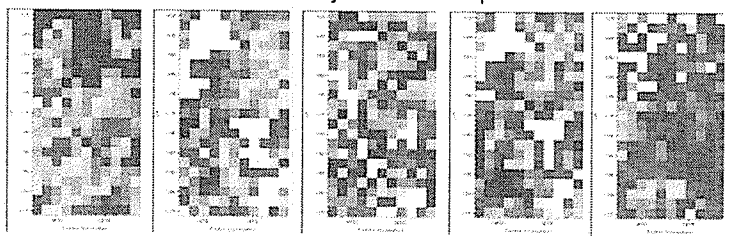

Collagen Phosphate Sugar 1014-1130 Sym CH_2

21 Day Que N71 Map 6

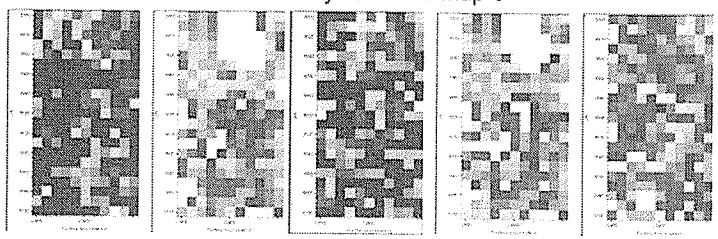

Collagen Phosphate Sugar 1014-1130 Sym CH_2

21 Day Saline

June 2003

Kathy Gough
Meghan Gallant
Vincent Okoli

4 YH TC2B_01.MAP

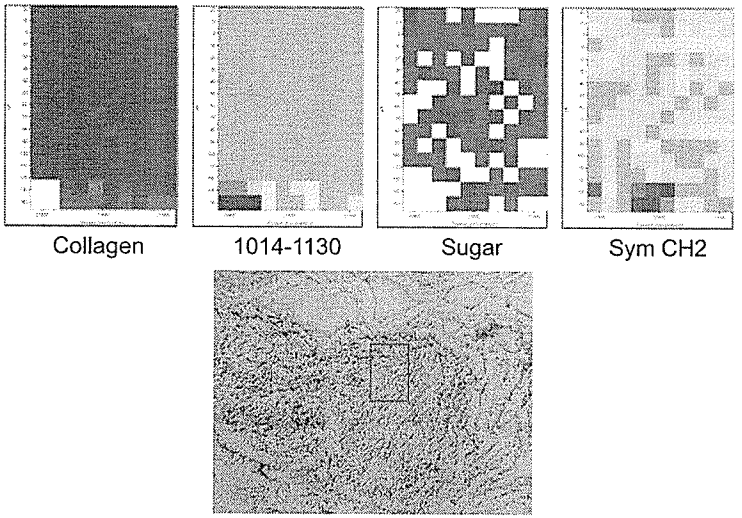

4 YH TC2B_01B.MAP

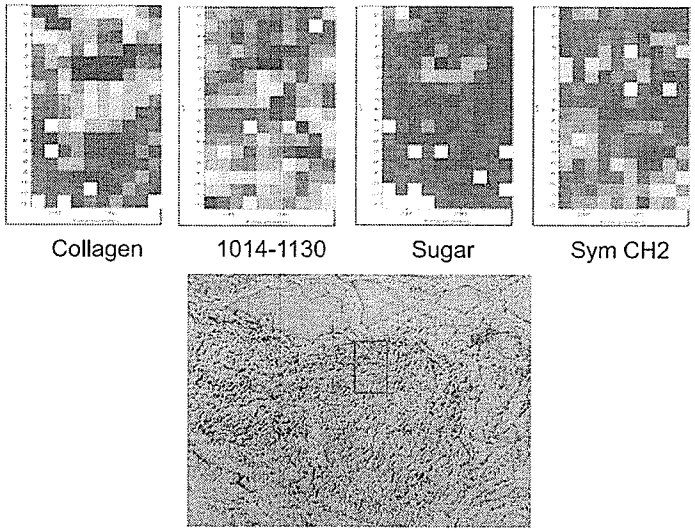

4 YH TC2B_02.MAP

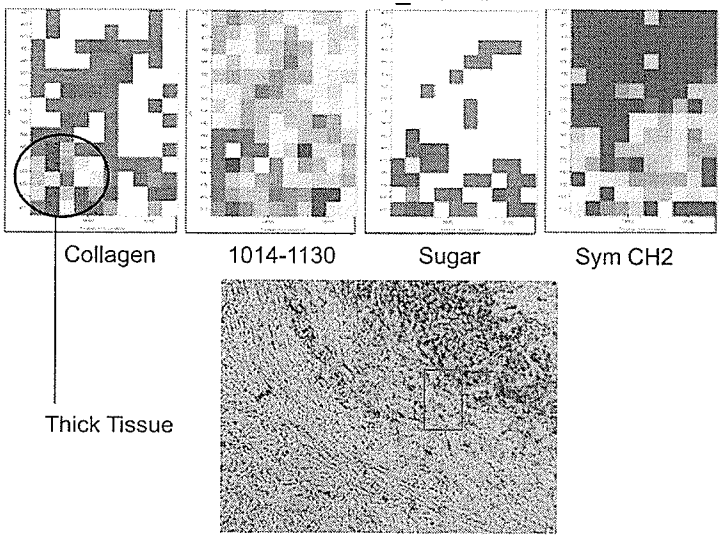

4 YH TC2B_03.MAP

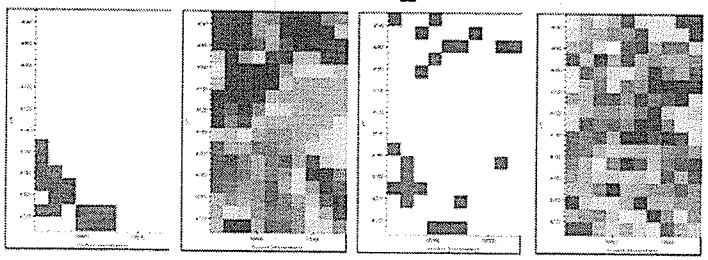

Collagen 1014-1130 Sugar Sym CH2

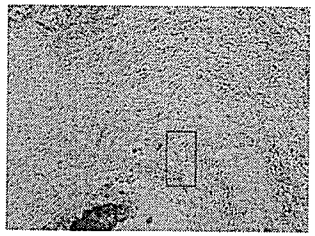

4 YH TC2B_04.MAP

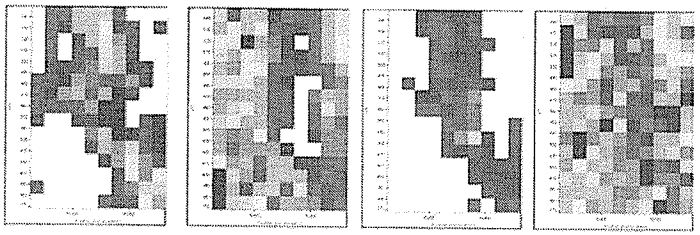

Collagen 1014-1130 Sugar Sym CH2

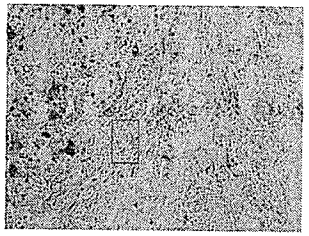

4 YH TC2B_05.MAP

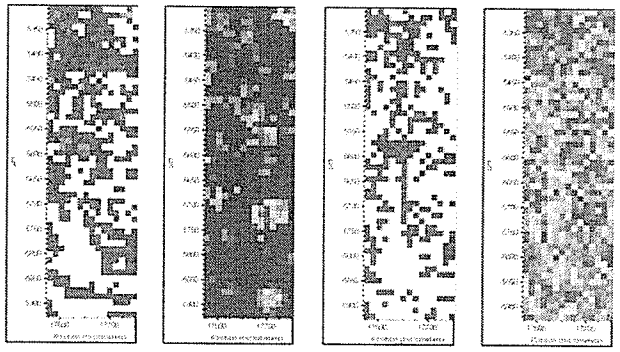

Collagen 1014-1130 Sugar Sym CH2

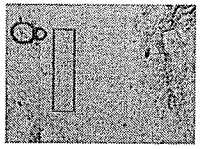

4 YH TC2B_06.MAP

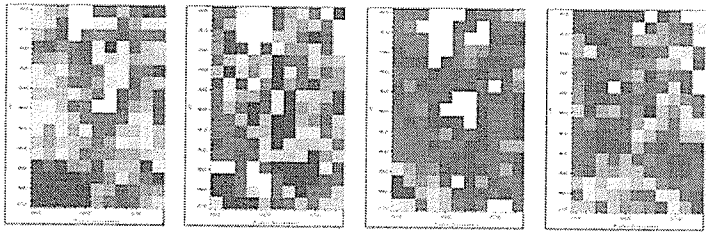

Collagen 1014-1130 Sugar Sym CH2

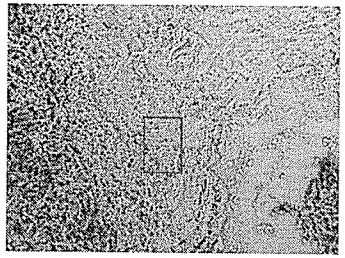

Top part of the map is out of focus, other parts have Amide I or II > 2

4 YH TC2B_07.MAP

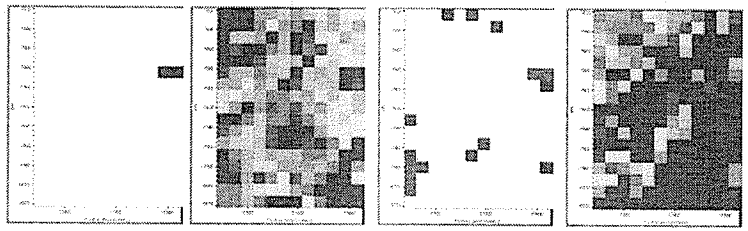

Collagen 1014-1130 Sugar Sym CH2

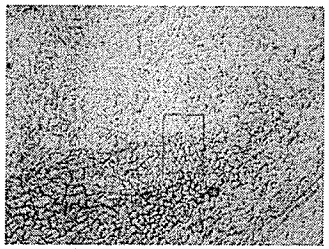

4 YH TC2B_08.MAP

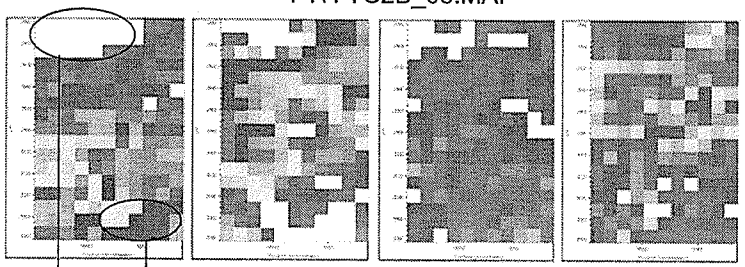

Collagen 1014-1130 Sugar Sym CH2

Thin Thick

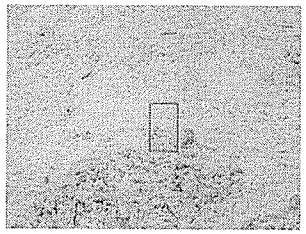

4 YH TC2B_09.MAP

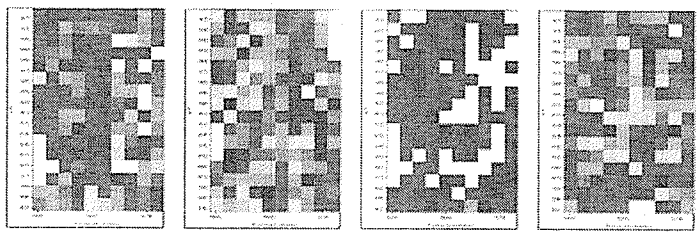

Collagen 1014-1130 Sugar Sym CH2

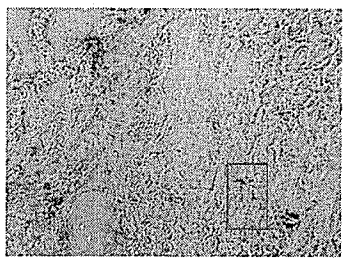

4 YH TC2B_10.MAP

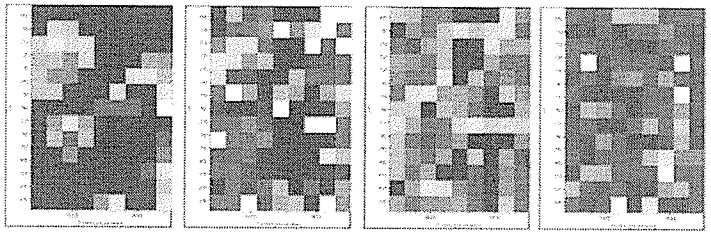

Collagen 1014-1130 Sugar Sym CH2

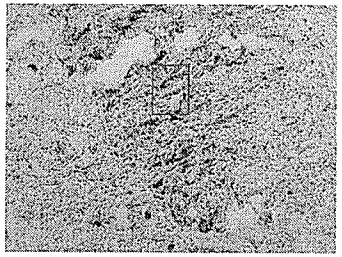

4 YH TC2B_11.MAP

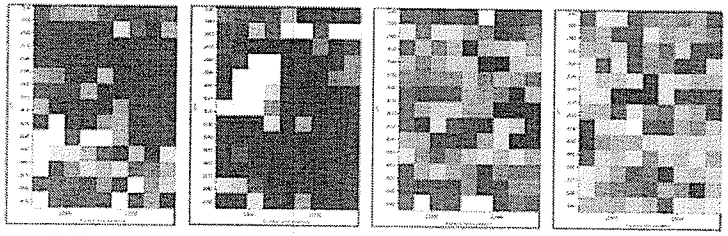

Collagen 1014-1130 Sugar Sym CH2

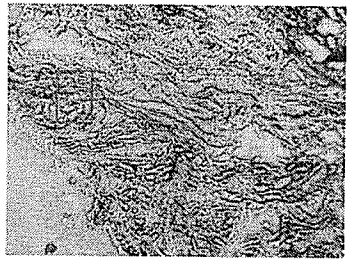

Lots of poor quality spectra

4 YH TC2B_12.MAP

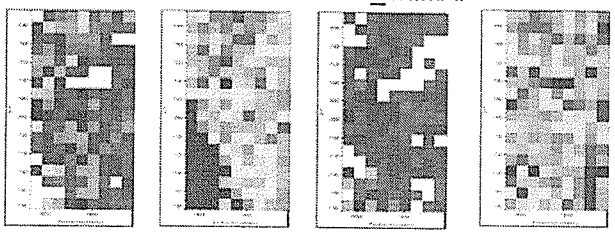

Collagen 1014-1130 Sugar Sym CH2

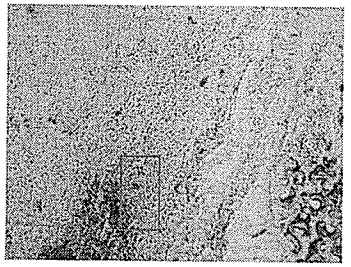

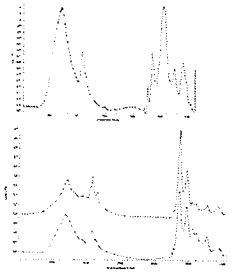

4 YH TC2B_13.MAP

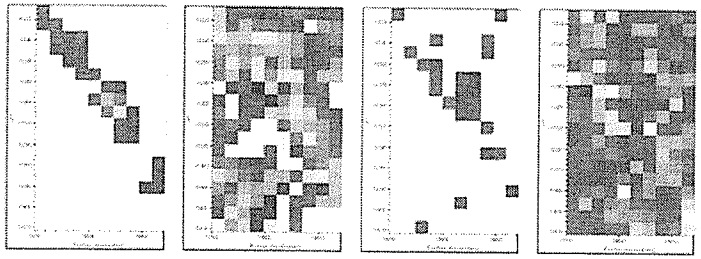

Collagen 1014-1130 Sugar Sym CH2

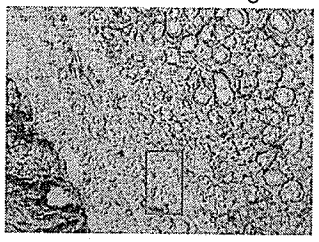

YH TC1A_01.MAP

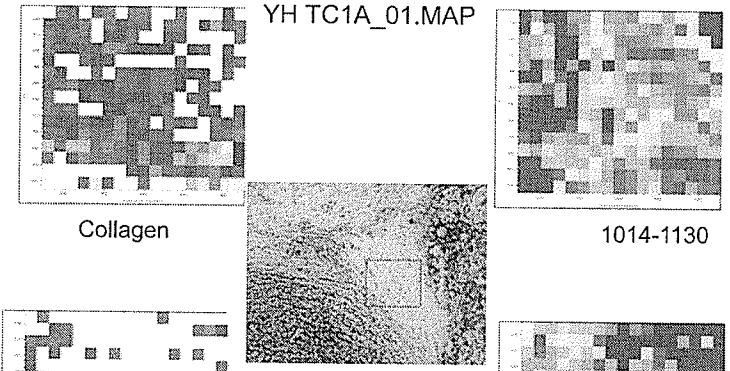

Collagen 1014-1130

Sugar Sym CH2

YH TC1A_02.MAP

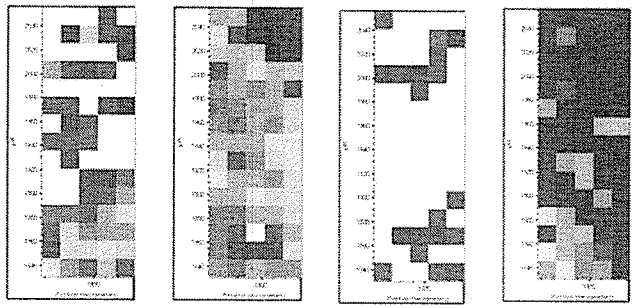

Collagen 1014-1130 Sugar Sym CH2

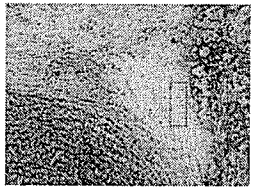

Baseline issues in top right corner, and occasional Amide I spikeyness

YH TC1A_03.MAP

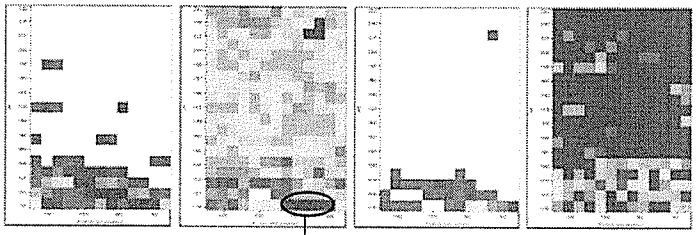

Collagen 1014-1130 Sugar Sym CH2

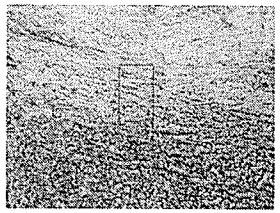

Out of focus, baseline starts at > 1

YH TC1A_04.MAP

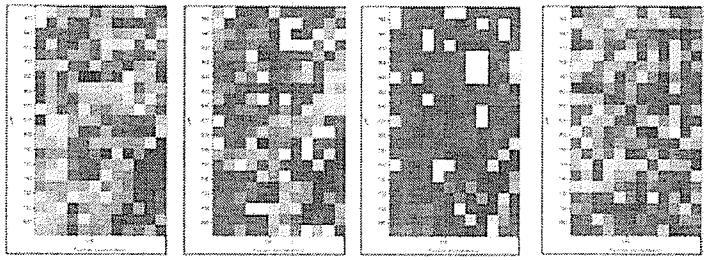

Collagen 1014-1130 Sugar Sym CH2

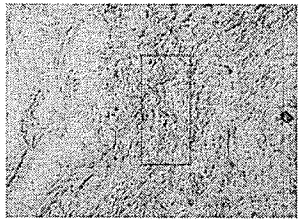

Lots of usual Amide I. We have low frequency ones, spikey ones, and split ones.

YH TC1A_05.MAP

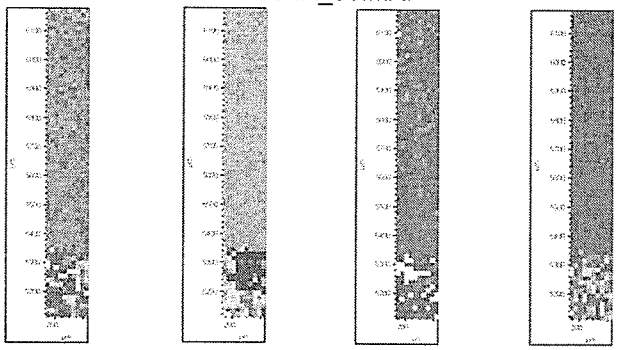

Collagen 1014-1130 Sugar Sym CH_2

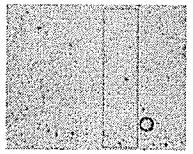

YH TC1A_05_blc.MAP

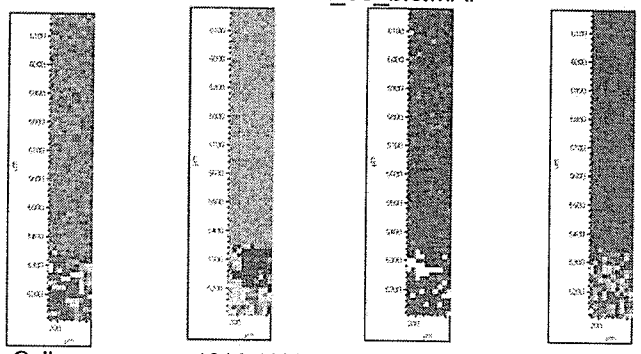

Collagen 1014-1130 Sugar Sym CH2

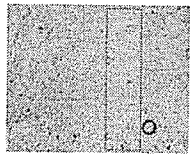

Same map, but baseline corrected.

YH TC1A_06.MAP

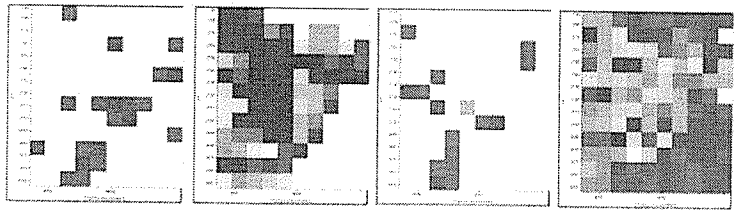

Collagen 1014-1130 Sugar Sym CH2

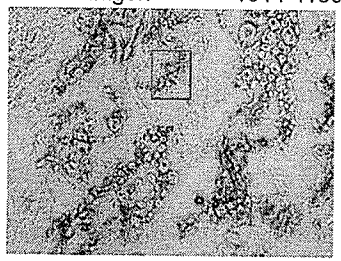

Amide I frequently > 2 and some areas of rolling baseline

YH TC1A_07.MAP

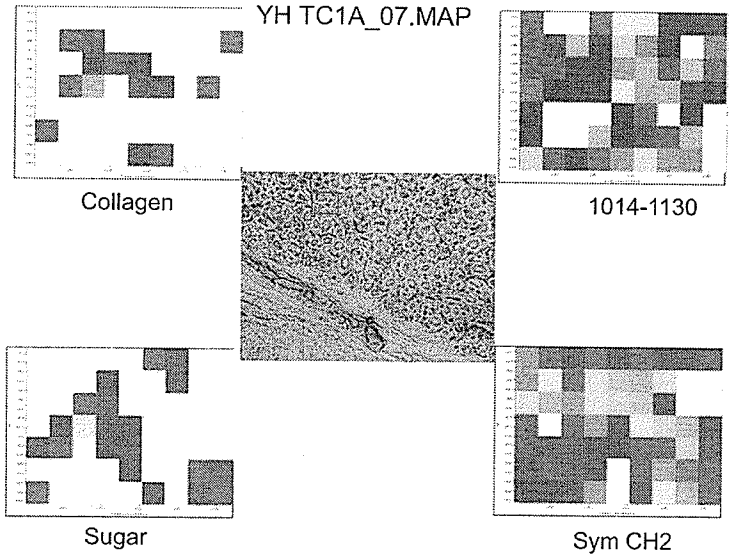

Collagen 1014-1130 Sugar Sym CH2

21 Day Saline

July 2004

Fred Zeiler
Richard Wiens
Margaret Rak

21 Day Saline Animal 25 Slide 10 map 1

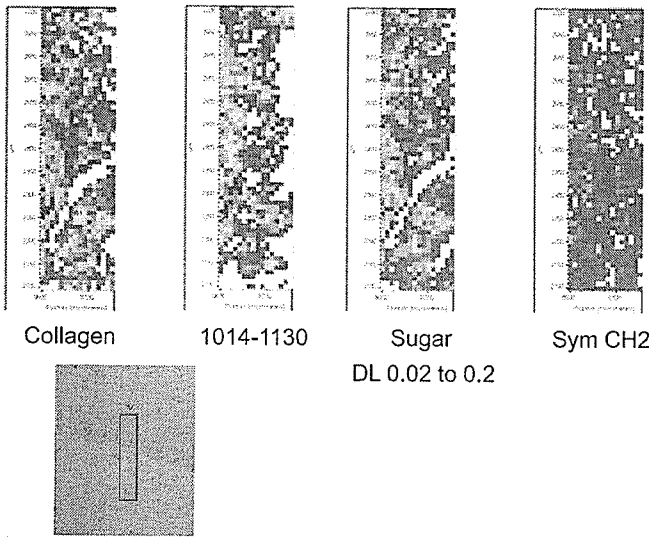

21 Day Saline Animal 25 Slide 10 map 2

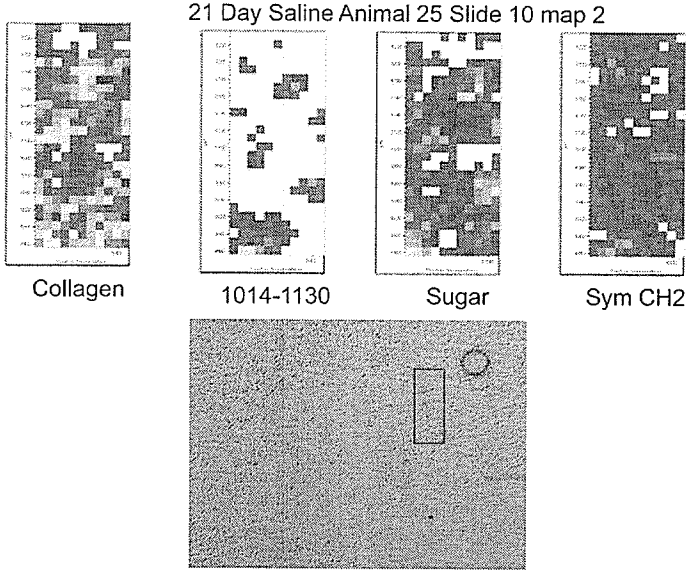

21 Day Saline Animal 25 Slide 10 map 3

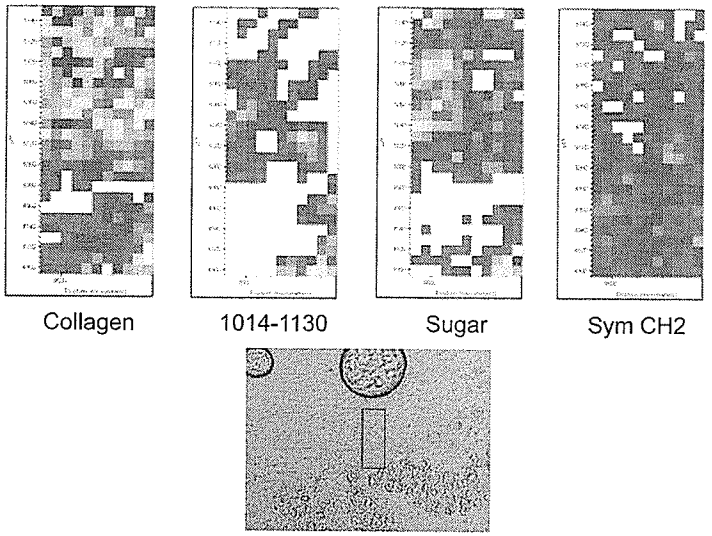

21 Day Saline Animal 25 Slide 10 map 4b

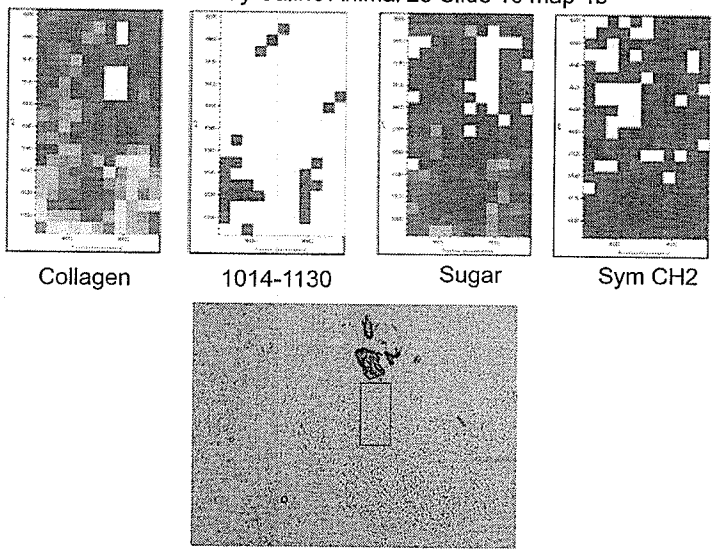

21 Day Saline Animal 25 Slide 10 map 5

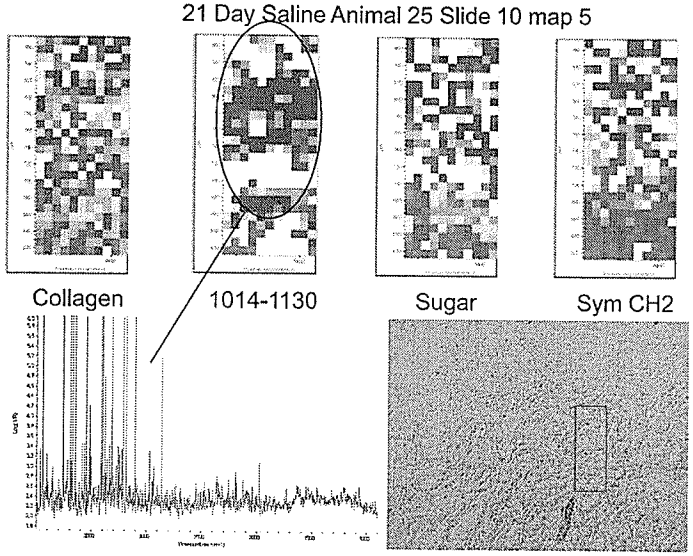

21 Day Saline Animal 25 Slide 10 map 6

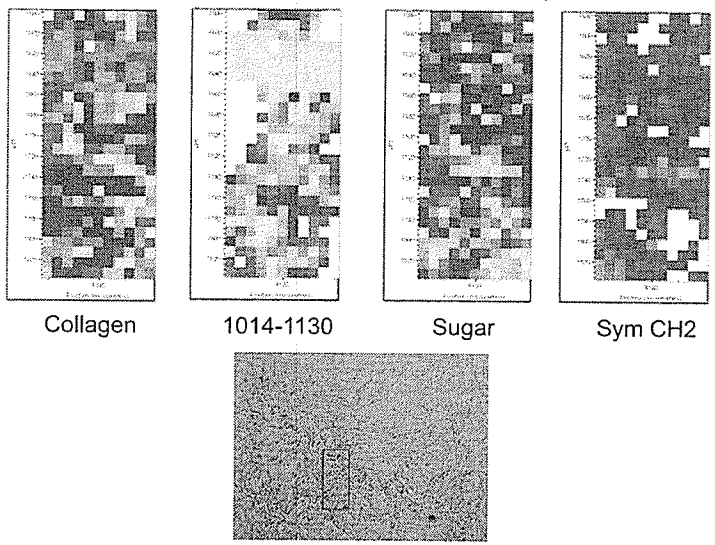

21 Day Saline Animal 26 Slide 10 map 1

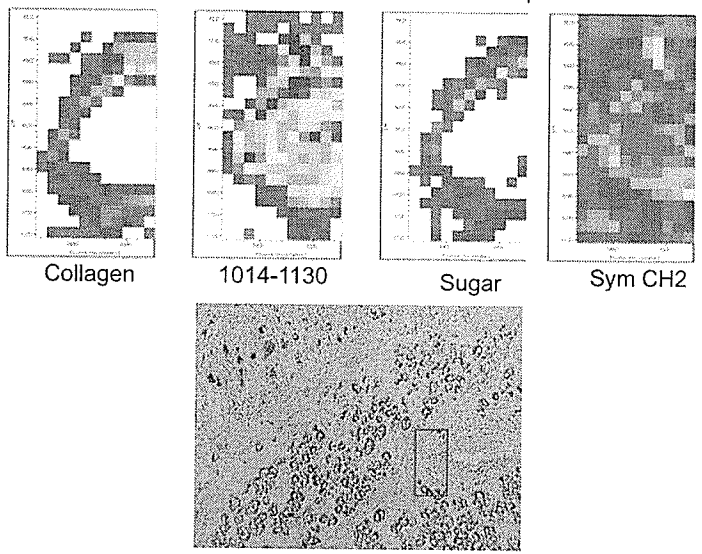

21 Day Saline Animal 26 Slide 10 map 2

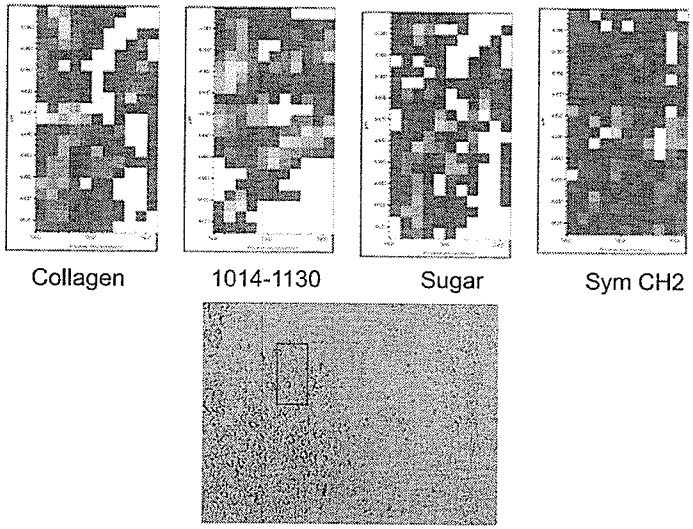

Collagen 1014-1130 Sugar Sym CH2

21 Day Saline Animal 26 Slide 10 map 3

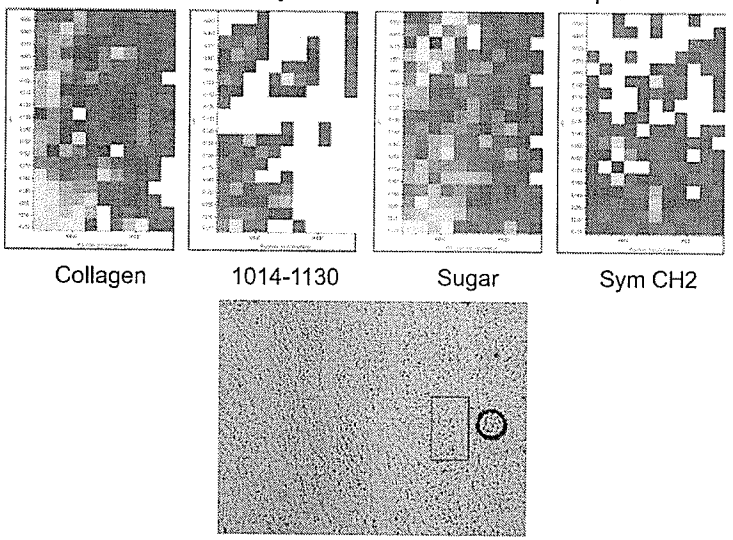

Collagen 1014-1130 Sugar Sym CH2

21 Day Saline Animal 26 Slide 10 map 4

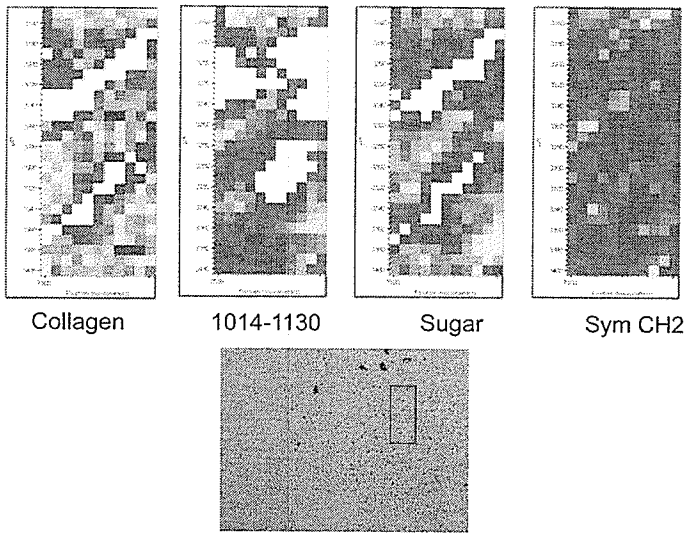

Collagen 1014-1130 Sugar Sym CH2

21 Day Saline Animal 26 Slide 10 map 5

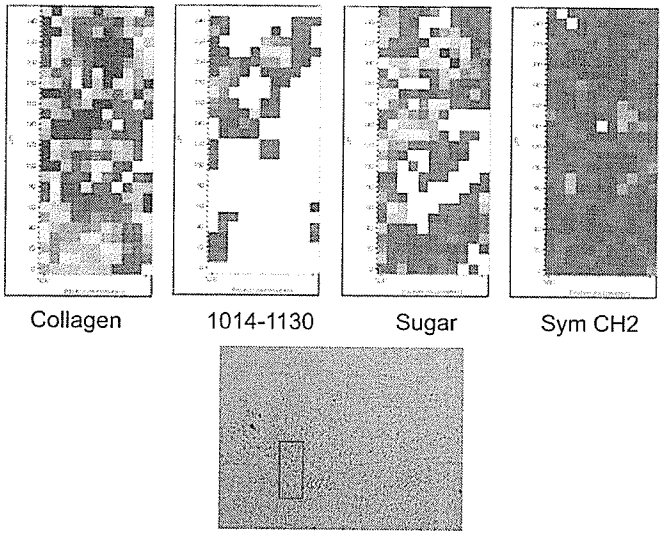

Collagen 1014-1130 Sugar Sym CH2

21 Day Saline Animal 26 Slide 10 map 6

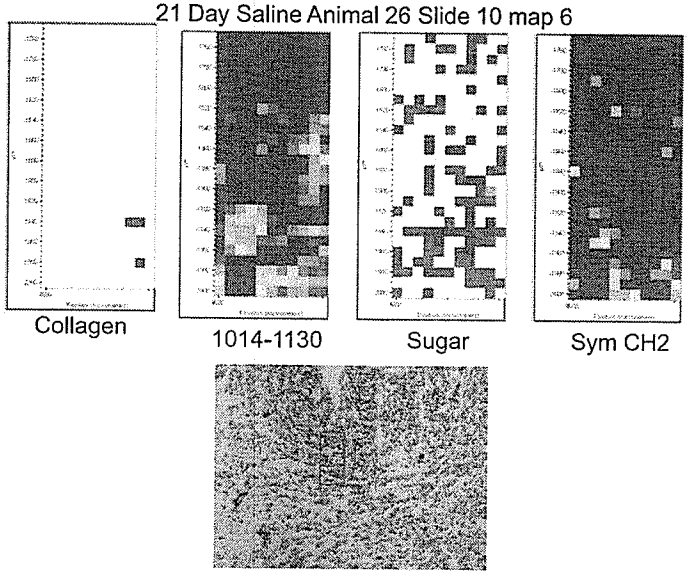

Collagen 1014-1130 Sugar Sym CH2

21 Day Saline Animal 27 Slide 10 map 1

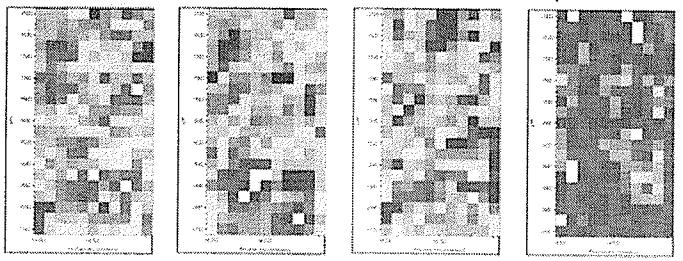

Collagen 1014-1130 Sugar Sym CH2

21 Day Saline Animal 27 Slide 10 map 2

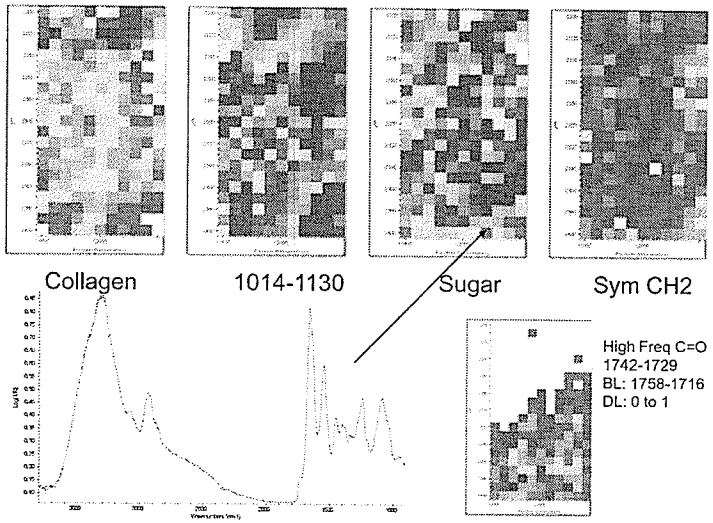

Collagen 1014-1130 Sugar Sym CH2

21 Day Saline Animal 27 Slide 10 map 3

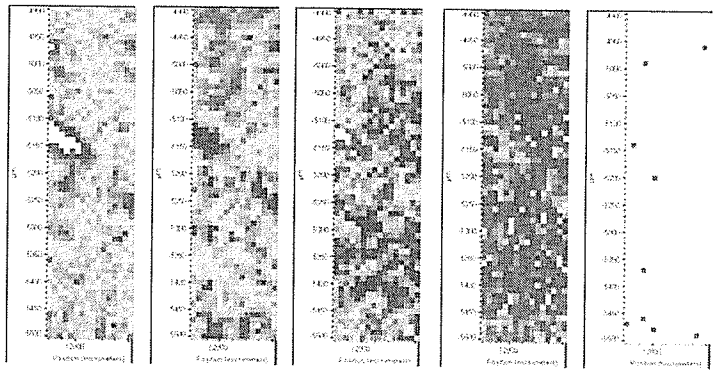

Collagen 1014-1130 Sugar Sym CH2 High Frequency (~1720) Carbonyl

21 Day Saline Animal 27 Slide 10 map 4

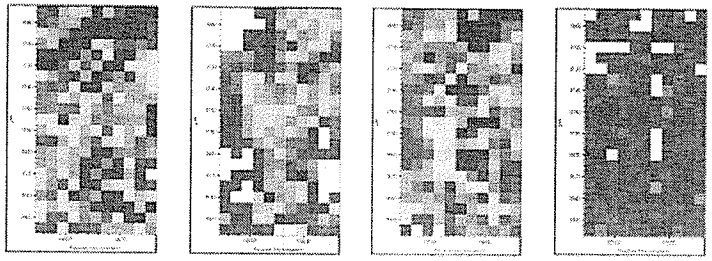

Collagen 1014-1130 Sugar Sym CH2

21 Day Saline Animal 27 Slide 10 map 5

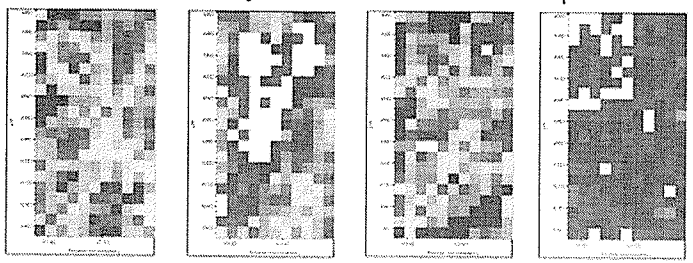

Collagen 1014-1130 Sugar Sym CH2

21 Day Saline Animal 27 Slide 10 map 6

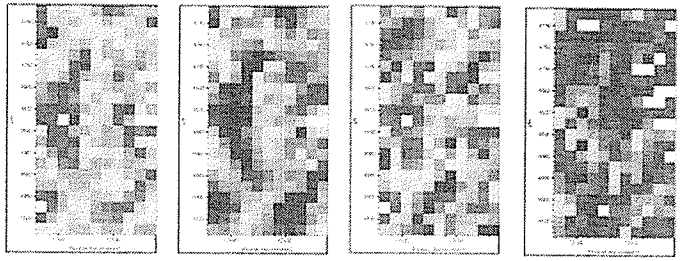

Collagen 1014-1130 Sugar Sym CH2

21 Day Saline

September 2004
Margaret Rak

21 Day Saline Animal 25 Slide 10 map 1

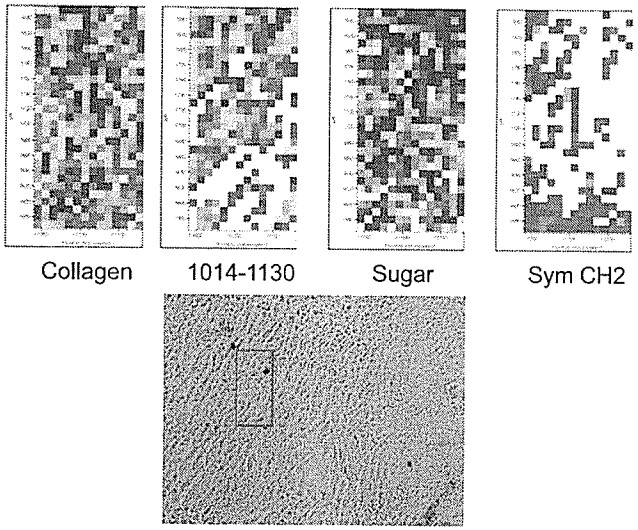

Collagen 1014-1130 Sugar Sym CH2

21 Day Saline Animal 25 Slide 10 map 2

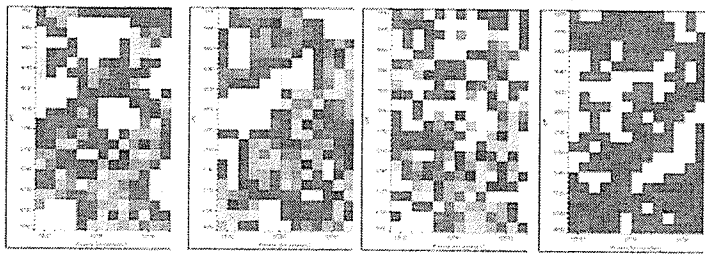

Collagen 1014-1130 Sugar Sym CH2

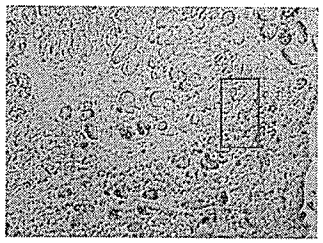

There seems to be a low periodicity baseline roll in some of the spectra that is affecting the calculation of the area of the 1014-1130 portion of the spectrum

21 Day Saline Animal 25 Slide 10 map 3

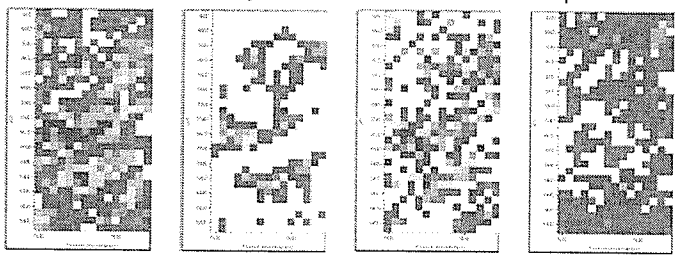

Collagen 1014-1130 Sugar Sym CH2

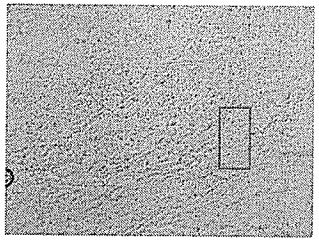

21 Day Saline Animal 25 Slide 10 map 4

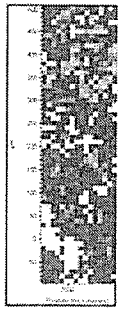
Collagen

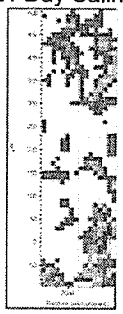
1014-1130


Sugar

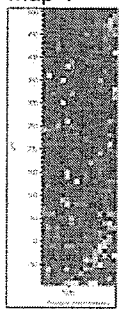
Sym CH2

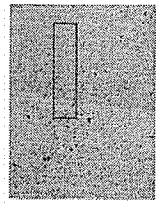

21 Day Saline Animal 26 Slide 10 map 1

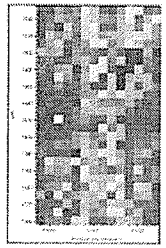
Collagen

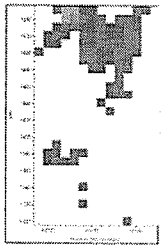
1014-1130

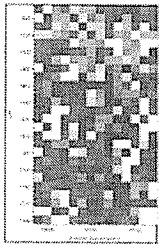
Sugar

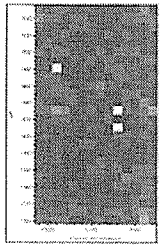
Sym CH2

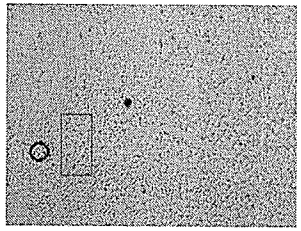

21 Day Saline Animal 26 Slide 10 map 2

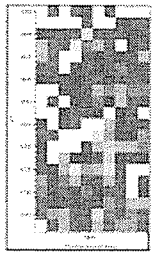
Collagen


1014-1130

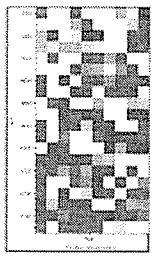
Sugar

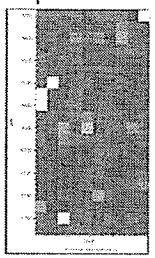
Sym CH2

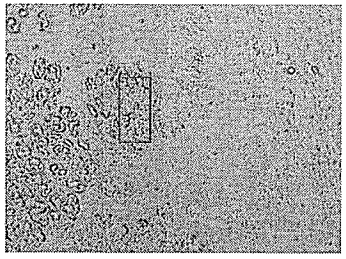

21 Day Saline Animal 26 Slide 10 map 3

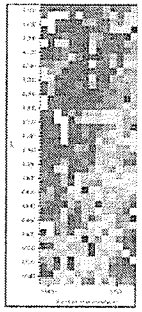
Collagen

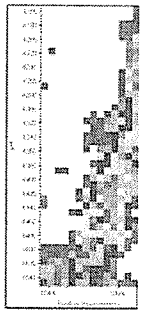
1014-1130

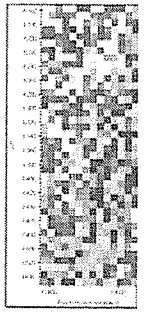
Sugar

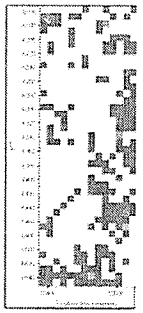
Sym CH2

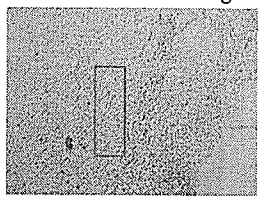

21 Day Saline Animal 26 Slide 10 map 4

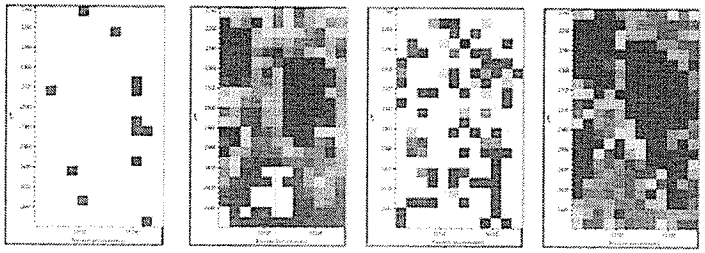

Collagen 1014-1130 Sugar Sym CH2

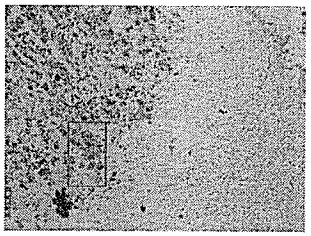

21 Day Saline Animal 27 Slide 10 map 1

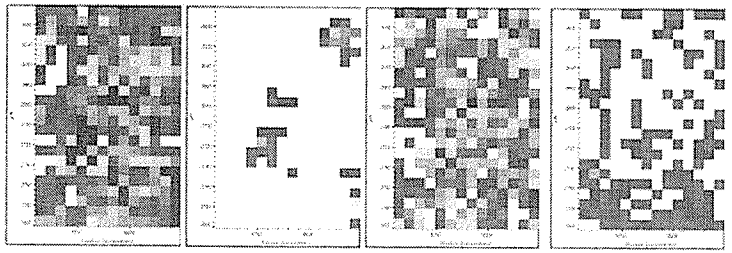

Collagen 1014-1130 Sugar Sym CH2

21 Day Saline Animal 27 Slide 10 map 2

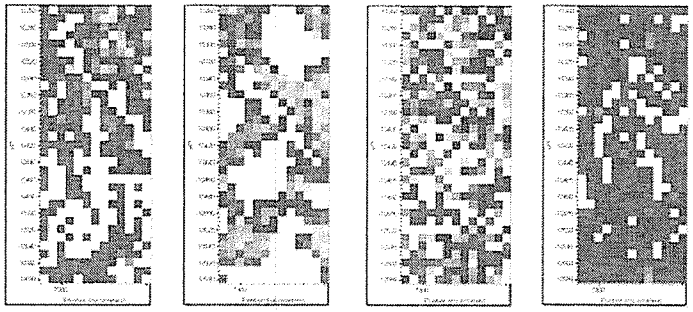

Collagen 1014-1130 Sugar Sym CH2

21 Day Saline Animal 27 Slide 10 map 3

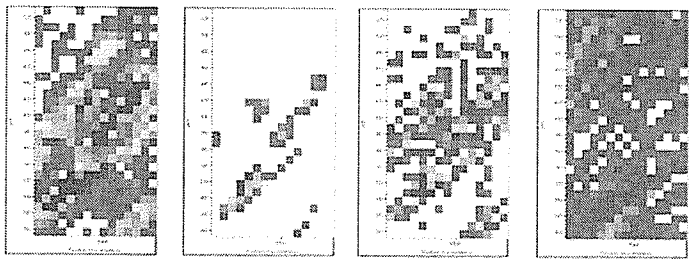

Collagen 1014-1130 Sugar Sym CH2

21 Day Saline Animal 27 Slide 10 map 4

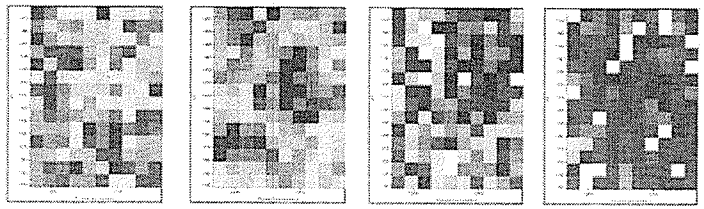

Collagen 1014-1130 Sugar Sym CH2

21 Day Saline Animal 27 Slide 10 map 5

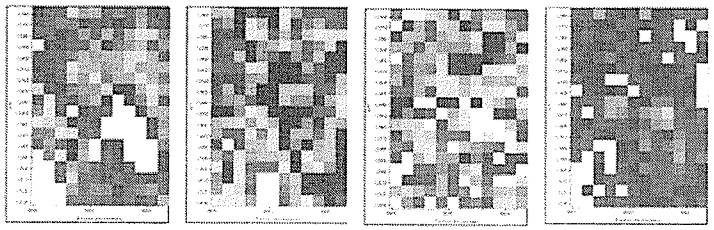

Collagen 1014-1130 Sugar Sym CH2

21 Day Saline

July 2005

Kathy Gough
Margaret Rak

21 Day Saline 25 Map 1 Slide 10A

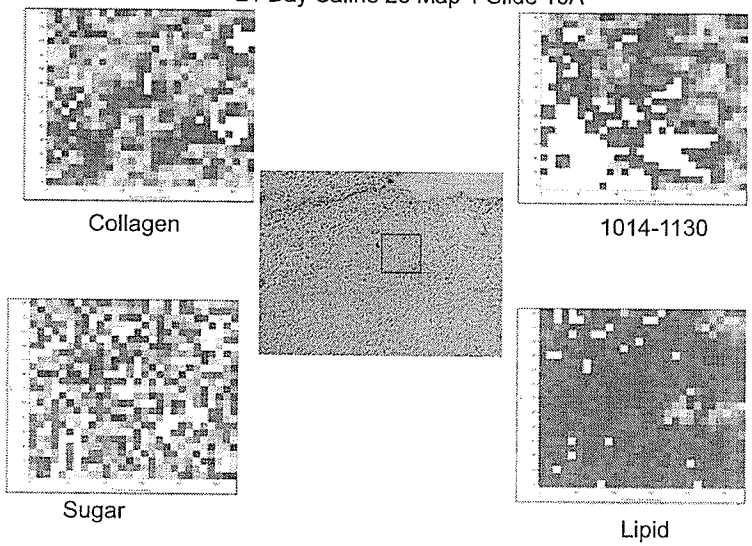

21 Day Saline 27 Map 1 Slide 10A

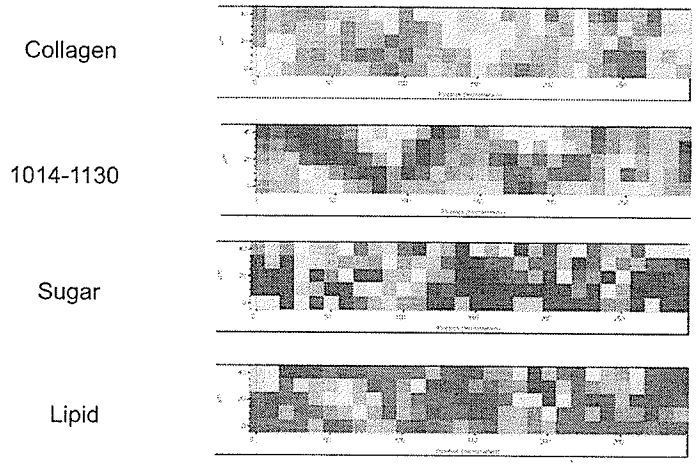

21 Day Saline 25 Map 1 Slide 10A

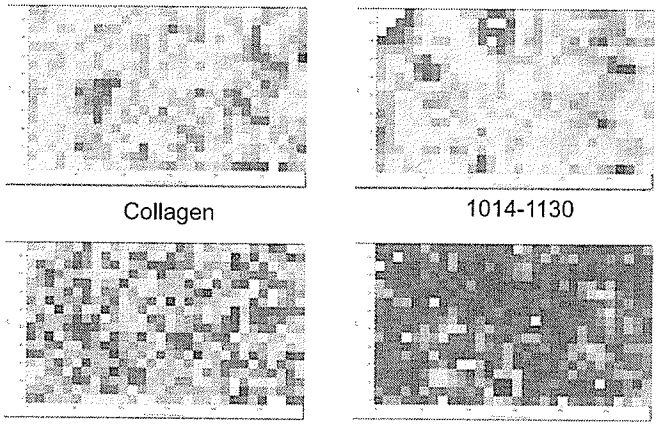

Map is not marked on image

63 Day OTC

June 2006
Richard Wiens
Mitch Bushuk

63 Day OTC N13 Slide 30 Map 7

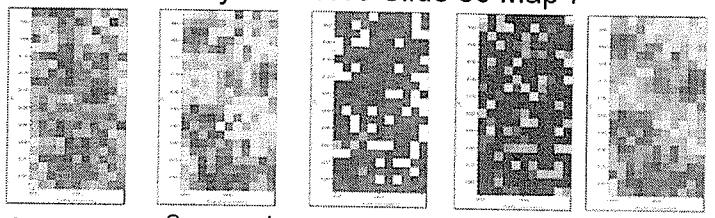

Collagen 1204 | Sugar and Phosphate | CH2 Sym | Sugar | 1080

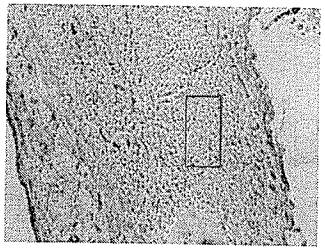

63 Day OTC N13 Slide 30 Map 8

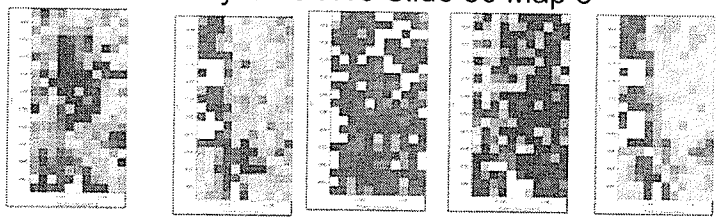

Collagen 1204 | Sugar and Phosphate | CH2 Sym | Sugar | 1080

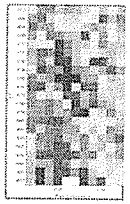

Collagen

DL: 0.025-0.55

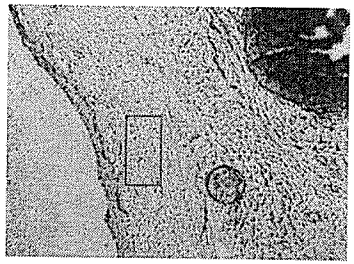

63 Day OTC N17 Map 1

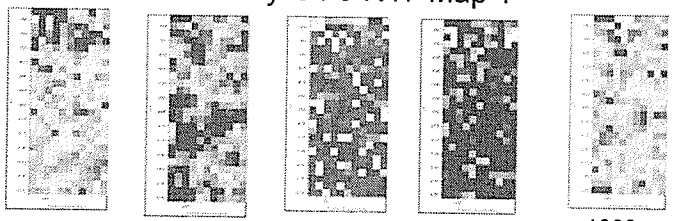

Collagen 1204 | Sugar and Phosphate | CH2 Sym | Sugar | 1080

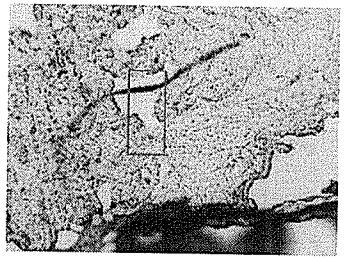

63 Day OTC N17 Map 2

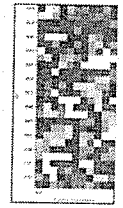
Collagen 1204

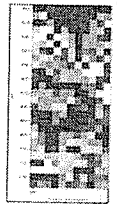
Sugar and Phosphate

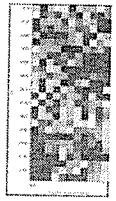
CH2 Sym

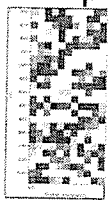
Sugar

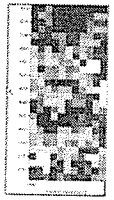
1080

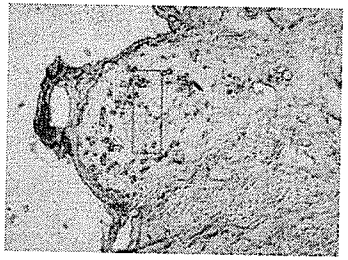

63 Day OTC N17 Map 3

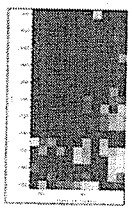
Collagen 1204

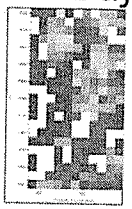
Sugar and Phosphate

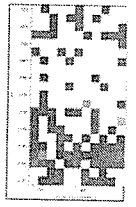
CH2 Sym

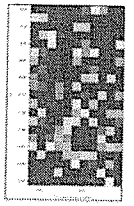
Sugar


1080

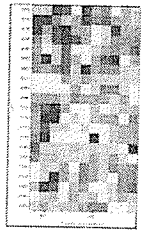
Collagen

DL: 0.025-0.8

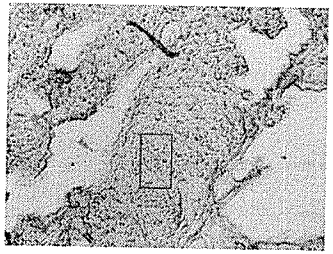

63 Day OTC N17 Map 4

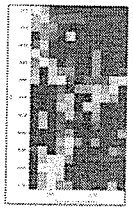
Collagen 1204

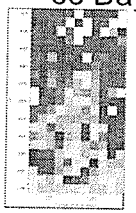
Sugar and Phosphate

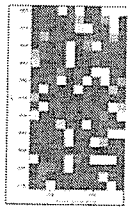
CH2 Sym

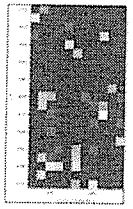
Sugar

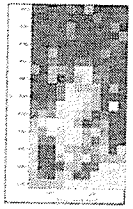
1080

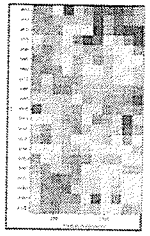
Collagen

DL: 0.025-0.8

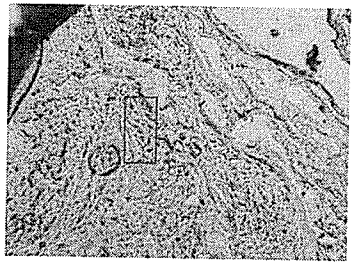

63 Day OTC N17 Map 5

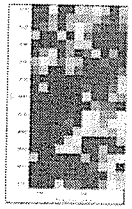
Collagen 1204

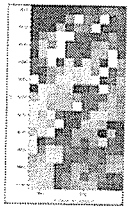
Sugar and Phosphate

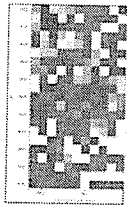
CH2 Sym

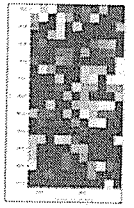
Sugar

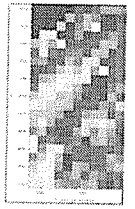
108 0

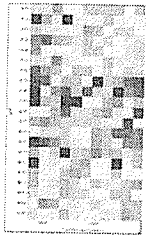
Collagen

DL: 0.025-0.7

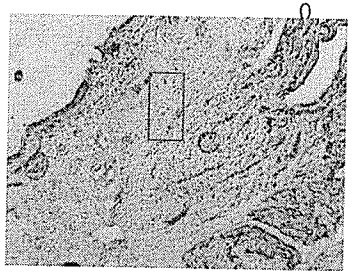

63 Day OTC N17 Map 6

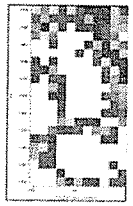
Collagen 1204

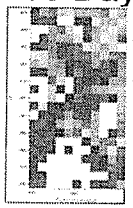
Sugar and Phosphate

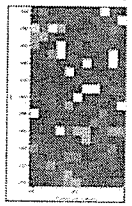
CH2 Sym

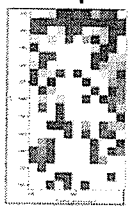
Sugar


1080

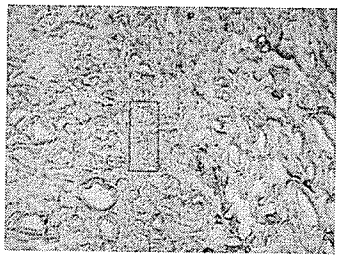

63 Day OTC N17 Map 7

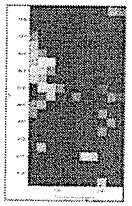
Collagen 1204

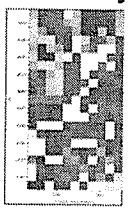
Sugar and Phosphate

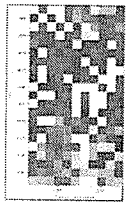
CH2 Sym

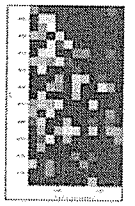
Sugar

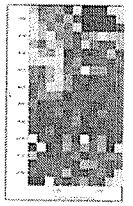
1080

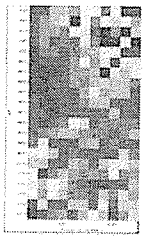
Collagen:

DL: 0.025-1.7

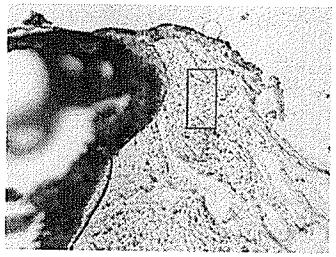

63 Day OTC N17 Map 8

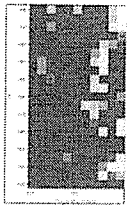
Collagen 1204

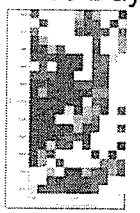
Sugar and Phosphate

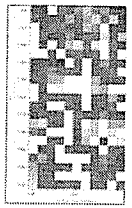
CH2 Sym

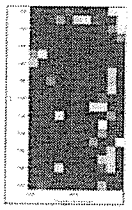
Sugar

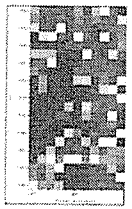
1080

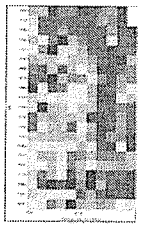
Collagen

DL: 0.025-1.7

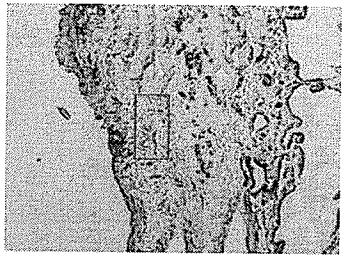

63 Day OTC N19 Map 1

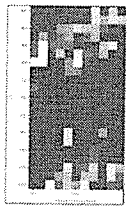
Collagen 1204

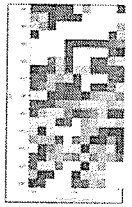
Sugar and Phosphate

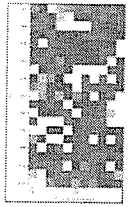
CH2 Sym

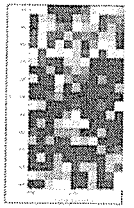
Sugar

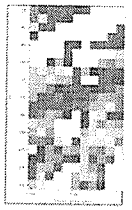
1080

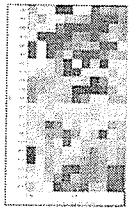
Collagen

DL: 0.025-1

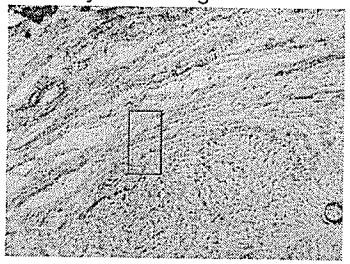

63 Day OTC N19 Map 2

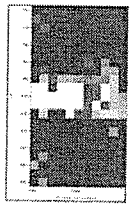
Collagen 1204


Sugar and Phosphate

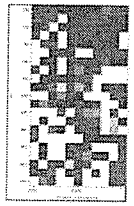
CH2 Sym

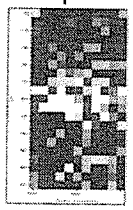
Sugar

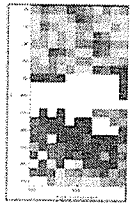
1080

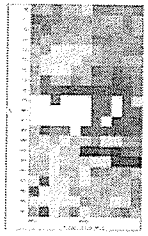
Collagen

DL: 0.025-1.3

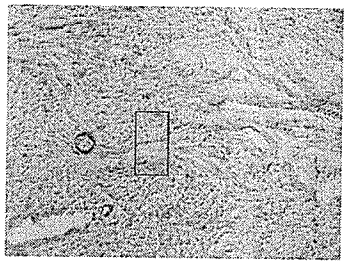

63 Day OTC N19 Map 3

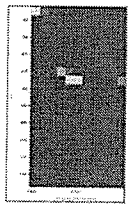
Collagen 1204

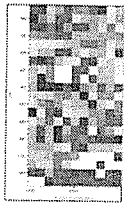
Sugar and Phosphate

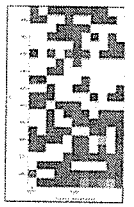
CH2 Sym

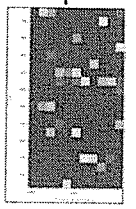
Sugar

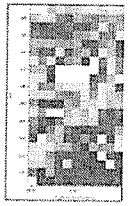
1080

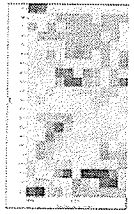
Collagen:

DL: 0.025-1.1

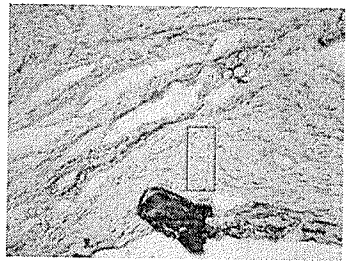

63 Day OTC N19 Map 4

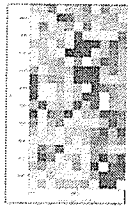
Collagen 1204

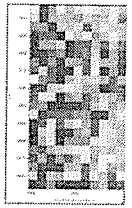
Sugar and Phosphate

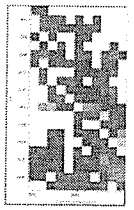
CH2 Sym

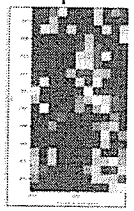
Sugar

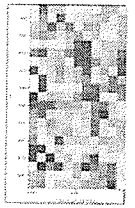
1080

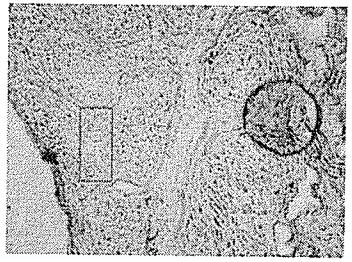

63 Day OTC N19 Map 5

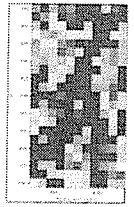
Collagen 1204

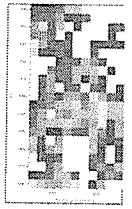
Sugar and Phosphate

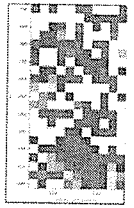
CH2 Sym

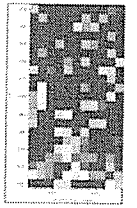
Sugar

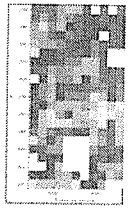
1080

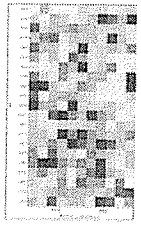
Collagen:

DL: 0.025-0.6

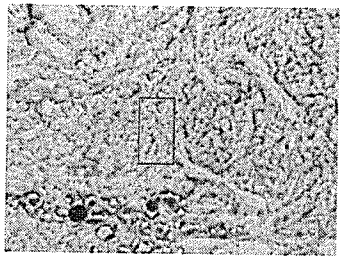

63 Day OTC N19 Map 6

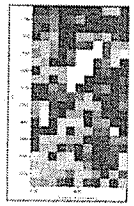
Collagen 1204

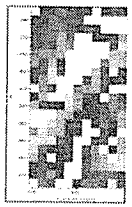
Sugar and Phosphate

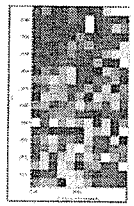
CH2 Sym

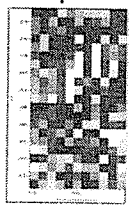
Sugar

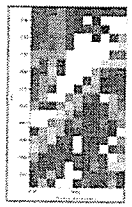
1080

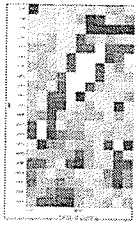
Collagen

DL: 0.025-0.7

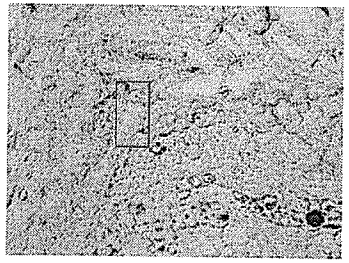

63 Day OTC N19 Map 7 Stage Died

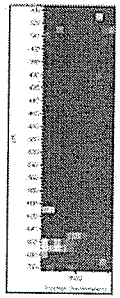
Collagen 1204

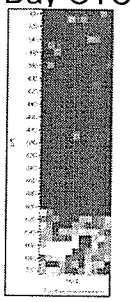
Sugar and Phosphate

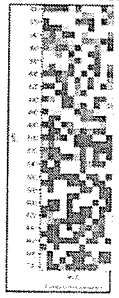
CH2 Sym

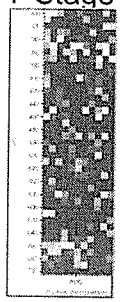
Sugar

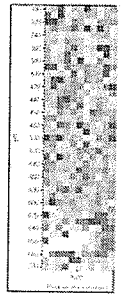
1080


Collagen

DL: 0.025-0.9

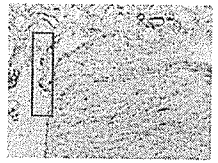

63 Day OTC N19 Map 7 Redo

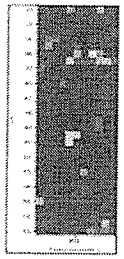
Collagen 1204

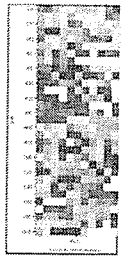
Sugar and Phosphate


CH2 Sym

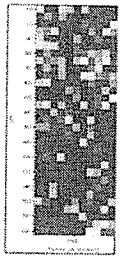
Sugar


1080


Collagen

DL: 0.025-0.9

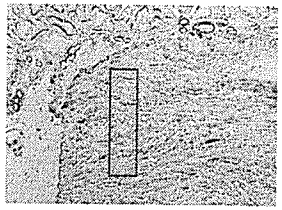

63 Day OTC N19 Map 8

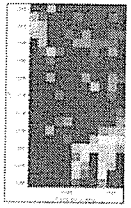
Collagen 1204

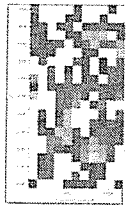
Sugar and Phosphate

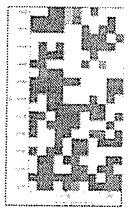
CH2 Sym

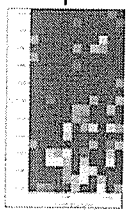
Sugar

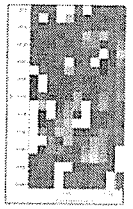
1080

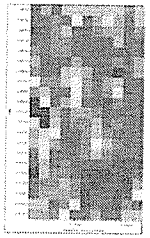
Collagen

DL: 0.025-1.6

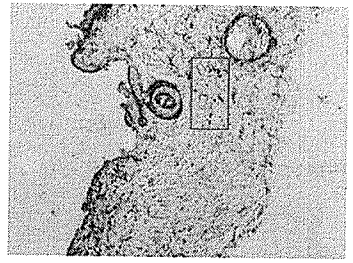

63 Day OTC N21 Map 1

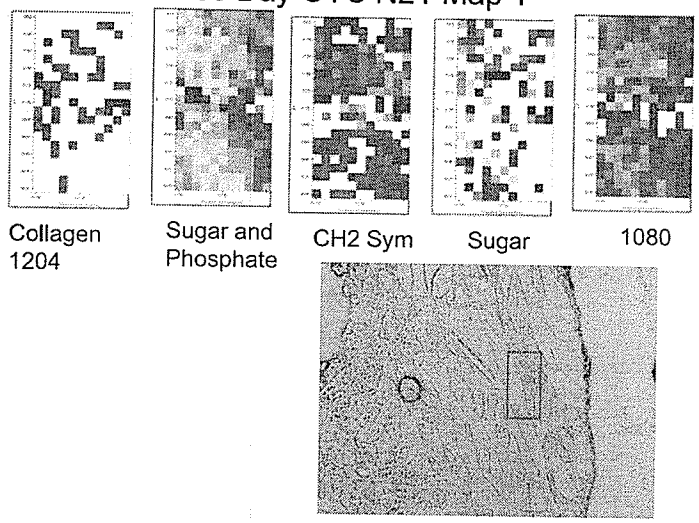

63 Day OTC N21 Map 2

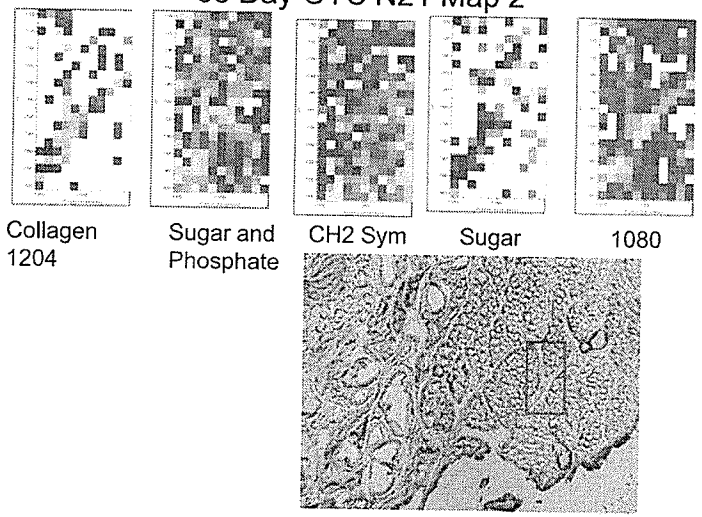

63 Day OTC N23 Map 1

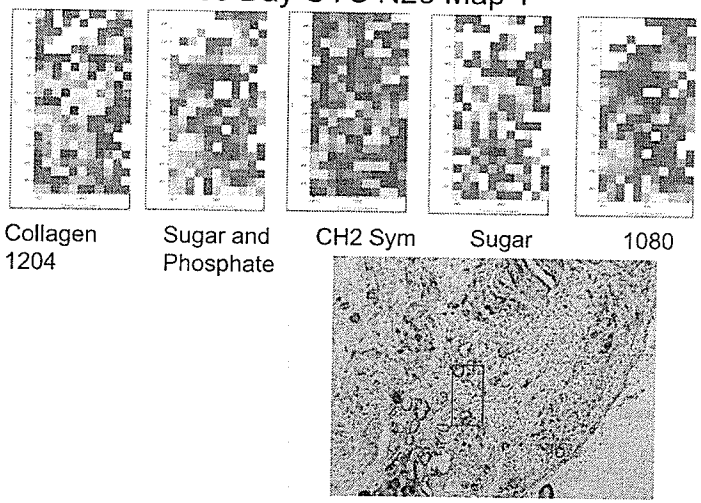

63 Day OTC N23 Map 2

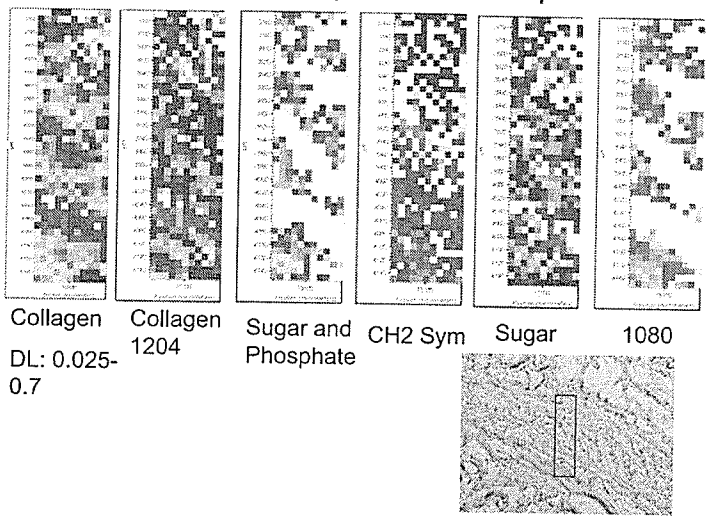

63 Day OTC N23 Map 3

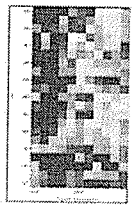
Collagen 1204

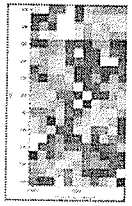
Sugar and Phosphate

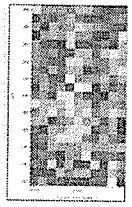
CH2 Sym

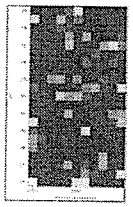
Sugar


1080

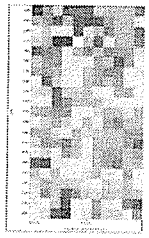
Collagen

DL: 0.025-0.6

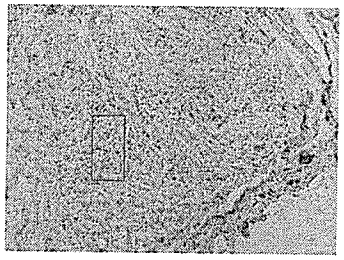

63 Day OTC N23 Map 4

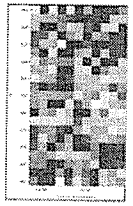
Collagen 1204

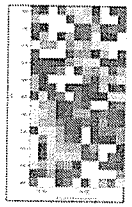
Sugar and Phosphate

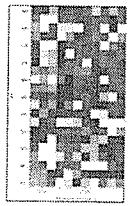
CH2 Sym

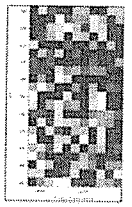
Sugar

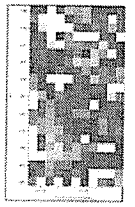
1080

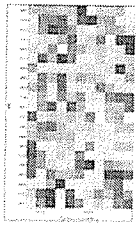
Collagen

DL: 0.025-0.6

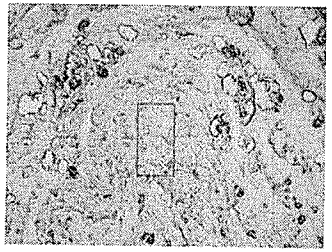

63 Day OTC N23 Map 5

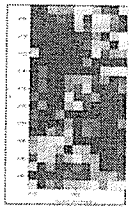
Collagen 1204

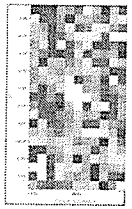
Sugar and Phosphate

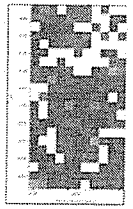
CH2 Sym

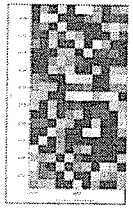
Sugar

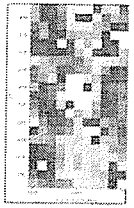
1080

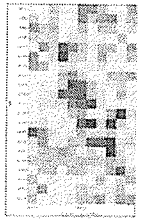
Collagen:

DL: 0.025-0.7

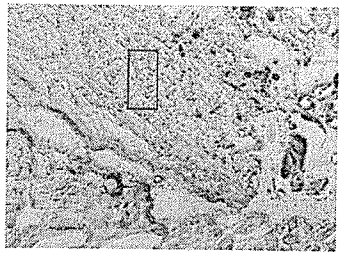

63 Day OTC N23 Map 6

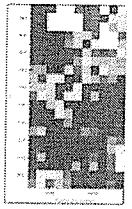
Collagen 1204

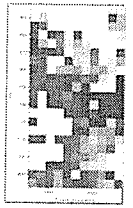
Sugar and Phosphate

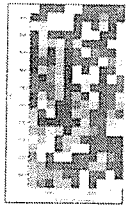
CH2 Sym

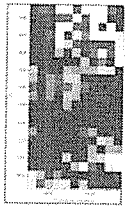
Sugar

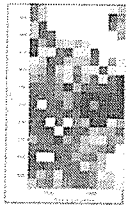
1080

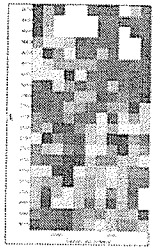
Collagen

DL: 0.025-1.2

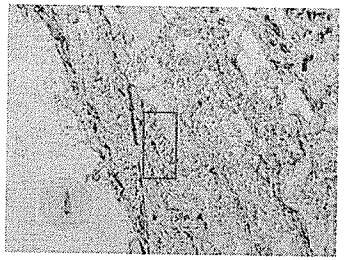

63 Day OTC N23 Map 7

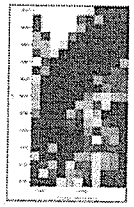

Collagen 1204

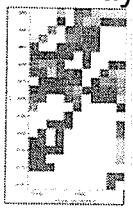

Sugar and Phosphate

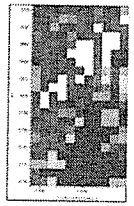

CH2 Sym

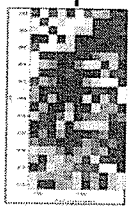

Sugar

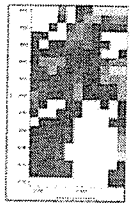

1080

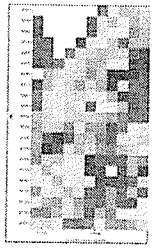

Collagen

DL: 0.025-0.8

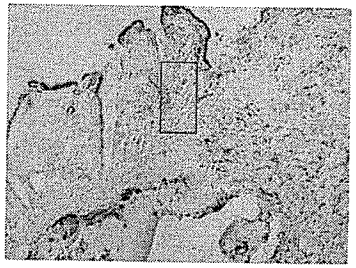

63 Day OTC N23 Map 8

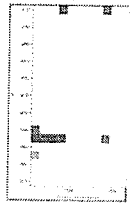

Collagen 1204

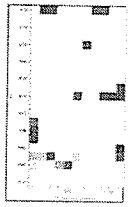

Sugar and Phosphate

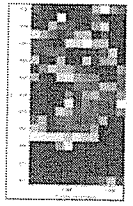

CH2 Sym

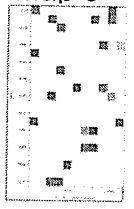

Sugar

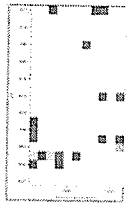

1080

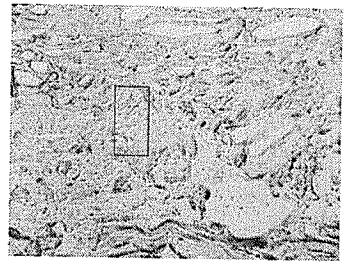

63 Day OTC

June 2007

Richard Wiens

63 Day OTC N19 Map 9

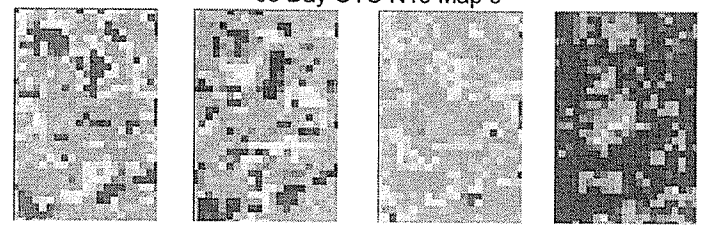

Collagen
0.0 to 0.75

Phosphate
0.6 to 1.6

Sugar
0.0 to 0.4

CH2 Sym
0.0 to 0.4

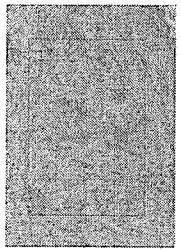

63 Day OTC N19 Map 10

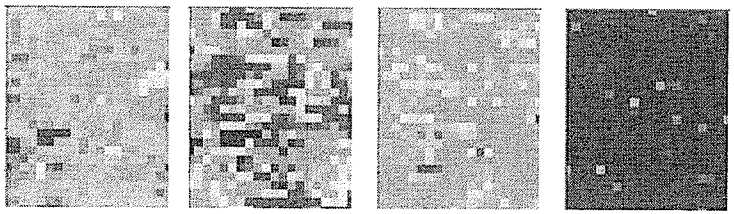

Collagen
0.0 to 0.5

Phosphate
0.6 to 1.6

Sugar
0.0 to 0.4

CH2 Sym
0.0 to 0.4

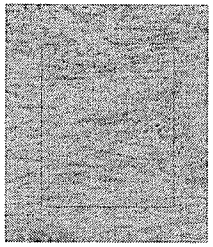

63 Day OTC N19 Map 11

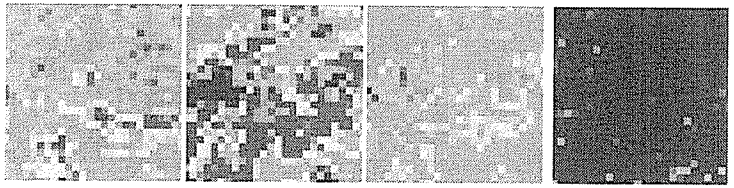

Collagen
0.0 to 0.5

Phosphate
0.6 to 1.6

Sugar
0.0 to 0.4

CH2 Sym
0.0 to 0.4

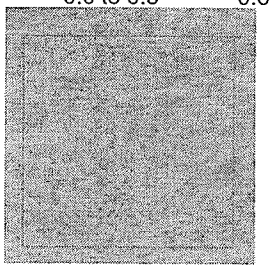

63 Day OTC N19 Map 12

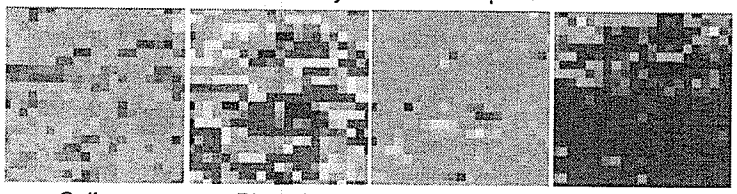

Collagen 0.0 to 0.5 | Phosphate 0.6 to 1.6 | Sugar 0.0 to 0.4 | CH2 Sym 0.0 to 0.4

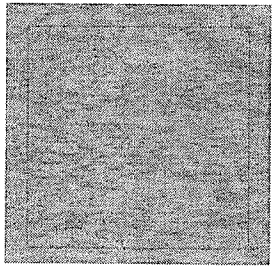

63 Day OTC N19 Map 13

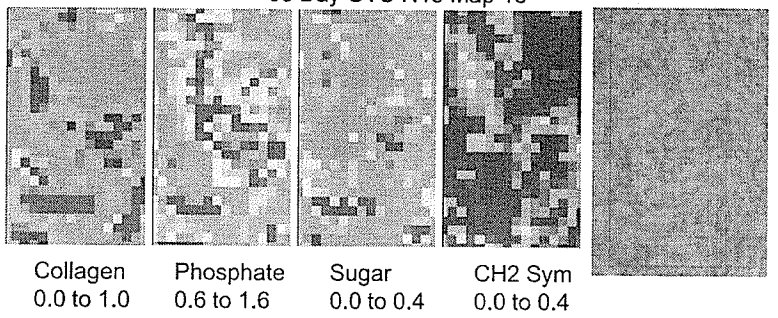

Collagen 0.0 to 1.0 | Phosphate 0.6 to 1.6 | Sugar 0.0 to 0.4 | CH2 Sym 0.0 to 0.4

- An interesting map. There are some spectra with split amide I's, as well as very high intensities around 3300 relative to the amides.

63 Day OTC N19 Map 14

Collagen 0.0 to 0.75 | Phosphate 0.6 to 1.8 | Sugar 0.0 to 0.4 | CH2 Sym 0.0 to 0.4

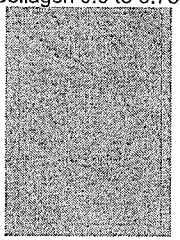

63 Day OTC N21 Map 3

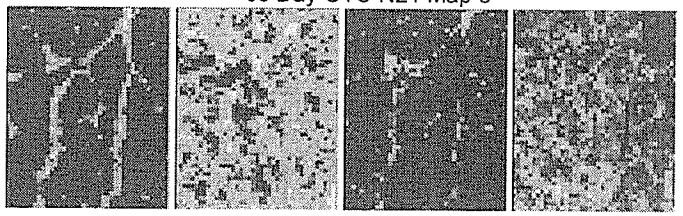

Collagen 0.0 to 0.5 | Phosphate 0.6 to 1.6 | Sugar 0.0 to 0.4 | CH2 Sym 0.0 to 1

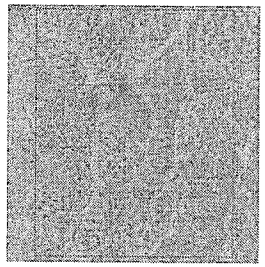

63 Day Que Rats

June 2006

Richard Wiens
Mitch Bushuk

63 Day Que N1 Map 4 Slide 30

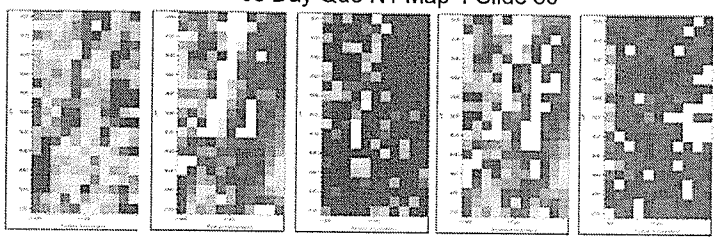

Collagen | Phosphate | Sugar | Total Phosphate and Sugar | Lipid

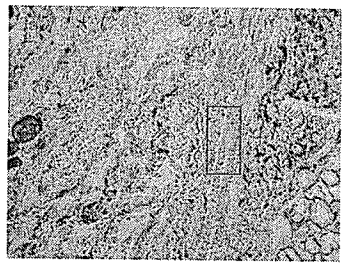

- More of the same old. Although glancing through the quercetin maps it does seem that there might be less intense collagen here

63 Day Que N1 Map 5 Slide 30

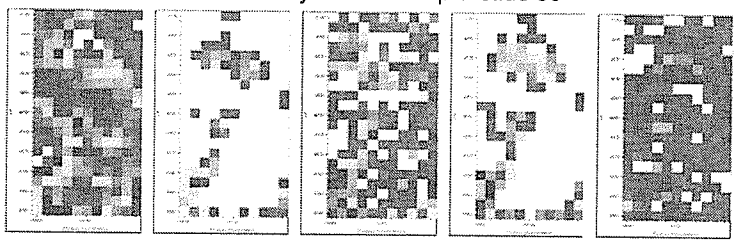

Collagen | Phosphate | Sugar | Total Phosphate and Sugar | Lipid

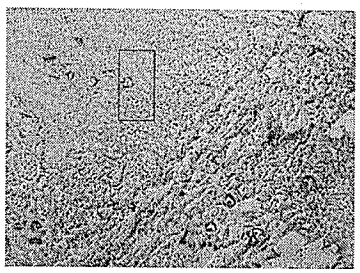

- Nice spectra in this map, the amides and OH/NH are a lot smoother than in some of the saline animals
- Below 1100 is somewhat noisy still though
- No mosaic for this map

63 Day Que N3 Map 1 Slide 30

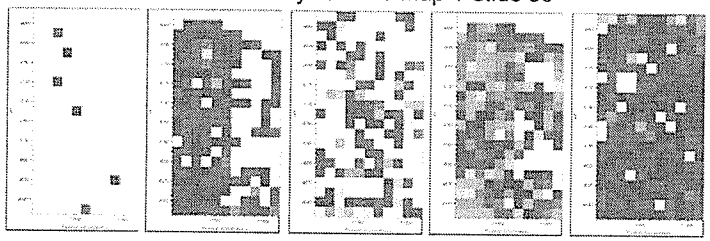

Collagen | Phosphate | Sugar | Total Phosphate and Sugar | Lipid

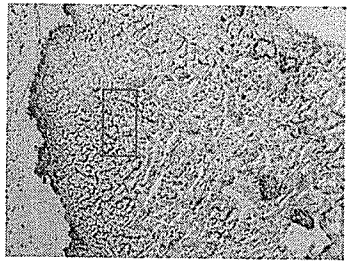

- Nice map, not much collagen

63 Day Que N3 Map 2 Slide 30

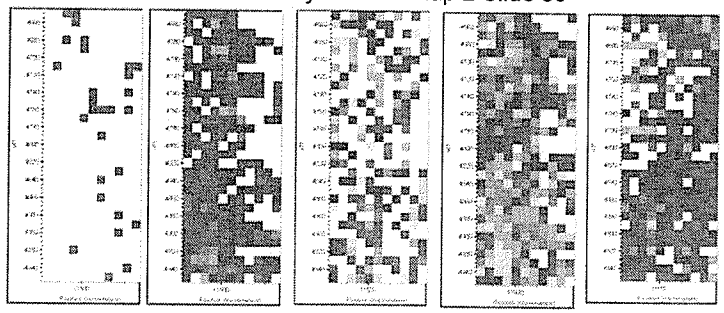

Collagen Phosphate Sugar Total Phosphate and Sugar Lipid

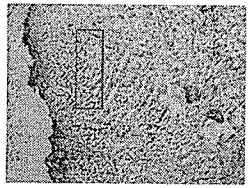

- Another good map, a bit of rolling baseline or spiky amides but nothing major

63 Day Que N3 Map 3 Slide 30

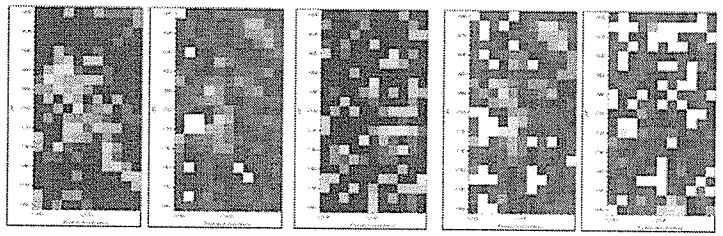

Collagen Phosphate Sugar Total Phosphate and Sugar Lipid

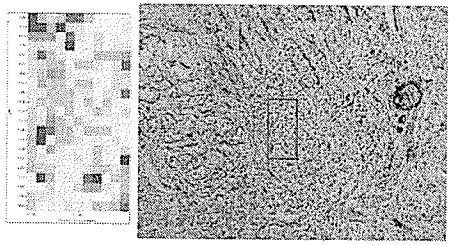

- Some spiky Amides and chopped off amides especially on the left hand side
- The Amide I bands don't match up well with the collagen spectra

DL: 0.025-0.7

63 Day Que N5 Map 1 Slide 10

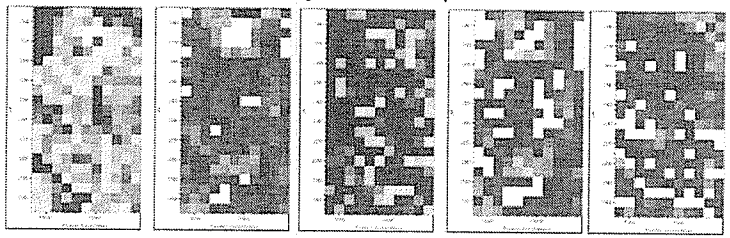

Collagen Phosphate Sugar Total Phosphate and Sugar Lipid

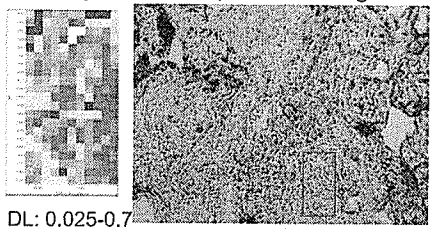

DL: 0.025-0.7

- More scraggly and spiky Amides and OH/NH stretches

63 Day Que N5 Map 2 Slide 10

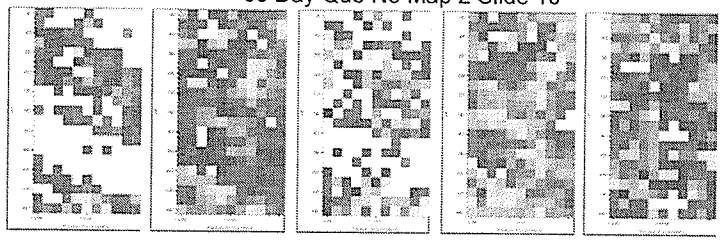

Collagen Phosphate Sugar Total Phosphate and Sugar Lipid

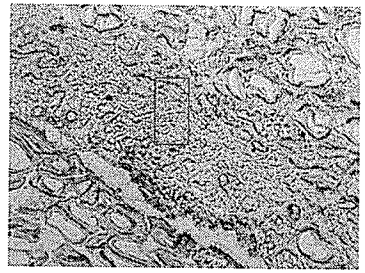

- Pretty standard fare for this trip, good collagen signature, not so good lipid and sugar/phosphate. Some cut off and spiky amides but not too bad

63 Day Que N5 Map 3 Slide 10

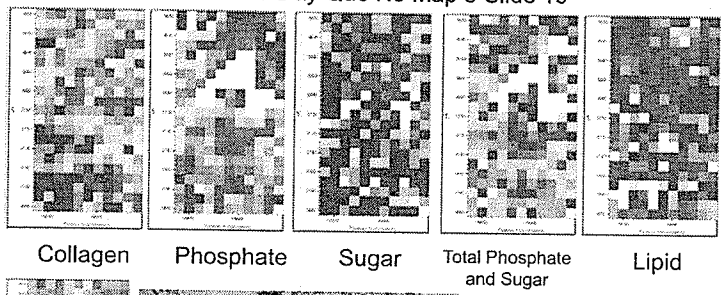

Collagen | Phosphate | Sugar | Total Phosphate and Sugar | Lipid

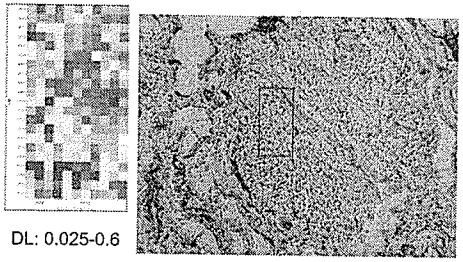

DL: 0.025-0.6

- Bottom portion of map is really nasty, especially the left hand part. Likely just really nasty tissue and not focus issues

63 Day Que N5 Map 4 Slide 10

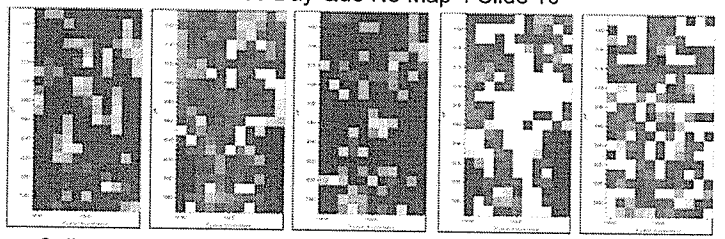

Collagen | Phosphate | Sugar | Total Phosphate and Sugar | Lipid

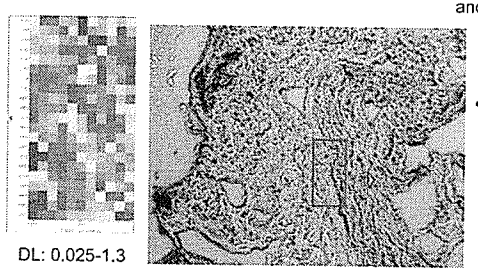

DL: 0.025-1.3

- Lots of spiky Amides in this map

63 Day Que N5 Map 5 Slide 10

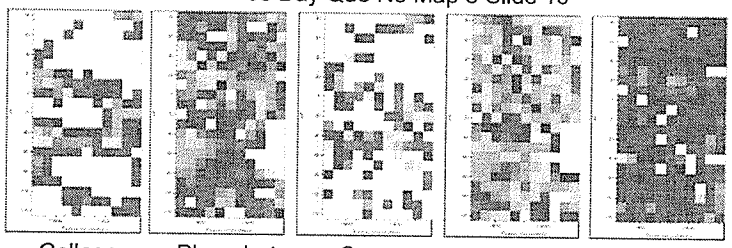

Collagen | Phosphate | Sugar | Total Phosphate and Sugar | Lipid

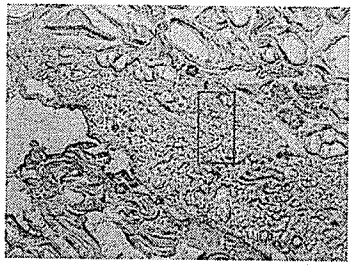

- Good spectra in this map although there are some baseline issues, but they don't really affect the profiles

63 Day Que N5 Map 6 Slide 10

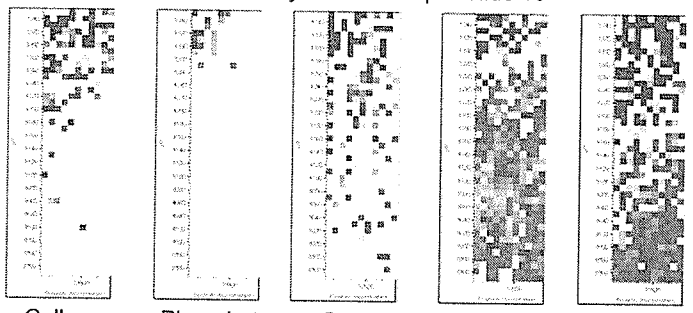

Collagen | Phosphate | Sugar | Total Phosphate and Sugar | Lipid

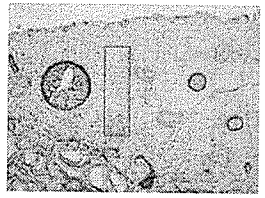

- It's an overnight map and it goes out of focus about 1/3 to ½ of the way through, and then it runs out of liquid nitrogen, so the top part is just junk
- In the end though it looks like it was taken in muscle area so we're not all that interested in it anyway

63 Day Que N5 Map 7 Slide 10

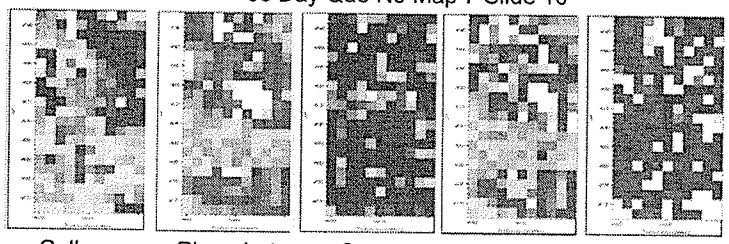

Collagen | Phosphate | Sugar | Total Phosphate and Sugar | Lipid

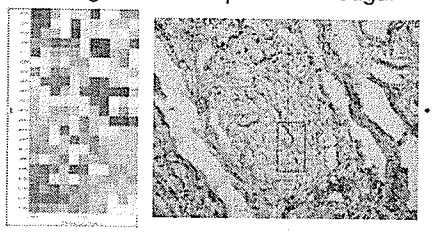

DL: 0.025-0.7

- Bottom part of map is better behaved than the top part, but the top part is ok too. There are a couple of small holes here and there, but nothing major to worry about

63 Day Que N7 Map 1 Slide 10

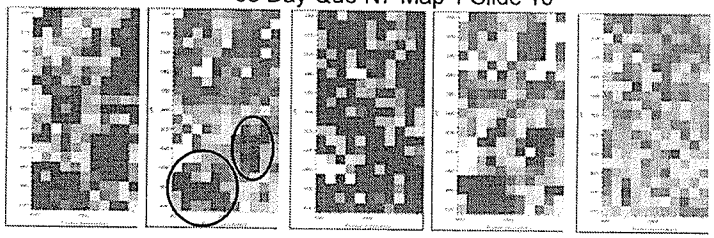

Collagen | Phosphate | Sugar | Total Phosphate and Sugar | Lipid

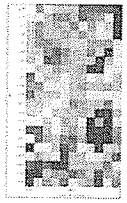

DL: 0.025-0.8

There are some seriously ugly spectra in this map, but there is information in them, I just don't know what it means →

There's also a frill running throughout the spectra here, more noticeably in the high frequency range of the spectra

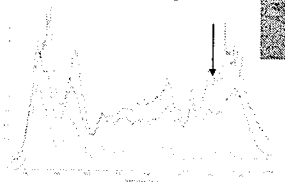

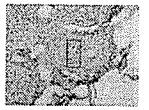

63 Day Que N7 Map 2 Slide 10

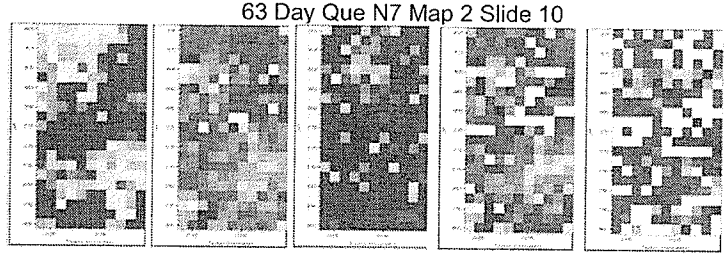

Collagen | Phosphate | Sugar | Total Phosphate and Sugar | Lipid

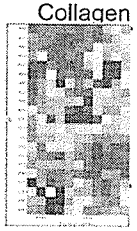

DL: 0.025-0.9

Pretty much every spectrum has something wrong with it, whether it be spiky amides, rolling baseline, ugly phosphate/sugar, or spiky CH2/OH/NH stretch

There also seem to be cases where the region from 1200 to 1500 cm-1 or so is elevated, and it doesn't really look like baseline issues

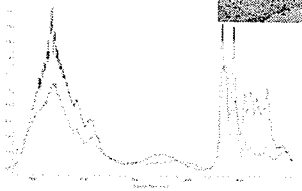

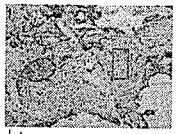

63 Day Que N7 Map 3 Slide 10

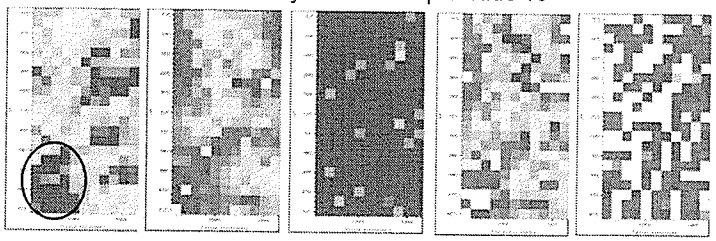

Collagen | Phosphate | Sugar | Total Phosphate | Lipid

- Spectra are ok here, but more evidence of nonstandard collagen Amide I profiles
- Pretty clean sugar/phosphate vibrations

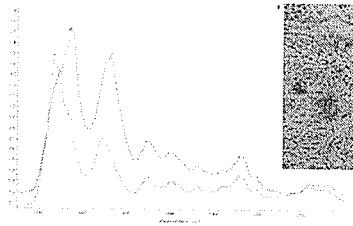

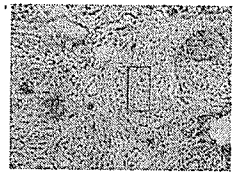

63 Day Que N7 Map 3 Slide 10

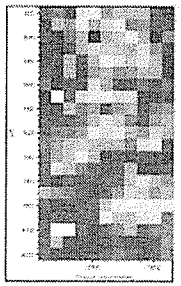

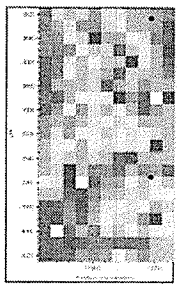

This probably shouldn't surprise me all that much. Even though the sugar/phosphate region in this map is pretty good, it isn't perfect and using baseline values that can be affected by the noise could cause problems.

Does that mean I need to go back and redo most of the sugar maps with the new values? Or at least new baseline values? No.

Alternate Sugar
1026 to 1039
BL: 985 to 1145

Same values for sugar band, but baseline the same as total phosphate and sugar and just phosphate

63 Day Que N7 Map 4 Slide 10

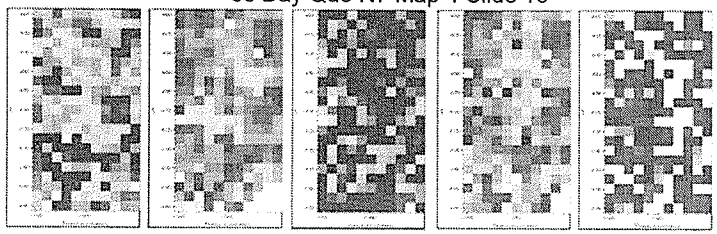

Collagen Phosphate Sugar Total Phosphate and Sugar Lipid

- Pretty standard map. Some spiky amides, some not. The CH/OH/NH region seems to be ok, but the sugar/phosphate region isn't well defined.

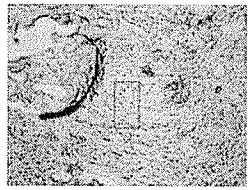

63 Day Que N7 Map 5 Slide 10

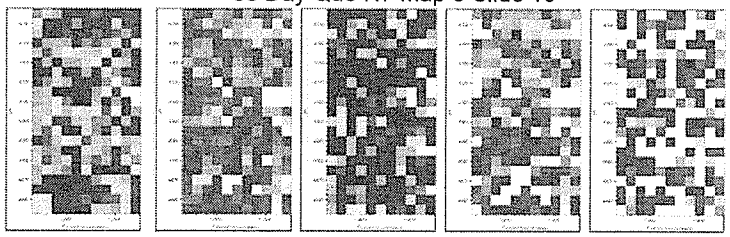

Collagen Phosphate Sugar Total Phosphate and Sugar Lipid

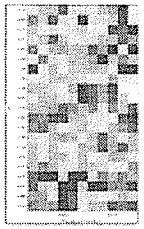

DL: 0.025-0.7

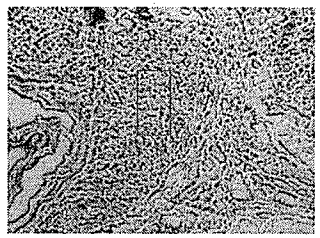

- Pretty much all the amides are spiky and/or cut off.
- The CH/OH/NH are noisy

63 Day Que N7 Map 6 Slide 10

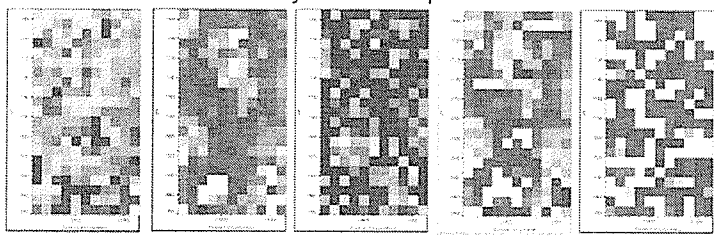

Collagen Phosphate Sugar Total Phosphate and Sugar Lipid

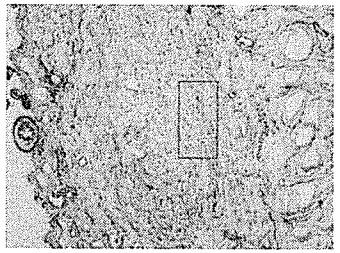

- Pretty typical for the 63 day animals. Good 1204 profiles, while the Amides tend to be rather scraggly and cut off.
- Sugar and phosphate region is awfully noisy

63 Day Que N9 Map 1 Slide 20

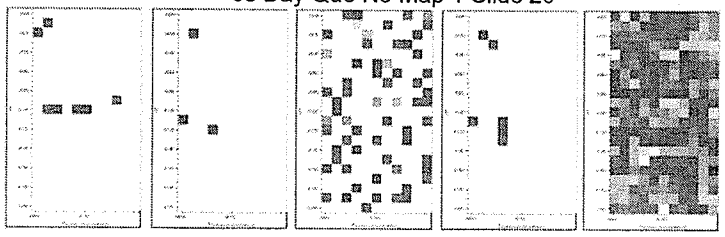

Collagen | Phosphate | Sugar | Total Phosphate and Sugar | Lipid

- This was the animal where the sections were placed on the wrong side of the MirrIR slide. We ended up collecting maps on slide 20 instead of slide 10 like we'd planned. We saved two mosaics for each map (one large image for location and another zoomed in to see where the map was taken). Mitch has since taken pictures of slide 20 and marked the maps on the image
- Decent spectral quality. The processed maps are believable, there isn't much collagen, but the CH2 str region is quieter and there is a bit of lipid around

63 Day Que N9 Map 2 Slide 20

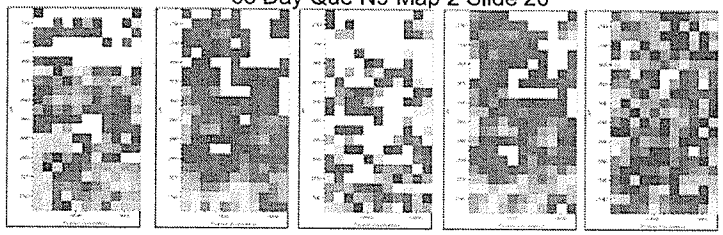

Collagen | Phosphate | Sugar | Total Phosphate and Sugar | Lipid

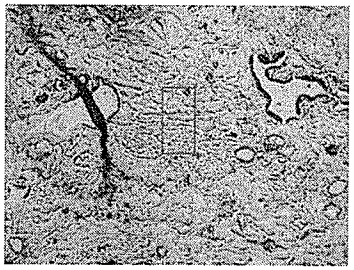

- Pretty standard quality for the 63 day animals. Some good pts, some bad pts.
- CH2 str isn't great, but that is real lipid. It's intense enough that it can be seen quite easily even over the noise
- Phosphate/Sugar region of the spectrum is just yucky

63 Day Que N9 Map 3 Slide 20

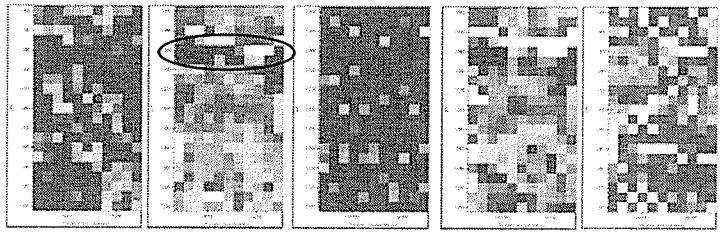

Collagen | Phosphate | Sugar | Total Phosphate and Sugar | Lipid

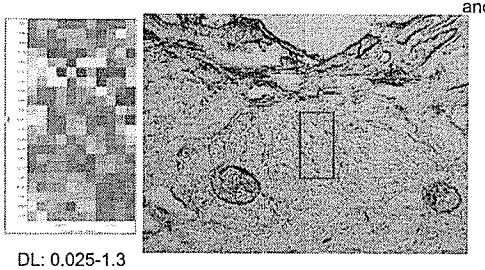

DL: 0.025-1.3

Not very good spectra here. The top and bottom are ok, but the middle is pretty ugly and there's an especially bad region marked

Sugar/phosphate region is useless in most of the spectra

63 Day Que N9 Map 4 Slide 20

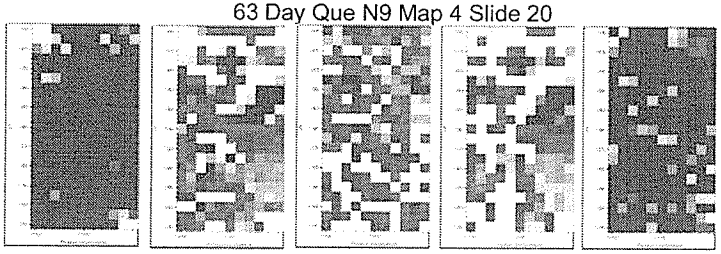

Collagen | Phosphate | Lipid | Total Phosphate and Sugar | Sugar

- Lots of collagen here. The Amide III is sometimes as high as the Amide I. I would chalk this up to orientational effects, but if that's the case then the Amide II should be more intense as well
- Some weird reflective issues in the top left and bottom right corner of the map
- If the baseline for the sugar is changed, the map looks like the phosphate and total phosphate/sugar maps. Are we imaging on baseline anomalies?

63 Day Que N9 Map 4 Slide 20

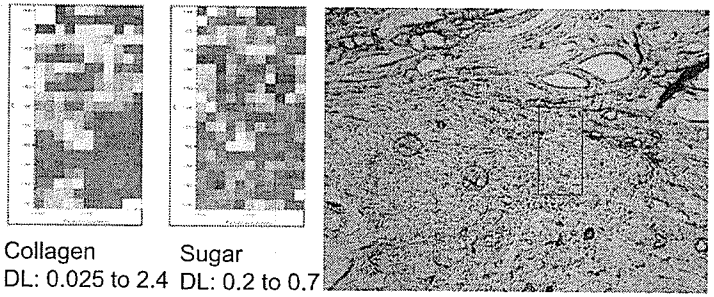

Collagen
DL: 0.025 to 2.4

Sugar
DL: 0.2 to 0.7

63 Day Que N9 Map 5 Slide 20

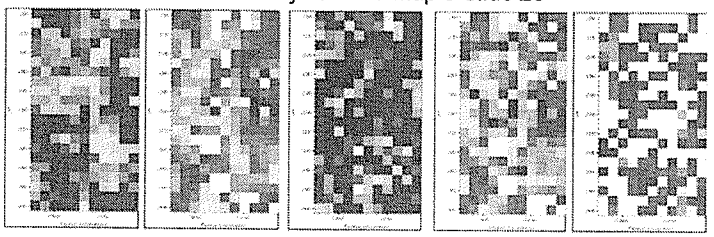

Collagen | Phosphate | Sugar | Total Phosphate and Sugar | Lipid

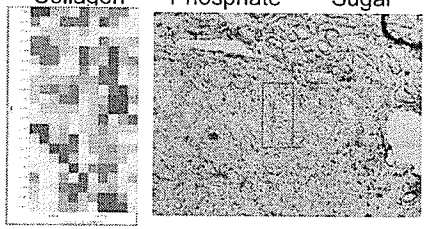

DL: 0.025-0.7

- About average. A fair amount of spiky amides and cut off tops.
- Overall sugar/phosphate is pretty lousy

63 Day Que N11 Map 1 Slide 10

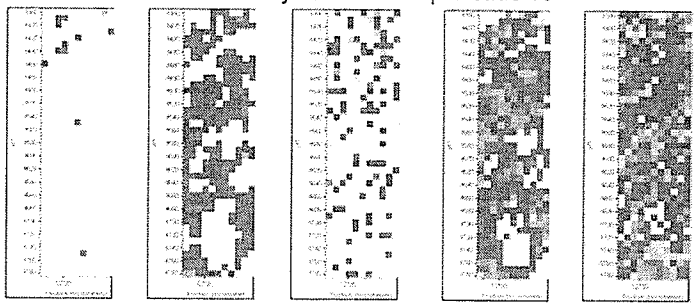

Collagen | Phosphate | Sugar | Total Phosphate and Sugar | Lipid

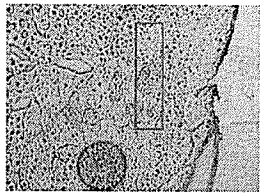

- An overnight map that actually stayed in focus
- The spectra are reasonable, but there are the usual problems with spiky amides, some rolling a baseline, and noisy phosphate/sugar

63 Day Que N11 Map 2 Slide 10

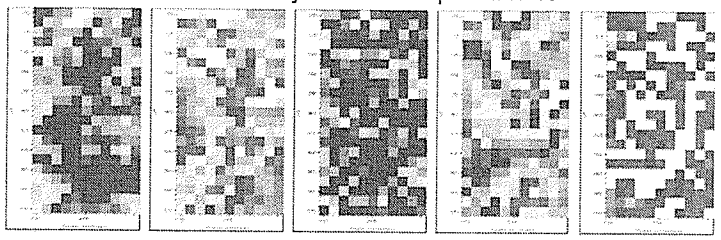

Collagen | Phosphate | Sugar | Total Phosphate and Sugar | Lipid

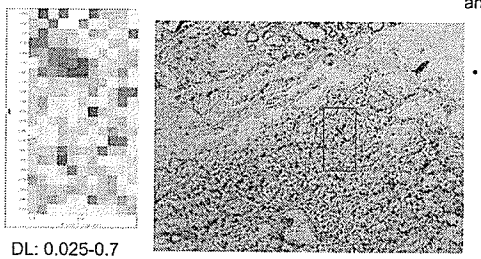

DL: 0.025-0.7

- This map turned out quite nice. There are minimal occurences of spiky amides, and the sugar/phosphate region is ok in most of the spectra

63 Day Que N11 Map 3 Slide 10

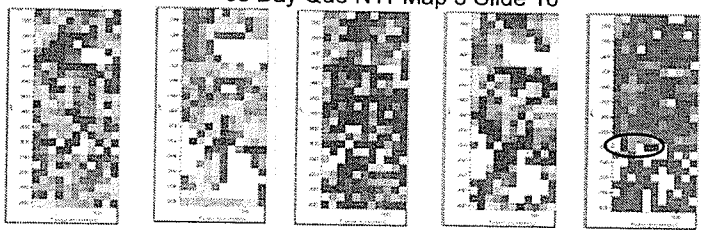

Collagen | Phosphate | Sugar | Total Phosphate and Sugar | Lipid

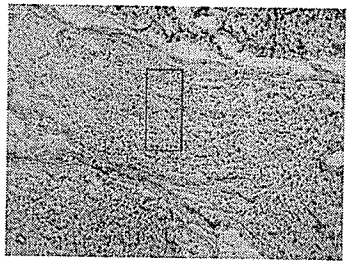

- Liquid nitrogen ran out for a few pixels, but the data is ok in the rest of the map
- The sugar/phosphate bands are still not useful though

63 Day Que N11 Map 4 Slide 10

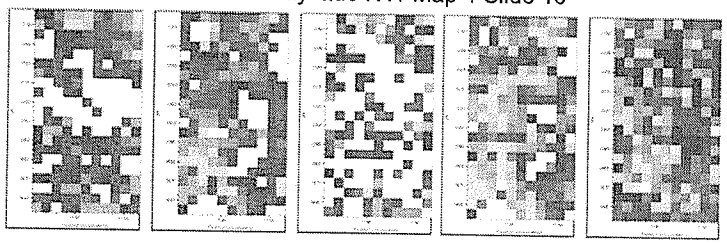

Collagen | Phosphate | Sugar | Total Phosphate and Sugar | Lipid

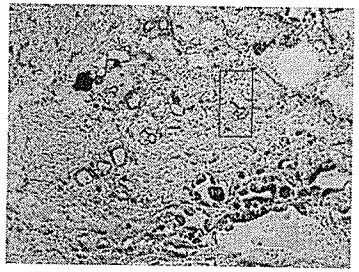

- Standard map. Nice collagen signal, pretty good lipid signal but lousy sugar/phosphate

63 Day Que N11 Map 5 Slide 10

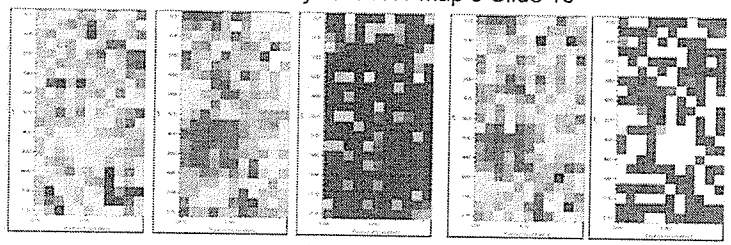

Collagen | Phosphate | Sugar | Total Phosphate and Sugar | Lipid

- Nice map except for the sugar/phosphate region of the spectrum

63 Day Que N11 Map 6 Slide 10

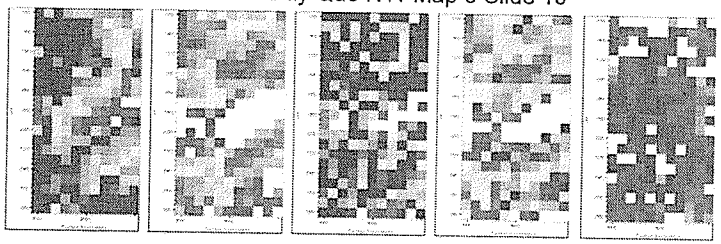

Collagen | Phosphate | Sugar | Total Phosphate and Sugar | Lipid

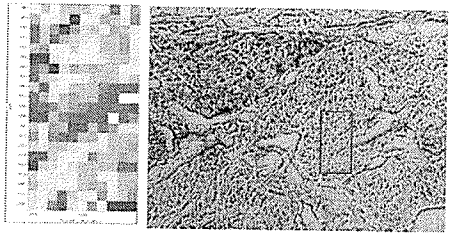

Ok, but not great. A fair bit of spiky amides and OH/NH stretch misbehaviour

DL: 0.025-0.7

63 Day Que Animals

June 2007

Richard Wiens

63 Day Que N5 Map 8

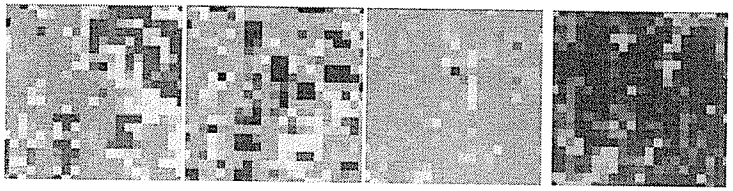

Collagen	Phosphate	Sugar	Sym CH_2
0 to 0.5	0.6 to 1.6	0.0 to 0.4	0.0 to 0.4

63 Day Saline Rats

June 2006 SRC

Richard Wiens
Mitch Bushuk

63 Day Saline N29 Map 1 Slide 10

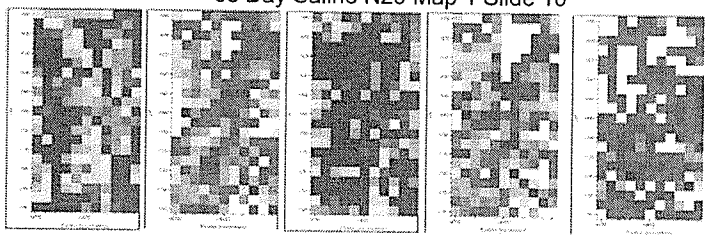

Collagen 1080 1030 1014-1130 Lipid

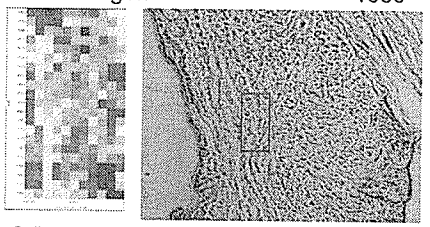

Collagen 0.025-0.9

Collagen region (1200-1400 cm-1) is pretty good throughout the map.

The 1000-1100 cm-1 region is a bit suspect though. I think the total sugar/phosphate might provide some information, but I'd be hesitant to read to much into the individual maps, especially the sugar.

CH2 str region is pretty lousy but visual inspection suggests there is little lipid when the spectra are good.

- Some cases of saturated spikey Amide I and II as well as OH/NH str above 3000 cm-1

63 Day Saline N29 Map 2 Slide 10

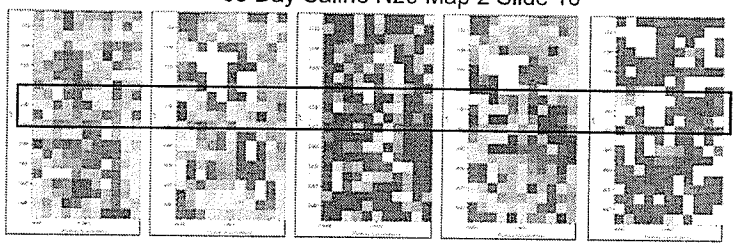

Collagen 1080 1030 1014-1130 Lipid

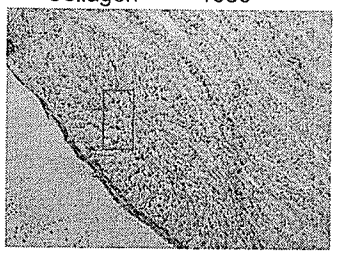

- About the same as the previous map. Decent collagen signature, less than pretty sugar/phosphate and CH2 str regions. A bit of cut off Amide I and II, but not too bad.
- A few lines in the center of the map seem to be thick tissue, or just out of focus.

63 Day Saline N29 Map 3 Slide 10

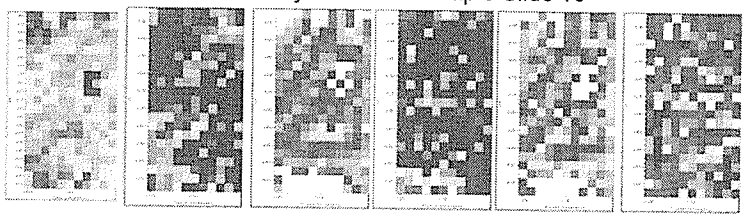

Collagen Collagen 1080 1030 1014-1130 Lipid

0.025-0.8

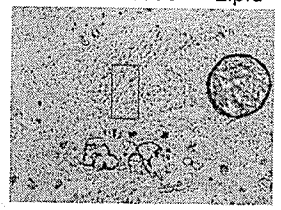

Not the greatest spectra ever, but that is real lipid. There seems to be a couple of different kinds of lipid though. In some of the spectra that show an elevated CH2 str there is no corresponding increase in lipid carbonyl around 1720 cm-1, while in other cases there is a bit of a blip of high frequency carbonyl. Point 57 and 140.

63 Day Saline N29 Map 4 Slide 10

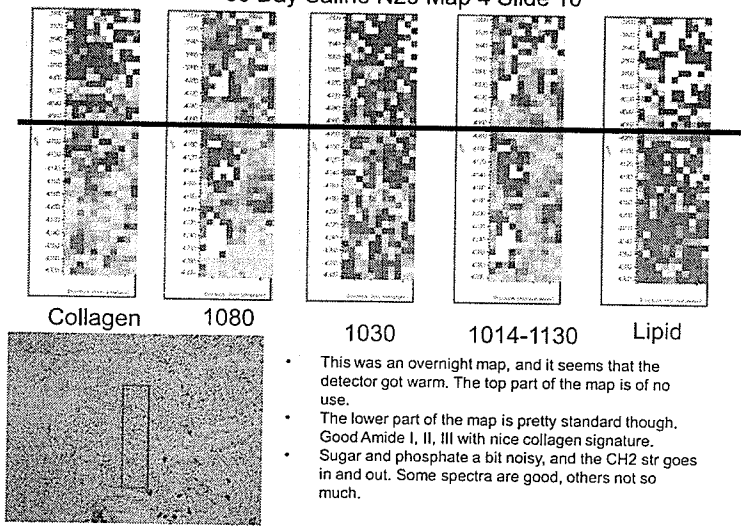

Collagen 1080 1030 1014-1130 Lipid

- This was an overnight map, and it seems that the detector got warm. The top part of the map is of no use.
- The lower part of the map is pretty standard though. Good Amide I, II, III with nice collagen signature.
- Sugar and phosphate a bit noisy, and the CH2 str goes in and out. Some spectra are good, others not so much.

63 Day Saline N29 Map 5 Slide 10

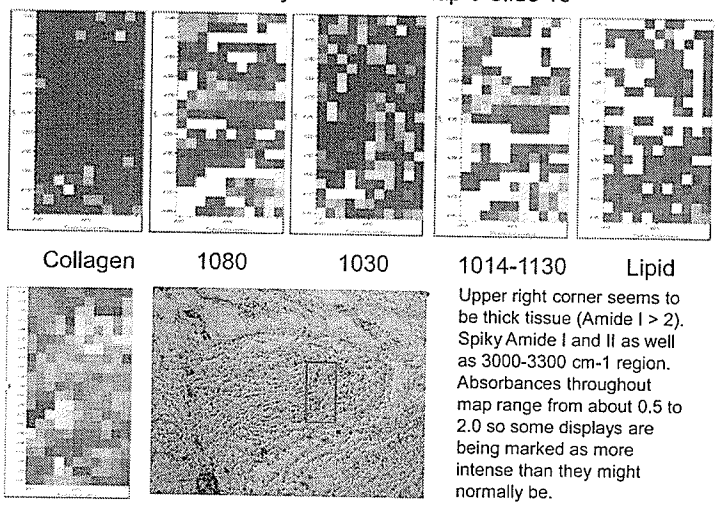

Collagen 1080 1030 1014-1130 Lipid

Collagen 0.025-1.9

Upper right corner seems to be thick tissue (Amide I > 2). Spiky Amide I and II as well as 3000-3300 cm-1 region. Absorbances throughout map range from about 0.5 to 2.0 so some displays are being marked as more intense than they might normally be.

63 Day Saline N29 Map 6 Slide 10

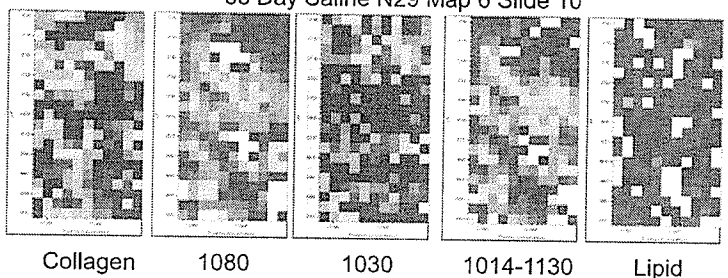

Collagen 1080 1030 1014-1130 Lipid

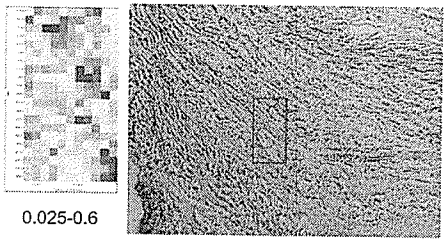

0.025-0.6

- Pretty much the same as all the previous N29 maps. There's a bit of a hole in the lower right, and the CH2 str seems better behaved in this map than some others, but that's offset by some cases of rolling baseline.

63 Day Saline N29 Map 7 Slide 10

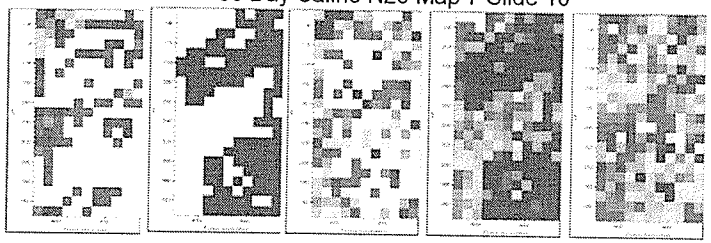

Collagen 1080 1030 1014-1130 Lipid

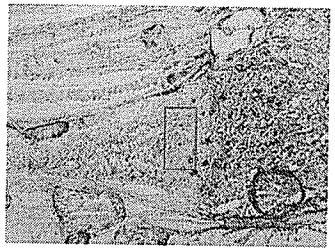

- This is one of the maps taken in a region with those odd cellular looking things. Oodles of phosphate, some CH2 stretch, and a variable high frequency carbonyl. See spectrum saved "N29 Map 7 point 196 – odd cell".
- Again, good spectra from about 1100 to 1800 cm-1 with the CH str and Phosphate/Sugar regions being less than smooth

63 Day Saline N29 Map 8 Slide 10

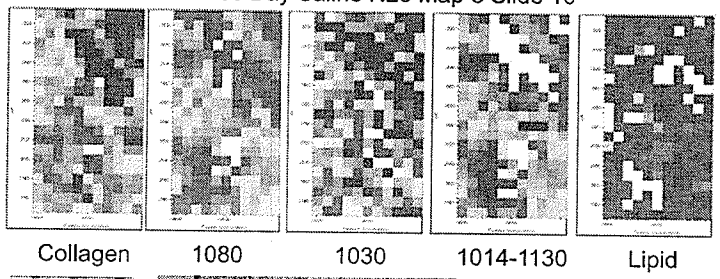

Collagen 1080 1030 1014-1130 Lipid

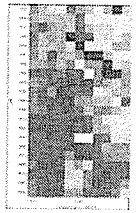

0.025-0.7

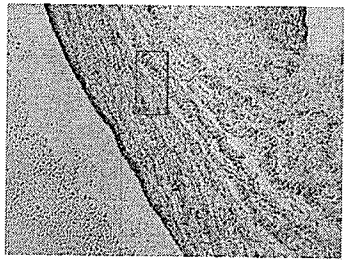

- Same old same old.
- I think the 1080 absorbance is due in part to baseline anomalies. There really doesn't seem to be that much there.

63 Day Saline N31 Map 1 Slide 10

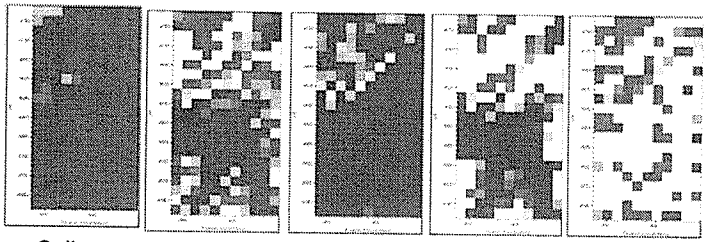

Collagen 1080 1030 1014-1130 Lipid

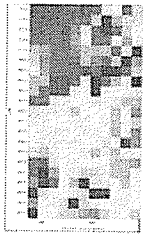

0.025-2.6

- Not the prettiest map ever. Some nasty tissue in the middle with lots of cut off amide Is and IIs, as well as scraggly 3000-3300 cm-1 regions. There are also some cases of spiking around 1450 cm-1
- The high 1080 also seems like it might be due to baseline variation.
- Looks like there is also some oriented collagen in the lower right hand corner

63 Day Saline N31 Map 2 Slide 10

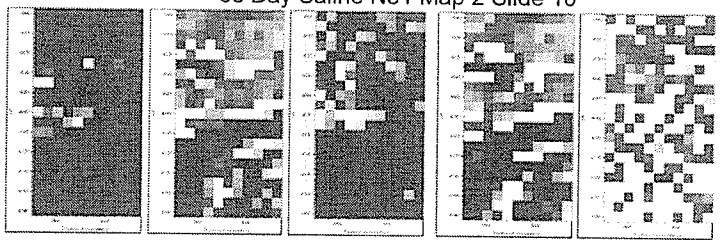

Collagen 1080 1030 1014-1130 Lipid

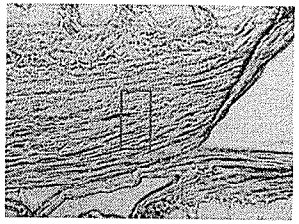

0.025-2.4

On the bad side of normal. Collagen fingerprint is there, but a lot of spikyness and noise at both high and low frequencies

Some nice oriented collagen in the lower part of the map

We may have to do some reprocessing with different display limits. The collagen area in 21 day animals displayed nicely from 0.025 to about 0.45, but in these 63 day animals it seems like collagen starts with an area of around 0.4 and goes up to over 3.0 in some cases

63 Day Saline N31 Map 3 Slide 10

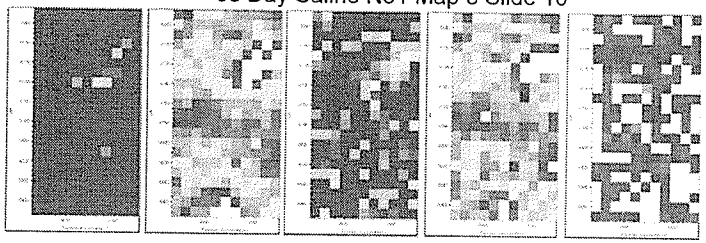

Collagen 1080 1030 1014-1130 Lipid

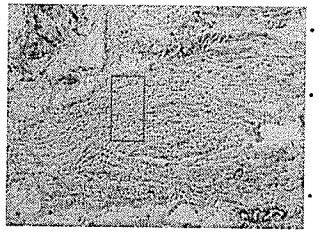

0.025-0.9

- Paused for beamfill at point 161. Alters absorbance value, but shouldn't affect data processing.
- Pretty standard data for this trip, although the CH2 region is better behaved than it has been in some other maps. Still noisy under about 1100 cm-1 though.
- Collagen varies from about 0.5 to 1.0

63 Day Saline N31 Map 4a Slide 10

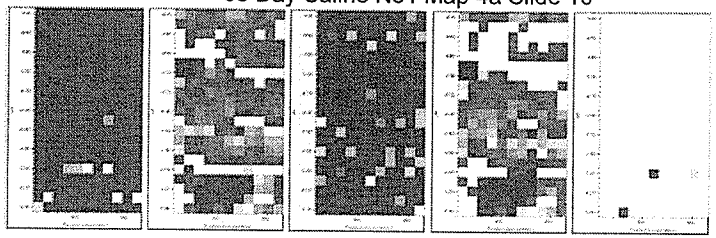

Collagen 1080 1030 1014-1130 Lipid

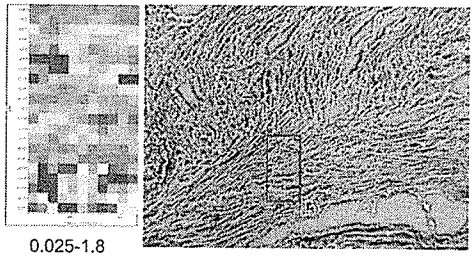

0.025-1.8

- This map got hit by the beam gremlins or something
- The spectra are noisy,
- Not only that, but there are very odd baseline occurences. Map was redone as 4b, see Lab Book 2 Page 41 for more details.

63 Day Saline N31 Map 4b Slide 10

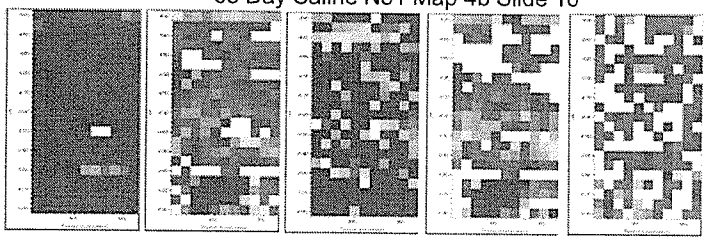

Collagen 1080 1030 1014-1130 Lipid

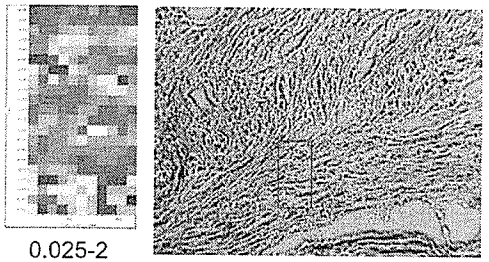

0.025-2

- This is the redone map of 4a, and it seems to have turned out better
- The lower area is still a bit icky due to tissue thickness, but the rest of it isn't too horrible.

63 Day Saline N31 Map 5 Slide 10

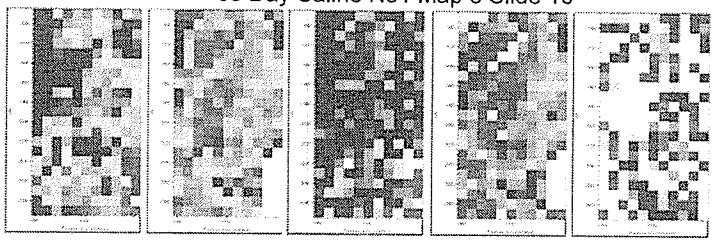

Collagen 1080 1030 1014-1130 Lipid

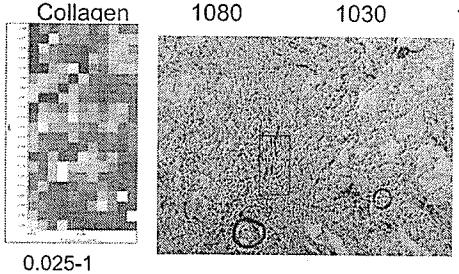

0.025-1

Pretty standard for these maps. Decent collagen profile, spiky amides and high frequency stretches, noisy under 1100 cm-1

It's a bit tough to say for sure, but there seems to be a fair bit of variable amide I. Sometimes shifted down to ~1620 and sometimes showing up as a split peak, but the spikyness makes conclusions dubious

63 Day Saline N31 Map 6a Slide 10

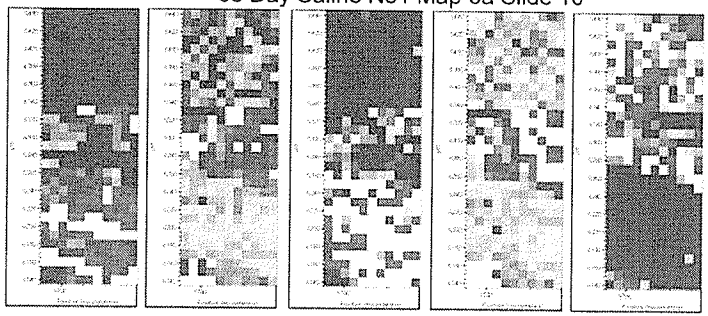

Collagen 1080 1030 1014-1130 Lipid

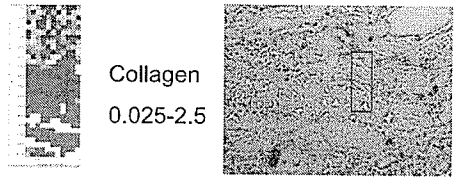

Collagen

0.025-2.5

An overnight map taken in one of the regions with the funny looking cells. The bottom half is good, but the top half went serioiusly outta focus. Was redone as 6b

63 Day Saline N31 Map 6b Slide 10

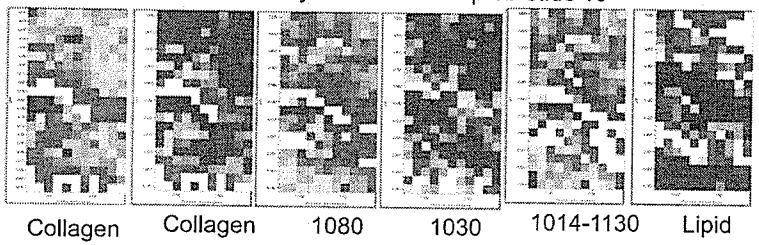

Collagen Collagen 1080 1030 1014-1130 Lipid

0.025-0.9

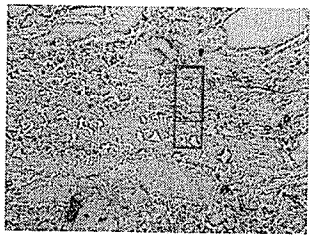

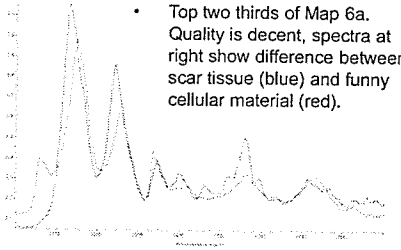

- Top two thirds of Map 6a. Quality is decent, spectra at right show difference between scar tissue (blue) and funny cellular material (red).

63 Day Saline N31 Map 7 Slide 10

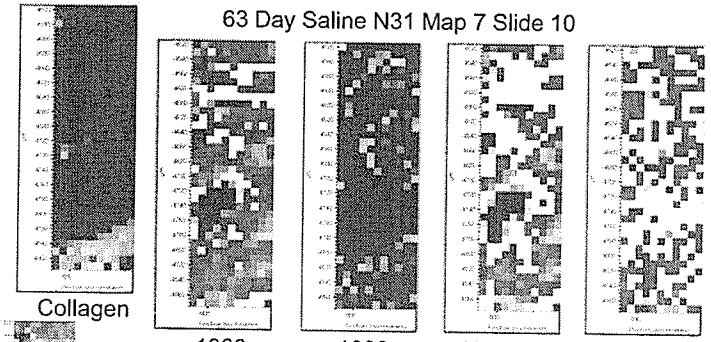

Collagen 1080 1030 1014-1130 Lipid

Collagen

DL: 0.025-2

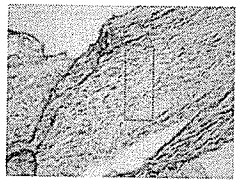

This map is odd. The lab book says it should be the standard 11 x 21 but it's actually 11 x 36, and the coordinates in the lab manual don't match up with the coordinates of the map or mosaic. The map and mosaic coordinates do match up, and it's drawn on the picture in the correct place.

63 Day Saline N33 Map 1 Slide 10

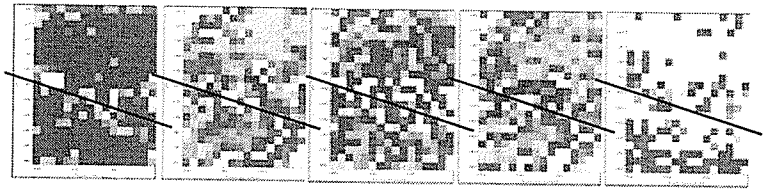

Collagen 1080 1030 1014-1130 Lipid

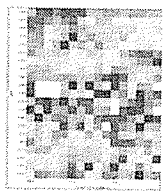

Collagen

DL: 0.025-0.9

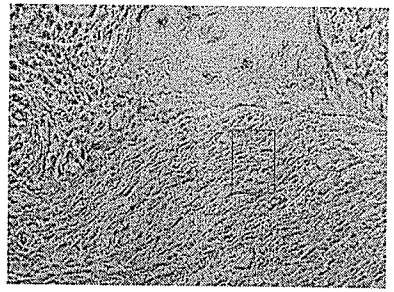

- Pretty good spectra top and bottom, but some thick tissue in the middle on either side of the line.

63 Day Saline N33 Map 2 Slide 10

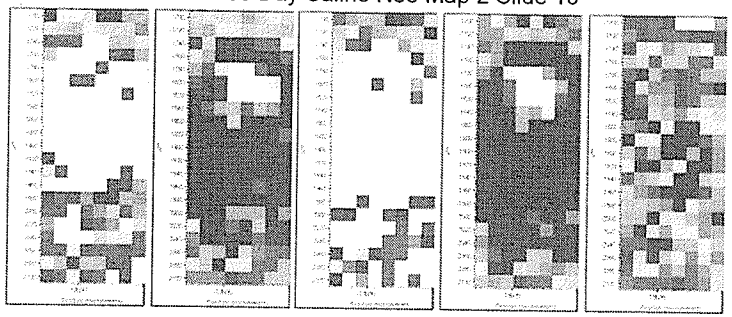

Collagen 1080 1030 1014-1130 Lipid

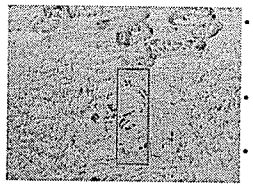

- Experimental map with 20 micron aperture and 20 micron step size to try and solve some of the problems we were having early on
- Good data, some more of those strange cells with really big lipid carbonyl and phosphate absorptions
- Also focused after every point, took about 2x the time as a normal map would've

63 Day Saline N33 Map 3 Slide 10

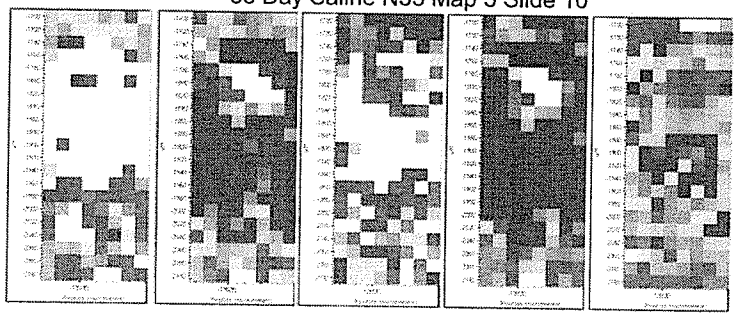

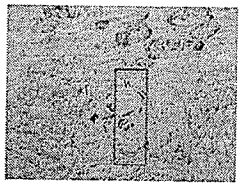

- Same map as map 2, but focusing every 3 rows or so. Not much of a noticeable difference between focusing every couple of rows vs after every pixel.
- 20 micron aperture, 20 micron step size

63 Day Saline N33 Map 4a Slide 10

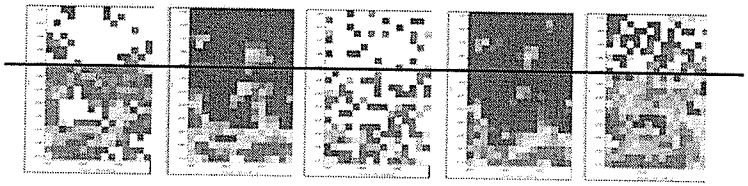

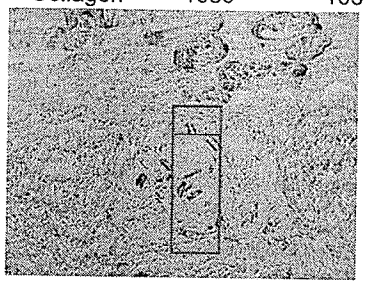

- Stage died at point 276, so map was stopped
- Map was to be same area as maps 2 and 3 with 12 micron aperture and 10 micron step size to see if amount of light would help
- Data acquired before stage stopped moving is ok

63 Day Saline N33 Map 4b Slide 10

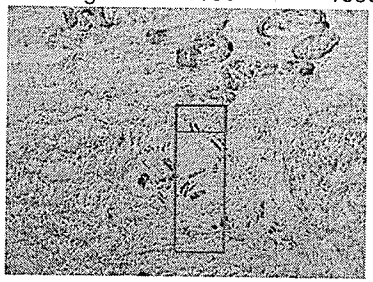

- This was to be the continuation of map 4a b/c of stage malfunctions, but the same thing happened again
- Decided that the point of the map had been fulfilled. We can get data with a 12 micron aperture, we just have to be very careful that things stay in focus. Tissue isn't nearly as uniform as it was in the 21 day animals

63 Day Saline N33 Map 5 Slide 10

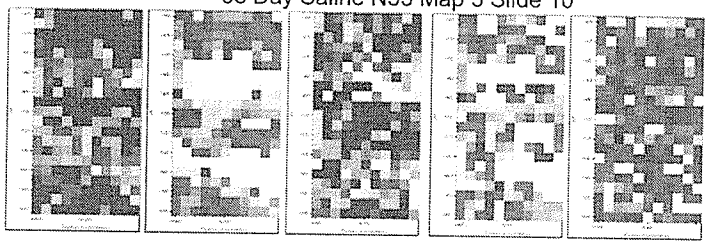

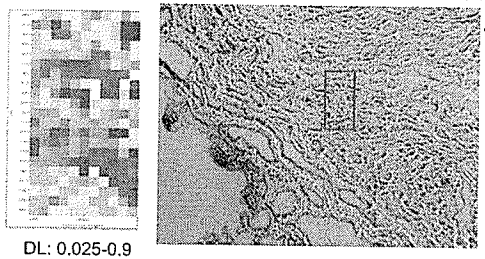

DL: 0.025-0.9

- Thick tissue leads to some nasty looking spectra in places, but pretty standard map for the 63 day animals. Decent collagen signature, tough to get info about sugar/phosphate and lipid regions though.

63 Day Saline N33 Map 6 Slide 10

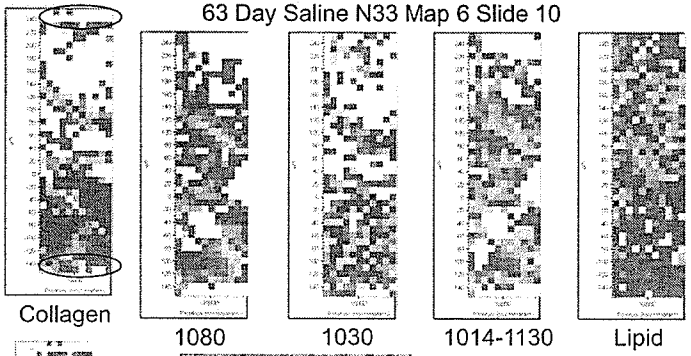

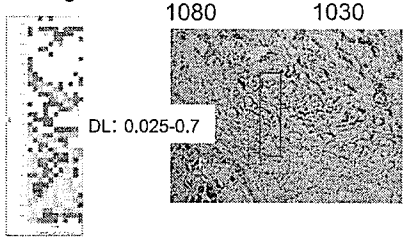

- An overnight map, this one isn't as out of focus as I would have feared. Some places aren't real good, but it looks to be more holes in the tissue than focus issues

63 Day Saline N35 Map 1 Slide 10

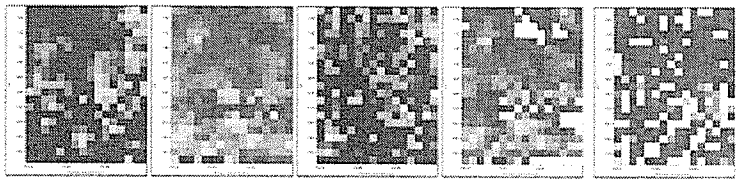

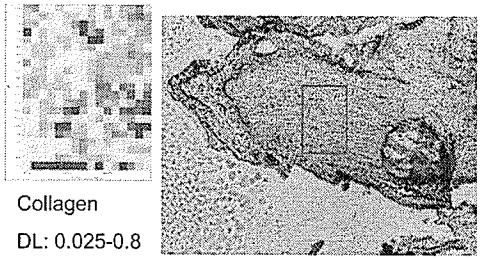

- This was the first sample we looked at
- Looking at the data now it doesn't seem to be nearly as bad as it seemed to be while we were there
- It's still not necessarily good, but you can get collagen information out of it, but the high frequency stretching vibrations and the low frequency sugar/phosphate aren't very useful

63 Day Saline N35 Map 2 Slide 10

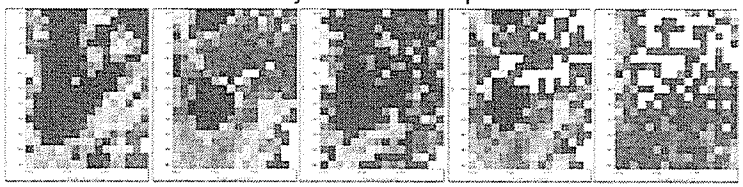

- Pretty nasty tissue, lots of spiky amides and things like that
- The lower left portion of the map has some spectra where the relative intensities of the OH/NH str are equal to that of the amide I,
- Redoing the collagen with a DL of 0.025 to 1.5 it seems like there's an outline of higher collagen around an area of moderate collagen but very high phosphate

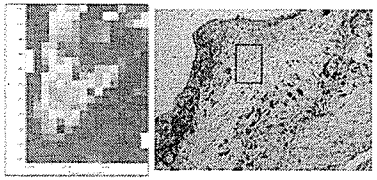

63 Day Saline N35 Map 3 Slide 10

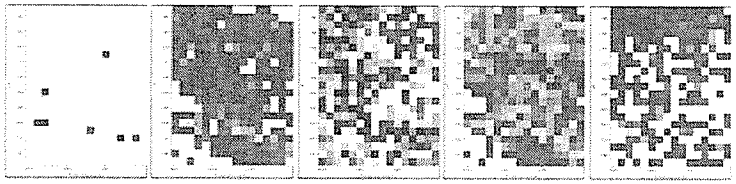

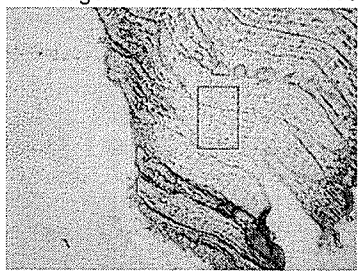

- Sugar/phosphate region is pretty useless, doesn't seem to be any collagen in this map. Probably taken in a muscle region

63 Day Saline N35 Map 4 Slide 10

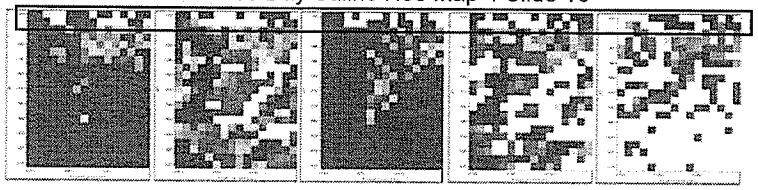

Collagen 1080 1030 1014-1130 Lipid

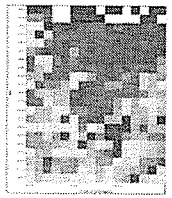

Collagen

DL: 0.025-2.5

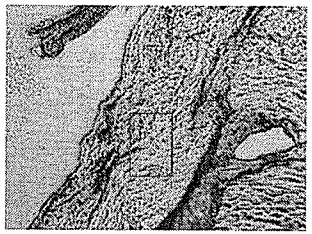

- Liquid nitrogen ran out at the end of the map, so the top two rows of the map are just noise
- Seems to be a fair bit of oriented collagen in the lower part, or at least the 1240 cm-1 region is very intense.
- 64 scans

63 Day Saline N35 Map 5 Slide 10

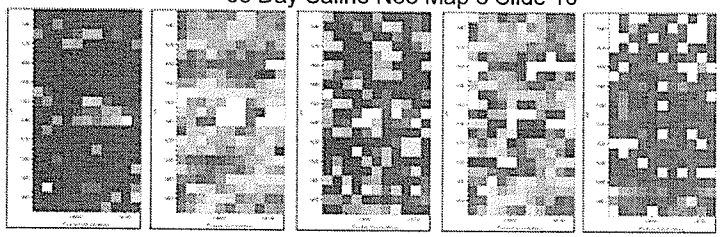

Collagen 1080 1030 1014-1130 Lipid

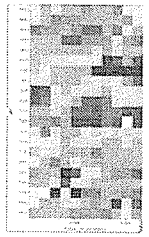

DL: 0.025-1.1

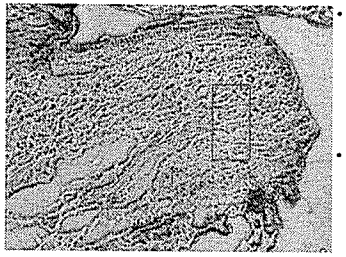

- These next four maps were done at the end of the two weeks while the first four were done at the beginning
- Spectra are decent, except for some spikeyness and noise below 1100 cm^{-1}.

63 Day Saline N35 Map 6 Slide 10

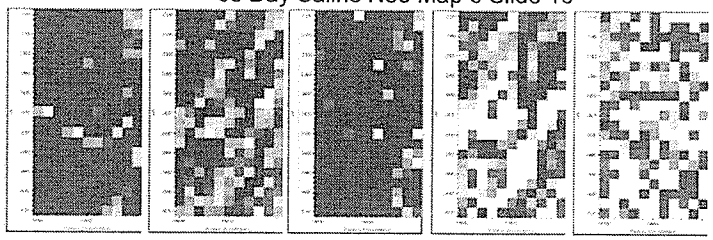

Collagen 1080 1030 1014-1130 Lipid

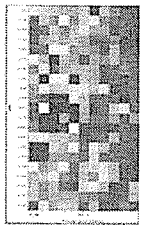

DL: 0.025-2.5

Pretty ugly spectra in this one

Lots of scraggly amide Is and OH/NH stretch

63 Day Saline N35 Map 7 Slide 10

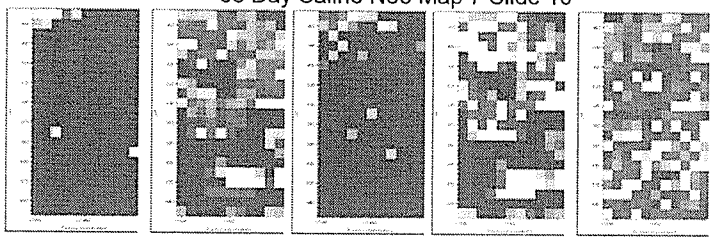

Collagen 1080 1030 1014-1130 Lipid

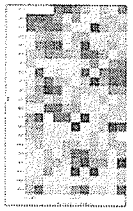

DL: 0.025-2.4

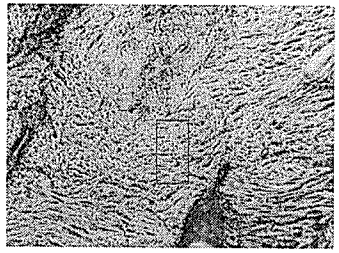

- Overall rather poor quality data, but some very intense amide III's, some of them even spike

63 Day Saline N35 Map 8 Slide 10

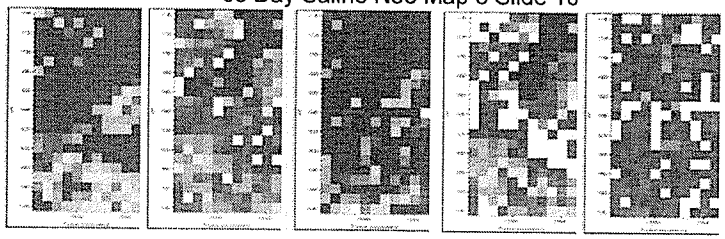

Collagen 1080 1030 1014-1130 Lipid

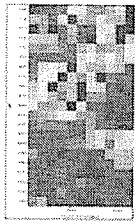

DL: 0.025-1.4

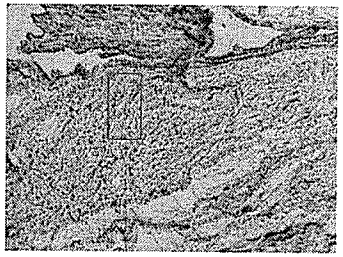

- Standard fare for these 63 day animals
- Good collagen signature, top half of the map is kind of raggedy

April and June 2007 SRC

Richard Wiens
New Omnic Software
And Microscope

63 Day Saline N29 Map 11

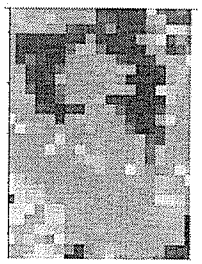

Collagen – 0 to 1
Phosphate 0.6 to 1.6

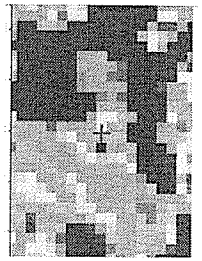

The Blue region in the C/S/P maps is just thin tissue. The phosphate/sugar region on the spectra isn't of very good quality, it's rather noisy. While there is a lot of lipid in some of the spectra, there is no corresponding increase in the carbonyl band to go with the high intensity C-H stretches. Also, there is quite clearly collagen present in the same spectra as the high C-H stretches.

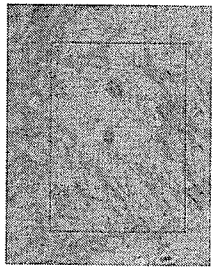

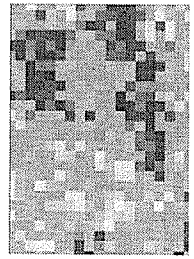

Sugar 0 to 0.4
Lipid 0 to 1.0

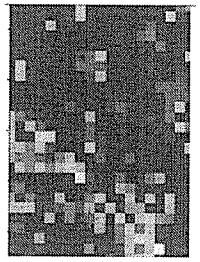

63 Day Saline N29 Map 12

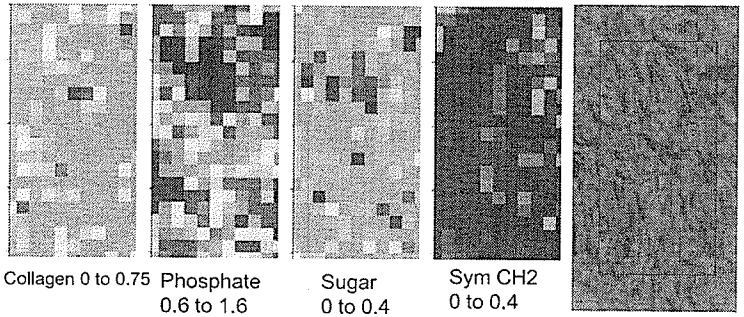

Collagen 0 to 0.75 | Phosphate 0.6 to 1.6 | Sugar 0 to 0.4 | Sym CH2 0 to 0.4

Data looks good. The phosphate/sugar is somewhat wobbly, but other than that, it's a good map.

63 Day Saline N31 Map 9

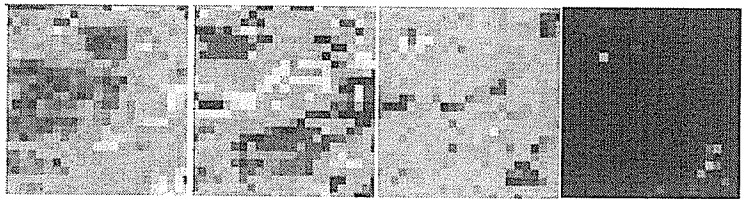

Collagen 0 to 1 | Phosphate 0.6 to 1.6 | Sugar 0 to 0.4 | Sym CH2 0 to 0.4

There was more water in the background spectrum than the tissue spectra, as a result there are negative peaks for water (and CO_2). The collagen, CH stretch and sugar/phosphate regions are all good though. There are some thick regions of tissue as well, with Amide I's and/or II's over 3.

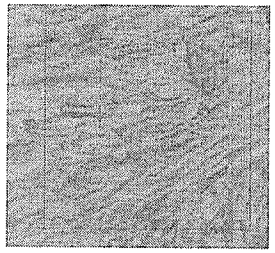

63 Day Saline N31 Map 10

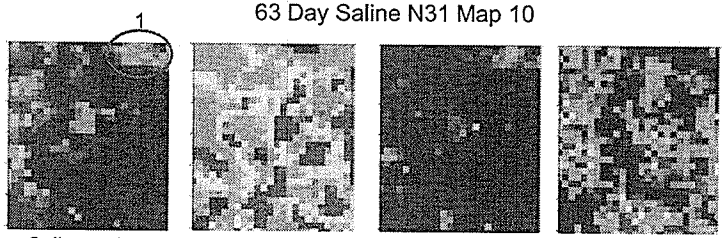

Collagen 0 to 1 | Phosphate 0.6 to 2.5 | Sugar 0 to 0.4 | Sym CH2 0.2 to 0.7

1) This is the only bit of collagen in the map. The other green bits aren't really collagen.

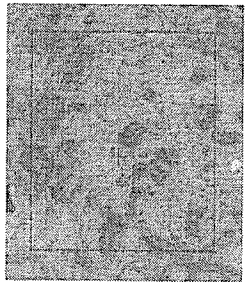

63 Day Saline N35 Map 9

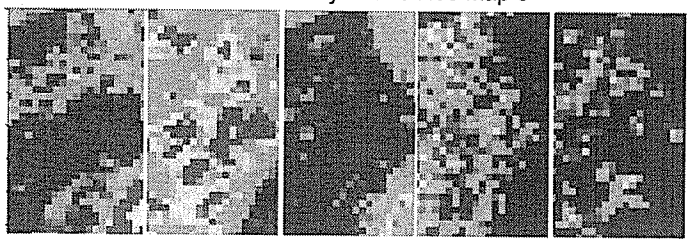

Collagen 0 to 0.5 | Phosphate 0.6 to 2.5 | Sugar 0 to 0.4 | Sym CH2 0.2 to 0.7 | Carbonyl 0 to 5

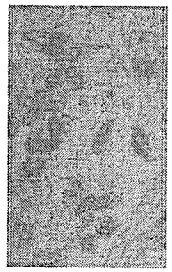

63 Day Saline N35 Map 10

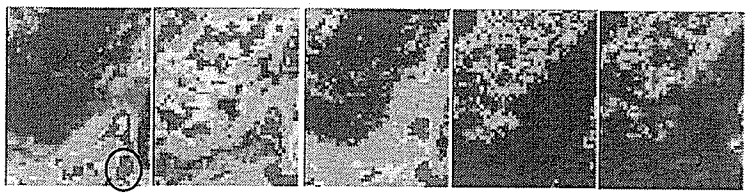

Collagen 0 to 1.5 | Phosphate 0.6 to 2.5 | Sugar 0 to 0.4 | Sym CH2 0.2 to 0.7 | Carbonyl 0 to 5

Possible Orientation